APPLICATIONS OF TWO-DIMENSIONAL IMAGE ANALYSIS TO MINERAL LIBERATION STUDIES
(BRUNSWICK MINING AND SMELTING, BATHURST, N.B.)

Gregg S. Hill

McGill University
Dept. of Mining and Metallurgy

April, 1990

Submitted in partial fulfillment of the requirements for the degree of Doctor of Philosophy in Science

DEDICATION:

I really thought that when I finished I would have something monumentally humorous to say. But now that the job is done it's almost as if an important part of me has disappeared with it.

This work is dedicated to my mom, Joan, who decided when I was still a baby that one day I would go to McGill. You were right.

To my dad, Stan; and Ross and Lesley.

To my friends Neil Rowlands and Jim Finch

To Steve and Joanna, who make my life a lot more fun.

To Bill Taggart

To Hélène

To Lise

God bless you all for your love and your friendship, and your support through the years. Now I'll have a bit more time enjoy life with you. I love you all.

ACKNOWLEDGEMENTS

The author would like to express his appreciation to Brunswick Mining and Smelting for providing funding and access to their facilities; to Noranda Inc. and to the National Sciences and Engineering Research Council (NSERC) for funding this research; to the New Brunswick Research and Productivity Council (RPC) for providing access to their facilities; to W. Petruk of CANMET for providing training on the KONTRON image analyser; and to INCO Ltd., for providing time to complete this work.

Thanks to Neil Rowlands and Jim Finch, my thesis advisors, for your friendship, support, and endless patience.

Thanks to Len Surges of Brunswick Mining and Smelting for your support and friendship.

Thanks to Dietrich Liechti and Peter Ryan of INCO Ltd. for encouraging me to finish writing and for providing the time and resources to get the job done.

ABSTRACT

A comprehensive analysis is carried out concerning the procedures and the problems applicable to fine-particle liberation studies employing two-dimensional image analysis, especially those employing backscattered electron imagery (BEI). It is found that BEI imagery, while presenting the most cost-effective method for automated liberation studies, is prone to errors on the data collection level. Specifications are provided for sample preparation and equipment setup, allowing errors to be minimized. A processing algorithm is developed for cleaning BEI images prior to data compilation, and statistical tests for data integrity are evaluated. It is found that the recalculated sample grade, the most commonly used test of data integrity, is inadequate and misleading. Some alternative methods of data evaluation are presented. The statistical basis of data reduction and data interpretation is reviewed. The effects of stereological bias upon two dimensional liberation data are assessed using a simple geometrical model, whereupon it is found that relatively simple translations may be made between uncorrected and corrected data. A case study of fine particle liberation and circuit assessment is presented using samples from the copper/lead separation circuit of Brunswick Mining and Smelting, Bathurst, N.B..

Un analyse compréhensif est effectué concernant les procédés ainsi que les problèmes applicables aux études de la liberation des particules fines employant l'analyse des images en deux dimensions, especiallement ceux employant l'imagerie par des électrons rebondant (BEI). Il est trouvé que l'imagerie BEI, qui constitut la méthodologie la plus economique pour les etudes de la liberation automatisées, produit des erreurs au niveau de la collection d'information. Des spécifications sont provisionées pour la preparation des échantillons et pour la choix des conditions analytiques, en permettant pour la minimisation d'erreurs. Une algorithme est dévelopée pour faire des adjustements aux images BEI avant la compilation d'information, et les méthodes statistiques sont developées pour l'evaluation de la qualité de l'information. Il est trouvé que l'analyse mineralogique recalculée, qui est utilisé fréquemment pour la verification de l'information, n'arrive pas aux bonnes conclusions. Des méthodologies alternatives sont discutées. Les effets du bias stéréologique sur l'information de la liberation en deux dimensions sont évaluées par une modèle géometrique simple. Il est trouvè que l'on peut effectuer les translations simples entre l'information brut et l'information adjusté. Une example d'une étude de la liberation des particules fines et de l'évaluation du procédé métallurgique est présentée, employant des echantillons du circuit de separation du cuivre et du plombe chez Brunswick Mining and Smelting, Bathurst, N.B..

CLAIMS TO ORIGINAL RESEARCH

Backscattered electron imaging (BEI) has been employed in two dimensional liberation studies for well over a decade. However, prior to this work there has been no comprehensive critical evaluation of the technique. It is demonstrated in this work that errors inherent both to the physics of BEI and the economic need for rapid analysis result in the inevitable collection of erroneous data, to such an extent that raw data sets are of little practical use. Moreover, it is demonstrated that the most common test for data integrity, ie. the recalculated sample grade, is inadequate and misleading. Neither of these conclusions can be reached by a survey of available literature. While conditions are specified in this work for optimal collection of BEI data it is concluded that such data cannot be used without extensive image processing.

Accordingly, an algorithm is developed for use at the data collection level which allows images to be processed in a manner which is both efficient and effective, yielding data sets which contain a superior description of the structural characteristics of the sample while effecting as few changes to the original images as possible. This is the first such algorithm to be published. The performance of the algorithm is critically assessed using an adaptation of the F-test, representing the first application of statistical methods to an assessment of the integrity (as opposed to the precision) of liberation data.

The effects of stereology upon two dimensional liberation data are assessed by means of a simple geometrical model involving spherical particles with planar boundaries. This is the first quantitative discussion of the effects of stereology upon two-dimensional size distributions and liberation data, and represents the first comprehensive solution to the two-dimensional model, the one dimensional case having been previously solved by Jones et.al.[11].

The results of the stereological model are used to provide a simple assessment of particle liberation, with provisions being given for both rigorous and approximate data analysis. This is the first model for the two-dimensional case which allows ready transformation to and from three dimensional data, with the possible exception of a computer-based sectioning simulation being developed by Lin et.al.[22]. It is certainly the first model to allow an approximate assessment to be made without the use of complex mathematical transformations.

A case study is given of liberation in the copper/lead separation circuit of Brunswick Mining and Smelting Limited, Bathurst, N.B.. Consideration is given both to the statistical limitations of the data and to stereological artifacts, allowing an accurate assessment of circuit performance to be made. This is one of the most comprehensive studies of its type, and represents an advancement in the methodology for circuit analysis using liberation data.

SUGGESTIONS FOR FURTHER RESEARCH AND DEVELOPMENT

While the principles and practice of the collection of accurate BEI-based liberation data are clearly outlined in this work, there is no easy way for such a study to be conducted. At the time that this research was conducted there was no way of transferring data directly from the image analyser to a PC-type computer. Thus, data transferral was performed by manual input. Similarly, the vast amount of data compilation and analysis was performed on a step-by-step basis using a spreadsheet program. While the procedure was semi-automated, employing several macro programs, the process still required a degree of manual manipulation which is not attractive for a commercial application. Thus, the logical progression from this work is to develop a means of performing the data analysis and verification in a more automated fashion. This task becomes easier as time progresses, since the current generation of personal computers is vastly more powerful and flexible than those which were available at the commencement of this research. The ideal case would be a program which would accept tabulated data directly from the image analyser, reduce it to a statistically significant form, then output both "raw" and stereologically adjusted liberation data with appropriate confidence intervals, along with the results of tests for the integrity of the structural data. This thesis provides the basis for performing all of these tasks to a reasonable degree of success. The practical application of this work is a development task as opposed to pure research.

The search for a valid way of transforming data from two dimensions to three is an ongoing one. The model used in this work is a simplification, which is intended simply to provide a semi-quantitative assessment of the magnitude of stereological errors which could be present in the data set. Better models will undoubtedly arise; however, a great failing of many such models is that they are more of a mathematical exercise than a practically applicable methodology. For example, it is known that liberation data sets are likely to contain erroneous data. The rigorous use of transformation matrices or transformation functions to correct from one or two dimensions to three dimensions must necessarily be accompanied by a sensitivity analysis - ie. an analysis of the extent to which the transformed data may be altered by small random alterations to the raw data set. Until a methodology is developed for transforming imperfect data sets one cannot progress far from the approximations and "rule of thumb" approaches employed in this work. Nonetheless, it is contended that even an approximate correction is better than interpretation of data with complete disregard for the systematic biases which are contained therein.

It is assumed that as technology provides us with more efficient detectors, microscope geometries and data processing capabilities less attention will have to be given to such factors as the tradeoff between image acquisition time and image processing time. However, the optimization of equipment set-up prior to data collection is relatively straightforward and could quite easily be aided by programs within the image analyser. A discussion of proposed methodologies would be beyond the scope of this work; however, it would be a reasonably straightforward task to input the names and size ranges of the minerals to be discriminated and the required data precision, and to be given the optimum conditions for accelerating voltage, spot size, sample height, image acquisition time and so forth.

TABLE OF CONTENTS

Page #

CHAPTER 1 : INTRODUCTION

CHAPTER 2 : COLLECTION OF DATA FROM THE IMAGE ANALYSER

TABLE OF CONTENTS ... Continued

Page #

CHAPTER 3 : DATA REDUCTION AND STATISTICAL ANALYSIS IN IMAGE ANALYSIS

TABLE OF CONTENTS ... Continued

Page #

CHAPTER 6 : DISCUSSION

TABLE OF ILLUSTRATIONS

Page #

CHAPTER 1 : INTRODUCTION

CHAPTER 2 : COLLECTION OF DATA FROM THE IMAGE ANALYSER

CHAPTER 3 : DATA REDUCTION AND STATISTICAL ANALYSIS IN IMAGE ANALYSIS

TABLE OF ILLUSTRATIONS ... Continued

LIST OF TABLES

CHAPTER 1 : INTRODUCTION

CHAPTER 3 : DATA REDUCTION AND STATISTICAL ANALYSIS IN IMAGE ANALYSIS

CHAPTER 4 : STEREOLOGICAL PROBLEMS IN LIBERATION STUDIES

LIST OF TABLES ... Continued

CHAPTER 5 : ANALYSIS OF COPPER CIRCUIT DATA

LIST OF TABLES ... Continued

CHAPTER 1: INTRODUCTION

1.0 : Project Description and Scope

Ore microscopy is one of the oldest tools of mineral processing, yielding information about process streams which is not available from wet chemical analysis. By direct examination of powder samples it is possible to observe mineralogy, mineral associations and the presence of or lack of mineral liberation. Thus, microscopy can be a tool for the development of flowsheets or the diagnosis of operating problems.

As a general rule, "classical" microscopic evaluations are highly qualitative in nature, relying upon subjective observations. For example, a liberation study would typically involve counting about a thousand particles, recording the minerals present in the sample and estimating their individual area grades. While this type of operation may often yield useful information, the scope of applications is limited; furthermore, the work is labor intensive, requires highly trained personnel, and tends to produce data which is not very reproducible. Many operations do not have the resources or the justification to maintain personnel and facilities for microscopic studies.

Demand for microscopic evaluation appears to be rising in response to technological challenges. Continued economic and environmental pressure has created a need for increased process efficiency. However, in operations which have existed for a decade or more the physical operating parameters (grind, pulp density, flotation retention time etc.) tend to have been optimized by the sum total of many small incremental changes over a period of time. Having reached a "practical limit of separation" using the existing processing scheme there is a call for understanding of the remaining metals losses or sources of contamination. However, this requires more precise quantitative information than conventional microscopic studies can provide, especially in cases where the streams to be analyzed contain only minor fractions of the mineral of interest.

Image analysis is currently finding applications as a high-technology alternative for manual liberation studies in the minerals industry. The image analyzer consists of an optical or electron microscope interfaced with a digitizer which converts the analog signals into a digital matrix, and a computer which interprets the digitized image. Since the image analyzer is capable of recording objective statistics from a great number of particles the technique shows promise for the production of precise, reproducible liberation data. Moreover, the use of electron microscopy as opposed to optical light microscopy allows the quantification of smaller features than could be observed under optical light.

Although there is a wide variety of image analysis equipment in use, very little of it has been adapted to perform liberation work. At the moment there are only two publicly available facilities for automated two dimensional liberation studies operated in Canada, one operated by CANMET in Ottawa and the other operated by the N.B. Research and Productivity Council (RPC) in Fredericton. Both facilities use the Kontron image analyzer, which is the first commercial image analysis equipment to have been provided with the required customized software.

Due to the scarcity of image analysis equipment capable of performing two dimensional liberation studies there has been little development work on the technique. For example, the methods for image collection and the algorithms for image processing are not widely published. Output data is typically tabulated in the form of particle area as a function of grade and size, and this is considered sufficient. However, it may be demonstrated that the results obtained from image analysis are highly dependent upon the methodology, and that there is only a tenuous link between area vs. grade/size data and the metallurgical information which is required. Moreover, data is generally released without an analysis of data precision or accuracy.

In its original conception the project focused upon the use of available techniques for the diagnosis of circuit performance and problems. However, as the work progressed it rapidly became apparent that two dimensional image analysis, the primary investigative technique, has not yet been developed into a fully effective method for the acquisition of mineral liberation data. The method contains many sources of bias and inaccuracy which have scarcely been mentioned in literature, having taken a far second place to discussion of image analysis results. Thus, it was necessary to develop the methodology for image analysis work prior to attempting circuit analysis. The focus of the project shifted away from applied circuit diagnostics towards critical examination and development of image analysis methodology.

The principal objective of this work is establish criteria for the collection of useful image analysis data. If image analysis is to expand as an analytical technique in the minerals industry then it is necessary to understand the major problems involved in collecting information. The discussion focuses largely upon potential sources of error, with statistical approximations or simple models invoked where applicable in an attempt to quantify these sources of error and to determine how to avoid them.

In order for image analysis to be useful it is necessary to simplify the analysis as much as possible. Thus, the approach taken here is not to determine the absolute best method for conducting a study; rather, it is the goal of this work to determine what one can realistically "get away with" before one is in danger of compromising the analysis. In order to make such an evaluation it is necessary to analyse and to understand all sources of error throughout the whole sequence of events, starting with sample preparation and progressing through equipment operating parameters, image processing, data compilation, stereological correction and data analysis.

A major problem in automated liberation work is verification of data integrity. It is easy to demonstrate a number of conditions under which erroneous data will be collected, sometimes yielding information which, though false, varies in a systematic manner which emulates common metallurgical behaviour. Since there is no single method for verifying that image analysis data is accurate one task of the work has been to develop tests for data integrity wherever possible.

The most widely used alternative method to microscopy is size-by-size analysis of circuit performance. This study includes a practical example of circuit analysis in which size-by-size data is collected and analysed, following which microscopic data is introduced. The real test of image analysis as a useful procedure lies in the amount of additional information which microscopy provides, over and above that which may be obtained from the much simpler and cheaper wet chemical method.

The format of the work is a step-by-step progression through the collection of image analysis data, culminating with the interpretation of a real data set and comparison with size-by-size analysis. Several digressions are made as individual problems are discussed, or as statistical tests of data integrity are introduced. Thus, the introduction of and interpretation of the data is a lengthy process. The work terminates with a recapitulation of the steps which are considered to be critical to a proper methodology.

It is recognized that there are distinct differences between the objectives of different image analysis studies. In some cases the objective may be a phenomenological study of circuit behaviour, perhaps looking at qualitative changes in the compositions of concentrates down a bank of flotation cells. In other cases a more quantitative description of circuit phenomena may be required. While both studies require the collection of accurate primary data, the collection of quantitative information requires a statistical assessment of error, and more caution in data handling. It is assumed here that quantitative data is required, resulting in a more detailed approach than may always be warranted. Again, the work focuses upon the most expedient ways to estimate error, using simplifying approximations wherever possible.

1.2 : Brunswick Mining and Smelting: Ore and Circuit Description

The practical study presented in this work involves the copper circuit at the Brunswick Mining and Smelting concentrator. The following is a description of the ore deposit and the processing flowsheet.

Brunswick Mining is located about 27 kilometers southwest of Bathurst, New Brunswick. The orebody is a stratiform deposit of massive sulfides which have been chemically precipitated and which are closely associated with metasedimentary and volcanogenic rocks. Footwall metasediments include massive to schistose argillites which may be locally silicified or chloritized. Some sericitic alteration is observed. The main ore zones consist of massive (80-90% sulfide) pyrite, sphalerite, galena, chalcopyrite and pyrrhotite. Silver is found in accessory tetrahedrite and other minor phases. The major non-sulfide phases in the massive zones are quartz, carbonates and chlorite, with minor amounts of sericite and graphite. Some of the ore zones contain layered to massive chlorite, and less commonly magnetite or siderite. Hanging wall rocks vary from massive to schistose argillite.[1]

The run of mill feed at Brunswick Mining is approximately 8.9% zinc, 3.5% lead and 0.3% copper with 99 g/t silver and 0.6 g/t Au. A typical mineralogical distribution is pyrite 58%, sphalerite 14.8% (at approximately 60% Zn), galena 4.1%, pyrrhotite 1.0% and chalcopyrite 0.9% with nonsulfides including quartz 12.0%, chlorite 7.0%, calcite 1.0% and others 1.2%.[2]

Ore is crushed on surface from 150 mm to -15 mm by two crushing lines, each consisting of an open-circuit standard crusher followed by two shorthead crushers in closed circuit with four rod decks. Grinding is accomplished in three parallel circuits, each of which employs an open circuit rod mill followed by two ball mills in series. Each of the ball mills operates in closed circuit with its own cyclopack, reducing the -0.55 mm rod mill discharge to 67% -37 µm at 50% solids. One of the grinding lines has two primary ball mills in parallel between the rod mill and secondary ball mill. The grinding circuit is illustrated in Figure 1.1.

Brunswick Mining treats a total of 10,250 mtpd. The flotation feed is aerated for 25 minutes in the presence of sodium carbonate (2.8 kg/t) and sulfur dioxide (150 g/t). The role of sulfur dioxide is to act as a catalyst to oxidation, which serves to depress pyrite. The aerated feed is floated with a mixture of 80% isopropyl xanthate, 20% amyl xanthate and Aero Promoter R241 to produce a CuPb rougher concentrate. This concentrate is reground to 92% -37 µm and fed to two-stage cleaning, producing a concentrate of 27.5% Pb, 2.4% Cu and 650 g/t Ag. The cleaner tailings are combined with the CuPb rougher tailings and routed to the zinc circuit (Figure 1.2).

The BMS zinc circuit consists of a roughing stage and three countercurrent cleaning stages. The feed is conditioned with 70 g/t/%Zn copper sulfate, lime, 80-isopropyl/20-amyl xanthate and Cyanamid S3894 dithionocarbamate. The rougher concentrate is reground to 92% -37 µm prior to cleaning. The first cleaner tailings are scavenged, with the scavenger tails and zinc rougher tails forming the plant tailings. The second cleaner tailings and cleaner scavenger concentrate are combined with the zinc rougher concentrate (Figure 1.3).

The CuPb concentrate passes to a copper flotation stage. The pulp is conditioned with activated carbon to absorb residual reagents and with wheat dextrine (starch) to depress galena. The pH is then lowered to 4.8 with sulfur dioxide prior to addition of Cyanamid S3894 dithionocarbamate. Copper flotation consists of a rougher and three cleaners. A low pulp density (in the order of 15-20% solids) is used in the rougher, increasing to 30% solids in the cleaner. The third cleaner concentrate constitutes the final copper concentrate, with all cleaner tailings recirculating back to the sulfur dioxide conditioner (Figure 1.4).

Tailings from the copper circuit are thickened, reground to 95% -37 μm then conditioned to 70°C with live steam to destroy residual starch and collector. The pulp is rediluted with cold water and conditioned to pH 10.8 with lime. Copper sulfate and xanthate are used to float sphalerite in a rougher and two cleaners, with the cleaner tailings recirculated to the conditioner (Figure 1.5). This produces a Pb-Zn bulk concentrate grading 32% Zn and 19% Pb, and a lead concentrate (rougher tailings) grading 4% Zn and 34% Pb.

An optional lead upgrading circuit can be used to produce a 36% Pb concentrate when necessary. This circuit floats pyrite out of the hot bulk concentrate feed prior to bulk conditioning. The pyrite concentrate is added to the plant tailings.

A list of reagents and their consumption is given in Table 1.1. All reagents are distributed in liquid form except for sulfur dioxide in the copper circuit, which is added as a gas. A typical plant metallurgical balance is shown in Table 1.2.

1.3 : Objectives of Circuit Analysis

The copper circuit produces a copper/silver concentrate by floating chalcopyrite and tetrahedrite while depressing galena, pyrite, sphalerite and silicates. There is a strong incentive for reducing recirculating loads in the copper circuit, since there is laboratory evidence that both the flotation rate of chalcopyrite and the selectivity of flotation deteriorate rapidly as a function of residence time in the circuit.

The copper circuit was studied by image analysis in an attempt to identify the constituents of recirculating loads, with the goal of determining the causes of both copper recirculation in the cleaner tailings and undesirable recovery of other minerals into the cleaner concentrate. This study attempts to define a quantitative path of locked and liberated particles through the circuit. The copper study uses image analysis in combination with mass balanced circuit assays to provide indications of the flotability of locked and liberated material at various points in the circuit.

TABLE 1.1

BRUNSWICK MINING AND SMELTING
MILLING REAGENT CONSUMPTION DATA

	Kg/DMT
Xanthate - Sodium Isopropyl	0.111
Xanthate - Potassium Amyl	0.033
Soda Ash	2.891
Copper Sulfate	0.935
Lime - Flotation	1.316
Lime - Pollution Control	2.215
Lime - Mine Water	1.596
Liquid Sulfur Dioxide	0.598
AERO Promoter R-241	0.021
AERO Promoter S-3894	0.004
Frother 41G	0.001
Activated Carbon	0.025
Starch	0.009
Percol 351	0.005

Brunswick L-3 Grinding Flowsheet

Figure 1.1

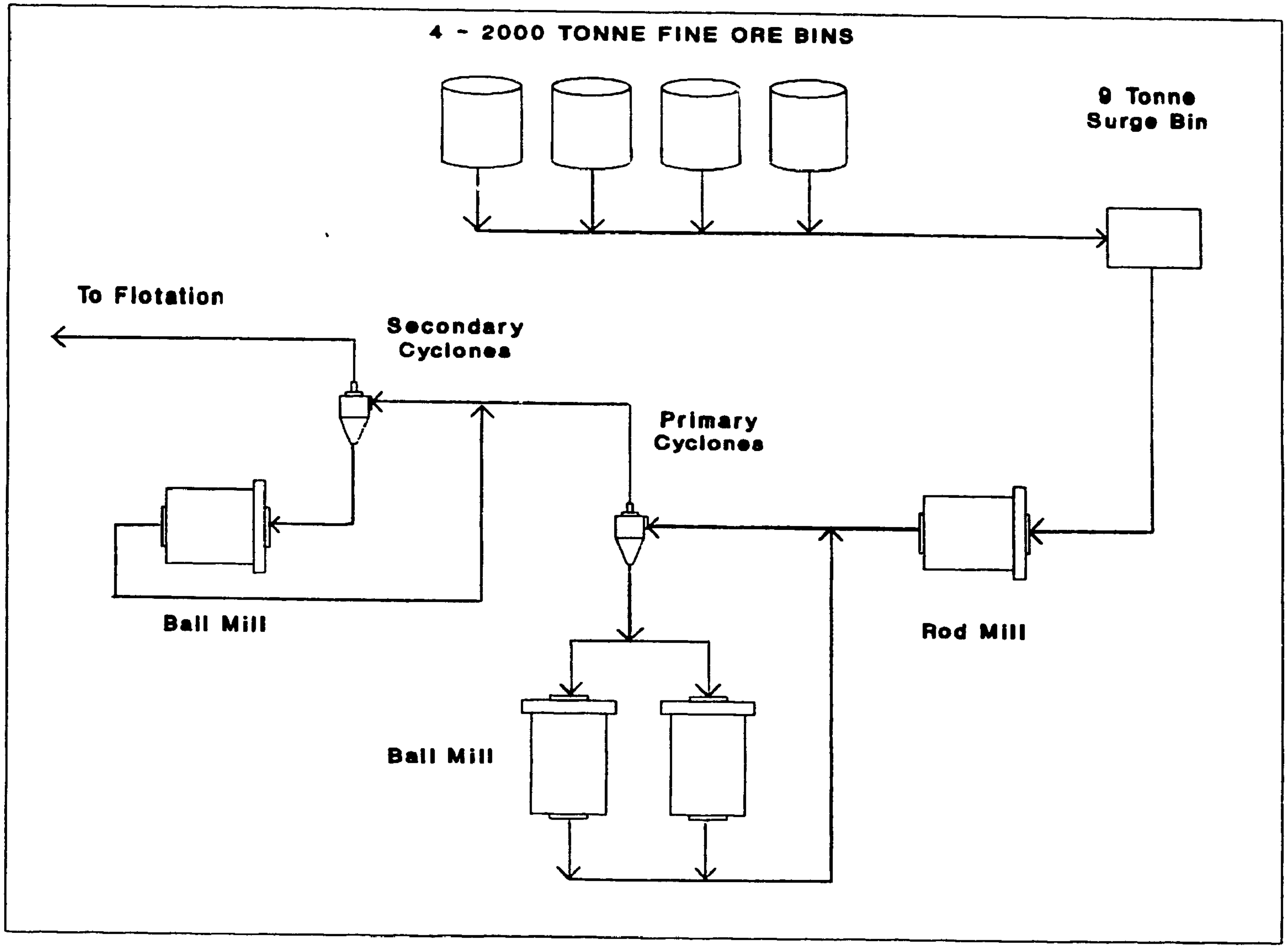

Brunswick CuPb Flotation Circuit

Figure 1.2

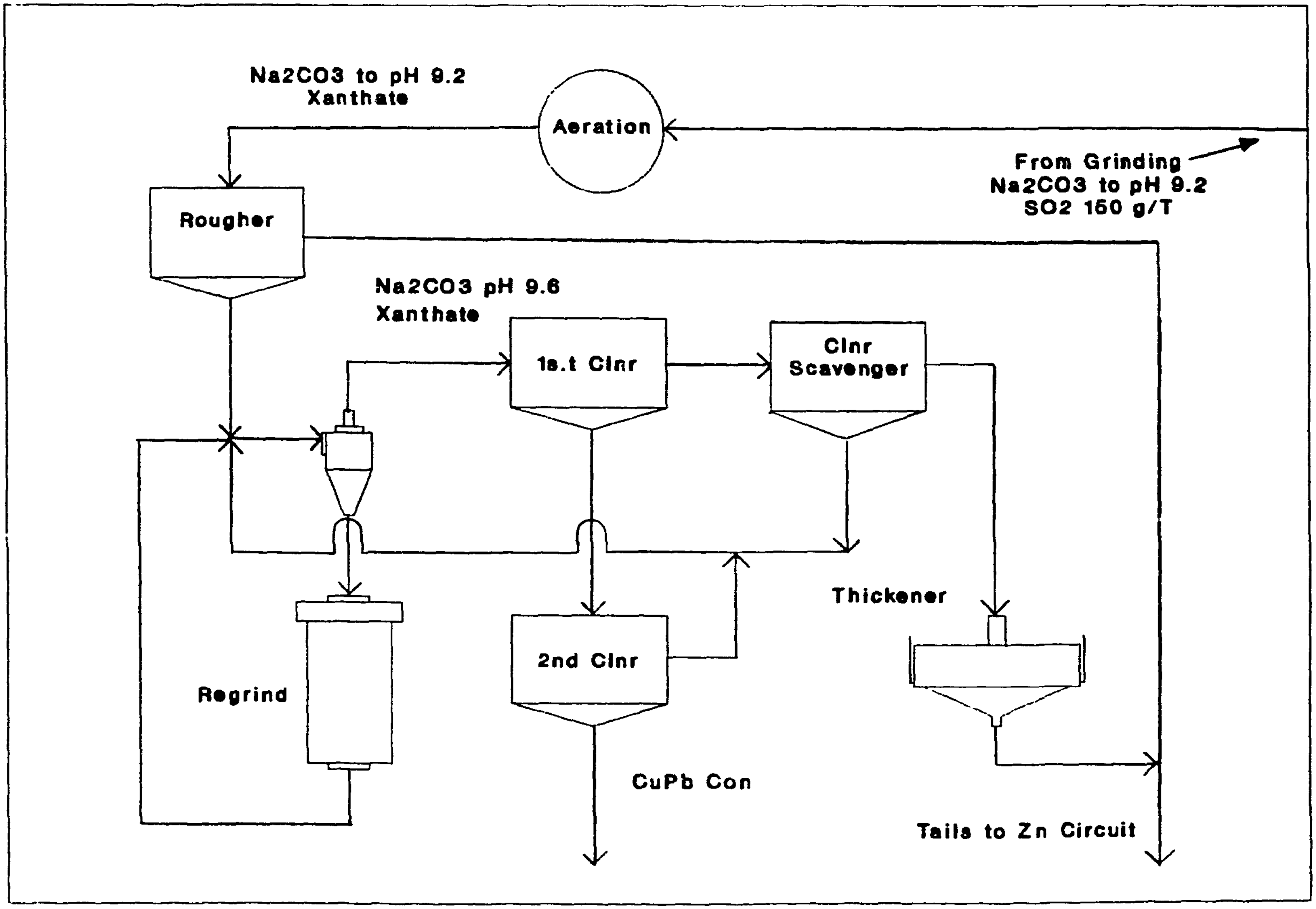

Brunswick Zinc Flotation Circuit

Figure 1.3

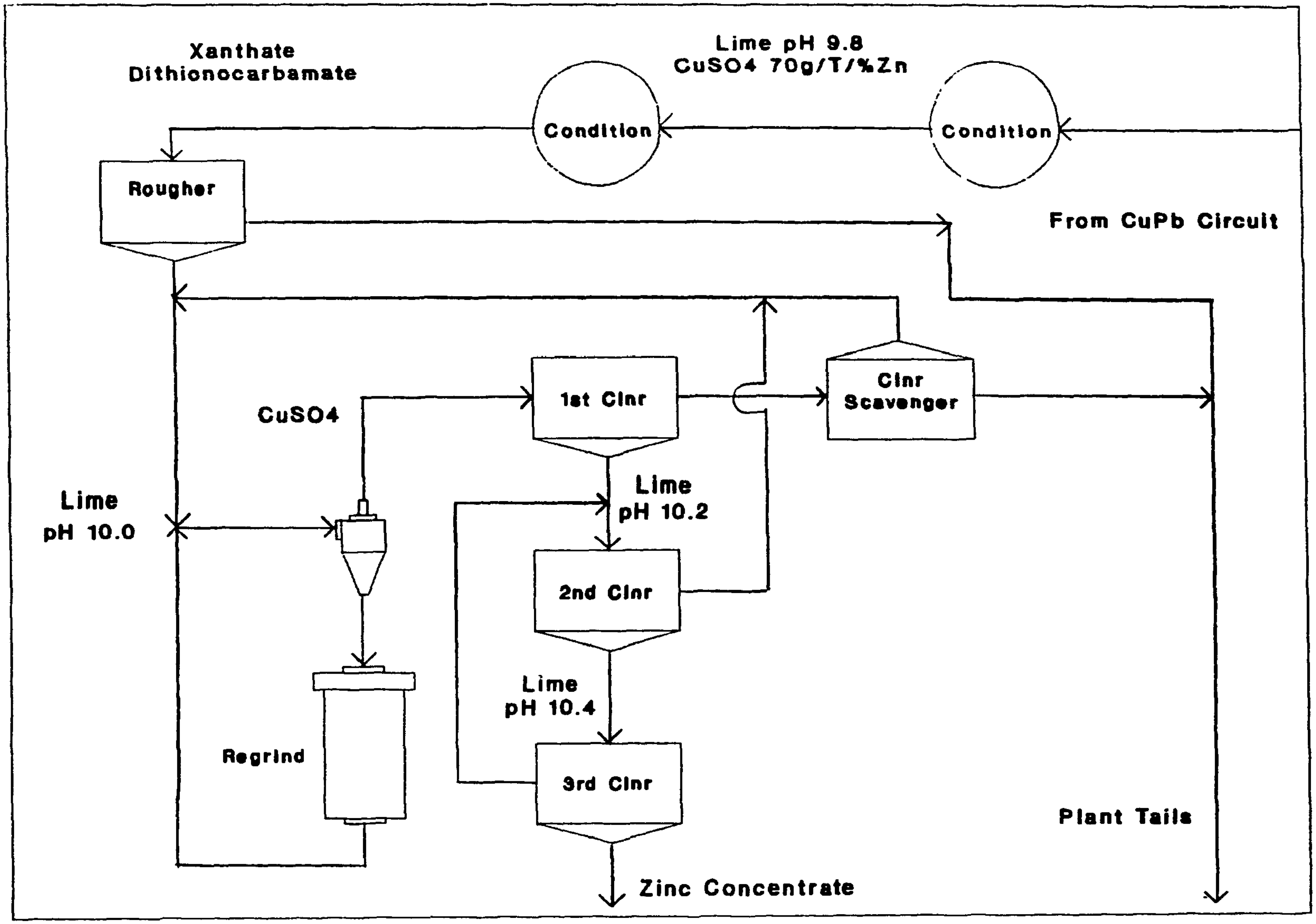

Brunswick Copper-Lead Separation Circuit

Figure 1.4

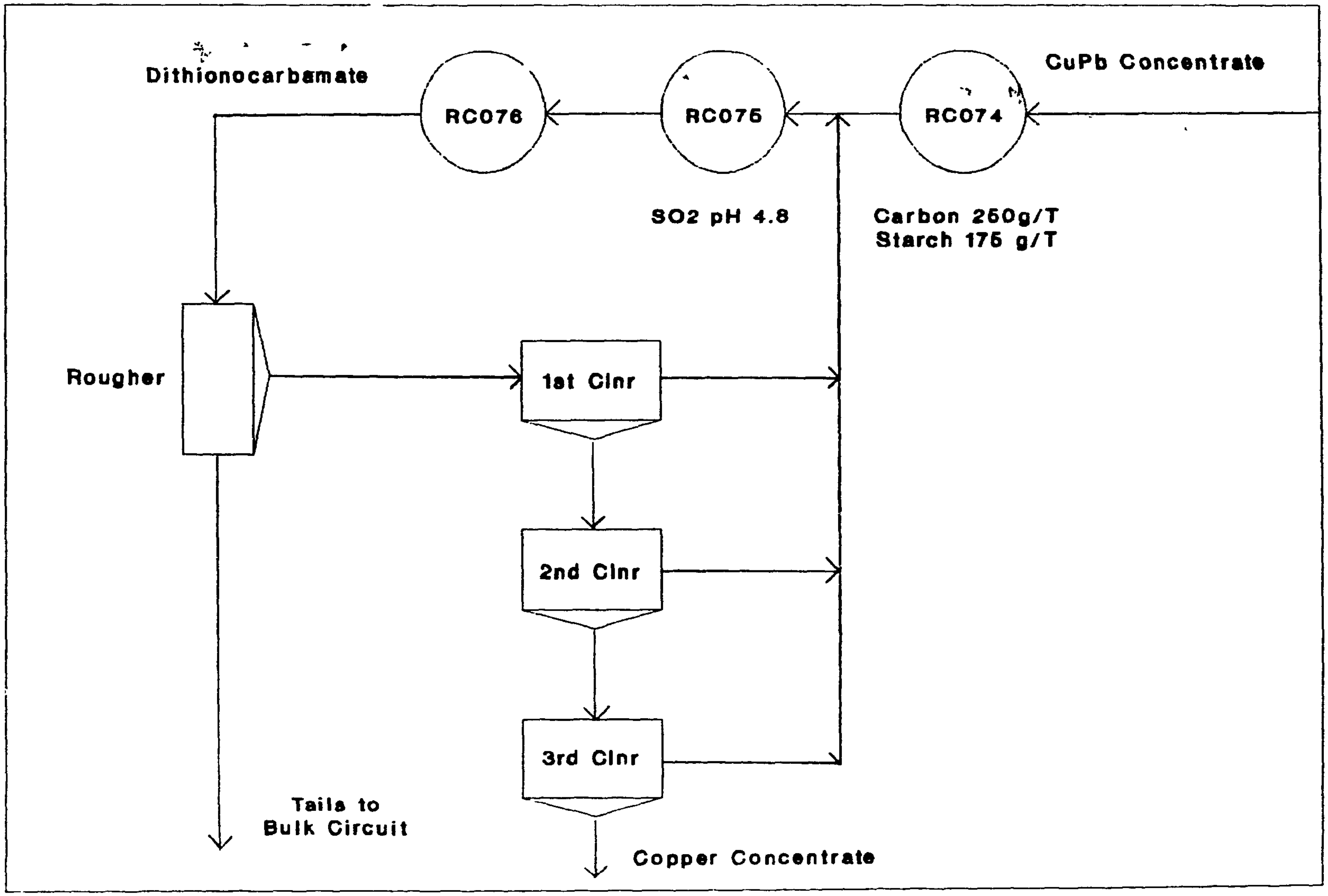

Brunswick Pb Upgrading / Bulk Circuit

Figure 1.5

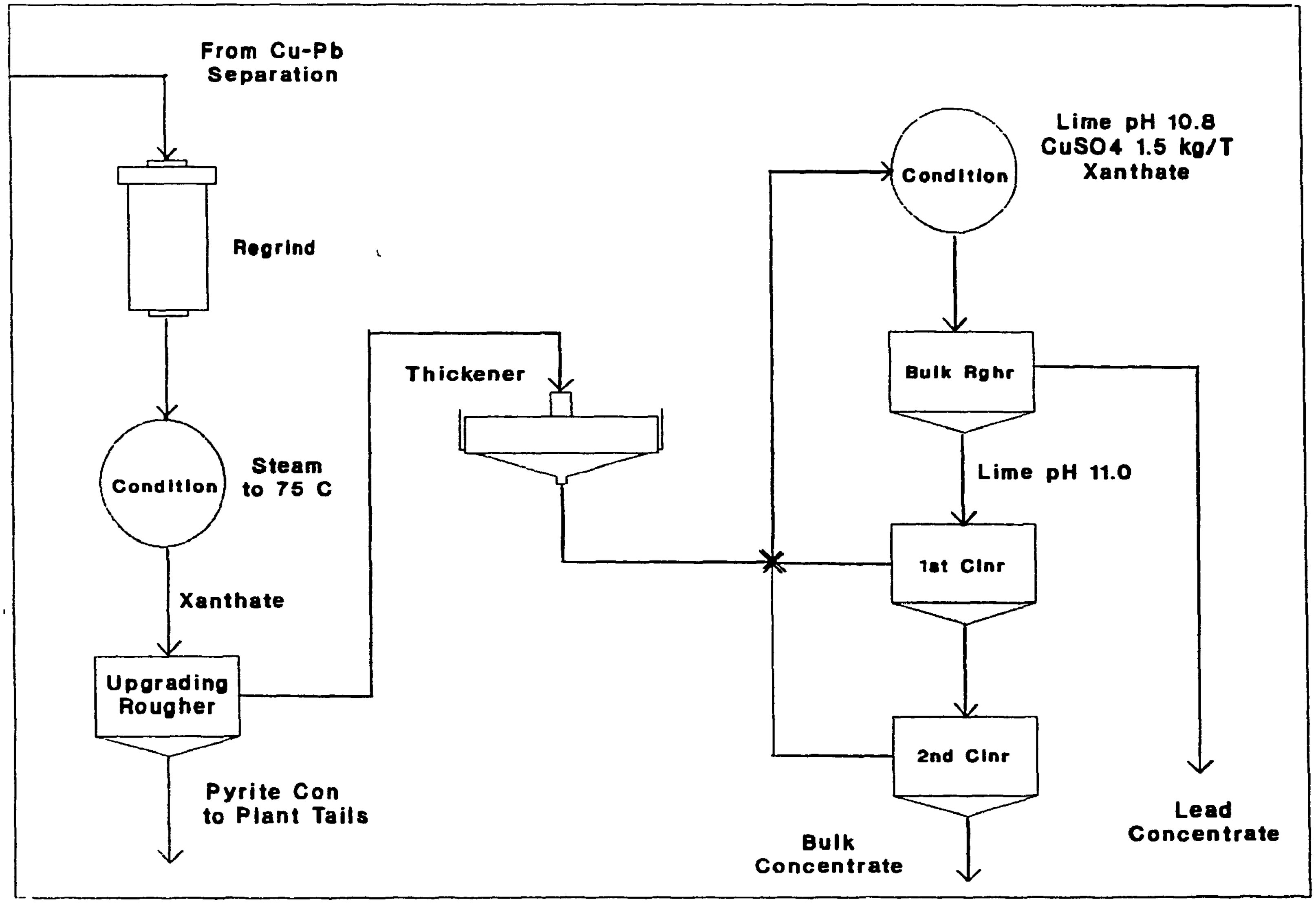

BRUNSWICK MINING AND SMELTING - PLANT METALLURGICAL BALANCE TABLE 1.2

			ASSAY, %				DISTRIBUTION		
Mill Product	Wt	Pb	Zn	Cu	Ag(gpt)	Pb	Zn	Cu	Ag
MILL FEED	100.0	3.55	8.85	0.32	99	100.0	100.0	100.0	100.0
CuPb Rghr Conc	16.3	16.70	10.50	1.50	420	76.7	19.3	76.4	69.2
CuPb Rghr Tail	83.7	0.99	8.53	0.09	36	23.3	80.7	23.6	30.8
CuPb Clnr Conc	8.9	27.50	9.50	2.58	680	68.8	9.5	71.6	61.0
CuPb Clnr Tail	7.4	3.78	11.65	0.21	109	7.9	9.8	4.8	8.2
CuPb Circ Tail	91.1	1.22	8.79	0.10	42	31.2	90.5	28.4	39.0
Zn Rghr Conc	21.5	2.00	34.00	0.30	100	12.1	82.6	20.2	21.7
Zn Rghr Tail	69.6	0.97	1.00	0.04	25	19.1	7.9	8.2	17.3
Zn Clnr Conc	13.0	1.80	51.50	0.25	90	6.6	75.9	10.2	11.9
Zn Clnr Tail	8.5	2.31	7.00	0.38	115	5.5	6.7	10.0	9.9
Zn Circ Tail	78.1	1.12	1.65	0.07	34	24.6	14.6	18.2	27.1
Cu/Pb Sep Feed	8.9	27.50	9.50	2.58	680	68.8	9.5	71.6	61.0
Cu Conc	0.9	6.00	3.00	22.00	2800	1.5	0.3	61.6	25.3
Cu/Pb Sep Tail	8.0	29.91	10.23	0.40	442	67.3	9.2	10.0	35.7
Pb Upgrd Pyrite	0.8	6.00	2.00	0.50	175	1.4	0.2	1.3	1.4
Pb Upgrd Tail	7.2	32.60	11.15	0.39	472	65.9	9.0	8.8	34.2
Bulk Conc	1.7	18.00	34.00	0.45	300	8.5	6.4	2.4	5.1
Pb Conc	5.5	37.04	4.20	0.37	525	57.4	2.6	6.4	29.2
Plant Tail	78.9	1.17	1.65	0.08	36	25.9	14.7	19.5	28.6

Payable Recoveries:
Pb = 65.9
Zn = 82.3
Cu = 61.6
Ag = 59.6

CHAPTER 2: COLLECTION OF DATA FROM THE IMAGE ANALYZER

2.0: Objectives of Liberation Studies

Size reduction in mineral processing has two objectives. The ore must be reduced to a size where the valuable mineral particles are amenable to treatment by the chosen separation method (usually less than about 150 μm for sulfide flotation) and the minerals must be liberated. Since size reduction is energy intensive most operations do not perform any more size reduction than that which is vital for mineral separation. After a certain point the incremental gains of grinding finer are offset by the need for increased capital and operating expenditure and by slower flotation kinetics. Most industrial processes seem to reach this cutoff at a point where the flotation feed still contains a fair amount of locked material.

Early studies employed some form of "liberation factor" to describe the ore. [3] Typically this represented the area fraction of a mineral of interest which appeared in a polished sample to be liberated. This method yields some measure of liberation, but fails to provide information of practical interest when the required or desired recovery lies above the degree of liberation of the ore. For example, if one is required to recover 90% of the sphalerite from an ore in which 70% of the sphalerite is liberated, the liberation factor does not reveal what the achievable grade will be. In ores where near perfect liberation is difficult to obtain (ie. most complex sulfide ores) it is found that the liberation factor is of little practical use.

One approach which has become more popular in recent years is the use of theoretical grade/recovery curves to describe liberation. Liberation data is tabulated as a grade/frequency histogram, and the theoretical separability of the ore described by constructing the best possible grade/recovery relationship. This is an inherently more useful approach; however, it is difficult to translate even this data into a useful description of practical separability. In flotation all particle compositions are selected at a finite rate, and the recovery rates for locked particles containing even a minimal amount of flotable material may be similar to the recovery rate for free material. Certainly liberation studies are useful as a descriptive method (eg. to see whether free gangue is being recovered into a concentrate). However, some type of kinetic consideration is warranted if the liberation data is to be used as a developmental tool to predict circuit performance or the impact of circuit modification.

There are several problems in the collection and interpretation of liberation data from microscopic studies. First of all, the polished sample is subject to the normal problems involving sampling and subsampling. Secondly, a large quantity of sections must be counted to assure a reasonable level of data precision. Thirdly, the observations must be made in an accurate and unbiased manner. Finally, the data obtained from two dimensional sections must be converted into a description of the phenomena present in three dimensional particles.

Needless to say, integrity of the raw data is a fundamental prerequisite for any study. In manual liberation studies the grades of sections must be estimated by the observer, leading to a loss of precision under any circumstances and to a loss of accuracy if the observer is in any way biased. Moreover, the number of sections which can be counted is limited by the slow and tedious nature of the procedure. This leads to an additional loss of data precision.

One rationale behind the promotion of automated image analysis studies over manual liberation studies is the precision with which data may be collected. Automated studies allow large particle counts to be obtained with a high degree of reproducibility; however, the high degree of precision does not necessarily imply high accuracy. Therefore, this discussion of the image analyzer as a tool for liberation work must initially embark upon a discussion of the requirements for collecting accurate primary data, including the various problems which may be encountered between sample collection and data compilation.

2.1: Choice of a Sample

Since the image analyzer is capable of recording size information as well as particle grade and frequency it is tempting to attempt to derive size vs. liberation data from a single analysis of an unsized sample. There are, however, several reasons why this should not be done. Problems are imposed by the physics of the analytical process, by the resolution of the image analyzer, and by stereological phenomena. All of these will be discussed in turn; however, it is simply stated at this point that samples for liberation work should contain no more than four or five size classes. In other words the smallest particle should have a diameter no less than about 1/4 to 1/6 of the diameter of the largest particle.

2.2: Preparation of Polished Samples

For liberation data to be meaningful it is necessary that the polished sample be an accurate representation of the stream to be examined. The acquisition of a representative sample is, in itself, a difficult task. Sampling methodology is well described in literature and it is assumed that an accepted method is used to obtain the powder sample needed for a liberation study. This discussion begins with methods for the preparation of polished samples. The basic requirements for a polished sample are that a representative portion of the powder sample appears in random orientation at the polished surface, and that the polished surface is as uniform a plane as possible.

The simplest and most common method for preparing a polished section is by mixing a powder sample with some type of resin, then polishing lower surface of the sample once the resin has hardened. Since this procedure involves some degree of settling, the sample tends to segregate. Thus, it is common to find that very dense materials are over represented at the exposed surface.

One way to bypass the segregation problem is to use a monolayer of particles on the bottom of the sample. While this avoids segregation it tends to induce preferential particle orientation. Locked particles tend to settle with the denser component oriented downward (Figure 2.1), and platy or fibrous minerals tend to rest upon cleavage planes (Figure 2.2).

A method proposed by Jackson [4] attempts to maintain random orientation of particles in the sample matrix by using an inert filler material to induce hindered settling. The powder specimen is thoroughly mixed with the filler and then impregnated with just enough resin to fill the void spaces. While some settling still occurs the viscosity of the resin combined with the large volume of filler material minimizes orientation problems. A recent variation of this method [5] includes the use of putty-type resins in which settling does not occur.

When using a hindered settling method it is essential that all gas be removed from the sample prior to final mixing. The powder sample and filler contain interstitial gas which inevitably becomes trapped in the resin when the two are mixed. Bubbles trapped at the surface interfere with polishing and bubbles rising through the resin induce settling. Thus, the sample should be subjected to a mild vacuum to remove the air then remixed (without introducing new air bubbles to the sample) prior to setting of the resin. Samples in this study employed a carbon filler and an epoxy matrix, into which powder samples

Figure 2.1

Preferential Orientation of Settled Galena/Quartz Composites

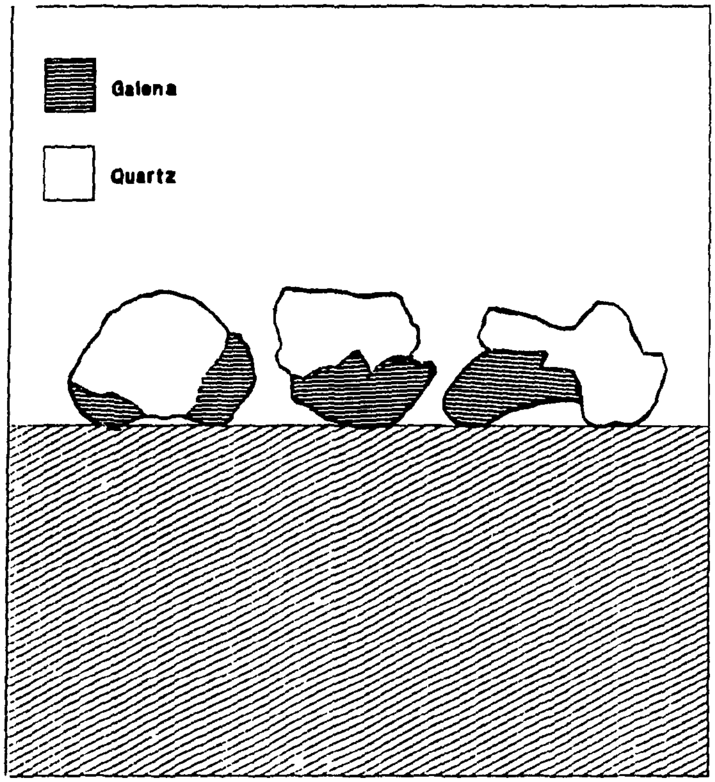

Figure 2.2

Preferential Orientation of Settled Sulfides and Amphiboles

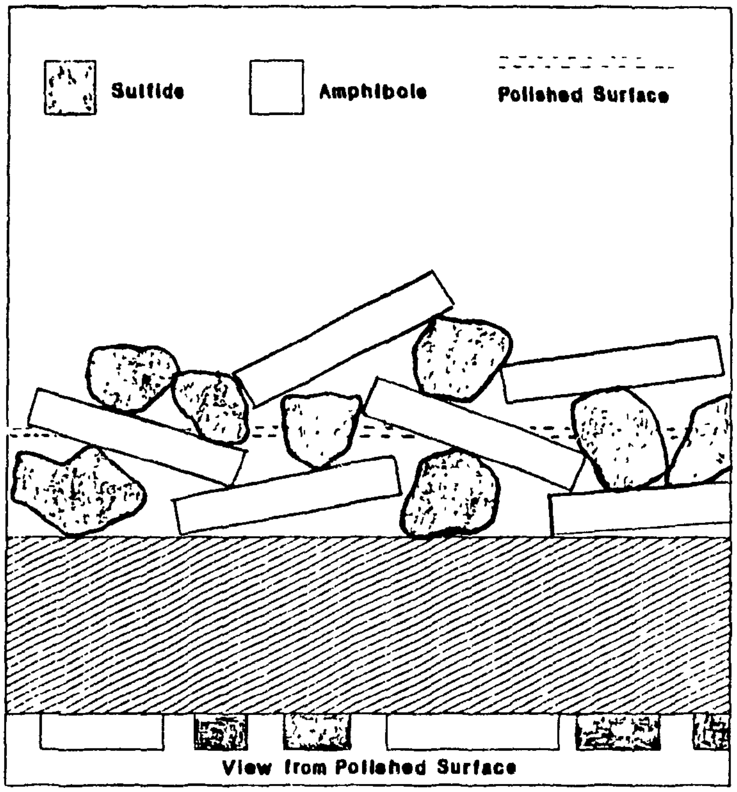

were introduced by the above method.

The use of a filler material is preferable to simply increasing the powder to resin ratio in samples. One of the major problems associated with automated image analysis studies is the distinction between locked and touching particles. Thus, the number of contact points between the individual mineral particles should be minimized. However, there is a practical limit to the amount of filler which can be used. The image analyzer requires a more or less constant amount of time per image to perform its analysis. The addition of filler material reduces the number of measured particles per image and therefore increases the analytical time. A volumetric ratio of 1:1 between filler and sample material is appropriate.

The desire to minimize contact points between individual mineral grains is one of the reasons why size-classified samples are preferable to unsized samples. The packing efficiency of mineral grains increases as the number of size classes is increased. Thus, unsized samples produce many point contacts between particles. During automated analysis there is always a problem of distinguishing point contacts from locked particles. The situation is aggravated when large particles are bordered by several small particles.

Polishing must be conducted in a correct manner to avoid the preparation of non-planar or biased samples. Grinding at too low a pressure allows the grinding medium to roll between the grinding wheel and the sample, inducing a gouging action rather than an abrasive action. This can result in deep pits which are not subsequently removed in the polishing stages. Polishing at too high a pressure may embed polishing medium in the softer minerals, leaving behind a hole when the polishing medium is eventually ripped out.

Since polishing usually employs a cloth wheel, there is a small amount of vertical flexibility of the polishing surface. Polishing at high pressure results in compression of the cloth under the sample, which allows the resin and soft minerals to be abraded at a faster rate than the hard minerals. This leads to the development of sample relief. The net effect of incorrect pressure in grinding and polishing is an over-representation of the hard species and an under-representation of the soft species at the surface, as well as the production of a surface which is non-planar.

Figure 2.3 illustrates some of the problems which may be caused by incorrect polishing. Four cases are illustrated, involving hard (black) and soft (shaded) mineral species. The differences are illustrated between the "observed" compositions of the particles, the "best interpretation" which could be made if the poorly-prepared features were properly identified, and the "actual" composition which would have been observed if the section had no relief.

Particle "A" is a composite with the hard species overlying the soft species. The hard species stands in relief, and results in the production of a non-horizontal edge to the particle. Thus, the particle will have a rim which is hard to identify. Even if the ambiguous area was to be properly identified then the particle would appear to have more of the hard phase than actually would have been exposed if the particle had been polished to the plane of the section. Particle "B" shows a composite particle oriented so that the soft mineral overlies the hard mineral. Again the hard mineral stands in relief. However, the soft mineral has been gouged below the plane of the section. The particle will appear to have a line of ambiguous composition running down the interface between the phases. Particle "C" has been plucked out, and will not be observed at all. Particle "D" has been gouged below the plane of the section, and will be hard to identify.

While pits and relief are ubiquitous features of any polished section they

Relief Effects in Polished Sections

Figure 2.3

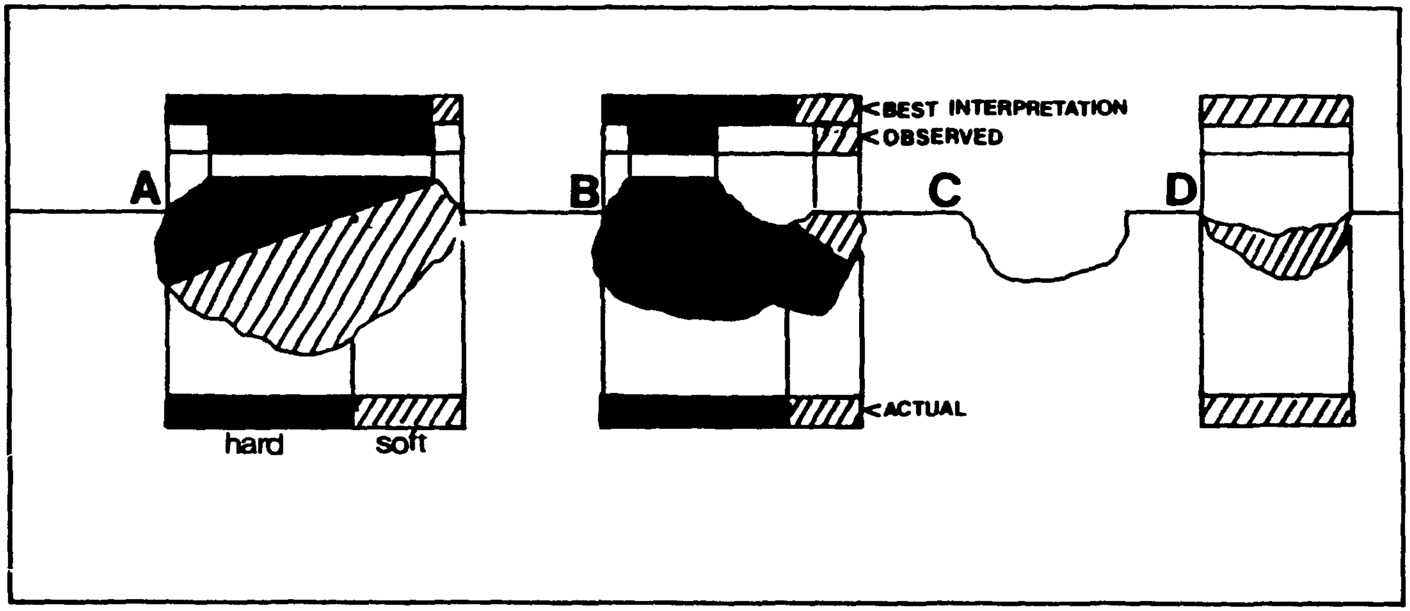

can be greatly reduced by using batch sample preparation equipment, in which the samples are held rigidly and an even pressure applied. It is also useful to chamfer the edges of the polished section to avoid binding between the polishing disk and the sample. Scratches, pits and excessive relief are all indicative of poor sample preparation and detrimentally affect analysis. In studies using backscattered electrons for imaging it is possible and even probable that poor sample preparation will lead to misidentification of particles and their structural features.

2.3: Signal Generation Using the Electron Microscope

There are several different ways in which an electron beam may interact with a sample (Figure 2.4) with the various signals being generated from different depths within the sample and different analytical volumes. Not all of these signals are useful in imaging, and even fewer are useful in liberation studies, since such work requires not only an image but also discrimination of individual mineralogical phases. Image analysis studies generally use one or a combination of secondary electron imagery (SEI), energy dispersive x-ray analysis (EDXA) and backscattered electron imagery (BEI).

The facilities used for this work were located in Fredericton at the New Brunswick Research and Productivity Council (RPC). The setup consisted of a JEOL 733 microprobe (SEM-BEI capable) interfaced to a Tracor 5500 EDXA system and a Kontron image analyzer. Thus secondary electron imagery, backscattered electron imagery and energy dispersive x-ray analysis were all available. Backscatter electron imaging (BEI) was chosen as the analytical method, since it is the fastest method for obtaining an image which has both acceptable resolution and compositional information. The three principal types of analysis are summarized below.

Figure 2.4

Signals Produced by an Incident Electron Beam

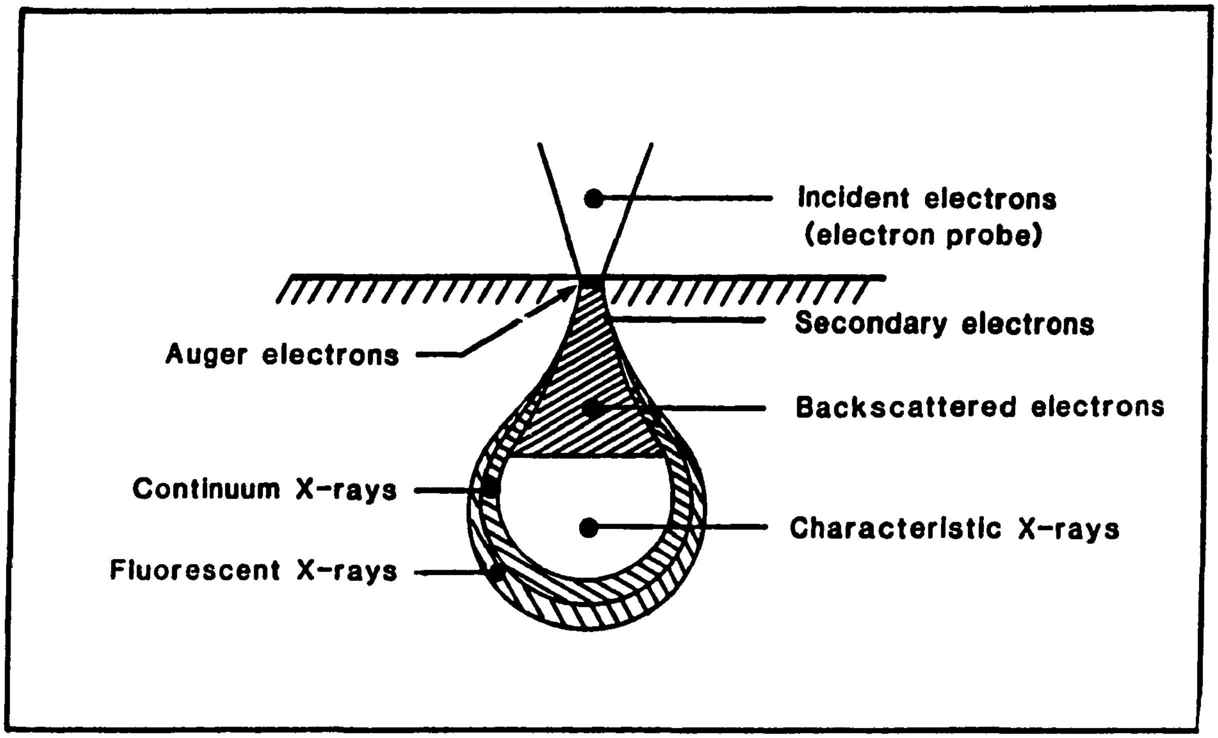

from Rowlands[6], Figure 2

2.3.1: Secondary Electron Imaging (SEI)

Some of the incident electrons interact by knocking low-energy electrons from atoms in the sample. These are referred to as secondary electrons, which have a low energy and which therefore do not move far within the sample before being recaptured. The normal depth from which secondary electrons are emitted is less than 0.05 µm [7]. The small sample volume allows the production of images with exceptionally high resolution; however, the signal shows only a minor change in intensity as a function of target composition. Thus, the method is not determinative and by itself is not used for liberation studies. Nonetheless the images are very useful for examining the quality of a polished section (looking for scratches, gouges, relief, etc.) and for determining the precise locations of grain boundaries.

2.3.2: Energy Dispersive X-ray Analysis (EDXA)

A high energy incident electron may under some circumstances interact with an atom in a sample by knocking a high energy inner-shell electron out of its orbital. The unstable configuration thus formed rapidly decays as an outer shell electron jumps to fill the vacant orbital space. The energy associated with the transition is one of a number of quanta which are characteristic of the atom involved. The quanta used for phase discrimination are in the x-ray wavelengths, which usually correspond to the transition of an electron from the K,L or M bands to the S band. Thus, the emissions are referred to as characteristic x-rays. A single atom will show a variety of peaks corresponding to different target orbitals being filled from different sources.

Most equipment is capable of detecting elements of atomic number 11 (sodium) or higher. The type of detector most commonly used for liberation work is a lithium drifted silicon crystal which converts incoming x-ray photons into a discrete number of free electrons. The electrons are collected by an applied bias into an integrator, which in turn gives a signal to a multichannel analyzer. The multichannel analyzer divides the x-ray spectrum into discrete energy ranges and keeps a record of the number of counts within each range. Thus, all elements can be counted simultaneously. This configuration is known as energy dispersive, and the method referred to as energy dispersive x-ray analysis (EDXA).

Characteristic x-ray emissions are generated within a large subsurface volume. Since the incident electrons must have an energy in excess of the energy required to generate the characteristic x-ray, the lower limit of accelerating voltage is about 25 KeV for transition elements. This results in deep beam penetration, with the signal typically emanating from a depth of 0.5-5.0 µm. Thus, images formed by EDXA have relatively low resolution. However, the method offers an advantage in that the wavelength of the emission is used for phase identification rather than the intensity of the emission. This makes EDXA relatively insensitive to surface irregularities. SEI is commonly used to form a high-resolution image of particle occurrences which is then overlaid with an EDXA image for compositional determination.

A major drawback in the use of characteristic x-rays is the large amount of time required to build an image. This is due in part to inelastic collisions between incident electrons and atoms in the specimen, in which the incident electron rapidly decelerates and releases part of its energy as x-ray radiation. Such x-rays form a continuum which is superimposed upon the x-ray peaks formed by characteristic emissions. Long count times are required in order to achieve an acceptable ratio of signal to noise. For example, in this study it would have taken seven minutes per frame (12 hours per sample) just to collect the primary images.

EDXA analysis is useful in cases where no other analytical methods are capable of making a reliable distinction between mineral phases; however, as a result of the low resolution and high image acquisition time this method of analysis is not preferred for liberation studies.

2.3.3: Backscattered Electrons:

Incident electrons colliding with atomic nuclei may rebound elastically as backscattered electrons. As a result of the relatively high energy of the incident electrons backscattered electrons may be scattered several times before exiting the sample and may therefore emanate from a relatively large sample area (typically from a depth of 0.1-1.0 µm). As a result of this the images formed by backscattered electron imagery (BEI) have lower resolution than those formed by SEI, although the resolution considerably exceeds that of optical microscopy.

The usefulness of BEI for phase determination results from a relationship between the atomic density of a sample and the number of electrons which will be backscattered. Minerals with high mean atomic densities scatter many electrons and therefore produce bright images compared to those of less dense minerals. Most sulfide minerals have a sufficiently unique mean atomic density to be differentiated, given sufficient analytical time. Typically a backscatter image useful for distinguishing sulfides may be obtained in 1-3 minutes, depending upon the density difference between the individual minerals.

One disadvantage in the use of BEI is the fact that signal intensity is not exclusively a function of density. Whereas the SEI detector uses an applied bias to attract electrons from quite a wide range of trajectories, the BEI detector collects electrons from a single trajectory. The net effect is that the sample appears as if it is under point illumination. Thus, the image will have bright and dark regions corresponding to different surface topography. The observed brightness is a function both of the sample density and its orientation with respect to and distance from the detector.

The presence of pits, cracks and relief have an obvious detrimental effect upon phase discrimination. Particles standing in relief will appear to have bright and dark edges, both of which may be identified as phases distinct from the bulk of the particle. Even minor irregularities on the surface will result in slight changes in signal intensity, sufficient to lead to ambiguous identification when sensitive phase discriminations are attempted.

Other difficulties associated with BEI are averaging and subsurface effects. Figure 2.5 illustrates a sample consisting of two particles. One is a composite of dense (dark) and less dense (light) minerals, while the other is a subsurface occurrence of the dense phase. As an electron beam traverses from left to right it will encounter the dense phase. While the actual atomic boundary between the mineral and the resin may be sharp, the emission intensity shows only a gradual increase. This is a result of the fact that the emissions originate from a finite subsurface volume, and do not reach a maximum until the complete analytical volume lies within the mineral phase. Similarly, as the beam traverses towards the less dense phase the emissions will gradually fall to a lower plateau, and then gradually fall to the baseline emission intensity for the mounting medium as the beam leaves the particle. Of course, if a third mineral has an emission level (backscatter "brightness") somewhere between that of the dense and the less dense mineral, than an image analyser will interpret the backscatter intensity profile as indicating a thin band of this third phase residing between the other two. Similarly, it may appear that a fourth phase exists at the particle boundary, forming a rim. This is referred to as the "edge effect", or "halo effect", and makes it difficult to conclusively

Figure 2.5

Backscatter Emissions
from Subsurface Particle

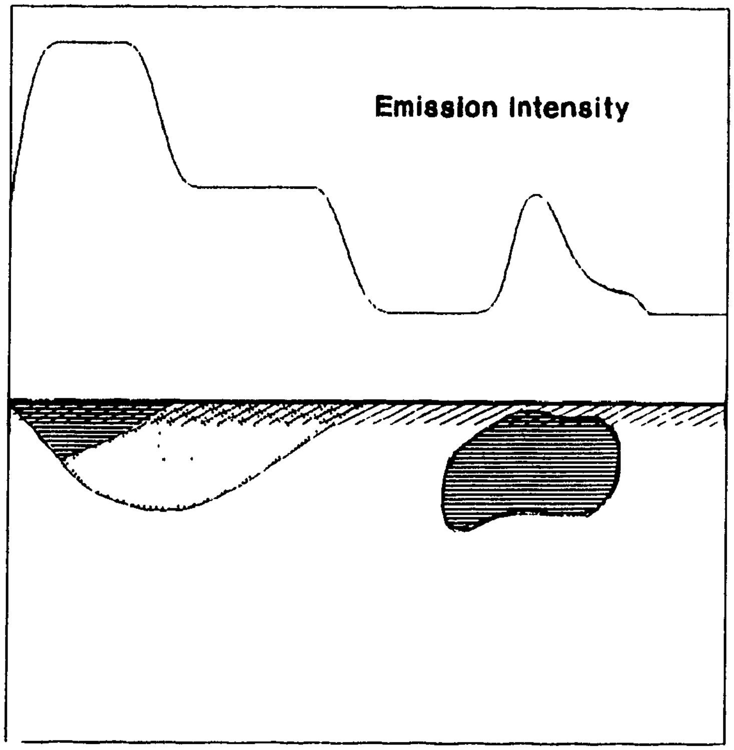

assign the locations and compositions of phase boundaries.

Continuing the traverse from left to right, the electron beam encounters a subsurface particle. Since the resin has very low density the electron beam penetrates quite deeply, encountering the particle. However, this particle has considerable surface topography and lies farther from the detector than particles at the surface. Furthermore, any backscattered electrons emitted from the particle will be slightly attenuated by the resin. As a result of these factors the backscatter intensity will vary across the sample, and will not achieve the brightness of a similar particle at the surface. Nonetheless, if dense phases lie close to the surface the intensity of their emissions may emulate the emission intensity of a less dense phase, leading to erroneous interpretation.

Since brightness is the determinative variable for phase identification in BEI it is essential that samples have low relief and as few surface defects as possible. Even so, all BEI images will contain a proportion of area which will ultimately be misidentified. Thus, it is necessary to process images in an attempt to eliminate artifacts of the data collection process.

2.4: Choice of Conditions for Backscatter Imaging

Given a sample which has been prepared as carefully as possible, the ability to distinguish phases of similar density is largely a function of signal acquisition time. In order to maximize the number of particles which can be economically measured by image analysis there is great pressure to reduce the analytical time to a minimum. One of the major determining factors for image acquisition time is the relationship between acquisition time and image contrast. This relationship is described by Poisson sampling statistics, since the backscatter detector records random emissions as a function of time. For example, if a mineral producing N counts per time period T is to be distinguished from a mineral producing (1.1)N counts per T then the 99% confidence interval for the number of counts expected from the first mineral is equal to N +/- $3*N^{1/2}$. Likewise, the 99% confidence interval for the second mineral is equal to (1.1)N counts per second +/- $3*(1.1\ N)^{1/2}$. To limit the brightness overlap to 0.5% of the sample area, $N+3N^{1/2} = (1.1N)-3(1.1N)^{1/2}$, or N must equal 3778 counts per time T. In other words the analytical time T must be chosen such that at least 3778 counts are obtained.

The required analytical time is obviously a function of the relative brightnesses of the two phases. If the second phase had a brightness of 2N, it is easy to calculate that the required value of N would equal only 53 counts, or about 1.5% of the analytical time required for the previously described case. It can be concluded, therefore, that under constant operating conditions there is a minimum theoretical data acquisition time which will allow two phases to be distinguished with a given degree of accuracy. As a general rule the analytical time is chosen such that the two phases with the most similar brightness level show about a 2% to 3% overlap, which can be effectively eliminated by image processing. Increasing image collection time past this point is usually counterproductive. In theory the analytical time would have to be increased by a factor of 2.25 to reduce the overlap from 2.5% to 0.5%, leaving much less time for image processing.

The number of backscattered electrons captured by the detector per unit time is highly dependent upon the experimental conditions. Thus, analytical time may be reduced by choosing conditions such that the rate of backscatter emissions is increased, or such that more of the emitted backscatter electrons reach the detector. The three primary variables are beam current, accelerating voltage and sample height.

Beam current is a direct measure of the number of electrons striking the sample per unit time (measured in coulombs per second). The greater the beam current the greater the number of electrons which will be backscattered. Since there is a finite rate at which energy can be dissipated from the sample there is a maximum beam current density which can be tolerated before the surface of the sample is actually vaporized. Current density can be reduced by increasing the width of the electron beam; however, this increases the analytical volume with a consequent reduction of resolution. The beam current is typically set between 10-20 nA.

Caution must be exercised in the collection of data over a long period of time, since the beam current has a tendency to drift. This is especially apparent when the line current varies or when the vacuum has been broken by changing the sample. Any change in the beam current will result in a change in the intensity of backscatter emissions, and will therefore lead to misidentification of minerals. It is advisable to check the beam current periodically using a Faraday cup. In this work a beam current of 15 nA was used, and it was found that a drift of +/- 0.1 nA could be tolerated without compromising the analysis.

A second way to increase the backscatter emissions is to bombard the sample with higher energy electrons. This can be accomplished by raising the accelerating voltage. Higher energy electrons have a greater depth of penetration and therefore a higher analytical volume. However, this decreases resolution. Typical accelerating voltages are 10-25 kV, with this study employing 10 kV.

Thirdly, the proportion of backscattered electrons which are recorded can be increased by moving the sample closer to the detector. As seen in Figure 2.6, the detector will record electrons encountered within some solid angle "A".

Figure 2.6

Effect of Sample Height upon Backscatter Signal

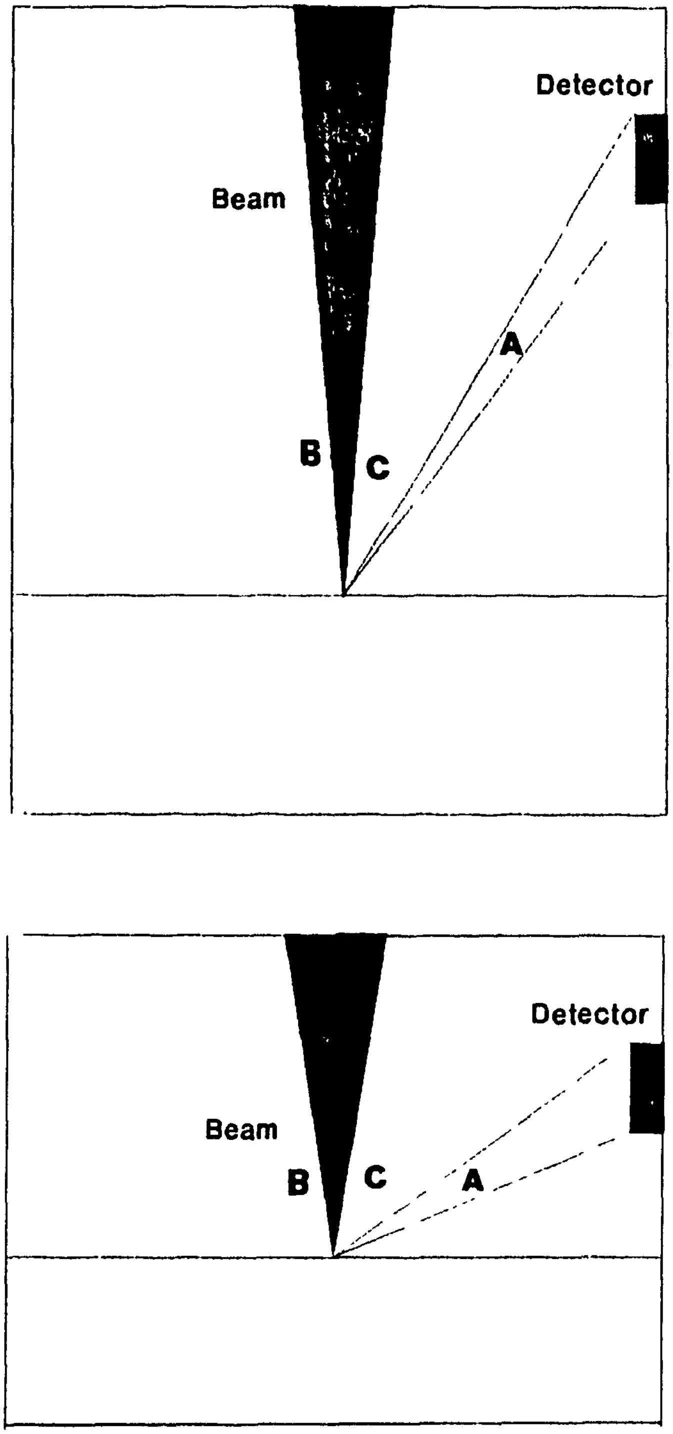

As the sample height is increased so will the value of "A", leading to a larger count rate. However, two detrimental effects are seen. The angle of convergence "B" of the incident electron beam will enlarge, leading to a lower depth of field. This is of relatively small importance for planar samples. The angle between the incident beam and the detector (angle C) will also widen, making it appear on the backscatter image as if the sample was illuminated from a more oblique light source. This increases the sensitivity of the analysis to relief and surface defects.

It is found, therefore, that a compromise must be made between analytical time, contrast and resolution. The best compromise depends largely upon the size of features within the sample. For example, if one requires quantitative liberation data from a sample in which the minor phase occurs as 2 µm or 3 µm wide dendrites then the boundary halos must be restricted to a fraction of a micrometer. A one micrometer halo on a two micrometer particle would obviously preclude quantitative data collection. To reduce the halo effect the accelerating voltage has to be reduced, at the expense of analytical time. The optimum conditions for examining very fine features or very fine particles are therefore not the same as for coarse particles. This is another reason for the sizing of samples prior to the collection of liberation data.

2.5: Creation of an Image

When an incident electron beam is directed against a spot upon the mineral surface the emission intensity may be measured at the target point. However, for liberation studies it is necessary to obtain photograph-type images. This is accomplished by moving the electron beam in synchronous motion with a cathode tube raster. In BEI or SEI the current across the detector is used to modulate the brightness of the cathode tube image, yielding a two dimensional representation of the sample. In EDXA the multichannel analyzer will send a pulse to the cathode tube every time an x-ray photon between selected energy limits is detected. This produces a dot-density map, which must be superimposed upon an SEI or BEI image in order to do liberation work.

The on-line image formed by such a method is not suitable for liberation work, since the cathode tube image is updated 30 times per second, resulting in an analytical time of only 0.033 seconds per image. The most satisfactory way to obtain a good image is to take a photograph of the cathode tube while the electron beam is very slowly rastered across the sample. A suitable photograph of BEI intensity can usually be obtained in about 60-120 seconds.

While liberation studies can be performed using photomicrographs in which features are counted manually, such a procedure is costly and time consuming. The method has never gained great popularity, having been largely replaced by digitization of the images and quantification of features by means of image analysis. However, the photographic method offers the advantage that the raw data is visible and available for textural interpretation in a way that tabulated image analysis data is not.

2.6: Examining the Quality of BEI Images

The usefulness of BEI images for liberation work is adversely affected by the fact that backscattered electron intensity, which is used as the determinative parameter, responds not only to composition but also to surface defects and phase boundaries. Before proceeding to a discussion of image digitization and interpretation it is useful to view photomicrographs of some BEI images to see the type and magnitude of problems which must be handled.

Figures 2.7 and 2.8 show photomicrographs at 350x magnification of a Brunswick Mining and Smelting (BMS) sample which consists primarily of silicates (Si, very dark gray), pyrite (Px, medium gray), chalcopyrite (Cp, medium gray), sphalerite (Sp, light gray) and galena (Gn, white) in a matrix of resin (black). The phases are identified in Figures 2.7B and 2.8B.

One problem in the identification of phases is the wide difference between the backscatter intensity of galena (the brightest mineral) and silicates (the darkest). In order to collect an image in which silicates are visible the brightness has to be increased. However, in order to keep galena from going off scale at this brightness the contrast must be reduced. This makes it impossible to differentiate minerals of similar contrast (eg. Cp vs. Px). Figure 2.7 employs a high brightness and a low contrast in order to allow silicates to be seen. However, under these conditions Cp and Px are indistinguishable. In Figure 2.8 the brightness is reduced and the contrast is increased. Under these conditions Cp can be distinguished from Px, but silicates are invisible. Figure 2.9 shows a better example of a pyrite/ chalcopyrite composite particle, presented at 500x magnification. Figures 2.7, 2.8 and 2.9 all employed identical microscope settings (ie. identical signals from the backscatter detector) but different CRT brightnesses and contrasts.

Upon close examination of Figure 2.9 it is seen that the individual minerals do not show uniform backscattered electron intensity; rather, they tend to contain patchy areas which may represent local variations in surface planarity or mineral composition, changes in crystallographic orientation or the presence of another species close to the plane of the polished section. Thus, in minerals such as pyrite and chalcopyrite which have similar gray levels there is some overlap in the observed backscattered electron intensity. Most of the grains visible in the photomicrographs also contain a number of dark areas which correspond for the most part to interfaces between individual mineral crystals.

A small locked particle is presented in Figure 2.10 at 3500x magnification.

The section has a long dimension of about 10 µm and is composed of galena and sphalerite. Diffuse boundaries are seen between both galena/sphalerite and mineral/resin. Figure 2.10B shows the actual section size and grain boundary locations reproduced from SEI imagery. Superimposed upon Figure 2.10B is the outline of the BEI image (shaded), showing that the halo effect causes an apparent increase in particle size. It will also be noticed that the apparent abundance of galena within the particle is increased, since halos extend not only into the resin but also into the area occupied by sphalerite. Halo width is independent of magnification, so that the effect has an equal magnitude in Figures 2.7 to 2.10; however, it is not until higher magnifications are employed that the halos are readily distinguished.

The magnitude of the halo effect is in part a function of the relative difference in gray level between the two interfacing phases. Thus, pyrite (the darkest sulfide) produces the smallest halos at particle boundaries while galena, the brightest mineral, produces the largest halos. Galena also tends to have a smaller size distribution than other sulfides in the BMS ore, giving it a larger interfacial area per unit of volume and therefore a greater opportunity to form halos. This results in a compositional bias which may elevate the apparent abundance of galena by a considerable amount.

In Figure 2.7 a small composite grain of galena, sphalerite and pyrite can be seen near the upper left hand corner of the figure. This grain is magnified to 1500x in Figure 2.11. The diffuse phase boundaries reveal the presence of a halo effect. When the accelerating voltage is lowered from 15 keV to 5 keV (Figure 2.12) the apparent size of the grain and the proportion of the area which is occupied by galena both decrease. Conversely, when the accelerating voltage is increased from 15 keV to 25 keV (Figure 2.13) the apparent size of the grain and the apparent proportion of galena both increase. The effect is seen most readily on the upper right hand side of the figures, in which subsurface material becomes involved in the production of halos.

The most accurate of the three images is Figure 2.12, produced at the lower accelerating voltage. However, this image required 180 seconds to acquire as opposed to 60 seconds for the images in Figures 2.11 and 2.13. Even at the higher acquisition time the contrast of Figure 2.12 is considerably less than that of the other two images. Thus, it is found that there is a practical limit requiring that the accelerating voltage be maintained at about 10-15 keV. Requirements may vary as a function of microscope geometry, spot size and sensitivity of the backscatter detector. For example, the photomicrographs presented here were obtained from a JEOL T-300 SEM at McGill University, and required a 15 kV accelerating voltage. The image analysis work conducted on the JEOL 733 microprobe at RPC could be carried out at 10 kV. Regardless of the differences between equipment it may be assumed that the practical limits for image acquisition time result in the collection of images which contain significant halo effects, or which in the case of Brunswick ores results in an overestimation of the abundance of galena.

In brief, one can say the following about the primary images obtained from BEI and the tasks which must be performed in image analysis:

1) The individual mineral species do not show uniform gray levels. Rather, they show a range of gray levels with effects caused by surface features, phase interfaces, grain boundaries and a variety of other factors. The image analyzer must recognize the locations of the various minerals and ignore the presence of pits, cracks, relief, and variations of gray level within mineral phases.
2) Interfaces between phases show halos which extend from bright phases into darker phases. The halo effect results in an overestimation of the abundance of bright minerals, which can be reduced in severity but not eliminated by lowering the accelerating voltage in the SEM to the lowest value which produces an acceptable image. The image analyzer must attempt to sharpen the boundaries by removing halos between mineral phases and at section edges.

FIGURE 2.7 A

BRUNSWICK ORE - 350 X, 15 kV

FIGURE 2.7 B

IDENTIFICATION OF MINERALS

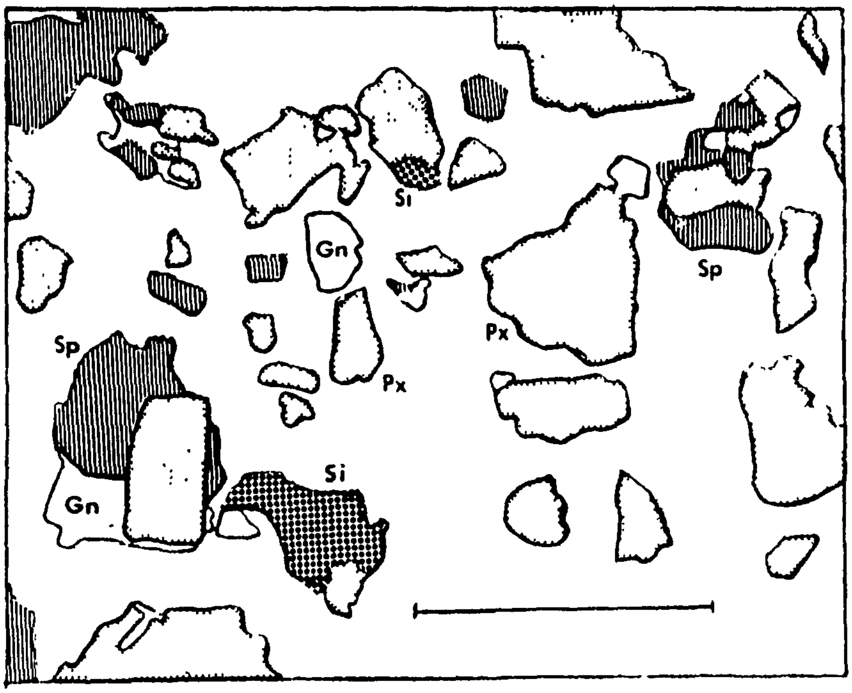

FIGURE 2.8 A

BRUNSWICK ORE - 350 X, 15 kV

FIGURE 2.8 B

IDENTIFICATION OF MINERALS

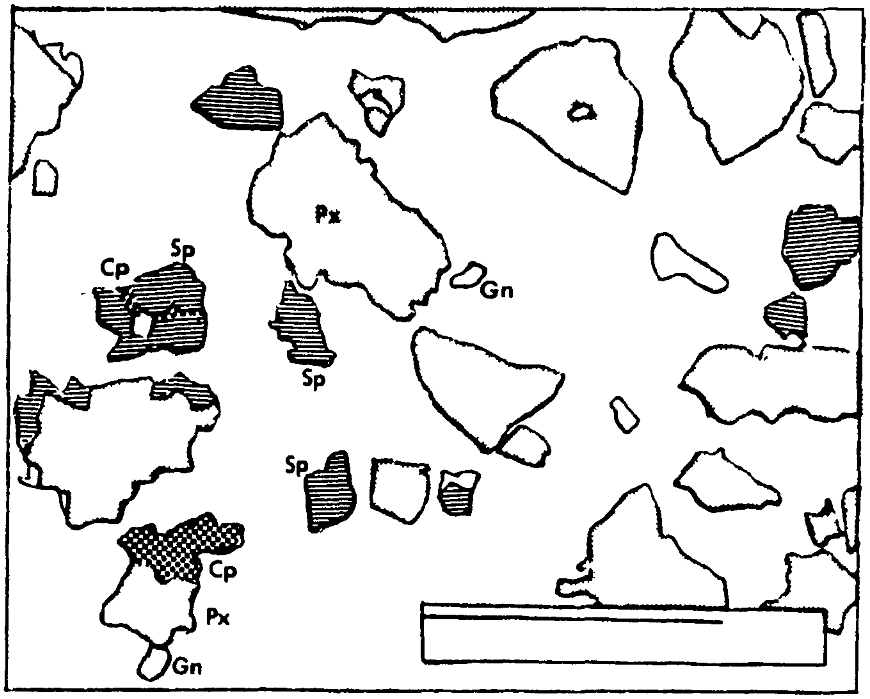

FIGURE 2.9 A

IRREGULAR SURFACE BRIGHTNESSES - 500 X, 15 kV

FIGURE 2.9 B

IDENTIFICATION OF MINERALS

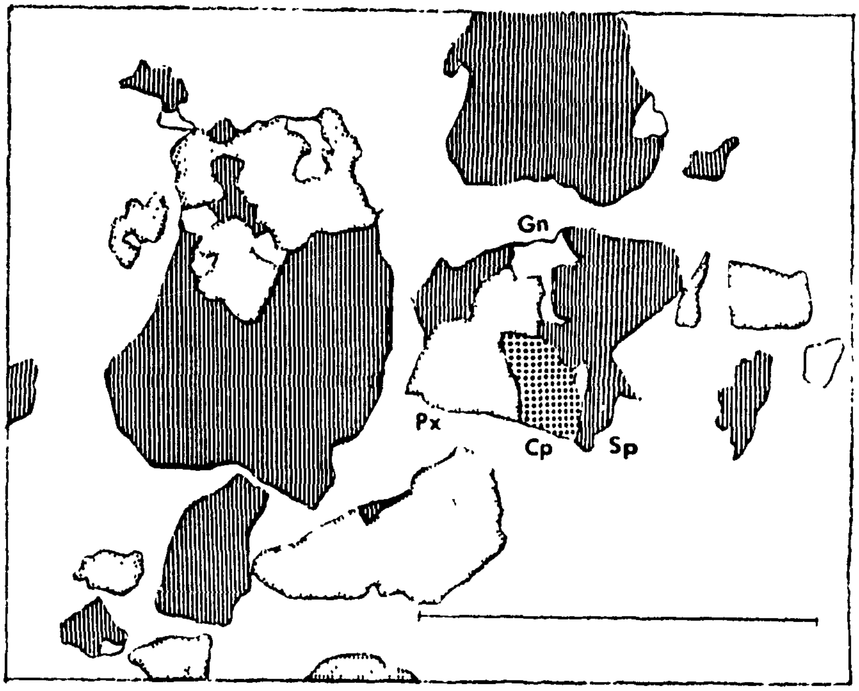

FIGURE 2.10 A

COMPOSITE PARTICLE - 3500 X, 15 kV

FIGURE 2.10 B

GRAIN BOUNDARIES (FROM SEI)

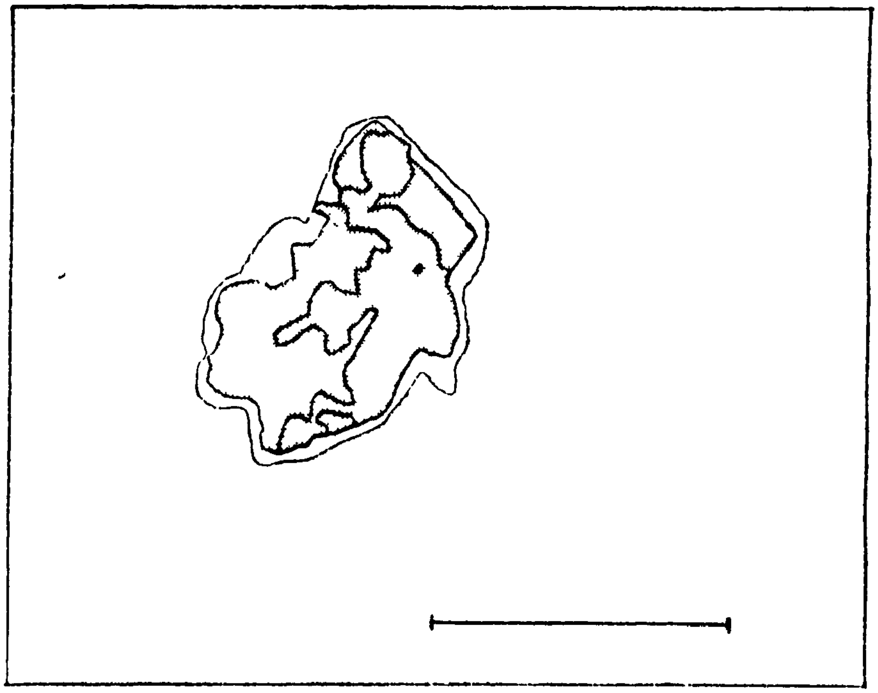

FIGURE 2.11 A

COMPOSITE PARTICLE - 1500 X, 15 kV

FIGURE 2.11 B

APPARENT GRAIN BOUNDARIES

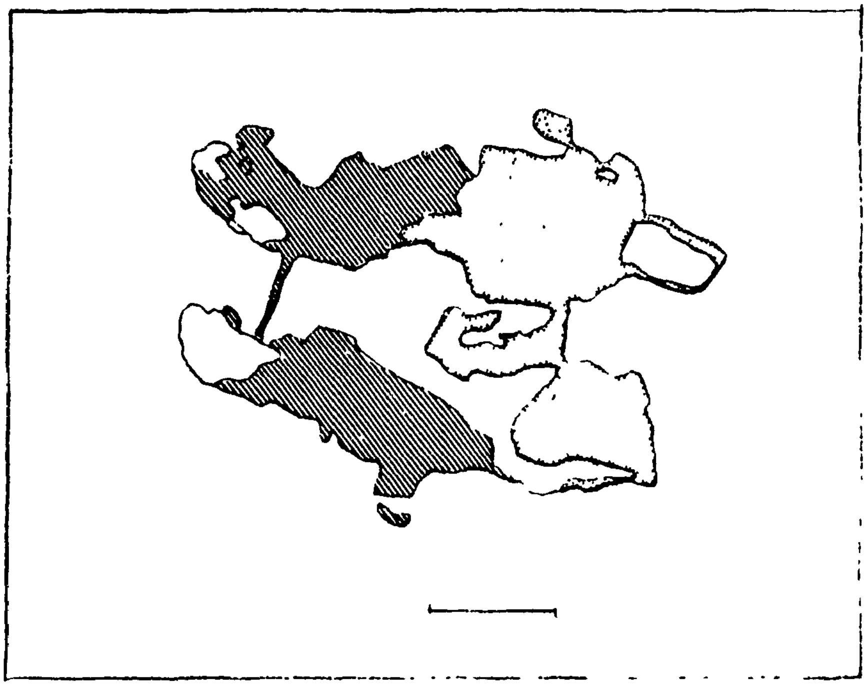

FIGURE 2.12 A

COMPOSITE PARTICLE - 1500 X, 5 kV

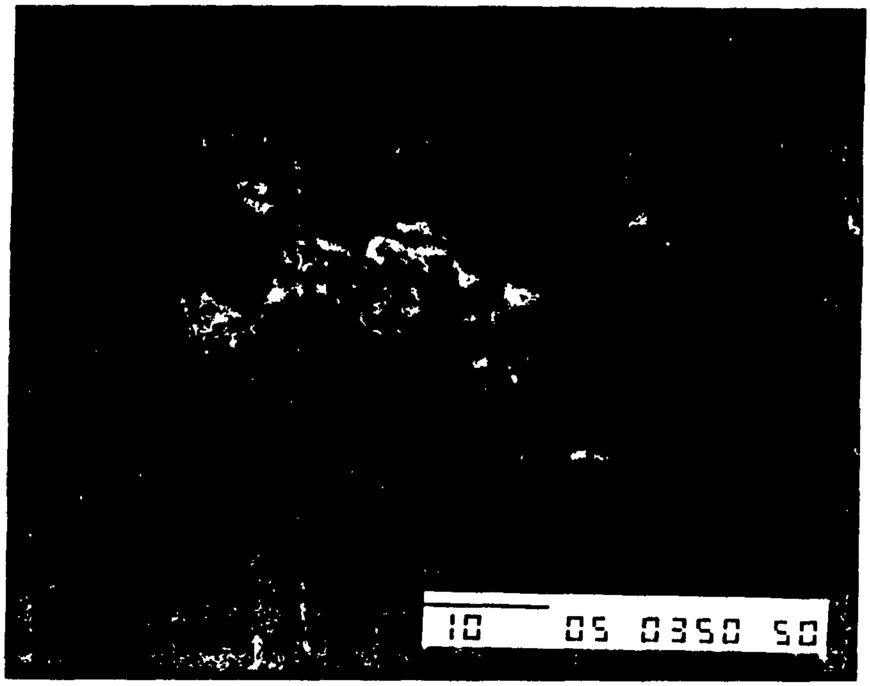

FIGURE 2.12 B

APPARENT GRAIN BOUNDARIES

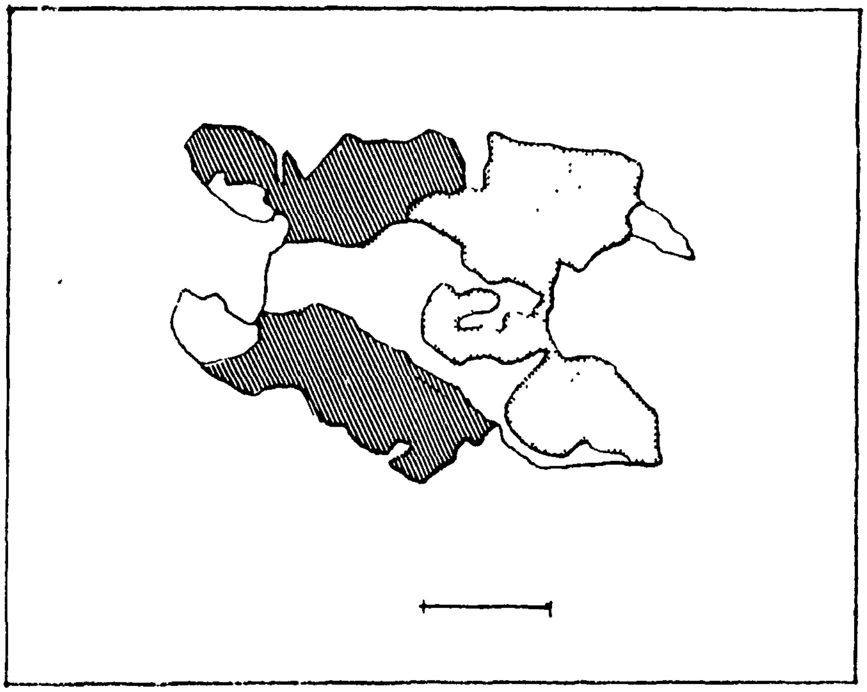

FIGURE 2.13 A

COMPOSITE PARTICLE - 1500 X, 25 kV

FIGURE 2.13 B

APPARENT GRAIN BOUNDARIES

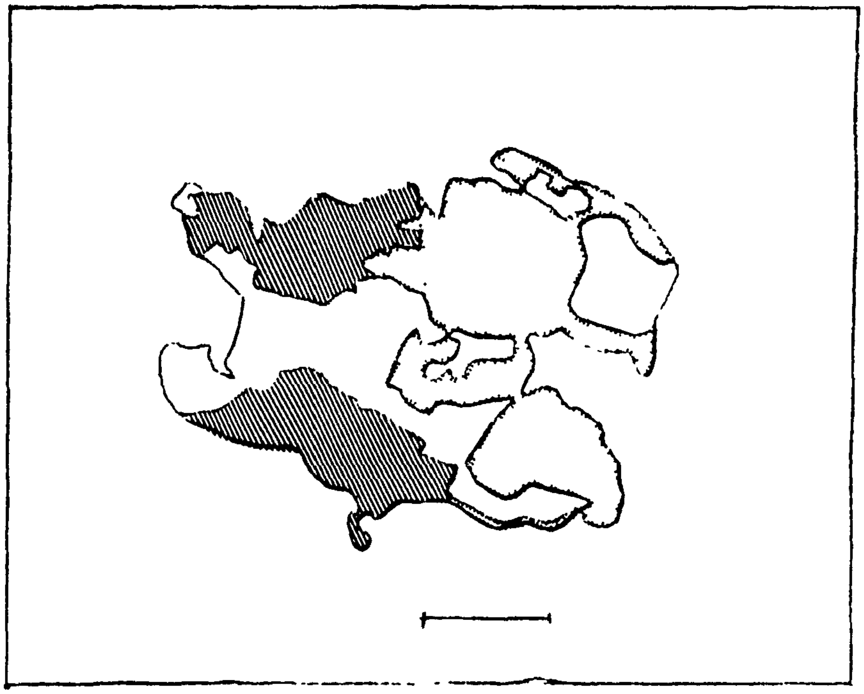

2.7 : Digitization of BEI Images

A major advance in liberation studies has been the development of digitized imaging capability. The signal from an optical or electron microscope can be fed into a computer which breaks the image into discrete packages referred to as pixels. The average intensity over the pixel area (for BEI) or the number of x-ray photon counts (for EDXA) is translated into a color or a gray level and plotted at the appropriate point on a computer monitor. The resolution of images varies from machine to machine but typically allows 256 gray levels with a linear resolution of either 512*512 pixels or 1024*1024 pixels. The major advantage of a digitized image is that it is in a format suitable for computer manipulation and evaluation.

2.7.1: Resolution Limits and Choice of Magnification:

The conversion of an analog signal into a digital representation results in loss of resolution, since each pixel represents an average over the area being represented. Thus, boundaries between a bright phase (eg. galena) and a dark phase (eg. resin) may be assigned the gray level of an intermediate phase (eg. sphalerite). This phenomenon is usually not observable, since errors introduced by the halo effect usually greatly exceed those generated by the frame averaging effect. However, a bright object small enough to occupy a single pixel could conceivably be represented by two to four pixels of an intermediate gray level. The limits imposed by resolution must be considered when deciding the size of object which can be considered significant at any given magnification. This work employed a 512*512 pixel linear resolution, half of what the image analyzer was capable of accommodating. If the linear resolution was to be doubled then the number of pixels per image would quadruple, with a corresponding increase in image processing time.

The image size and resolution impose limits on the largest and smallest particle sizes which can be quantified within a single image. In practice it is not practical for a field to contain less than about 50 objects, otherwise too much time is spent in image acquisition and stage movement. However, if too low a magnification is chosen then each object will occupy so few pixels that it is impossible to process the image without radically altering the shapes and compositions of individual sections. The magnification should be chosen such that in a typical field the largest particle section should have a diameter no more than about 10% of the image diameter. This means that on a screen with a linear resolution of 512 pixels the largest section should have a diameter of about 50 pixel widths, and will therefore occupy about 2500 pixels. In a sized sample containing about three or four size classes this will tend to yield about 50-100 objects per image.

Image processing, as discussed in Section 2.8.5, tends to obliterate features with linear dimensions less than about four or five pixels. This imposes constraints upon the smallest particle size for which liberation can be effectively quantified. If, for example, the largest particle in a sample is 270# (54 μm) then a magnification should be chosen such that the entire image is about 540 μm wide, or so that one pixel represents about one square micrometer. If a locked section is described as one which contains 5% or more of a minor phase then this minor phase would have to possess a linear dimension in excess of four micrometers (or an area of about 16 square micrometers) to avoid being eliminated during image processing. This means that the total particle would have to have an area of about 16/.05, or 320 pixels, or a linear dimension of about 18 μm. Thus, it is seen that when the magnification is chosen to accommodate a 54 μm top-size the smallest particle for which quantitative information may be obtained is about 18 μm, or about three size classes smaller.

Even under the best of analytical conditions the maximum number of size classes (using the Tyler progression) must not exceed four or five within a given polished section. Any sections smaller than the about the fourth size class below the top size will contain erroneous data.

In samples containing more than one particle size the use of too high a magnification in an attempt to measure finer particles also generates erroneous data. At high magnifications larger sections will tend to be truncated at the frame boundaries. In the previous example the magnification was chosen such that the largest particle had about 0.1 times the linear dimension of the image. Thus, if a section through the center of this particle was randomly placed within the image there would be a 90% chance of failing to intersect the top or bottom of the image, and a 90% chance of failing to intersect the sides. This produces an 81% chance that the section would lie completely within the image, and a 19% chance that only part of the section would be seen. Doubling the magnification would increase the chance of boundary intersection to 36%. Thus it is found that although the lower size limit for quantitative evaluation can be pushed down by increasing the magnification, the upper size limit is simultaneously affected. The use of too high a magnification also increases the chance that a large particle will occupy the whole image frame, lowering the amount of quantitative data obtained during the analysis.

The limits described above can be altered by doubling the pixel resolution to 1024*1024. Using the same example of a sample with a 54 µm top size and a 540 µm frame width the lower size limit for quantitative data would be 9 µm, or five size classes below the top size. Of course, increasing linear resolution does not alter the lower analytical size limits imposed by the halo effect. In a 9 µm particle composed of 95% phase "A" and 5% phase "B" the minor phase would have a linear dimension of only about two micrometers, imposing a requirement for special analytical conditions in order to collect quantitative data.

Since there are lower limits to resolution in BEI imaging there are also upper limits to the magnification which can be considered useful. It may be useful, for example, to have an image resolution which is up to about four times the pyhsical limits of BEI resolution. Image processing can be used to sharpen a halo which is about four pixels wide, and may result in a more interpretable image than the primary image. However, increasing the magnification beyond this point simply lowers the number of particles which are counted without adding anything to the interpretability of the data. Under the conditions used in this study the halo effect extended over about a one to two micrometer width. Thus, the maximum useful resolution would be about 1/4 micrometers per pixel, or about a 130 micrometer total image width (=512 pixels). This corresponds to an SEM magnification of about 770x. A magnification of 720x was used for the finest particles examined in this study.

2.7.2 : Contrast and Brightness - Calibration of Gray Scales

Digitization consists of converting the BEI image (primary image) into gray levels between 0-255. The counts from the backscatter detector must be calibrated such that the gray levels of the minerals of interest are separated as much as possible, or in other words so that the gray scale resolution is utilized as fully as possible. This is done at the microscope by adjusting brightness and contrast. Brightness is simply an offset bias which is applied to the signal from the backscatter detector, while contrast is synonymous to gain. Both controls are simple signal processing controls, and do not affect what is physically occurring within the sample chamber.

Just as there is a limit to the maximum useful magnification, so there is a limit to the maximum useful contrast. If a mineral "A" has a backscatter intensity of 1.000 +/- 0.080 while a second mineral "B" has an intensity of 1.100 +/- 0.100 (arbitrary numbers) then the overlap in intensity will occur between 1.000 and 1.080. In physical terms the regions with an observed intensity of 1.000 to 1.020 will be predominantly "A" while those in the range 1.060 to 1.080 will be predominantly "B". Both phases will contribute about equally to the observed intensity range of 1.020 to 1.060. Under these conditions one would want to have a gray scale resolution of at least about 0.005 per gray level, or a total gray scale range of 256*0.005 or 1.28 intensity units. This would allow the ambiguous range of intensities to be characterized by (1.060-1.020)/.005 or eight individual gray levels. Increasing the resolution very much beyond about 0.0025 per interval would add little to the analysis, while decreasing the resolution much below 0.005 per interval would lower the confidence with which the minerals could be discriminated.

By fixing the range of intensities per gray level interval one fixes the range of gray levels which can be simultaneously measured. For example, the total gray scale range in the above example can be no higher than 1.280 intensity units before one of the minerals goes off scale either on the high or on the low side (since 1.280/.005 equals 256, the total number of possible gray levels). This becomes a problem when, for example, bright galena and dark silicates must be measured simultaneously. Since a wide range of gray levels must be measured, the gray scale resolution is lowered and it becomes difficult to discriminate similar minerals such as pyrite and chalcopyrite.

This problem can be solved in part by allowing the bright mineral to go off scale. The contrast is adjusted such that there is sufficient resolution to discriminate the two similar minerals, at which point the bright mineral may have an equivalent gray level as high as 500-1000, which is off scale and therefore represented by gray level 255. However, this is considerably disadvantageous, since wide halos and even subsurface occurrences of the bright mineral may also be off scale, and could no longer be distinguished from true occurrences. As a general rule, no minerals which are to be measured should be allowed to off scale on either the upper or the lower boundary. The reason will become more apparent in Section 2.8.1, which discusses image filtering and enhancement.

It may therefore be concluded that when two minerals of similar brightness must be discriminated there is a limit to the range of brightnesses which may be simultaneously measured within the sample. For example, the major species in the BMS ores are silicates, iron sulfides (mostly pyrite), chalcopyrite, sphalerite, galena, and arsenide/sulfarsenide species. (The latter, though of relatively minor abundance, are of interest due to the silver content of some of their constituents). The silicates are of low atomic density and are therefore much darker in backscatter imaging than the sulfides, although they show variations in brightness among themselves. Next in intensity is pyrite, followed by chalcopyrite and then sphalerite. Iron-rich sphalerite grains appearing similar to chalcopyrite, while iron-deficient sphalerite grains approach the brightness of arsenopyrite. Other sulfarsenides and arsenides tend to be considerably brighter, followed by galena which is far brighter than any of the other minerals. Given the existing constraints upon image acquisition time it was difficult to distinguish chalcopyrite from the iron sulfides when both silicates and galena were being measured. Thus, it was decided in the copper circuit study to omit silicates from the analysis and to quantify iron sulfides (pyrite and pyrrhotite, Px), chalcopyrite (Cp), sphalerite (Sp), and galena/arsenides/sulfarsenides (Gn).

It should be noticed that the gray scale resolution required for proper identification of the minerals is a function of the amount of gray level overlap between the various mineral species, which in turn is a function of the image acquisition time. Thus, the use of longer acquisition time could allow the discrimination of silicates, galena and all other sulfides simultaneously. This is not necessarily identical to the acquisition time at which the human observer can distinguish the mineral species. The contrast at which the image analyzer can effectively separate minerals is lower than the contrast required by the human observer. For example, the difference in gray levels between pyrite and chalcopyrite in Figure 2.8 appears to be small but is quite sufficient for mineral identification using digital images.

2.8 : Image Manipulation

The primary digital BEI image collected from the SEM is not in the form which is eventually used for quantification of liberation. For liberation measurements the digital images, which contain 256 possible gray levels per pixel, are converted into a number of binary images which simply record the presence or absence of a mineral species of interest at any particular X,Y coordinate in the image. A variety of tasks must be performed before the digital image is converted into binary images. The image must first be cleaned of artifacts such as halos and variations in gray level within mineral species, and the gray level envelopes for the various mineral species must be selected.

Image cleaning continues in the binary images. Once satisfactory binary representations of the mineral occurrences have been obtained a structural correction is applied, designed to discriminate minerals locked within a single particle from point contacts between particles. The particle types and their compositions are then measured.

The algorithm used in this study is a compromise between a desire to fully utilize the features of the Kontron image analysis system and a need to maintain as rapid an analysis as possible. The need for somewhere between 5000-10000 objects per analysis was considered to be inflexible on statistical grounds. However, there was an economic constraint strictly limiting the analytical time to 6 hrs per sample. The magnification was chosen for each sample to allow about 50-100 objects to be present within a given field, requiring that about 100 frames be analyzed at an approximate rate of one frame per three and a half minutes.

In this study the accelerating voltage was set at 10 kV and the beam current at 15 nA. These settings were the lowest at which a useful real-time image could be obtained on the cathode tube of the microprobe. The availability of a real-time image was considered to be greatly advantageous, since it facilitated sample set-up and gray level calibration. Under these operating conditions it was found that about eighty seconds were needed in order to collect an acceptable image. Including stage movement the total image acquisition time was just under ninety seconds, leaving just a little over two minutes for image processing. Image processing therefore had to be streamlined as much as possible for rapidity of analysis. A 512*512 image was used in place of the 1024*1024 maximum in order to reduce processing time, and the data was reduced to as small a tabular format as possible.

2.8.1 : Image Filtering and Enhancement

It may be appreciated that once a binary image has been created in which all variations in gray level have been removed the discrimination of real features from artifacts can be accomplished only on the basis of the shape or size of the occurrence. Thus, one could decide to eliminate all occurrences under 10 or 20 pixels in area in order to get rid of spurious pixels, or to eliminate any feature which is very long and thin, which could represent a halo. However, the amount of image alteration required in order to remove all unwanted features by this method is often so large as to seriously alter many real features of the sample. It is therefore advantageous to transfer at least some of the image processing to the primary digital image.

Discrimination of artifacts in digital images can be at least partially accomplished by looking at the gradation of gray levels across the sample. For example, in an ideal image one would expect a uniform gray level within a section which would abruptly change at the section boundary to the uniform gray level corresponding to the mounting matrix. However, in real images the minerals are seen as relatively uniform gray levels which grade systematically over a distance of one to several micrometers into a different gray level. One may apply image filters to seek these gradations and to convert them to abrupt transitions. In reference back to Section 2.7.2 it is essential that no minerals go off scale in brightness otherwise a large proportion of their halos will also be off scale and indistinguishable from the bulk of the occurrence.

A wide variety of filters are available in image analysis for the removal of unwanted features. A cursory description of some filters available on the IPS system is included here. Only those filters which are considered to be typical of all image analysis systems and of immediate use to liberation studies are included. The IPS reference manuals (Copyright 1984, Kontron Electronik) provide a more complete description.

SHADE	Performs brightness and contrast corrections on an image. Performing corrections is obviously inferior to providing a primary image with appropriate brightness and contrast.
SIGMA	(Gaussian averaging) Reduces gray level fluctuation caused by statistical variations in image intensity. As previously discussed, the variance of the gray level is a function of signal acquisition time. This phenomenon results in grainy images when acquisition time is insufficient. SIGMA allows the user to define a matrix size over which values will be averaged, along with the standard deviation for gray levels within the matrix. All pixels with values

within two standard deviations of the local mean are replaced by the mean value within the matrix. This is an effective algorithm for cleaning grainy images, but is obviously not as effective as collecting an image over an appropriate signal acquisition time.

LOWPAS (Lowpass filter) Averages the gray levels within a specific area. The size (in pixels) in the X and Y directions is specified, along with the number of times which the operation should be iterated. Lowpass filters eliminate rapid changes in gray levels from pixel to pixel, and therefore act as smoothing algorithms for evening out background gray levels. The overall visual effect is similar to putting the image slightly out of focus.

HIGHPA (Highpass filter) Defined as the weighted difference between the lowpass image and the original image. This removes all slowly varying information from an image, with the area of influence of the filter being varied by changing the size of the lowpass matrix. This filter has applications in removing halo effects from images. The visual effect is similar to assuming that the original image is out of focus, then inferring what the focused image should look like.

The major use of image filters in mineral liberation studies is for reduction of the halo effect. If the halo is not removed then free sections may appear to be surrounded by a second phase, while locked two-phase sections may appear to have a third phase at the interface between the two actual phases or at the particle boundary. The filter used in this study was DELIN, designed specifically for delineating phase boundaries. The filter uses a highpass algorithm to find phase boundaries at or below a selected width, then masks the primary image so that only these boundaries will be altered. A second highpass filter assigns approximately half of the boundary to the phases on either side of the interface. The filtered primary images, exhibiting sharpened boundaries, are subsequently referred to as secondary images.

2.8.2 : Choice of Gray Level Envelopes

The gray levels assigned to individual compositions are ranges which are intended to encompass the mean gray level and the statistical scatter of gray level produced by a given mineral composition. However, it can be seen from the photomicrographs that surface imperfections can widen the range of gray levels pertaining to individual mineral species to the point where the minerals show some overlap. Artifacts resulting from halo effects and their attempted removal also widen the effective range of gray levels which must be used to describe a mineral composition. Thus, no ranges of gray levels can be chosen which will outline the individual mineral occurrences without including an unacceptable number of misidentified pixels.

The most common approach to the problem is to divide the gray level envelope (0--255 gray levels) into continuous regions such that all pixels are assigned a mineral composition. Figure 2.14 shows the profiles of gray level vs. frequency of observation (represented as normal curves) which could be produced by three different minerals. The overlapping regions are cleanly divided so that each gray level is assigned to a single mineral.

This procedure is convenient, since all pixels with a gray level above that of the matrix are assigned to one (and only one) mineral. However, this constitutes a deliberate misidentification of at least some of the pixels. The amount and type of image processing required to remove unwanted features by this method is so large as to obliterate many real features. A more effective discriminatory approach must be devised.

In this study two gray level ranges are defined for each mineral, using the secondary (filtered) image as a source. The first gray level range (low range) is that which encompasses the mean gray level for the species, plus or minus about one standard deviation (Figure 2.15). If the mineral is either the brightest or the darkest in the analysis, one tail of the gray level frequency distribution may be retained. The low range image corresponds to pixels which be identified with a high degree of confidence. Depending upon the amount of overlap observed between minerals a greater or lesser proportion of the total area may be positively identified. About 2/3 of the Cp pixels could be included in the low-range image in this work, as compared to almost 100% for Gn.

The second gray level range (high-range) encompasses the mean gray level for the mineral species, plus or minus about three standard deviations (Figure 2.16). This range produces a solid, well-defined binary image of all occurrences of the mineral of interest, but also contains many falsely identified pixels. The high range image therefore records all possible occurrences of the mineral of interest. If the binary high range image does not record a mineral at a particular location, the chances of the mineral actually existing at that location are very slim.

The use of the low range and high range images to pinpoint the various mineral occurrences is an image processing function, and is discussed in detail at a later point. In brief, the low-range image shows where a mineral "is", while the high-range image shows where the mineral "could be". (The inverted high-range image defines where the mineral of interest "could not be"). The procedure involves exaggerating the sizes of the occurrences which "are", then eliminating the areas which "could not be". This procedure extorts the maximum possible amount of information from the secondary image, and thus reduces the need for subsequent image cleaning.

One decision which must be made is how many minerals will be quantified by the analytical procedure. In the case of the BMS samples the mineralogy includes a number of silicates and a small amount of iron oxides, pyrite, pyrrhotite, chalcopyrite, sphalerite, galena, tetrahedrite and a wide variety of accessory minerals. It is obviously preferable to quantify all minerals individually rather than creating combinations within a single gray level envelope; however, there are practical limits to both the gray level resolution, as previously discussed, and the analytical time which can be afforded for quantification of the various species. The possible number of two-phase locked

Assignment of Gray Level Ranges
(Conventional Division of Ranges)

Figure 2.14

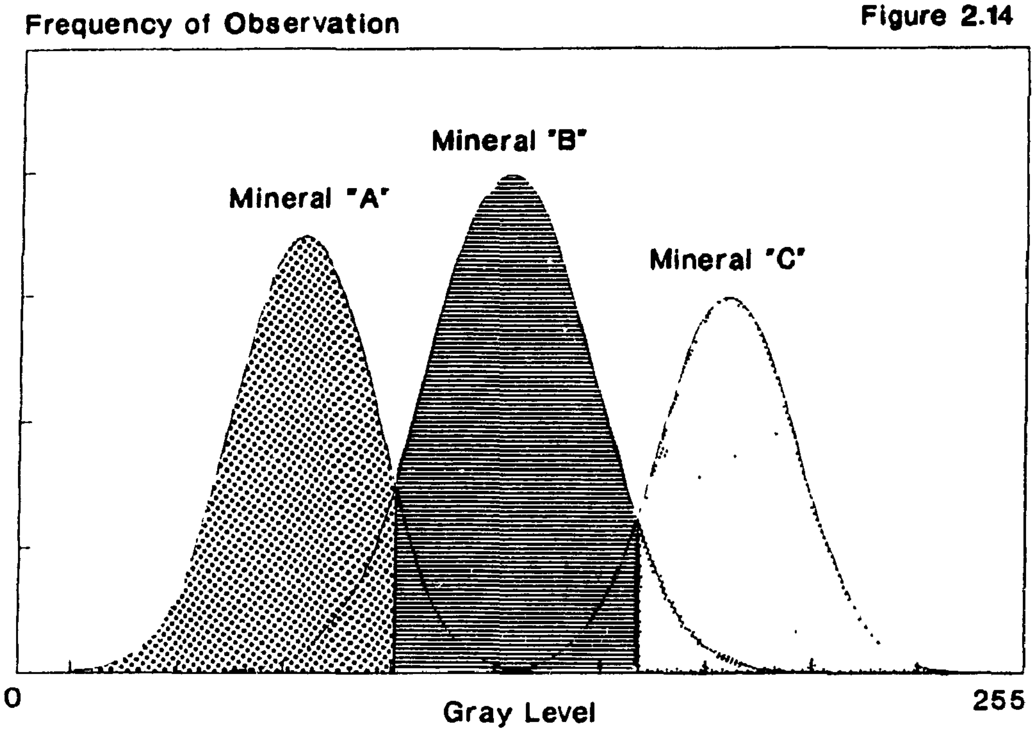

Assignment of Gray Level Ranges
(Low-Range Assignment)

Figure 2.15

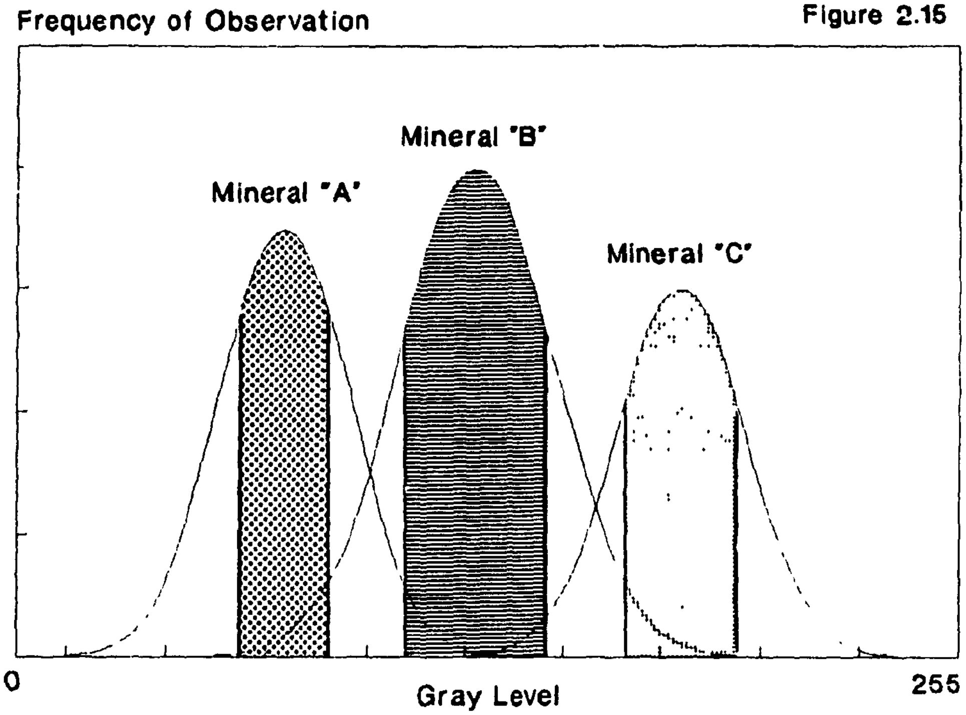

Assignment of Gray Level Ranges
(High-Range Assignment)

Figure 2.16

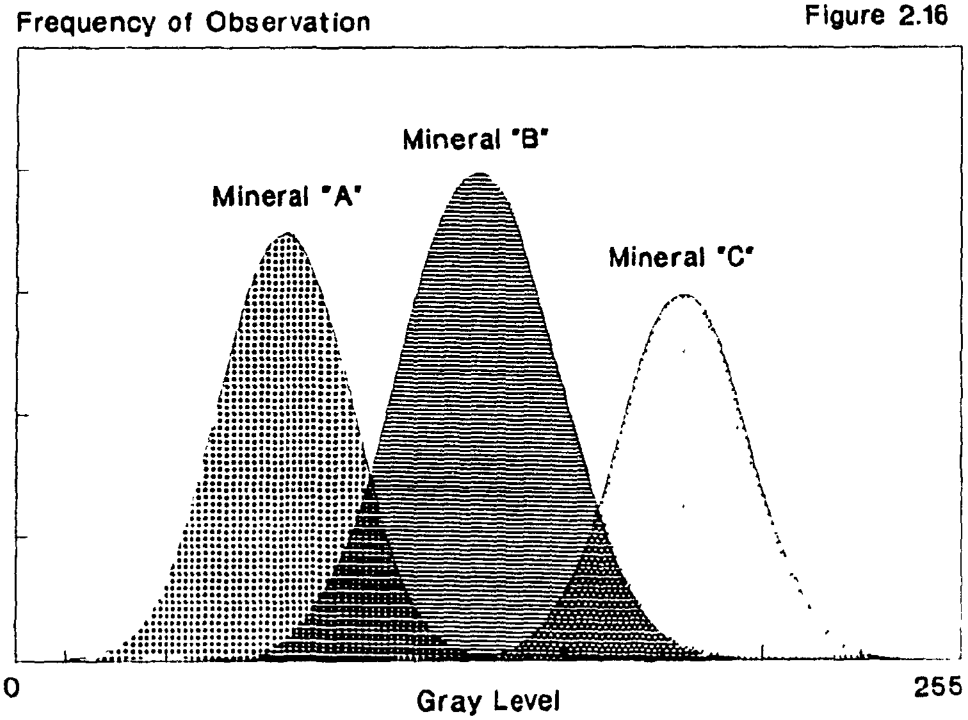

particle types for (N) gray levels is equal to $(N^2 - N)/2$, or six for four gray levels. Increasing this to five gray levels would create ten possible binary combinations, and so on, resulting in large increase in analytical time. Therefore a compromise has been made in this work, with the study employing four gray level envelopes (Px, Cp, Sp, Gn).

2.8.3 : Objectives of Image Processing

Image processing is defined for the purpose of this discussion as a series of mathematical operations performed upon binary images. Binary images are those which record either presence or absence of a mineral phase by setting the pixel value either to on (present) or off (absent). If one might imagine a mineral with a gray level range of 145-165 it is of no relevance in a liberation study whether individual pixels have gray levels of 145, 165 or somewhere in between. One simply wants to know whether the mineral is present or absent at a particular location.

The purpose of prior image filtering is to extract as much information as possible out of gray level gradations, since all gradations are lost in the binary image. Likewise, the use of carefully selected low range and high range gray level envelopes preserves some of the gray level intensity data for use by the processing algorithm. Once the secondary image has been reduced to a number of binary images recording the locations of the mineral phases all subsequent operations must be performed exclusively on the basis of the size and the shape of features within the image.

Image processing has two major objectives. The first is the removal of artifacts which could not be eliminated by image filtering. The second objective is identification and structural evaluation of all individual objects within the sample. The latter is not a simple task, since sections may be in physical contact. As far as the image analyser is concerned a single section is any non-matrix feature bounded by a continuous border of matrix. This means that if two sections touch they will be identified as a single particle. Likewise, if the halos around two sections overlap and happen to exhibit a non-matrix composition then the two sections will be identified as a single object.

Since processing involves an alteration of both compositional and structural features, there is an inevitable elimination of at least some of the smaller valid features. It is important, therefore, that processing be as non-aggressive as possible and that difficulties in the procedure be identified and taken into account in construction of the algorithm. The following discussion elaborates upon the problem of discriminating touching particles from locked mineral phases, and some of the difficulties in applying a processing algorithm to correct the problem.

Figure 2.17 shows a view of a BMS sample at 500x magnification. Six sections near the center of the sample touch or come very close to touching each other. One possible interpretation of the section boundaries which could be made using image analysis is presented in Figure 2.17B. The two light gray sphalerite sections in the center of the figure are in physical contact, and will be identified as a single section no matter how the gray levels are set up. (These two sections are represented as a single section in Figure 2.17B using coarse dots). The medium gray chalcopyrite grain and the white galena grain (represented together as fine dots) will be treated as a single section if the halo region between the two sections is assigned a mineralogical composition. Likewise, the dark gray silicate grain and the small sphalerite grain (represented as horizontal lines) will appear as a single particle if the halo region between them is assigned a mineralogical composition. If all halos in the image were assigned mineral compositions then it is conceivable that all six sections could be combined as a single section. Sections will therefore be combined (false locking) if they approach each other close enough to display physical contact or significant halo overlap. This tends to be more of a problem at small particle sizes than at larger ones. It may be inferred that false locking will appear more commonly with galena than with other particle compositions, since galena produces the largest halos.

Figure 2.18 shows another image at the same magnification (500x). If the mineral grains are closely examined it may be observed that dark lines are found at some phase boundaries. This is a relief effect, and may produce false liberation. It may be appreciated that the image analyzer cannot distinguish very well between the thin dark lines separating some mineral phases and the thin dark lines separating individual sections in close proximity to one another. Any attempt to aggressively separate touching or close-lying sections from each other will inevitably result in the separation of some locked particles along their phase boundaries. Figure 2.18B shows an exaggerated view of the individual sections which could potentially be identified from the image in Figure 2.18 if the image was to be aggressively processed to separate touching particles. For example, the large Gn/Sp/Px particle just left of the centre could be identified as two small sphalerite sections (at the top), one large Sp/Gn composite (at the left) and one Px/Gn/Sp composite (at the right).

FIGURE 2.17

TOUCHING PARTICLES - 500 X, 15 kV

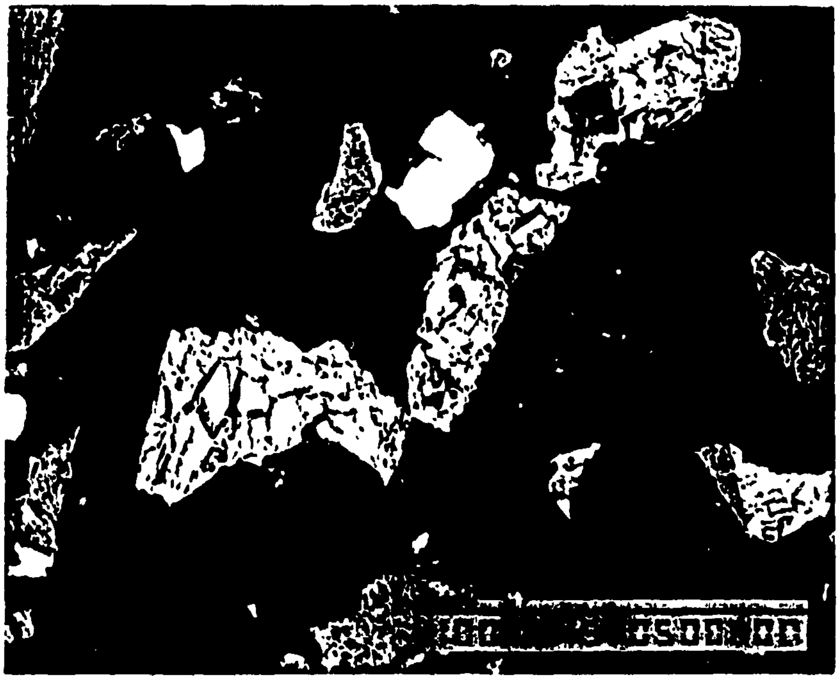

FIGURE 2.17 B

POSSIBLE INTERPRETATION BY IMAGE ANALYSER

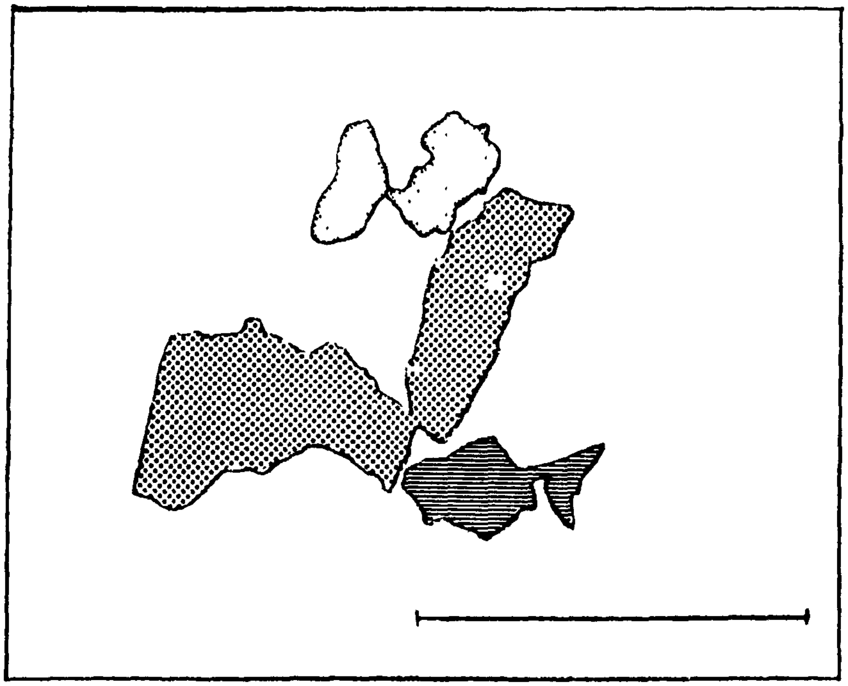

FIGURE 2.18

DARK INTERCRYSTALLINE BOUNDARIES - 500 X, 15 kV

FIGURE 2.18 B

POSSIBLE INTERPRETATION BY IMAGE ANALYSER

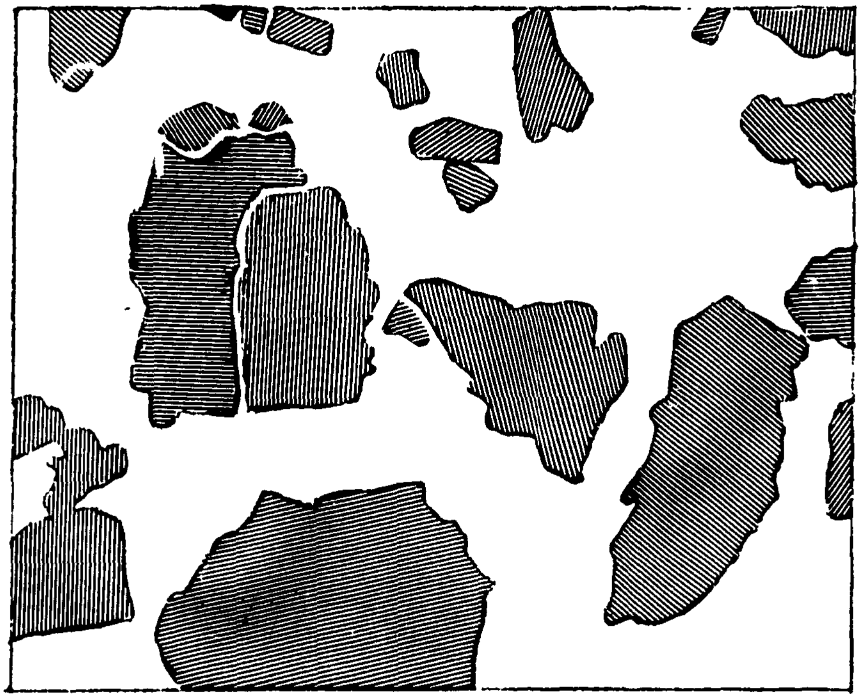

2.8.4 : Guidelines for the Image Processing Algorithm

The image analyser is simply a dedicated computer, for which the rules of operation must be defined. Thus, a program must be written in order to collect liberation data. There are no fixed methods for the construction of liberation algorithms; however, in this study a few guidelines were adopteds as follows:

1) The changes to an image should be as minor as possible.
2) The output should be reduced to a minimum.
3) When necessary the algorithm should emphasize preservation of structural features over compositional integrity.
4) The algorithm and parameters should be chosen such that a reasonable number of particles may be analyzed within economically dictated time constraints.

The first guideline is self-explanatory. The more the image is tampered with the lower the integrity of the resultant data. The second is designed to overcome the common computer problem of generating too much information for useful interpretation. The third is based upon the necessity for eliminating or modifying at least some of the data in order to obtain a useful image for liberation work. (By definition, modification of a pixel represents modification of the observed image composition. However, processing must proceed far enough to remove artifacts and false structural data). The fourth guideline reflects the limited availability and costliness of use of the image analysis equipment, and recognizes the fact that the optimum amount of processing and sophistication of the algorithm may not be achievable within reasonable economic constraints.

2.8.5 : Conversion of Gray Level Envelopes to Binary Images

The low range and high range gray level envelopes provide two binary images of each mineral occurrence, the former recording known locations of the mineral of interest and the latter recording all possible locations of the mineral. Neither is used as the binary image for mineral quantification, since each of the images contains only a part of the known information. The procedure for identifying the mineral occurrences is described below, and illustrated in Figure 2.19.

Figure 2.19a shows a simulated field of view containing five particles consisting of two phases, "A" (dark shading) and "B" (light shading). All particles have halos, and the interface between the two locked particles is of indeterminate composition. The two larger occurrences of the lighter phase contain small areas which could represent inclusions of the darker phase, or possibly surface defects.

Interpretation of the image is difficult, since it is not known how much of the halo region should be considered as part of the mineral occurrence. Neither is it known exactly where the interface is on the locked particles, or whether the small ambiguous areas in the light phase should be counted as inclusions or imperfections. Probably the particle boundaries depicted in Figure 2.19b are somewhat close to a proper interpretation.

The low-range and high-range images of the dark phase are shown in Figures 2.19c and 2.19d. The low-range image of the phase does not fill the whole area occupied by the phase. (In actual fact on the screen of the image analyser the real occurrences of the phase will appear as grainy clusters of pixels instead of solid objects). Nonetheless, the low-range image still contains some pixels at the particle boundaries and inside the light phase which do not fit the definition of "known occurrences". The high-range image includes most of the ambiguous area as well as the actual occurrences of the dark phase, and gives a description of all possible occurrences.

The low range image is eroded in Figure 2.19e. Erosion is accomplished by searching the image for uniform blocks pixels (usually 3*3), marking the centers of the blocks, then removing all unmarked pixels. The operation is

Interpretation of Phases and Boundaries **Figure 2.19**

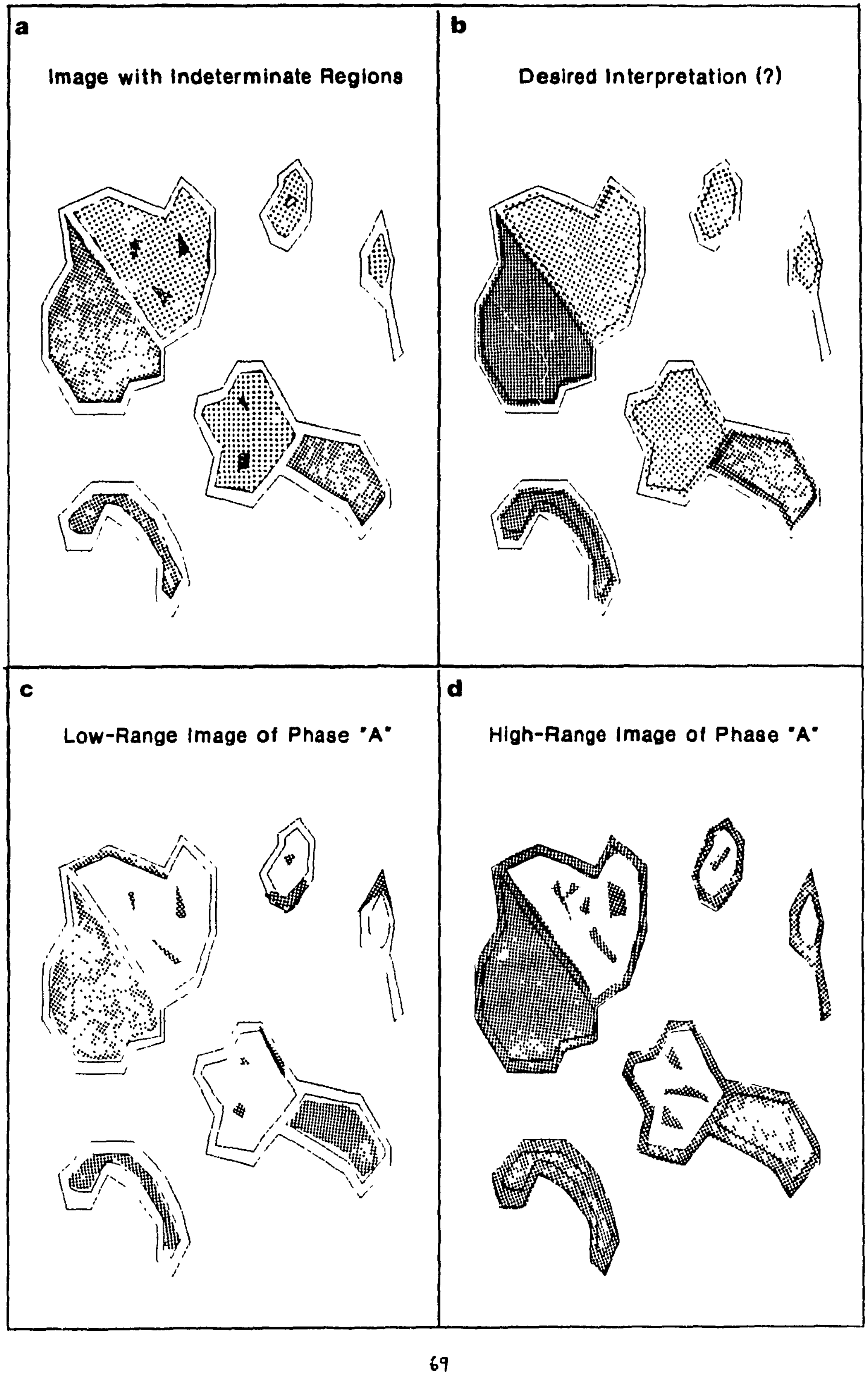

a Image with Indeterminate Regions

b Desired Interpretation (?)

c Low-Range Image of Phase "A"

d High-Range Image of Phase "A"

Figure 2.19 ... continued

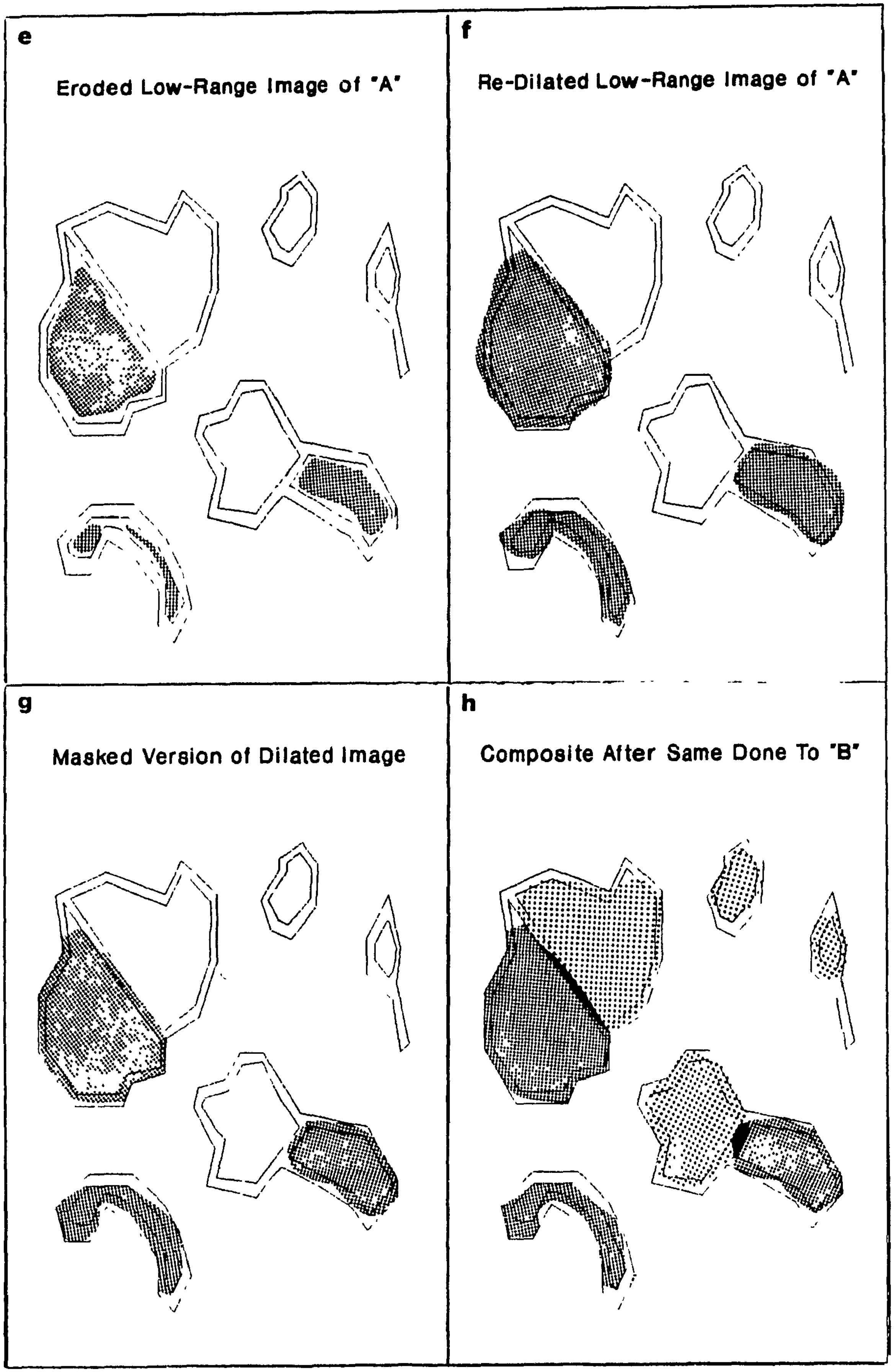

roughly equivalent to contracting the boundaries of the eroded phase by one pixel width. Following erosion the image is cleaned of objects less than a specified number of pixels (typically fifteen or thereabouts). Scrapping small objects results in the loss of some real occurrences (eg. one or more of the small ambiguous areas in the light phase could have been real inclusions of the dark phase), but effectively removes the vast majority of the remaining artifacts. Figure 2.19e is an accurate marker of the known locations of the dark phase.

Although Figure 2.19e contains almost no misidentified pixels, it does not adequately depict the true occurrences. The image is filled in by means of repeated dilations (Figure 2.19f). A dilation consists of replacing all pixels of "A" with a matrix (usually 3*3) of "A" pixels, so that the borders of "A" grow outwards by one pixel per dilation. The image thus formed contains a reasonable approximation of the occurrences of the phase of interest; however, the occurrences may have been dilated sufficiently to extend beyond the true boundaries of the particle. Typically about two or three dilations are needed to fill the images, meaning that an "average" occurrence may experience a significant increase in area by addition to the perimeter.

The perimeters of objects in the dilated image are corrected by combination with the high-range image using the Boolean operator "AND" (Figure 2.19g). This allows the individual pixels to show a mineral occurrence only if they are in a location which could potentially be a true occurrence (ie. the pixel is covered in Figure 2.19f) and which has also been previously marked as a possible occurrence (ie. the pixel is also marked in Figure 2.19d). The low range image therefore pinpoints the true locations of occurrences while the high-range image is used to define the shape and area.

The variable parameters (erosion cycles, dilation cycles and size of objects to be scrapped) are set interactively for the first frame of each sample. Figure 2.19 is meant to be illustrative of the process, and grossly exaggerates the corrections which are made. On the image analysis equipment the difference between frames is quite small, and could not be reproduced in a format suitable for presentation.

By following this procedure for each individual mineral species one obtains binary images of all mineral occurrences in the sample. The images are then combined using the Boolean operator "OR" to produce a composite binary image of all minerals (identified areas) in the sample (Figure 2.19h). During setup of the parameters it is verified that the composite binary image (referred to as the #1 binary image) is very similar to the image formed by converting the filtered BEI image into binary form.

This discrimination algorithm offers both advantages and disadvantages over algorithms which use only one source image per mineral. Algorithms with only one source image require aggressive scrapping of small objects to remove false occurrences, and tend to assign false compositions to ambiguous areas of the sample. This becomes an important source of error when small particle sizes are analyzed. In contrast, the algorithm presented in this study retains all but the smallest of real occurrences while either leaving ambiguous areas of the sample unassigned, or assigning them to an adjacent known occurrence. Ambiguous areas are generally unusually wide halos, the centers of pits, or particles close enough to the surface of the polished section to yield gray levels higher than that of the matrix.

The disadvantages of this algorithm are that it consumes more analytical time than the single source method, and that portions of the halos at mineral interfaces may be assigned twice. For example, in Figure 2.19h there are areas at the boundary between the phases which are assigned to both phases (shaded black). This corresponds to about a two-pixel overlap for most interfaces, and was not considered to be worth the analytical time required to correct the problem. A method of evaluating the error generated by this overlap is provided in the Chapter 3, which discusses methods of data verification.

2.8.6 : Discrimination of Structural Features

A procedure was written which provided a satisfactory method of separating touching particles, using as its starting point the #1 binary image. An overview of the processing algorithm is given, followed by a more detailed description of the individual operations:

1) The #1 binary image is inverted to black (minerals) on white (matrix) as shown in Figure 2.20a.
2) The white areas are dilated to separate the particles (Fig. 2.20b)
3) The white structure formed in Fig. 2.20b is skeletalized by eroding the white areas while maintaining connectivity (Fig. 2.20c).
4) The skeletal image is inverted and combined with the original binary particle image using the Boolean operator (AND). This produces the final image (Fig. 2.20d).

STEPS 1,2: Inversion and Dilation

By dilating the inverted image it is possible to separate the individual particles. For example, if two touching particles have an interface which is five pixels wide, then three successive dilations of the background will rupture the interface and create continuity of the background around the particles. The number of dilations required to separate the particles is determined interactively for each sample and tends to be higher for fine particles, which appear locked by halo overlap, than for coarse particles which tend to appear locked by physical contact.

Algorithm for Particle Separation Figure 2.20

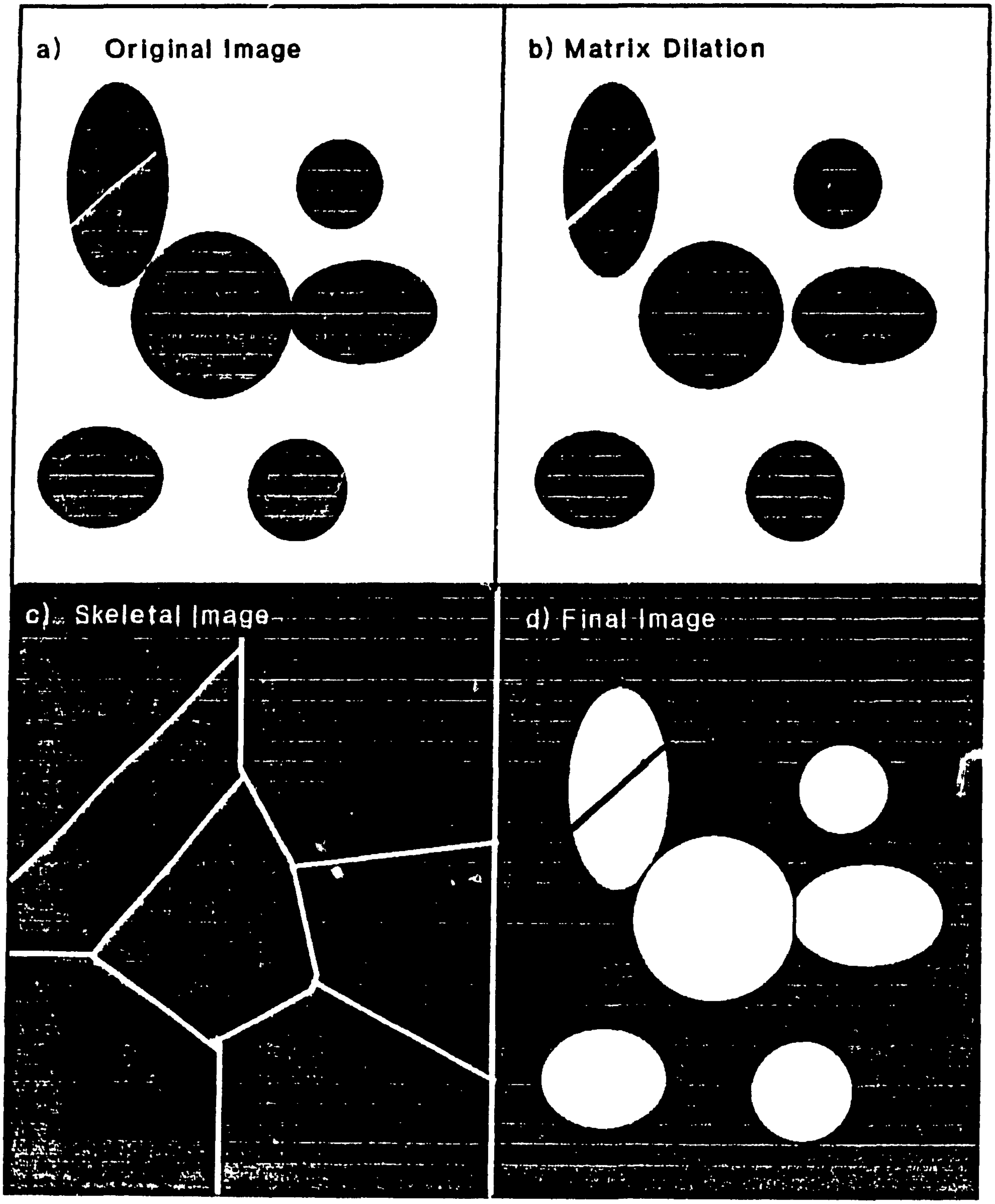

STEPS 3,4: Binary thinning and Combination

Although the altered image (Figure 2.20b) discriminates touching sections from each other, it is not particularly useful for liberation work. The areas and shapes of sections are irrevocably altered, and all sections with a diameter less than or equal to 2*N pixels (where N is the number of dilations) disappear completely. Thus, the dilated image is used only to identify section boundaries between particles with diameters greater than 2*N. This is accomplished by eroding the white areas of the inverted image (ie. the mounting matrix) down to one-pixel thickness without actually rupturing any lines (ie. thinning while maintaining connectivity). In the IPS program this is termed the BTHINN binary thinning instruction, which has an equivalent in most image analysis packages. The end result of the algorithm is that a skeleton is formed representing the bisecting lines between all objects in the field. The skeleton is then used as a mask for altering the interfaces between touching particles. The mask is inverted and combined with the #1 binary image using the Boolean operator "AND". Any pixel on the #1 binary image which is white (a mineral) but which is also white on the mask (ie. which should be background) is set to black (converted to background). The resultant image is referred to as the #2 binary image (Figure 2.20d).

The algorithm allows particles to be separated by altering only the minimum number of pixels required to create a continuous boundary between them. The variable parameter in the algorithm is the number of dilations required to adequately separate the particles. If the number of dilations (N) is too large then two effects will be seen: first, small objects (diameter <= 2*N) will not be separated from their neighbors, since they will disappear from the inverted and dilated image. Secondly, cracks and dark interfaces within particles will be expanded to the point where they bisect the particles (ie. produce false liberation). For example, one particle in Figure 2.20 was depicted as having a dark feature (a crack or dark interface) which was expanded in the dilation operation, resulting in the erroneous division of the particle into two separate particles. On the other hand, if the number of dilations is too small then larger sections will not be adequately separated. In practice, the number of dilations is chosen on a sample-by-sample basis to produce about the same amount of false liberation as there is false locking. This is not meant to imply that the errors cancel, since all errors add progressively to the variance of observations. The discriminatory power of this algorithm is about 99% under typical conditions, with about 1% of the observations representing false locked or liberated particles. As a point of reference, it may be stated that failure to process the #1 binary image at all typically results in about 20% false locking, and this in a sample in which inert filler has been added in a deliberate attempt to avoid such problems.

2.8.7 : Measurement and Data Compilation

Measurement and data compilation are relatively simple tasks, but which nonetheless consume a fairly large proportion of the total analytical time. The data inputs are the #2 binary image described above and the images recording the individual mineral occurrences.

There are 12 memories (M01-M12) available in the Kontron system for storing images, and an auxiliary memory used during image manipulation. In this algorithm the #2 binary image is in M02 and the binary images corresponding to the four mineral phases are stored in M03-M06. The copper study will be used for illustration, in which M03-M06 are occupied respectively by the binary images for chalcopyrite (Cp), iron minerals (Px), galena/arsenides (Gn) and sphalerite (Sp). The possible section types are Cp/Px (including free

Cp and free Px), Gn/Sp (including free Gn and free Sp), Cp/Gn, Cp/Sp, Px/Gn, Px/Sp and TQ (ternary and quaternary particles). The designations [U], [I] and [N] as used below represent union (Boolean "OR"), intersection (Boolean "AND") and non-intersection (Boolean "AND NOT"). The "OR" and "AND" functions are straightforward. The "AND NOT" operation may be read as follows: M05 = M05[N]M06 means that any sections which are in M05 "AND NOT" in M06 are stored in M05.

Step	Operation	Resultant Image
1)	M12 = M03[U]M04	(All sections except Gn, Sp, Gn/Sp)
2)	M11 = M05[U]M06	(All sections except Cp, Px, Cp/Px)
3)	M10 = M03[I]M04	(Cp/Px, Cp/Px/Gn, Cp/Px/Sp, Cp/Px/Gn/Sp)
4)	M09 = M05[I]M06	(Gn/Sp, Cp/Gn/Sp, Px/Gn/Sp, Cp/Px/Gn/Sp)
5)	M01 = M09[U]M10	(Cp/Px, Gn/Sp, TQ)
6)	M07 = M02[N]M11	(Cp, Px, Cp/Px)
7)	M01 = M01[N]M07	(Gn/Sp, TQ)
8)	M08 = M02[N]M12	(Gn, Sp, Gn/Sp)
9)	M01 = M01[N]M08	(All ternaries and quaternaries)
10)	M09 = M03[I]M05	(Cp/Gn, Cp/Px/Gn, Cp/Gn/Sp, Cp/Px/Gn/Sp)
11)	M09 = M09[N]M01	(Cp/Gn)
12)	M10 = M03[I]M06	(Cp/Sp, Cp/Px/Sp, Cp/Gn/Sp, Cp/Px/Gn/Sp)
13)	M10 = M10[N]M01	(Cp/Sp)
14)	M11 = M04[I]M05	(Px/Gn, Cp/Px/Gn, Px/Gn/Sp, Cp/Px/Gn/Sp)
15)	M11 = M11[N]M01	(Px/Gn)
16)	M12 = M04[I]M06	(Px/Sp, Cp/Px/Sp, Px/Gn/Sp, Cp/Px/Gn/Sp)
17)	M12 = M12[N]M01	(Px/Sp)

The resultant images are as follows: Cp,Px,Cp/Px sections (M07); Gn,Sp,Gn/Sp sections (M08); Cp/Gn (M09); Cp/Sp (M10); Px/Gn (M11); Px/Sp (M12); ternary/quaternary (M01). The binary images of Cp, Px, Gn and Sp remain in M03-M06.

The compositions of the sections are evaluated by individually choosing sections, measuring one of the mineral constituents, then comparing the area of the measured mineral with the area of the section. Cp is used as a mask for Cp/Fe, Cp/Gn and Cp/Sp; Px is used as a mask for Px/Gn and Px/Sp; Gn is used as a mask for Gn/Sp. The ternary/quaternary particles are evaluated four times, once for each mineral.

It may be observed in the above description that free observations were included with locked observations instead of being quantified individually. Free Cp and Px are included with Cp/Px binaries, while free Gn and Sp are included with Gn/Sp binaries. This is done simply because there are limits to the confidence which can be placed in the phase composition of a single pixel, which is all that is required to change the definition of a particle from free to locked. A particle occupying 2500 pixels would be considered locked if even one pixel (.0004 of the sample area) represented a phase different from that of the bulk of the particle. The expected error in the assessment of free particle abundance would therefore be expected to be high even in an image where 99.99% of the pixels were assessed accurately. Nonetheless, it was considered important in this study to distinguish free particles from low-grade locked particles. This is done by inference in Chapter 3.

2.9 : Summary and Critique of the Image Analysis Algorithm

It is evident that image analysis presents several problems which are not encountered in manual liberation studies. In a manual study the microscopist can usually recognize surface defects, cracks, edge effects and other sample imperfections, and can always distinguish touching particles from locked particles. These tasks are a major stumbling block for automated studies. Image analysis will always give reproducible results, in that the same data field analyzed twice under stable instrument conditions will always produce an identical distribution of particle areas and compositions. However, this does not imply that the data is accurate. In actual fact, the image analyzer's discriminatory algorithms operate upon much simpler rules than human observation and intelligence. The validity of data from image analysis based liberation studies is highly dependent upon a multitude of variables including particle size and range of sizes within a single sample, sample preparation, operating parameters for the microscope, image acquisition time, and the quality of the discrimination algorithm which is used. Thus, there are many points at which errors in the analysis may be generated. By opting for automated liberation data in preference to manually collected liberation data it must be carefully considered whether the increased precision of the data justifies the high cost of the work and the lower accuracy of structural information. The reproducibility of image analysis and the large number of particles which can be analyzed are both major advantages; however, the weaknesses of the method must not be discounted.

In this work great effort is expended in attempting to transform the primary digital BEI image into an accurate representation of the sample. In fact, this cannot be done in a wholly satisfactory manner. Ambiguous areas of the sample are an unavoidable element of BEI analysis. Unfortunately, the ambiguous areas tend to be concentrated at mineral interfaces and particle boundaries, where all structural interpretations must be made. Thus, it is not possible to simply ignore these areas of the sample. Rules must be developed which allow the discriminatory algorithm to interpret the image in a manner which will be rapid, accurate and as non-destructive to the composition of the sample as possible. The halo effect can never be completely eliminated, especially in so far as disproportionately bright phases such as galena tend to be overestimated. Thus, there is also a question as to whether known artifacts should be allowed to pass into the data, or whether some effort at correction should be made at the processing level. It was decided in this study that artifacts such as erroneously large galena occurrences would be allowed to pass into the data as long as the structural information within the image remained correct. Thus, image processing concentrates on the interfaces between minerals, such as can be found in locked or touching particles. Relatively little effort is expended in trying to rigorously interpret the precise positions of boundaries between minerals and the mounting matrix.

Since interactive parameters are set individually for each mineral the minerals will each undergo a different degree of processing. For example, there is almost no doubt that even a single "galena" pixel records a true galena occurrence, since it is very unlikely that any one of the other phases could produce a brightness equivalent to that of the average galena brightness. On the other hand, it is considerably more difficult to determine whether or not a scattering of chalcopyrite pixels in a pyrite section marks a valid chalcopyrite occurrence. The net result is that pixels from minerals which are difficult to identify are deleted preferentially from the image. In the case of the copper circuit study galena needed very little processing. Sphalerite and pyrite generally required a moderate amount of processing, and chalcopyrite the most of all. Thus, the reconstructed assay of galena is expected to be high relative to the other phases, while the reconstructed assay of chalcopyrite is expected to be low.

The introduction of such compositional bias into the reconstructed assay is a conscious decision, based upon the principal that valid data should not be deleted from the image. Since galena can be distinguished readily from the other minerals it is found that fine features such as small inclusions are retained down to a size at which identical features of a different composition are lost. This is a departure from the usual method for conducting liberation studies, in which processing and scrapping parameters are set globally for all mineralogical occurrences. The usual assumption is that the size of feature which may be analyzed is governed by the most difficult discrimination which must be made. This approach results in the deletion of much useful information, for no apparent reason. The objectives of the liberation study must be borne clearly in mind. One usually wants to determine, on an absolute basis, whether a mineral is locked or liberated at a particular point in the circuit, and how liberation changes through the circuit. In such a case all available structural data should be collected and considered. The only reason for standardizing the analytical limits for the different minerals would be to allow direct comparisons to be made between the liberation of the various mineral species. However, the question of whether one species is "more locked" or "more liberated" than another does not lend itself to practical applications. Thus, it was not considered to be worth the sacrifice of data to be able to make the comparison.

The steps involved in the image analysis procedure are reiterated below. An interactive parameter is set interactively only in the first frame, with all subsequent frames adopting the same values.

1) A primary image is obtained from the sample at an appropriate magnification. The DELIN algorithm is used to thin the halos (ie. form the secondary image), using an interactively determined highpass discrimination level for masking the image. The primary and secondary images are checked against each other to verify that they correspond.
2) The gray levels corresponding to the low-range and high-range images for each mineral are set interactively.
3) Binary low-range and high-range images are obtained for all minerals. The low range images are eroded for an interactively determined number of cycles, then dilated for the same number of cycles using a 3*3 matrix. A size is interactively chosen (# of pixel points per object) below which objects on the eroded low range images will be scrapped. The interactive parameters are determined separately for each mineral.
4) An interactively determined number of dilations is performed upon the low-range images. The logical AND of the low-range and corresponding high-range images is then determined. The resultant outout is taken to represent the true mineral occurrences. The four mineral occurrence images are combined using a logical "OR" to form the #1 binary image. The #1 binary image is checked against a binary version of the secondary image to verify that they correspond.
5) The #1 binary image is inverted, and the matrix dilated an interactively determined number of times to separate touching particles. The dilated image is then thinned to a skeletal structure. The logical AND of the inverted skeletal structure and the #1 binary image forms the #2 binary image, in which the vast majority of particles are separated. The individual particles in the #2 binary image are highlighted in separate colors, to provide visual confirmation that touching particles are being separated without causing unacceptable amounts of false liberation.
6) The individual particle types are discriminated and stored in seven different image memories. The algorithm then measures one phase abundance for each of the binary types and four phase abundances for the ternary & quaternary particles. The data is stored in ten tables which record cumulative measured particle area as a function of particle grade and equivalent spherical diameter.

The algorithm described above relies heavily upon correct assignment of the several interactive parameters. The complexity is necessitated by a desire to collect liberation data at sizes where the halo effect becomes a significant problem. It is not difficult to design an algorithm which is functional for particles in the 50-100 micrometer range of sizes. The magnifications which are employed are such that the halos only occupy one or two pixel widths, and can be scrapped without significantly affecting the analytical area. However, in fine particle work it is essential that the algorithm be able to reduce halo effects and separate touching particles in more effective a manner than is afforded by simple erosion/dilation or scrapping algorithms using binary images from a single gray level source image. The algorithm presented here is capable of making a highly efficient discrimination of real features from artifacts in the primary image while eliminating only a minimal amount of data and while creating very few artifacts of its own (eg. false liberation) during processing.

The issue of recalculated grade in image analysis samples is a pertinent one in this study, since comparison of the recalculated assay to wet chemical assays is the global test used in image analysis to offer "proof" of the validity of the data. In actual fact, it is proposed in the following chapter that the compositional and structural information within a sample are two separate entities, and that in BEI analysis one tends to be maintained at the expense of the other. In this work the preservation and reconstruction of structural information was accomplished with no regard to the preservation of recalculated grade. This is possibly the most contentious issue in the research, and leads to a need for some type of objective proof of the validity of the data. Since there is virtually no way of verifying the accuracy of structural data, most studies present well-correlated grade data and leave the reader to infer from this that the accuracy of the verifiable parameter (grade) is a test of accuracy of the unverifiable parameter (structure).

Of course, the best way to assure that the data is valid is to audit the operation of the image analyzer while data is being collected. However, it is also necessary to provide methods by which a person other than the equipment operator may examine the quality of the data set. It is also necessary to provide guidelines for handling the data which is generated. Thus, the next discussion focuses upon data reduction, statistical estimation of data precision, and data quality assessment.

CHAPTER 3: DATA REDUCTION AND STATISTICAL ANALYSIS IN IMAGE ANALYSIS

3.0: Introduction

Image analysis studies tend to generate about 10,000 observations per sample, resulting in a need for some form of data reduction. In many cases data reduction is performed with the sole objective of reducing the quantity of output into an interpretable format; however, it may also be necessary in some cases to combine data for statistical reasons. This chapter is concerned primarily with methods which can be used to calculate statistical confidence limits for measured sample parameters.

It is unusual to ever see the raw data from image analysis, since first level of data reduction is usually performed at the data collection level. In this study, for example, the individual observed sections were classified into seven section types, twelve sizes and eleven possible compositions. Thus, the number of unique descriptions (bins) was (7 types * 11 compositions * 12 sizes), or 924 per analysis. This is a very mild amount of data reduction, corresponding to a 11:1 ratio from the original 10,000 or so objects which were measured. For stereological reasons which will be presented in the next chapter it was undesirable to try to extract information for size-related phenomena from the data set. Thus, data for all size classes within a single sample were combined together. This yielded information about 7 types * 11 compositions, or 77 bins, corresponding to a data reduction of about 129:1.

Data reduction of some form is often required at the data collection level for the simple reason that a list of 10,000 observations is not particularly useful. A smaller table of summary information may be used either for direct data interpretation or as input for further data manipulation using a small computer. An obvious future development in image analysis is the interfacing of image analysis equipment with other, less expensive hardware. The image analyzer is too valuable for its time to be occupied with the type of data manipulation conducted in this study.

One decision which must be made is a determination of the amount of data reduction required to yield statistically significant observations. For example, the tabular output from the image analyzer corresponds to about an 11:1 data reduction, or 924 bins. Taking into account the fact that the ten most abundant bins could easily contain half of the observations, it would not be at all surprising to find many empty bins. This does not necessarily imply that the true probability of finding a section with that bin description is equal to zero. The problem of empty bins could be solved by increasing the number of particles analyzed (eg. to 1,000,000). However, the number of particles per analysis is largely governed by practical or economic considerations and must be considered a more or less fixed variable.

One problem with the combination of data is that it inevitably results in loss of information, and should therefore not be overdone. Statistics is invoked in an attempt to maximize the amount of information which can be obtained from the sample, while assuring that the individual units of information bear significance.

3.1: The Binomial and Poisson Distributions

Binomial and Poisson statistics are well known in sampling and data analysis, and require only a summary description. Binomial statistics describes the probability of observing an event (X) times in (N) trials based upon the actual probability (P) of the event occurring and the actual probability (Q = 1-P) of the event not occurring. The precise probability formula is:

$$p(X) = N!\, P^{x} Q^{(N-X)} / X!(N-X)!$$

It is common in statistical treatment to view the binomial distribution as being approximately normal with a mean of NP and a variance of NPQ. For rare events where Q approaches unity the variance of the distribution (NPQ) approaches the mean (NP). This is the basis of the Poisson distribution.

When a feature has some frequency "X" in an image analysis study one may calculate the approximate probability of occurrence: $X = NP^*$, or $P^* = X/N$. The relationship between P and P^* may be derived by assuming that the observed value P^* is no more than 1.96 standard deviations from the true value P. In other words, one may calculate a 95% confidence interval for P. This is done by solving the following quadratic equation:

$$(N^2 + N)\, P^2 + (2NP + N)\, P^* + P^2 = 0$$

In most instances where the parameter of interest is the variance associated with a measurement it is sufficient to approximate $P = P^*$, with a variance of P approximately equal to NP^*Q^*.

The relative error of a measurement can be defined as the 95% confidence interval, or two standard deviations from the mean. In metallurgical applications a measured parameter tends to be of little use if the relative error is more than about 20%. Thus, it may be easily calculated that the parameter must be defined by at least 100 observations. It follows that in a 10,000 section study where at least 100 observations are required per bin the level of data reduction must be at least 100:1. In practice, some bins contain a very large number of observations and others very few. Thus, it is advantageous to use a data reduction ratio of at least about 200-300 to one, or a total of 30-50 bins. Reduction of the data past this point leads to the loss of useful information, while failure to reduce the data to about this point leads to the collection of many non-quantitative observations.

The quantitative nature of observations (or the required data reduction ratio) is obviously strongly dependent upon the number of observations which are collected. For example, it is calculated above that in a study involving 10,000 observations no more than 30-50 separate categories of observations may be recorded if the data is to be considered quantitative. In a study involving only 1,000 observations only about 3-5 separate categories of observations could be quantitatively defined. This imposes definite statistical limits on the minimum sample size which may be used, and is the principal factor responsible for the attempts in Chapter 2 to minimize analytical time. A processing algorithm which collects perfect data in inadequate quantities is not much more useful than an algorithm which collects huge amounts of inaccurate data, requiring that a compromise be established.

3.2: Error Calculation for Compound Observations

Compound observations (such as recalculated assays) which are combinations of simple observations (such as locked particles of a particular area and grade) may be calculated by weighting the variances of the simple observations. For example, if an assay is to be recalculated on the basis of 100 free particles of chalcopyrite and 300 locked particles of 50% grade (assuming a study involving 10,000 observations) one can calculate the assay as follows:

$$(100/10000 * 100\%) + (300/10000 * 50\%) = 2.5\%$$

The variance associated with the individual observations can be approximated as NP^*Q^* (equal to 99 for the free particles and 291 for the locked particles) and the variance of the assay can be written as follows:

$(99 * 100\%^2 / 10000^2) + (291 * 50\%^2 / 10000^2)$
$= .0163 \%\%$

The standard deviation of the assay is the square root of the variance, or about 0.13%. The general formula for error propagation is as follows:

$C = aA + bB .... + nN$
Variance of $C = a^2 (A) + b^2 (B) ..... + n^2 (N)$

The use of an error propagation formula accommodates the fact that a unique compound observation may be derived from a variable number of simple events, and consequently does not possess a unique variance. The observation of 100 free particles out of 10,000 leads to an assay of 1% with a standard deviation of about 0.1%. However, the observation of 1000 locked particles with a grade of 10% leads to an identical assay of 1% with a standard deviation of only about 0.03%.

3.3: Data Reduction for Copper Circuit Samples

Data reduction and calculation of precision is illustrated by example, using data from the study of the Brunswick Mining and Smelting copper circuit. The circuit and samples are briefly described, followed by a discussion of the image analyzer output and the methodology for data reduction.

3.3.1: Copper Circuit Sample Description and Measurement Parameters

The Brunswick copper circuit was described in Chapter 1 (Figure 1.4). The circuit samples will be discussed in greater detail in Chapter 5, and are only briefly described here. Three sized samples for image analysis were prepared from each of six measured streams. The size fractions are referred to as "A", or coarse, "B", or medium, and "C", or fine. The six sampling points were as follows: RC074 discharge, equivalent to circuit feed and subsequently referred to as "74"; RC076 discharge, equivalent to rougher feed and referred to as "76"; Rougher tailings, or "RT"; Cleaner feed, or "CF" (equivalent to rougher concentrate); Cleaner tailings or "CT"; and Cleaner concentrate, or "CN" (equivalent to circuit concentrate). To completely describe a sample the size range is added to the stream mnemonic. For example, "CNC" refers to fine cleaner concentrate, and "76B" to medium rougher feed.

Measurement parameters for the copper circuit samples are presented in Table 3.1. The analytical area (and total number of analyzed objects) is strongly dependent upon magnification. For example, samples 74B and RTB were both analyzed at 720X magnification, resulting in a lower analytical area than the other medium size fraction samples. (The slightly higher magnification was used to facilitate the quantification of low-grade Cp occurrences, which tended to be abundant in these samples).

The table also shows the percent analyzed, or the percentage of analytical area which was occupied by sulfides. The values are relatively uniform for all samples except CFC and CTC. These samples showed a slight tendency towards agglomeration, and benefitted from the use of less sample material in the polished section. Of course, this resulted in a lower density of sulfide particles, lowering the overall number of objects which were quantified.

3.3.2: Methodology for Data Reduction

The primary output from the image analyser was in tabular format, with each table recording eleven possible grade classes and twelve possible size classes for a given type of section. As outlined in Section 2.8.7 the section types were defined as the six binary types Cp/Px, Cp/Gn, Cp/Sp, Px/Gn, Px/Sp, Gn/Sp and four descriptions of the ternary/quaternary sections (Cp/TQ, Sp/TQ, Px/TQ and Gn/TQ). Thus, ten individual tables were produced per sample.

MEASUREMENT PARAMETERS FOR COPPER CIRCUIT SAMPLES TABLE 3.1

		Coarse	Medium	Fine
AREA: (1000 um^2)	RC074 (Circuit Feed)	6006	760	690
	RC076 (Rghr Feed)	6926	2271	585
	Rghr Tails	7661	674	663
	Rghr Con	5257	2326	315
	Clnr Tails	2448	2244	237
	Clnr Con	5469	1853	627
MAGNIFICATION:	RC074 (Circuit Feed)	240	720	720
	RC076 (Rghr Feed)	240	400	720
	Rghr Tails	240	720	720
	Rghr Con	240	400	720
	Clnr Tails	360	400	720
	Clnr Con	240	400	720
FRAMES:	RC074 (Circuit Feed)	100	100	100
	RC076 (Rghr Feed)	100	100	86
	Rghr Tails	100	100	100
	Rghr Con	80	100	105
	Clnr Tails	100	100	100
	Clnr Con	100	100	114
ANALYZED AREA PER FRAME: (1000 um^2)	RC074 (Circuit Feed)	60.1	7.6	6.9
	RC076 (Rghr Feed)	69.3	22.7	6.8
	Rghr Tails	76.6	6.7	6.6
	Rghr Con	65.7	23.3	3.0
	Clnr Tails	24.5	22.4	2.4
	Clnr Con	54.7	18.5	5.5
AREA% ANALYZED:	RC074 (Circuit Feed)	35%	39%	36%
	RC076 (Rghr Feed)	40%	36%	35%
	Rghr Tails	44%	35%	34%
	Rghr Con	38%	37%	16%
	Clnr Tails	32%	36%	12%
	Clnr Con	32%	30%	28%

The eleven descriptions of section grade used in the output were 0-5%, 95-100%, and nine intervals of 10% width (5%-15%, 15%-25%, etc.). The twelve size ranges were equivalent spherical diameters corresponding to the standard Tyler mesh series. Table 3.2 is an example of the image analyser output, showing data for Cp/Px binaries in sample 74A. The data entries record measured area in µm², as opposed to section counts. For example, the entry of 39 µm² at Size = 6.54-9.25 µm , Grade = 25-35 %Cp represents a single section of equivalent spherical diameter 7.0 µm.

It is obvious from examination of the table that a large amount of the data bins do not contain quantitative data. This could be anticipated, since the data reduction ratio at the primary data collection stage is only about 11:1. As previously mentioned, the size data was not used in the analysis. Thus, the primary data was converted from 10 tables of (grade vs. size) into one table of (type vs. grade). This increases the data reduction ratio to about 130:1. Table 3.3 shows the resultant output table for sample 74A. The measured areas are converted to percentages in Table 3.4. At this level of data reduction only one bin is empty; however, many still contain non-quantitative data. In the analysis (Chapter 5) the data is further reduced to four descriptions of grade, yielding a data reduction ratio of about 350. This was considered to be the optimum compromise between data precision and information loss, and is consistent with the statistical guidelines for data reduction.

In this work it is necessary to devise a method for determining how many of the observations in the 00-05% and the 95-100% composition ranges are free, as compared to how many are locked. The need to make such a distinction depends largely upon the type of application for which the liberation study is intended. In this study the total flow of each mineral past each sampling point is calculated and characterized according to section grade. Of course, in the

RC074 (COPPER CIRCUIT FEED) COARSE FRACTION TABLE 3.2

Measured Area (μm^2) as a Function of Section Size (Equivalent Spherical Diameter and Section Grade (%Cp) : Cp/Px Binary System

Percent Chalcopyrite in Chalcopyrite/Pyrrhotite Binary System
(Includes Free Observations)

Size	00-05	05-15	15-25	25-35	35-45	45-55	55-65	65-75	75-85	85-95	95-00	TOTAL
<1.63	0	0	0	0	0	0	0	0	0	0	0	0
2.31	42	0	0	0	0	0	0	0	0	0	4	46
3.27	1800	0	0	0	0	0	0	0	0	0	30	1830
4.62	4250	0	0	0	0	0	0	16	0	0	256	4520
6.54	6790	0	0	0	0	29	0	75	0	0	2580	9470
9.25	16400	0	0	39	44	94	34	209	138	213	4350	21500
13.1	24700	0	317	234	0	0	0	220	256	467	4360	30600
18.5	36200	1240	504	0	142	0	204	0	150	590	9140	48200
26.2	75800	1150	1330	1230	0	462	416	1500	991	275	12300	95500
37.0	164000	1510	1590	0	952	0	918	0	0	1200	26500	197000
52.3	141000	0	1350	1090	1450	0	2760	1820	1170	1130	13600	165000
>52.3	45000	0	2150	0	0	0	0	0	3650	0	2340	53700
TOTAL	516000	3900	7240	2590	2590	585	4340	3840	6360	3880	76000	628000

RC074 COARSE: MEASURED AREA (100's of µm²) AS A FUNCTION OF SECTION TYPE AND FRACTIONAL COMPOSITION

TABLE 3.3

	PROPORTION OF FIRST MENTIONED PHASE (EG. Cp in Cp/Px)										
TYPE	00-05	05-15	15-25	25-35	35-45	45-55	55-65	65-75	75-85	85-95	95-00	TOTAL
Cp/Px	5160	39	72	26	26	6	43	38	64	39	760	6273
Cp/Gn	285	45	7	5	12	13	0	32	33	34	93	559
Cp/Sp	133	15	7	8	15	24	11	26	13	7	89	348
Gn/Sp	5790	1700	750	596	362	287	350	264	306	237	7980	18622
Px/Sp	1180	179	27	43	40	85	39	87	132	366	347	2525
Px/Gn	912	36	181	297	292	443	585	881	1420	3370	4050	12467
Px/TQ	7390	1300	800	859	800	1080	1360	1200	1680	2240	554	19263
Cp/TQ	18600	248	118	59	38	69	15	24	11	58	37	19277
Gn/TQ	6030	6170	2640	1480	911	658	510	323	245	204	110	19281
Sp/TQ	3760	2740	1210	1480	1050	1160	992	1110	1490	2560	1730	19282
												60070

RC074 COARSE: PERCENTAGE OF TOTAL MEASURED AREA AS A FUNCTION OF SECTION TYPE AND COMPOSITION

TABLE 3.4

	PROPORTION OF FIRST MENTIONED PHASE (EG. Cp in Cp/Px)										
TYPE	00-05	05-15	15-25	25-35	35-45	45-55	55-65	65-75	75-85	85-95	95-00	TOTAL
Cp/Px	8.59	0.06	0.12	0.04	0.04	0.01	0.07	0.06	0.11	0.06	1.27	10.44
Cp/Gn	0.47	0.07	0.01	0.01	0.02	0.02	0.00	0.05	0.05	0.06	0.15	0.93
Cp/Sp	0.22	0.02	0.01	0.01	0.02	0.04	0.02	0.04	0.02	0.01	0.15	0.58
Gn/Sp	9.64	2.83	1.25	0.99	0.60	0.48	0.58	0.44	0.51	0.39	13.28	31.00
Px/Sp	1.96	0.30	0.04	0.07	0.07	0.14	0.06	0.14	0.22	0.61	0.58	4.20
Px/Gn	1.52	0.06	[illegible]	0.49	0.49	0.74	0.97	1.47	2.36	5.61	6.74	20.75
Px/TQ	12.30	2.16	1.33	1.43	1.33	1.80	2.26	2.00	2.80	3.73	0.92	32.07
Cp/TQ	30.96	0.41	0.20	0.10	0.06	0.11	0.02	0.04	0.02	0.10	0.06	32.09
Gn/TQ	10.04	10.27	4.39	2.46	1.52	1.10	0.85	0.54	0.41	0.34	0.18	32.10
Sp/TQ	6.26	4.56	2.01	2.46	1.75	1.93	1.65	1.85	2.48	4.26	2.88	32.10

absence of prior knowledge of liberation it is suspected that low-grade chalcopyrite particles make up a significant proportion of the rougher tailings, while low-grade Gn, Sp and Px contribute significant proportions of the concentrate contamination. If all occurrences in the 95-100% and 00-05% classes are treated as free sections then the contributions of low-grade Cp to the tailings and of low-grade Sp, Gn, and Px to the concentrate will disappear from the data, invalidating the analysis. Conversely, if all such sections are treated as being locked, the relative contributions of their minor constituents will be grossly overestimated, since a substantial proportion are expected to be free. Solving the problem at the data collection level is difficult, as explained in Section 2.8.3.

In this work the approach to the problem is to make a mathematical extrapolation. It is assumed that the observations, when assembled into a cumulative grade/frequency histogram, should define a smooth curve. In other words, there should be no sharp discontinuity in the frequency of occurrence of any particular locked composition class with respect to its neighboring classes. This makes intuitive sense; for example, if 100 observations were 25%-35% and 70 were 15-25%, then it would be reasonable to expect 40 or 50 sections to be 5%-15%.

The extrapolation for sections with 0%-5 grade is conducted by calculating the slope (b1) of the cumulative frequency histogram between the 15-25% and 25-35% grade classes, and comparing it to the slope (b2) between the 5-15% and the 15-25% grade classes. The difference in slopes (b1-b2) can be called d(b). The slope between the 0-5% and 5-15% grade classes is then considered to be equal to (b2 + d(b)), allowing an intercept to be calculated. To illustrate, using the Gn/Sp data in Table 3.4, it can be seen that the frequency of Gn/Sp binaries as a function of %Gn is as follows: 0.99 (25-35%), 1.25 (15-25%), 2.83

(5-15%). The slopes are as follows:

b1 = 1.25-0.99 = 0.26;
b2 = 2.83-1.25 = 1.58;
d(b) = 1.58-0.26 = 1.32;
b3 = 1.58+1.32 = 2.90

The number of locked sections in the 0-5% class is calculated as being equal to the number in the 10-20% class plus b3, or 2.83 + 2.90 = 5.73. Since the 0-5% class is only half as wide as the 10-20% class this result must be divided by two, to yield 2.87%. The same procedure in mirror image is applied to the data for sections in the 95%-100% class. Table 3.5 shows the resultant output when the data from Table 3.4 is processed. The intercepts are obviously not allowed to fall lower than 0% or to exceed 100%.

3.4: Estimation of Data Confidence Intervals

The collection of image analysis data for a number of particles is equivalent to describing a very small sample of the constituent process stream. A number of different types of events are measured (eg measurements may fall in any one of a number of data bins); however, for rare events the error in the estimated abundance of the event will be high.

Table 3.5 describes the data for 74C in terms of thirteen possible grades and seven possible types of section. This means that there are 91 unique "structural assays" for the sample, each of which possesses its individual variance.

In order to be rigorously correct in estimating the variance of observations (measured areas) it is necessary to know the number of events (individual sections) making up the observations. The individual sections have different areas; thus, their abundances and variances must be weighted and added together using the error propagation method described in Section 3.2.

RC074 COARSE: PERCENTAGE OF TOTAL MEASURED AREA AS A FUNCTION OF SECTION TYPE AND FRACTIONAL COMPOSITION (AREA OF FREE SECTIONS INFERRED)

TABLE 3.5

	PROPORTION OF FIRST MENTIONED PHASE (EG. Cp in Cp/Px)												
TYPE	00	00-05	05-15	15-25	25-35	35-45	45-55	55-65	65-75	75-85	85-95	95-00	100	TOTAL
Cp/Px	8.59	0.00	0.06	0.12	0.04	0.04	0.01	0.07	0.06	0.11	0.06	0.00	1.27	10.44
Cp/Gn	0.38	0.10	0.07	0.01	0.01	0.02	0.02	0.00	0.05	0.05	0.06	0.03	0.13	0.93
Cp/Sp	0.19	0.03	0.02	0.01	0.01	0.02	0.04	0.02	0.04	0.02	0.01	0.01	0.14	0.58
Gn/Sp	6.77	2.87	2.83	1.25	0.99	0.60	0.48	0.58	0.44	0.51	0.39	0.05	13.24	31.00
Px/Sp	1.55	0.42	0.30	0.04	0.07	0.07	0.14	0.06	0.14	0.22	0.61	0.58	0.00	4.20
Px/Gn	1.52	0.00	0.06	0.30	0.49	0.49	0.74	0.97	1.47	2.36	5.61	5.60	1.14	20.75
Px/TQ	10.34	1.96	2.16	1.33	1.43	1.33	1.80	2.26	2.00	2.80	3.73	0.92	0.00	32.07
Cp/TQ	30.59	0.37	0.41	0.20	0.10	0.06	0.11	0.02	0.04	0.02	0.10	0.06	0.00	32.09
Gn/TQ	0.00	10.04	10.27	4.39	2.46	1.52	1.10	0.85	0.54	0.41	0.34	0.17	0.02	32.10
Sp/TQ	1.21	5.05	4.56	2.01	2.46	1.75	1.93	1.65	1.85	2.48	4.26	2.88	0.00	32.10

Although the number of section counts was not directly recorded during the data collection stage, the size intervals used in the output tables are spaced narrowly enough to allow the number of counts to be estimated with high accuracy. Thus, it is possible in principle to calculate the variances of all the compound events recorded in Table 3.5. However, the task is exceedingly time-consuming, since variances have to be calculated for the (11*12*7) or 926 original data bins in the image analyser output, following which the data has to be added together using the error propagation formula to produce the compound observations presented in Table 3.5. A simpler method is required, since it could take upward of 15 minutes just to calculate the variance of a single compound observation.

A method has been derived whereby a Poisson approximation may be used to measure the variances. To illustrate the method the binomial probabilities are calculated by the long method, then compared to the variances calculated by the approximate method.

Table 3.6 shows the various section types in sample 74A, this time combined to omit the grade data. This is done for illustrative purposes, since calculation of variance requires the size data. The section types measured in the sample are the four free mineral species Cp, Px, Gn, and Sp, (here represented for the sake of simplicity by the number of sections containing over 95% of the mineral of interest), the six types of binary sections, the measured area of ternary/quaternary sections, and the total measurements of Cp, Px, Gn, and Sp in the form of ternary/quaternary sections. The table records the measured areas of these section types as a function of section size.

Table 3.7 converts these measured areas into measured events. An event is defined as a single sectional observation, and will occupy a variable area depending upon the section size. The section size within a class is defined as

RC074 COARSE: SECTION AREA, BY TYPE AND MEAN EQUIVALENT SPHERICAL DIAMETER TABLE 3.6
(Measured in 1000's of μm^2)

Size um	Measured Area	Cp	Px	Gn	Sp	CpPx	CpGn	CpSp	PxGn	PxSp	GnSp	TQ	CpTQ	PxTQ	GnTQ	SpTQ
1.4	0	0	0	0	0	0	0	0	0	0	0	0	0	0	0	0
2.0	0	0	0	0	0	0	0	0	0	0	0	0	0	0	0	0
2.8	6	0	2	4	0	0	0	0	0	0	0	0	0	0	0	0
4.0	13	0	4	7	1	0	0	0	0	0	0	0	0	0	0	0
5.7	30	3	7	9	9	0	0	0	1	0	0	0	0	0	0	0
8.0	78	5	17	20	23	1	1	0	5	2	3	1	0	1	1	1
11.3	124	5	25	30	28	2	1	1	16	4	8	4	1	4	4	4
16.0	252	10	42	70	46	3	3	1	34	6	19	19	3	14	16	17
22.7	692	17	111	206	90	7	2	2	105	15	52	85	8	63	60	72
32.1	1679	32	310	359	190	7	8	3	274	32	120	344	24	238	263	278
45.3	1915	18	347	191	291	10	3	5	264	23	173	588	22	404	445	470
64.1	1253	8	146	32	206	6	0	0	85	17	109	644	5	409	524	537
	6041	98	1011	929	884	35	18	12	784	100	485	1685	63	1132	1313	1378

RC074 COARSE: MEASURED "EVENTS" (SECTIONS) AS A FUNCTION OF SIZE AND SECTION TYPE TABLE 3.7

Size um	μm^2 per Section	Cp	Px	Gn	Sp	CpPx	CpGn	CpSp	PxGn	PxSp	GnSp	TQ	CpTQ	PxTQ	GnTQ	SpTQ
1.4	1.6	0	0	0	0	0	0	0	0	0	0	0	0	0	0	0
2.0	3.1	2	13	20	4	0	0	0	1	0	0	0	0	0	0	0
2.8	6.3	12	286	666	18	0	1	0	6	1	1	0	0	0	0	0
4.0	13	26	338	561	63	1	1	0	8	2	3	0	0	0	0	0
5.7	25	105	270	359	355	4	4	2	51	12	18	3	1	2	3	2
8.0	50	96	328	399	465	15	12	3	103	40	62	16	4	15	14	13
11.3	101	50	247	302	273	15	12	5	156	44	82	43	8	39	41	39
16.0	202	50	208	349	227	14	13	5	167	31	93	92	14	69	80	82
22.7	404	42	274	511	223	18	5	6	261	36	128	209	19	156	150	178
32.1	807	39	384	445	236	8	10	4	340	39	149	426	30	295	326	345
45.3	1611	11	216	119	181	6	2	3	164	14	107	365	14	251	276	291
64.1	3223	2	45	10	64	2	0	0	26	5	34	200	2	127	163	167
	TOTALS :	437	2609	3740	2108	84	61	29	1283	225	677	1354	92	954	1052	1118

All Types: 12607 Sections (CpTQ, PxTQ, GnTQ and SpRQ are subsets of TQ, and are not counted) being the root mean square of the upper and lower limits of the size class. To illustrate, the size class 37.0 µm to 52.3 µm is defined as having a mean size of 45.3 µm, while the area per mean particle equals 1611 µm^2 (or $\pi D^2 / 4$). It may be observed at the bottom of Table 3.7 that the total number of sections is equal to 12607.

The observed number of sections (X) is equal to NP*, which is used as an approximation of P. The variance (S^2) is equal to NPQ, where Q is approximated by $(N-X)/N$. Thus, NPQ equals ($X(N-X)/N$), or ($X - X^2/N$). Variances for the measured events are calculated in Table 3.8. In most cases the value of Q is close to unity, so that the variance is close to the measured number of sections. The relative errors (ie. the 95% confidence intervals) of the individual observations are presented in Table 3.9, calculated as ($1.96 \sqrt{S^2} / X$).

It may be seen in Table 3.9 that few of the measurements are quantitative, in that their individual relative errors tend to exceed 20%. The level of data reduction at this point is about 85:1, and is clearly inadequate.

In order to reconstruct the abundances of the various section types it is simply required to divide the weighted sum of section observations of that type by the weighted sum of all observations. The weighting factor is, of course, the section area. Similarly, the variance is calculated by taking the weighted sum of variances for the individual size fractions, with the weighting factor equal to the square of the particle area, then dividing by the square of the total measured area.

Table 3.10 shows the summary "assays", or observational frequency as a proportion of total area, as well as the variances for the different section types. The standard deviations are the square roots of the variances, and the relative errors are 1.96 standard deviations, expressed as a percentage of the observational frequency. It can be seen that at this level of data reduction (11

RC074 COARSE: VARIANCE OF OBSERVED EVENTS CALCULATED FROM BINOMIAL THEORY TABLE 3.8

Size um	Cp	Px	Gn	Sp	CpPx	CpGn	CpSp	PxGn	PxSp	GnSp	TQ	CpTQ	PxTQ	GnTQ	SpTQ
1.4	0	0	0	0	0	0	0	0	0	0	0	0	0	0	0
2.0	2	13	20	4	0	0	0	1	0	0	0	0	0	0	0
2.8 .	12	279	630	18	0	1	0	6	1	1	0	0	0	0	0
4.0	26	329	535	62	1	1	0	8	2	3	0	0	0	0	0
5.7	104	264	349	345	4	4	2	51	12	18	3	1	2	3	2
8.0	95	319	386	447	15	12	3	102	40	61	16	4	15	14	13
11.3	50	242	295	267	15	12	5	153	44	82	43	8	39	41	39
16.0	50	204	339	223	14	13	5	165	31	92	91	14	69	80	82
22.7	42	268	490	219	18	5	6	255	36	126	206	19	154	148	176
32.1	39	372	429	231	8	10	4	331	39	147	411	30	287	317	335
45.3	11	212	118	178	6	2	3	162	14	106	354	14	246	270	284
64.1	2	45	10	64	2	0	0	26	5	34	197	2	126	160	164

RC074 COARSE: RELATIVE ERROR (95% CONFIDENCE INTERVAL) IN OBSERVED EVENTS TABLE 3.9
CALCULATED FROM BINOMIAL THEORY

Size um	Cp	Px	Gn	Sp	CpPx	CpGn	CpSp	PxGn	PxSp	GnSp	TQ	CpTQ	PxTQ	GnTQ	SpTQ
1.4	0%	0%	0%	0%	0%	0%	0%	0%	0%	0%	0%	0%	0%	0%	0%
2.0	131%	54%	44%	93%	0%	0%	0%	174%	0%	0%	0%	0%	0%	0%	0%
2.8	56%	11%	7%	46%	0%	220%	0%	79%	220%	174%	0%	0%	0%	0%	0%
4.0	38%	11%	8%	25%	186%	174%	0%	68%	148%	105%	0%	0%	0%	0%	0%
5.7	19%	12%	10%	10%	98%	103%	136%	27%	56%	46%	118%	189%	138%	118%	152%
8.0	20%	11%	10%	9%	51%	56%	105%	19%	31%	25%	49%	96%	50%	52%	54%
11.3	28%	12%	11%	12%	50%	57%	86%	16%	29%	22%	30%	71%	31%	31%	31%
16.0	28%	13%	10%	13%	52%	53%	84%	15%	35%	20%	20%	52%	23%	22%	22%
22.7	30%	12%	8%	13%	46%	84%	81%	12%	33%	17%	13%	45%	16%	16%	15%
32.1	31%	10%	9%	13%	69%	62%	97%	10%	31%	16%	9%	36%	11%	11%	10%
45.3	59%	13%	18%	14%	77%	141%	112%	15%	52%	19%	10%	53%	12%	12%	11%
64.1	124%	29%	63%	24%	147%	0%	0%	38%	85%	34%	14%	152%	17%	15%	15%

observations, or a data reduction ratio of 1100:1) the compound events have a reasonable statistical precision. Tables 3.11 and 3.12 show the summary information for samples 74B and 74C, with the intermediate calculations omitted.

A much simpler method is available for error calculation, making use of the Poisson distribution. It may be approximated that the observational frequency (NP*) is similar to the variance (NP*Q*). Comparison of Tables 3.7 and 3.8 shows this to be the case. The variance of an individual bin is therefore equal to the weighted observational frequency, expressed as a number of events.

A second approximation is applied, which converts all observations into "mean events", arising from particles of "mean size". The mean size is obtained by evaluating size vs. cumulative measured area for the total data set. For example, the three size classes "A", "B" and "C" of sample RC074 are evaluated individually by plotting the cumulative measured area as a function of the logarithm of size (Figure 3.2, Table 3.13). In the case of sample 74A it is seen that 50% of the area occurs in particles below 38 µm in size. Therefore, the mean event is 38 µm, with a mean area of 1134 μm^2. The total analyzed area for the sample is 6.01E+6 μm^2 (from Table 3.6) leading to a calculation of 6.01E+6 divided by 1134, or E=5296 "mean events" derived from this polished section. Similarly, the "B" fraction has a mean diameter of 19.5 µm and a mean area of 299 μm^2, while the "C" fraction has a mean diameter of 10.3 µm and a mean area of 83 μm^2. The respective measured areas are 7.60E+5 and 6.90E+5 um^2, leading to calculations of 760,000/299, or 2542 mean events for the "B" class, and 690,000/83, or 8317 mean events for the "C" class. The measured sample areas for all copper circuit samples and their calculated mean events are summarized in Table 3.14. All samples within a given prepared size range are assumed to have the same size of mean event.

RC074 COARSE: SAMPLE STATISTICAL SUMMARY

TABLE 3.10

	Cp	Px	Gn	Sp	CpPx	CpGn	CpSp	PxGn	PxSp	GnSp	TQ	CpTQ	PxTQ	GnTQ	SpTQ	Total
OBS. FREQUENCY:	1.62	16.73	15.38	14.63	0.58	0.30	0.21	12.98	1.65	8.02	27.89	1.05	18.74	21.74	22.81	100
VARIANCE:	0.02	0.36	0.21	0.36	0.01	0.00	0.00	0.26	0.03	0.21	0.90	0.02	0.59	0.71	0.74	
STD DEVIATION·	0.16	0.60	0.46	0.60	0.11	0.06	0.06	0.51	0.19	0.45	0.95	0.14	0 77	0.84	0 86	
REL. ERROR.	19%	7%	6%	8%	37%	39%	54%	8%	22%	11%	7%	27%	8%	8%	7%	
SIMPLE ERROR:	21%	7%	7%	7%	35%	49%	59%	7%	21%	9%	5%	26%	6%	6%	6%	

MEAN DIAMETER (µm) : 38

MEAN EVENT (µm^2) . 1134

RC074 MEDIUM: SAMPLE STATISTICAL SUMMARY

TABLE 3.11

	Cp	Px	Gn	Sp	CpPx	CpGn	CpSp	PxGn	PxSp	GnSp	TQ	CpTQ	PxTQ	GnTQ	SpTQ	Total
OBS. FREQUENCY.	3.66	23.23	21.51	8.75	1.21	0.61	0.98	9.51	0.85	5.29	24.42	5.72	15.65	18.30	16.95	100
VARIANCE:	0.15	0.99	0.72	0.51	0.04	0.02	0.02	0.42	0.03	0.35	1.73	0.32	1.05	1.40	1.32	
STD DEVIATION:	0.39	0.99	0.85	0.71	0.19	0.12	0.16	0.65	0.18	0.59	1.31	0.56	1.03	1.19	1 15	
REL. ERROR:	21%	8%	8%	16%	31%	40%	31%	13%	40%	22%	11%	19%	13%	13%	13%	
SIMPLE ERROR.	20%	8%	8%	13%	35%	50%	39%	13%	42%	17%	8%	16%	10%	9%	9%	

MEAN DIAMETER (µm) : 19.5

MEAN EVENT (µm^2) . 298

RC074 FINE: SAMPLE STATISTICAL SUMMARY

TABLE 3.12

	Cp	Px	Gn	Sp	CpPx	CpGn	CpSp	PxGn	PxSp	GnSp	TQ	CpTQ	PxTQ	GnTQ	SpTQ	Total
OBS. FREQUENCY	3.48	30.09	22.19	4.34	2.67	0.09	1.05	3.80	0.18	1.10	31.01	20.91	22.71	18.02	19.13	100
VARIANCE.	0.06	0.38	0.21	0.08	0.03	0.00	0.01	0.05	0.00	0.01	0.60	0.43	0.44	0.35	0.37	
STD DEVIATION:	0.25	0.61	0.45	0.28	0.18	0.02	0.10	0.22	0.03	0.11	0.78	0.66	0.57	0.59	0 61	
REL. ERROR:	14%	4%	4%	13%	13%	53%	19%	11%	37%	20%	5%	6%	6%	6%	6%	
SIMPLE ERROR:	12%	4%	5%	10%	13%	71%	21%	11%	51%	21%	4%	5%	5%	5%	5%	

MEAN DIAMETER (µm) : 10.3

MEAN EVENT (µm^2) : 83

RC074 (COPPER CIRCUIT FEED) IMAGE ANALYSIS AREA FREQUENCY VS. SIZE TABLE 3.13

Equivalent Spherical Diameter	COARSE FRACTION		MEDIUM FRACTION		FINE FRACTION	
Mean Size	Measured Area (um^2)	Cumulative Frequency	Measure Area (um2)	Cumulative Frequency	Measured Area (um^2)	Cumulative Frequency
1.63	0	0.0%	481	0.1%	1927	0.3%
2.31	131	0.0%	1648	0.3%	3257	0.8%
3.27	6236	0.1%	3030	0.7%	7929	1.9%
4.62	12623	0.3%	6143	1.5%	18560	4.6%
6.54	29745	0.8%	12542	3.1%	56097	12.7%
9.25	77501	2.1%	34651	7.7%	192610	40.6%
13.10	124050	4.1%	103180	21.3%	280670	81.3%
18.50	252070	8.3%	205380	48.3%	110869	97.3%
26.20	691760	19.8%	228370	78.4%	16204	99.7%
37.00	1678590	47.6%	148430	97.9%	2200	100.0%
52.30	1915100	79.3%	16080	100.0%		100.0%
+++	1253010	100.0%		100.0%		100.0%
Mean Diameter (um) :		38		19.5		10.3
Mean Event (µm^2) :		1134		299		83

Cumulative Area vs. Section Diameter

(Sample RC074)

Figure 3.1

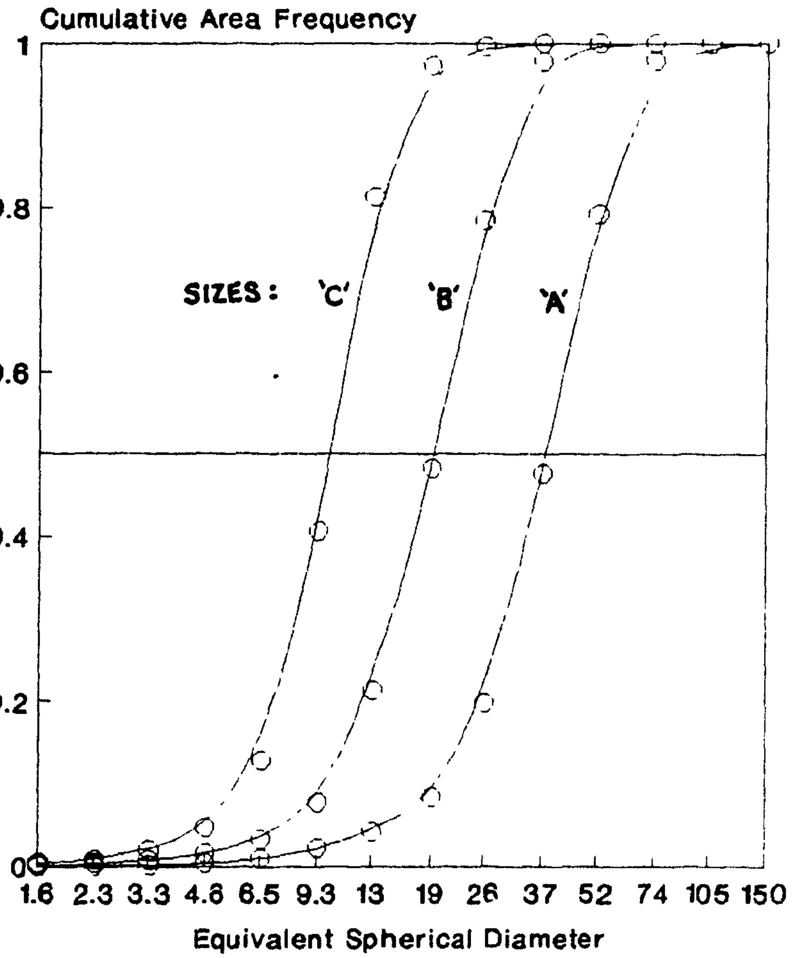

Expression of measured area as a number of mean events allows a simple error calculation to be carried out. For example, it is seen in Table 3.11 that free chalcopyrite has an observational frequency of 1.62%, or 0.0162. Since a total of 5296 mean events were recorded from the sample, it follows that free chalcopyrite constituted 85 mean events. The variance is then equal to 85 (ie. the variance equals the number of observations, from Poisson statistics), yielding a relative error of (1.96 $\sqrt{85}$ / 85), or 21%. The approximations of relative error based upon the Poisson distribution are included in Tables 3.10, 3.11 and 3.12 under the heading of "simple error", and correspond closely to the errors calculated from the more rigorous binomial approach.

Thus, a greatly simplified method is available for the calculation of the variance of a compound observation from a narrowly sized sample. All that is needed is the analytical area of the event of interest (A_1), the analytical area of all events (A_t), and the size of mean event (A_e). For events expressed as a a fraction of total area ($A = A_1/A_t$) the relative standard deviation is equal to:

$$S\%_A = 100\% \sqrt{A_e} / (\sqrt{A}\ \sqrt{A_t}) = 100\% / \sqrt{(A*E)} \quad (E = \text{sample mean events})$$

For example, Cp had an observational frequency of .0162 (1.62%) based upon 5296 mean events in the sample. The relative standard deviation of A equals 100% / $\sqrt{(.0162 * 5296)}$, or S%A = 10.8%. The relative error is 1.96 standard deviations, or 21%.

This method adds a lot of power and flexibility to error calculations, since only one number (E, or the total number of mean events) is required in order to calculate the standard deviations of any number or combination of compound observations. Thus, Table 3.14 is all that is needed to reconstruct the error margins in recalculated parameters for the whole of the copper circuit study.

EQUIVALENT EVENT COUNTS FOR POISSON ERROR ESTIMATION TABLE 3.14

		Coarse	Medium	Fine
AREA: (000's of μm²)	RC074 (Circuit Feed)	6006	760	690
	RC076 (Rghr Feed)	6926	2271	585
	Rghr Tails	7661	674	663
	Rghr Con	5257	2326	315
	Clnr Tails	2448	2244	237
	Clnr Con	5469	1853	627
EVENT SIZES:	(000's of μm²)	1.134	0.299	0.083
MEAN EVENTS:	RC074 (Circuit Feed)	5296	2542	8317
	RC076 (Rghr Feed)	6107	7596	7042
	Rghr Tails	6756	2253	7988
	Rghr Con	4636	7778	3800
	Clnr Tails	2159	7506	2850
	Clnr Con	4823	6197	7551

3.5: Recalculation of Mineral Assays and Assay Variance

Once the image analysis data is in a form such as that shown in Table 3.5 it is possible to calculate the grade/recovery relationships and other relevant metallurgical parameters for the sample. The mineral assays are compound events formed by taking the weighted sum of all sections containing the mineral of interest. In this case the weighting factor is the proportion of the mineral of interest contained within the section.

Data for the copper study occupies a fair amount of space, and is therefore included as Appendix 1. Tables A1.1 to A1.6 show the areas of the various section types and grades. In Tables A1.7 to A1.24 the area of free sections is estimated and the areas of all section types and grades recalculated to a total sample frequency of 100%.

Recalculation of the sample grades and confidence limits is a straightforward application of the calculation procedure demonstrated in the previous section, and is not further elaborated upon. Tables 3.15 and 3.16 present the recalculated mineralogical assays and the confidence intervals (95%) calculated using the mean event method. The 95% confidence intervals are also expressed as relative errors.

It may be observed that all of the recalculated assays fit the normal definition of what would be called quantitative numbers (ie. relative error less than 20%). Nonetheless, image analysis is is not a precise method for assay recalculation, due to the relatively low number of particles which are analyzed compared to wet assay techniques. The statistical errors associated with the analysis tend to lie in the region of about 5% of the measured assay for species with abundances in the range of 10% to 50%.

COPPER CIRCUIT SAMPLES: SUMMARY OF ERROR IN RECALCULATED ASSAYS TABLE 3.15

		Cp	Px	Gn	Sp	Events
RC074 COARSE	OVERALL SAMPLE GRADE:	2.5	38.0	27.3	32.1	5296
	ERROR (95%):	0.4	1.1	1.1	1.0	
	RELATIVE ERROR (%):	14.7	2.8	4.0	3.3	
RC074 MEDIUM	OVERALL SAMPLE GRADE:	6.3	40.0	31.6	22.2	2542
	ERROR (95%):	0.8	1.9	1.8	1.1	
	RELATIVE ERROR (%):	12.4	4.6	5.8	4.9	
RC074 FINE	OVERALL SAMPLE GRADE:	9.8	46.8	29.6	15.7	8317
	ERROR (95%):	0.4	1.2	1.0	0.6	
	RELATIVE ERROR (%):	4.1	2.6	3.5	3.6	
RC076 COARSE	OVERALL SAMPLE GRADE:	5.0	34.4	30.0	30.7	6107
	ERROR (95%):	0.5	0.9	1.1	0.7	
	RELATIVE ERROR (%):	9.6	2.8	3.5	2.4	
RC076 MEDIUM	OVERALL SAMPLE GRADE:	7.5	37.6	35.8	19.2	7596
	ERROR (95%):	0.5	1.0	1.2	0.7	
	RELATIVE ERROR (%):	6.6	2.7	3.4	3.5	
RC076 FINE	OVERALL SAMPLE GRADE:	13.3	43.3	29.7	18.5	7042
	ERROR (95%):	0.4	1.2	1.2	0.6	
	RELATIVE ERROR (%):	3.4	2.8	3.9	3.4	
RGHR TLS COARSE	OVERALL SAMPLE GRADE:	3.4	33.9	30.1	32.5	6756
	ERROR (95%):	0.4	1.0	0.9	0.8	
	RELATIVE ERROR (%):	10.7	2.9	3.1	2.5	
RGHR TLS MEDIUM	OVERALL SAMPLE GRADE:	2.5	47.4	28.6	21.6	2253
	ERROR (95%):	0.4	2.3	1.9	1.4	
	RELATIVE ERROR (%):	15.9	4.9	6.8	6.4	
RGHR TLS FINE	OVERALL SAMPLE GRADE:	1.4	47.7	31.3	19.6	7988
	ERROR (95%):	0.1	1.2	1.1	0.6	
	RELATIVE ERROR (%):	8.4	2.6	3.5	3.1	

COPPER CIRCUIT SAMPLES: SUMMARY OF ERROR IN RECALCULATED ASSAYS TABLE 3.16

		Cp	Px	Gn	Sp	Events
RGHR CON COARSE	OVERALL SAMPLE GRADE:	16.1	29.4	46.6	7.8	4636
	ERROR (95%):	0.9	1.1	1.8	0.5	
	RELATIVE ERROR (%):	5.8	3.8	3.9	6.5	
RGHR CON MEDIUM	OVERALL SAMPLE GRADE:	12.5	33.2	44.9	9.5	7778
	ERROR (95%):	0.7	1.0	1.4	0.5	
	RELATIVE ERROR (%):	5.2	3.1	3.1	5.2	
RGHR CON FINE	OVERALL SAMPLE GRADE:	19.3	36.6	32.0	14.8	3800
	ERROR (95%):	0.8	1.1	1.6	0.7	
	RELATIVE ERROR (%):	4.3	3.1	5.1	5.0	
CLNR TLS COARSE	OVERALL SAMPLE GRADE:	10.5	35.3	44.2	10.0	2159
	ERROR (95%):	1.1	1.8	2.6	0.9	
	RELATIVE ERROR (%):	10.4	5.0	5.9	9.4	
CLNR TLS MEDIUM	OVERALL SAMPLE GRADE:	12.7	33.2	43.8	10.4	7506
	ERROR (95%):	0.7	1.0	1.4	0.5	
	RELATIVE ERROR (%):	5.4	3.1	3.3	5.2	
CLNR TLS FINE	OVERALL SAMPLE GRADE:	19.2	39.2	30.8	11.2	2850
	ERROR (95%):	1.3	1.9	1.9	0.8	
	RELATIVE ERROR (%):	6.9	4.8	6.1	7.2	
CLNR CON COARSE	OVERALL SAMPLE GRADE:	65.9	23.1	5.6	6.0	4823
	ERROR (95%):	2.1	1.0	0.6	0.5	
	RELATIVE ERROR (%):	3.2	4.6	10.3	8.8	
CLNR CON MEDIUM	OVERALL SAMPLE GRADE:	74.1	20.8	1.6	3.6	6197
	ERROR (95%):	2.0	0.9	0.3	0.4	
	RELATIVE ERROR (%):	2.7	4.4	15.8	11.6	
CLNR CON FINE	OVERALL SAMPLE GRADE:	74.1	14.5	7.2	4.3	7551
	ERROR (95%):	1.9	0.8	0.6	0.4	
	RELATIVE ERROR (%):	2.5	5.2	8.0	9.3	

3.6: Verification of Data Integrity

The images used for data acquisition represent highly processed versions of the original BEI image. Thus, liberation studies using image analysis rely upon data which, though precise, may not be correct and for which there are few independent checks of integrity. The most common test of image analysis data sets is comparison of recalculated grades with grades obtained from chemical analysis.

The confidence intervals provided in the previous discussion for streams in the copper circuit represent statistical limits of precision, based upon the number of sections which were counted. By comparing the recalculated assay to a chemical assay it is theoretically possible to observe whether or not the discrepancy is large enough to be attributed to an inaccurate analysis. However, it is already recognized that factors such as the halo effect tend to bias the recalculated mineralogical analysis, and that the image analysis mineralogy will therefore contain inaccuracies. One can find several problems associated with the use of recalculated assays to test data:

1) Subjective bias is introduced even in the first level of processing, where gray levels are converted into the various minerals. The assignment of gray levels often involves deciding a cutoff point between two minerals of similar gray level (for example, chalcopyrite and iron minerals in this study). By biasing the choice of gray level boundaries it is possible to induce an apparently correct composition. However, the gray levels at which the assays are correct do not necessarily represent the gray levels at which the structural features are best revealed.

2) There are known physical phenomena in BEI which bias the analysis towards overestimation of denser species. This cannot be counteracted without applying a compensatory bias to the processing algorithm. Addition of a bias does not serve to increase the quality of the data set, since it simply superimposes two independent sources of error. The data can be made to correspond more closely to the chemical analyses, but at the expense of increasing the variance.

3) Once the primary image has been digitized it must be further processed to reconstruct structural features. While there is a definite limit to the amount of processing which may be considered beneficial, there is also a minimum amount of processing which is required. Processing inevitably changes compositional features, since it involves changing some fraction of the pixels in the image. Changes to individual pixels represent, by definition, changes to the composition of the sample. Thus, an under-processed image may have a better reconstructed assay than a properly processed image.

4) The brightest and darkest minerals in BEI analysis will require less aggressive processing than the minerals of intermediate brightness, since there is less ambiguity in their identification. For example, there is little doubt whether or not a bright point in an image constitutes galena; however, there is considerably more ambiguity in whether a point of intermediate gray level constitutes chalcopyrite. A decision must therefore be made during analysis whether only ambiguous data will be eliminated (in which case the recalculated assays will be biased) or whether valid information will be scrapped from the image (in which case sufficient useful information will be deleted to maintain the assay). In this work the deletion of useful information was

considered to be counterproductive.

5) Data is recorded in discrete intervals, for example 15%-25% Cp. This introduces considerable problems when attempting to reconstruct the grade of streams in which one of the constituents occurs in the form of low-grade locked particles. For example, if many of the particles in a study contain 0-5% of the mineral of interest it makes a large difference to the assay whether these particles are classified as being free or locked.

6) Errors in the recalculated assay may sometimes be attributed to segregation in the polished section which, if small, does not necessarily invalidate the structural data which is collected.

It should be evident from the above that the recalculated grade of a sample may not bear a fixed relationship to the usefulness of the data for liberation work. In fact, the apparent grade from image analysis can be manipulated by biasing the selection of gray levels, the assignment of ambiguous areas of the sample, and the aggressiveness of the scrapping algorithm for each mineral during formation of the binary images. Such operations may result in a good recalculated assay but compromise the validity of the structural data which is collected. Thus, it should not be construed that alterations to the processing algorithm which help to maintain the recalculated grade close to wet chemical values are beneficial to the collection of accurate structural data.

Errors and bias occur not only in the collection of image analysis data but also in the conversion of image analysis and chemical data into a form where they can be compared. Either the image analysis data has to be converted into chemical assays or the wet chemical data has to be converted into equivalent mineralogy. This is not as easy as it may appear, presenting additional problems as outlined below:

1) Not all minerals follow a fixed stoichiometry; for example, sphalerite has a widely variable composition, with variations seen within a given orebody or even a given hand sample. Thus, an average assay must be assigned which, in the absence of a detailed microprobe study, may not be absolutely correct.
2) Reconciliation of wet chemical iron assays with observed iron sulfides is difficult, since neither of the constituent elements is unique to pyrite or pyrrhotite. Iron is very difficult to balance since it occurs in various quantities within a number of silicate species, each of which may show different flotation behavior. Therefore, the observed quantity of iron minerals must be compared to the chemical assay for residual sulfur, or the amount of sulfur left unaccounted for by the other major sulfide species. Residual sulfur has about four times the variance of the original sulfur chemical assay, since it is a subtractive composite of four assays. Moreover, the sulfur assay is usually the least precise in any given chemical analysis.
3) In an image analysis study where silicate species are not quantified the comparison between image analysis and chemical assays requires normalization of the sulfide assays to 100% total sulfide content. This adds additional error to all assays, since the factor used for normalization combines the errors in all individual sulfide assays.
4) Due to a variety of practical reasons it is common for minerals to be combined in image analysis within a single set of gray level boundaries. Thus, in the copper circuit study we see that all

arsenides, sulfarsenides and various other minerals are combined with galena. Since all minerals exhibit different flotation characteristics the assemblage described by the gray level boundaries cannot be described by a unique composition or specific gravity. For example, it is expected that the gray level region described as "galena" contains a substantially higher fraction of sulfarsenides (eg. tetrahedrite) but less arsenopyrite in the concentrate than in the tailings.

The various compounded errors and sources of bias described above tend to invalidate recalculated assays as a test of data integrity. Nonetheless, the principal errors tend to add compositional bias as opposed to compositional variance. Thus, it is expected that if the image analyzer is functioning correctly there will exist a nearly linear correlation between image analysis and wet chemical results, but not necessarily an absolute match.

It may be concluded that automated image analysis studies are almost totally lacking in external quality control, in that once results are collected an independent examiner has no reliable means to quantify the accuracy of the measurements. Much of the usefulness of an image analysis study depends upon the researcher's ability to set subjective parameters in as objective a manner as possible, on a sample by sample basis, and to carefully audit the operation of the equipment and the processing algorithm as the data is being collected. If image analysis equipment is set up to operate in "batch" mode and left to run without supervision then there is no way to verify the integrity of structural features after the fact.

One internal check was designed into the processing algorithm used in this study to allow identification of any gross errors generated by over-aggressive image processing. It may be recognized in Section 2.8.6 that the image processing algorithm tends to assign ambiguous areas of the sample (halos etc.) to whichever phase is being measured. If all phases in TQ sections are measured then every interface will be counted somewhere between 0 times (if the interface is assigned to neither of the adjoining phases) and twice (if the interface is assigned to both of the adjoining phases). The objective while setting up the interactive processing parameters was to divide the ambiguous halo areas such that half of each halo was assigned to each of the adjoining phases. However, if any unassigned area was left between the phases then the sequence of operations leading to separation of touching particles would also lead to the production of false liberation. Therefore, the algorithm was most set up so that there was some overlap when assigning the interfacial boundaries. The amount of ambiguous area and the amount of overlap required are both a function of particle size, since halos may constitute a substantial proportion of the area of fine particles.

Ternary/quaternary sections, by definition, tend to contain a greater interfacial area than binary sections. The errors associated with the processing algorithm are multiplied by up to a factor of three in the TQ sections relative to the binary sections, since up to four species may be present. It is considered that a recalculated assay of about 105% in the TQ particles is acceptable, indicating an error of no more than about 2-3% in the grade estimation of the binaries. A recalculated assay over 105% may indicate that a significant amount of sections are placed into erroneous grade classes, and that the image quality was low enough to require exceedingly aggressive processing.

The recalculated assay balances for the TQ sections is presented in Table 3.17. The mean balances are 100.5 for the coarse (A) size fraction, 101.1 for the medium (B) size fraction and 105.0 for the fine (C) size fraction, revealing the more aggressive processing required for fine particle analysis. The particle size of the "C" fraction was 9-13 µm, which is evidently close to the lower size limit for liberation work using the microscope setup parameters chosen for this study. At least two of the samples (RFC, CFC) required more aggressive processing than would be considered optimal.

At the given operating conditions it was found that halos had a 1 µm to 2 µm thickness at most interfaces. To limit the area of a 1.5 µm halo to about 10% of the section area it can be calculated that the section would have to have a size of about 28 µm. This calculation is for a free section, in which the only interface is at the perimeter. By using the DELIN algorithm it was possible to thin the halo down to about half of its width, allowing particles of about 13 µm to be quantified with no more than 10% of the area remaining ambiguous. However, particles of 9-13 µm size (ie. the "C" fraction) can produce many sections with diameters in the range of 5-10 µm or even smaller, under which circumstances the ambiguous area can easily exceed 25% of the section area. Thus, the errors in recalculation of TQ grade reflect fundamental problems in BEI resolution as opposed to problems in the processing algorithm. This emphasizes the need for special setup parameters for ultrafine liberation work (ie particles <10 µm) and demonstrates the futility of trying to obtain quantitative data for fine sections in unsized samples, in which the setup parameters are optimized for fast analysis of coarser particles. Unfortunately, the recalculated assay method is not an affirmative indication of the structural integrity of the data. All that can be said is that samples which display assay balances over about 105% are so aggressively processed as to cast some doubt upon the integrity of structural information. The remainder of the samples are believed to contain reliable data.

The overall test of data integrity, which should be used whenever possible in any study, is internal consistency of the data set. When samples originate

Recalculated Analysed Area for TQ Sections Table 3.17

	Coarse (A)	Medium (B)	Fine (C)
Circuit Feed (74)	100.0	100.3	104.8
Rougher Feed (76)	100.4	100.5	110.7
Rougher Tail (RT)	99.9	101.1	100.8
Cleaner Feed (CF)	100.0	101.4	109.0
Cleaner Tail (CT)	100.5	101.0	103.1
Cleaner Con (CN)	102.7	102.4	101.3
Average	100.6	101.1	104.9

Numbers represent (Px+Cp+Sp+Gn), which should equal 100.0%

from different points within a processing circuit it is expected that they should bear some reasonable relationship to each other. For example, the copper circuit contains no grinding stage. It is therefore expected that no particle types should appear or disappear within the circuit. Referring back to Figure 1.4, one could expect the following relationships between the six sample points:

74 = 76 - CT
76 = 74 + CT = RT + CF
RT = 76 - CF
CF = 76 - RT = CN + CT
CT = CF - CN
CN = CF - CT

The observation of locked particles entering a junction from which they do not exit or leaving a junction without any apparent source is obviously a suspect event. However, it must also be considered that samples are rarely collected simultaneously and may therefore reflect circuit variations. It must also be cautioned that the variance associated with quantifying certain binary particle types is high in some streams, so that a mass balance may not be conclusive. Even a good mass balance is fallible, since a systematic error in analysis (eg. an algorithm which makes all particles appear to be locked) will have internal consistency but may bear no relation to reality.

In summary, there is no independent way of checking automated liberation data for accuracy. The available tests make it possible to identify individual samples which are anomalous in reference to other similar samples; however, it is not possible to verify the accuracy of data from a suite of samples which appear to bear internal consistency. Systematic errors in the determination of structural features will pass unnoticed. It is therefore essential when dealing with image analysis liberation data to be aware of the parameters used for acquisition of the BEI image and of the discriminatory ability of the image processing algorithm which is employed. A knowledge of the operating conditions and processing algorithm allow some qualitative estimation to be made concerning the type and magnitude of errors which are generated.

3.7: Testing Image Analysis Data against Recalculated Mineralogy

Portions of the powder samples used for the image analysis study were analyzed by ICP at the Research and Productivity Council in Fredericton, NB. The ICP assays were converted into mineralogical assays using the copper, lead, zinc and sulfur values (Table 3.18). Copper was assigned to chalcopyrite and lead to galena according to normal stoichiometry, and zinc to sphalerite assuming 60% Zn content in the sphalerite (a typical value for BMS ores). Residual sulfur (S_R) was assigned to pyrite. Unaccounted mass was assumed to be silicates, designated "Rock" in the table. To make the comparison between image analysis and ICP the results from ICP were normalized to 100% total sulfide content, since silicates were ignored in the image analysis study.

Image analysis data was collected as area percentage of each phase. The ICP mineralogical data therefore converted to area (volume) percentages by assuming specific gravities of 4.2 (Cp), 4.0 (Sp), 5.0 (Px), 7.5 (Gn). The image analysis and ICP area percentages are presented side by side in Table 3.19.

Figures 3.2 to 3.5 show a comparison of ICP and image analysis assays for the four mineral species. The statistical confidence limits for assay precision (from Tables 3.15 and 3.16) are included in the figures as dots above and below the mean (represented by circles).

Several things may be noted concerning the image analysis assays. First of all, they show some type of correlation with wet chemical assays. Secondly, they do not correlate 1:1, since the image analysis assays do not scatter around the wet chemical assays. In other words, there is an assay bias.

ICP DATA - CONVERSION FROM ASSAYS TO MINERALOGY TABLE 3.18

	ICP Assay				Recalculated Mineralogy (Mass%)					Normalized Mineralogy			
Stream	Cu	Pb	Zn	S	Cp	Px	Gn	Sp	Rock	Cp	Px	Gn	Sp
74A	1.1	24.0	16.6	31.2	3.1	32.3	27.7	27.8	9.3	3.5	35.5	30.6	30.4
74B	2.0	26.2	11.2	31.4	5.7	35.9	30.2	18.6	9.6	6.3	39.7	33.4	20.6
74C	2.4	23.7	8.9	32.4	7.0	40.0	27.4	14.9	10.9	7.8	44.8	30.7	16.7
76A	1.5	28.7	14.1	29.4	4.2	29.2	33.1	23.5	9.9	4.7	32.4	36.8	26.1
76B	2.4	30.2	9.7	30.2	6.8	33.3	34.8	16.1	9.0	7.5	36.6	38.3	17.7
76C	2.9	27.6	7.8	30.1	8.2	35.0	31.9	13.0	12.0	9.3	39.7	36.2	14.7
RTA	0.2	25.9	14.5	27.6	0.7	28.6	29.9	24.2	16.6	0.8	34.3	35.8	29.0
RTB	0.3	25.5	11.1	30.6	0.8	37.8	29.5	18.6	13.4	0.9	43.7	34.0	21.4
RTC	0.3	26.4	10.5	31.6	1.0	40.0	30.5	17.5	11.0	1.1	45.0	34.2	19.7
CFA	5.2	36.2	4.3	25.2	14.9	22.5	41.8	7.2	13.6	17.2	26.0	48.4	8.3
CFB	4.8	32.8	5.0	28.6	13.8	29.7	37.9	8.3	10.3	15.4	33.1	42.2	9.3
CFC	5.6	27.8	5.9	28.7	16.1	29.0	32.0	9.8	13.0	18.6	33.4	36.8	11.2
CTA	4.7	36.3	4.3	25.8	13.4	24.5	42.0	7.2	12.9	15.4	28.1	48.2	8.3
CTB	5.5	31.9	4.8	27.0	16.0	25.6	36.8	8.1	13.3	18.5	29.8	42.5	9.3
CTC	5.3	26.5	5.8	28.9	15.4	30.3	30.6	9.7	14.0	18.0	35.3	35.5	11.3
CNA	23.1	4.1	3.0	34.0	66.6	15.8	4.8	5.0	7.9	72.3	17.1	5.2	5.4
CNB	23.5	4.4	2.6	33.8	67.8	14.9	5.1	4.4	7.9	73.6	16.1	5.5	4.8
CNC	25.7	4.6	2.3	32.5	74.2	8.5	5.3	3.8	8.2	80.8	9.3	5.8	4.2

ICP MINERALOGY (AREA%) COMPARED TO IMAGE ANALYSIS MINERALOGY (AREA%) TABLE 3.19

	ICP Assays Normalized Mineralogy				ICP Assays Recalculated Area%				Image Analysis Assays Observed Area%			
Stream	Cp	Px	Gn	Sp	Cp	Px	Gn	Sp	Cp	Px	Gn	Sp
74A	3.5	35.5	30.6	30.4	4.2	36.2	20.8	38.8	2.5	38.0	27.3	32.1
74B	6.3	39.7	33.4	20.6	7.9	41.7	23.4	27.0	6.3	40.0	31.6	22.2
74C	7.8	44.8	30.7	16.7	9.7	47.0	21.5	21.8	9.8	46.8	29.6	15.7
76A	4.7	32.4	36.8	26.1	5.9	34.1	25.8	34.3	5.0	34.4	30.0	30.7
76B	7.5	36.6	38.3	17.7	9.5	39.3	27.4	23.7	7.5	37.6	35.8	19.2
76C	9.3	39.7	36.2	14.7	11.9	42.5	25.8	19.7	13.3	43.3	29.7	18.5
RTA	0.8	34.3	35.8	29.0	1.0	36.0	25.0	38.0	3.4	33.9	30.1	32.5
RTB	0.9	43.7	34.0	21.4	1.1	46.4	24.1	28.4	2.5	47.4	28.6	21.6
RTC	1.1	45.0	34.2	19.7	1.4	48.0	24.4	26.3	1.4	47.7	31.3	19.6
CFA	17.2	26.0	48.4	8.3	23.0	29.2	36.2	11.6	16.1	29.4	46.6	7.8
CFB	15.4	33.1	42.2	9.3	20.0	36.3	30.9	12.8	12.5	33.2	44.9	9.5
CFC	18.6	33.4	36.8	11.2	23.5	35.5	26.1	14.9	19.3	36.6	32.0	14.8
CTA	15.4	28.1	48.2	8.3	20.6	31.6	36.1	11.6	10.5	35.3	44.2	10.0
CTB	18.5	29.8	42.5	9.3	24.0	32.5	30.9	12.7	12.7	33.2	43.8	10.4
CTC	18.0	35.3	35.5	11.3	22.6	37.3	25.1	14.9	19.2	39.2	30.8	11.2
CNA	72.3	17.1	5.2	5.4	75.9	15.1	3.0	5.9	65.9	23.1	5.6	6.0
CNB	73.6	16.1	5.5	4.8	77.3	14.2	3.2	5.3	74.1	20.8	1.6	3.6
CNC	80.8	9.3	5.8	4.2	84.0	8.1	3.4	4.6	74.1	14.5	7.2	4.3

Cu Circuit Chalcopyrite Assays

(Image Analysis vs. ICP)

Figure 3.2

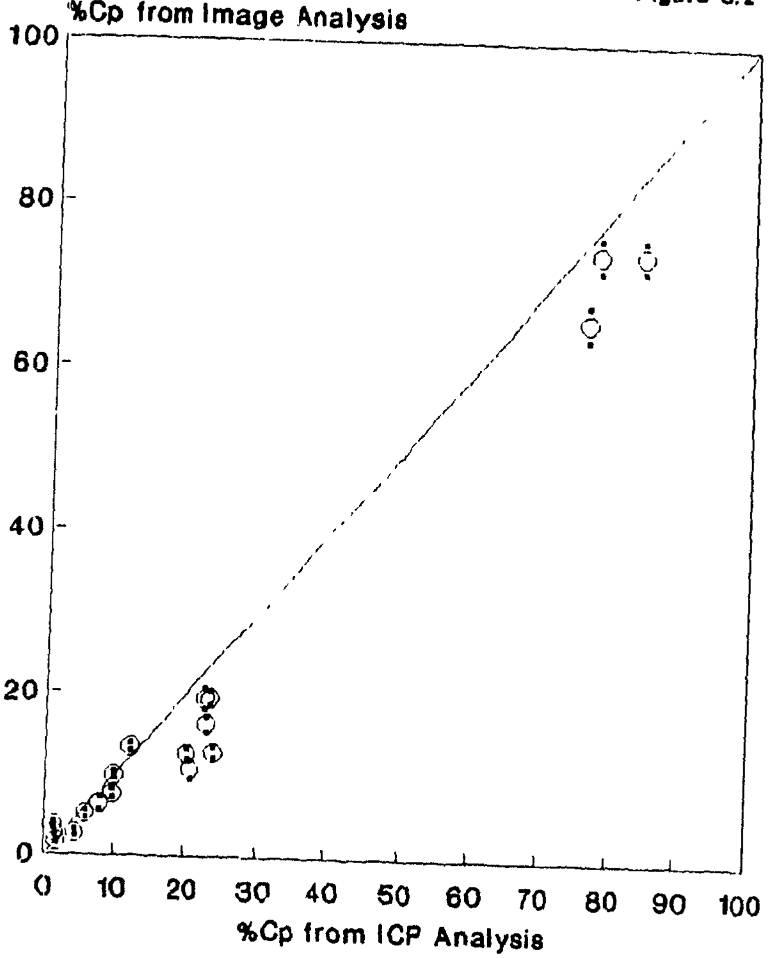

Cu Circuit Galena Assays

(Image Analysis vs. ICP)

Figure 3.3

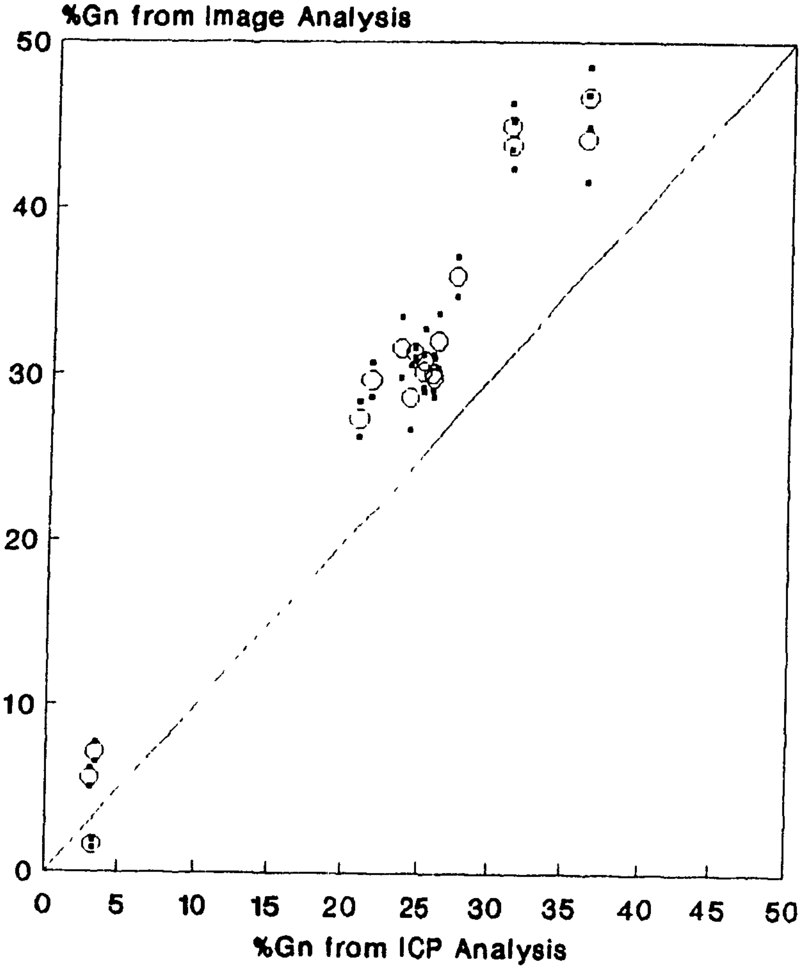

Cu Circuit Iron Mineral Assays

(Image Analysis vs. ICP)

Figure 34

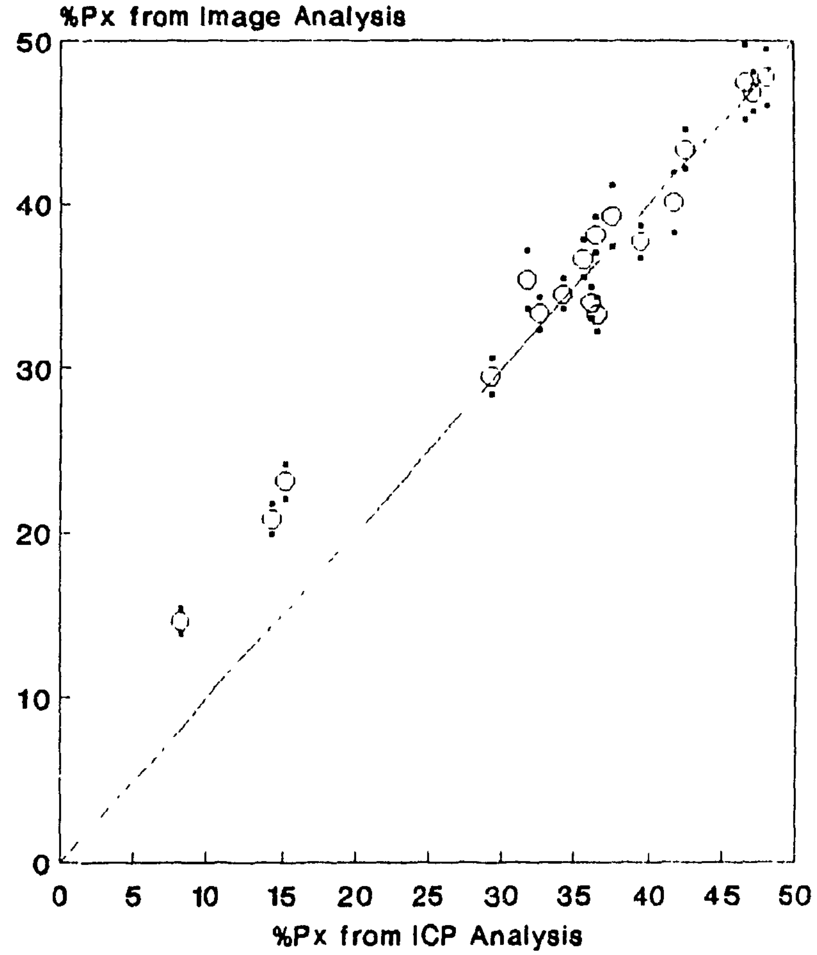

Cu Circuit Sphalerite Assays
(Image Analysis vs. ICP)

Figure 3.5

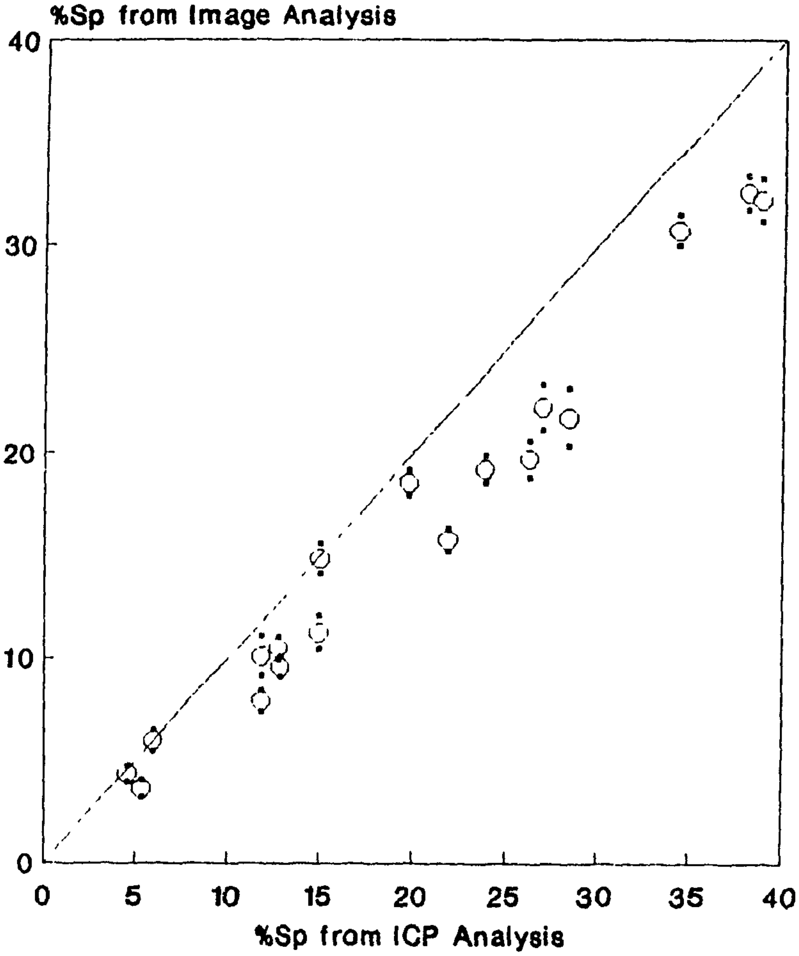

Thirdly, the deviation of the image analysis assays from linearity (i.e. the scatter) is greater than that which can be explained by sampling precision.

There is a need for further investigation of the image analysis assays and chemical assays, since a straight comparison of the two reveals the presence of anomalies but offers no quantitative explanation. The general direction of the bias (eg. overestimation of galena and underestimation of both sphalerite and chalcopyrite) could be anticipated from the halo and data scrapping effects as previously described; nonetheless, the fact that assay comparison is so extensively used as a quality check for image analysis data requires that the lack of correlation be further investigated.

The first task is to verify that the reconstructed mineralogy from ICP is a true reflection of the actual mineralogy. In other words, some confirmation is required both that the ICP analyses are correct and that the expected mineralogy is that which actually was present in the sample. This can be done by statistical reconstruction of the mineral assemblage, as follows:

1) The assays for iron, copper, zinc, lead and sulfur are added, yielding a number somewhat less than 100%. The unaccounted mass (UA) is assumed to be silicates, etc. which contain very little copper, zinc, lead or sulfur but which are expected to contain significant quantities of iron.
2) The iron assay is regressed against copper, zinc, lead, sulfur and UA with the regression forced to pass through zero. This reflects the fact that iron must associate with at least one of the other species. The amount of iron associated with silicates is deducted from the iron assay and added to unaccounted mass. This leaves sulfide iron, copper, zinc, lead and sulfur.
3) Sulfur is regressed against iron, copper, zinc and lead. Iron is expected to cross-correlate with both copper and zinc, so that no minerals can be isolated from these elements on the basis of the sulfur regression. However, the sulfur associated with lead is not expected to cross-correlate with any of the other species and is therefore removed from the total sulfur assay.
4) Iron is regressed against copper, zinc and sulfur.
5) Two equations have now been obtained for four variables. These equations calculate i) sulfur in terms of copper, zinc, and iron; and ii) iron in terms of copper, zinc and sulfur. The equations are combined to solve for sulfur in terms of copper and zinc, and iron in terms of

copper and zinc. It is assumed that no cross-correlation exists between copper and zinc.

6) The amounts of copper-iron-sulfur mineral and zinc-iron-sulfur mineral are calculated, with residual sulfur and iron assigned to the iron minerals using the ratio calculated in (4).

8) The sulfur and iron residuals are regressed against the iron, copper and zinc minerals to ensure that the residuals do not correlate against any of the minerals.

This procedure yielded results as follows:

1) Unaccounted mass was calculated as having a composition of 81.2% unaccounted and 18.8% iron. The standard error of the Fe/UA ratio was 36%. This is a reasonable value for the type of iron-bearing silicates which host the BMS deposits.

2) The Pb mineral was calculated as containing 85.9% Pb and 14.1% S, with the standard error for the S/Pb ratio was equal to 11%. Theoretical values for galena are 86.6% Pb and 13.4% S.

3) The iron minerals were calculated as having an assay of 47.8% Fe and 52.2% S, with a standard error for the Fe/S ratio equal to 3%. The theoretical value for pyrite equals 46.6% Fe and 53.4% S.

4) The copper mineral was calculated as having an assay of 30.5% Cu, 32.1% Fe and 37.5% S. The theoretical value for chalcopyrite equals 34.7% Cu, 30.4% Fe and 34.9%S. The recalculated assay can also be expressed as 88% stoichiometric chalcopyrite with 12% iron minerals of composition 44.0% Fe and 56.0% S. The standard errors for the Fe/Cu and S/Cu ratios were 54% and 44%, respectively.

5) The zinc mineral was calculated as having an assay of 36.2% Zn, 30.0% Fe and 33.8% S. The theoretical value for BMS sphalerite equals 60% Zn, 6.7% Fe and 33.3% S. The recalculated assay can be interpreted as 36% sphalerite with 64% iron minerals containing 47.1% Fe and 52.9% S. The standard errors for the Fe/Zn and S/Zn ratios were 12% and 10%, respectively.

6) Iron and sulfur residuals averaged 0% with a standard deviation of 0.25%.

The procedure suggests that three populations of iron minerals exist, one occurring by itself and one each with sphalerite and chalcopyrite. This gives rise to a calculated zinc mineral which includes an associated sulfur-deficient iron mineral, as well as a calculated copper mineral which includes a sulfur-rich iron mineral. However, the relative errors of the postulated iron mineral compositions are too large to provide statistical evidence for more than one iron mineral. The results indicate that the ICP analyses are essentially correct, and demonstrate the utility of this statistical method.

mineralogy, suggesting that both the assays and the assumed mineralogy are correct.

It is attractive to attempt a regression based analysis of whether or not the image analysis mineralogy corresponds to the ICP mineralogy. However the halo and scrapping effects result in a non-linear correspondence. For example, if the halo effect systematically increases the apparent galena area by a fixed proportion, then there will be a non-linear increase in the image analysis galena assay, the magnitude of which depends upon the absolute assay. To demonstrate, a case is described where the assay quantity of Galena (G_{ass}) is multiplied by some constant "a" to obtain observed galena (G_{obs}), while other area (A_{ass}) is multiplied by "b" to obtain observed other area (A_{obs}):

$$G_{ass} + A_{ass} = 1$$
$$G_{obs} = aG_{ass} / (aG_{ass} + bA_{ass})$$
$$G_{obs} / G_{ass} = a / ((a-b)G_{ass} + b) \quad \text{(slope varies as a function of } 1/G_{ass}\text{)}$$

Thus, one cannot simply compare observed mineralogy to assay mineralogy. Some attempt must be made to estimate the halo and scrapping bias to see whether or not this can explain the discrepancy.

In this analysis galena had significant halo effects, but required little scrapping to remove ambiguous features. Both the presence of halos and the comparatively low degree of scrapping tend to increase the apparent galena assay. Sphalerite was relatively easy to identify, and therefore required only a moderate amount of scrapping. Chalcopyrite required quite aggressive processing since it was difficult to identify. Chalcopyrite also tended to form smaller occurrences than sphalerite and pyrite, leading to a greater loss of data when small features were removed. Pyrite lay at the low end of the gray level scale, and therefore required very little scrapping to remove unwanted artifacts. However, pyrite was not particularly prone to elevation of the assay by halo effects. It was therefore expected that the major bias in the recalculated assay would be dominated by the elevation of the galena assay, and to a lesser extent by the diminution of the chalcopyrite assay.

The equation derived above can be rearranged to yield a relationship between the microscopically observed and true assays of galena, as follows:

$Gn_{obs} = aGn_{ass} / [(a-b)Gn_{ass} + b]$ or if $b=1$,
$a = (Gn_{obs}Gn_{ass} + Gn_{obs}) / (Gn_{obs}Gn_{ass} - Gn_{ass})$

The value of "b" is arbitrarily set to one, since it is only the relative elevation of the galena assay which is of importance. This allows the value of "a" to be calculated from the observed and assayed vaues for galena, yielding an initial estimate of the galena bias. Starting with this initial estimate, biases are added by trial and error to the other minerals to produce the best linear data fit between ICP and area mineralogy.

A set of biases which produced good results was Gn=1.6, Px=1.2, Sp=1.0, Cp=0.8. In other words, one unit of galena appears in the assay as 1.6 units of area, while one unit of Px appears as 1.2 units, etc.. It is the relative shift in assays which is of importance. For example, the above numbers could be equally well expressed as Gn=1.0, Px=0.75, Sp=0.63, Cp=0.5. To convert assays into observations the ICP area percent analyses are multiplied by the appropriate bias factor, then the result abundances scaled to 100%. This produces the data of Table 3.20, which is plotted in Figures 3.6 to 3.9.

It can be seen the failure of the image analysis data to correspond to the ICP data can be more or less corrected by applying a fixed multiplier to the individual minerals, making it unneccessary to postulate the misidentification of mineral species. This does not constitute a proof of correct mineralogical identification; however, it does demonstrate that the observed errors can be explained by expected and systematic phenomena.

In summary, recalculated assays from image analysis do not necessarily correspond to chemical analyses. Thus, image analysis data cannot be adequately tested by this manner. The procedures which lead to the collection of correct structural information in appropriate quantities tend to alter the apparent composition, since the various mineral species may have different tendencies to form halos, different grain sizes which vary the proportion of occurrences which will appear as ambiguous pixels, or different ease of identification.

The effort in this work to identify the sources of error in recalculated assays and to explain the observed deviations is necessitated by the fact that recalculated assays are used almost universally in image analysis based liberation studies to make some comment upon data validity. It is proposed in this work that the comparison is not useful, and may in fact lead to a conscientious effort to preserve recalculated grade at the expense of both the quantity and quality of structural data. It is certainly possible to preserve mineralogical abundances in image analysis; however, for the purposes of liberation work it is not necessarily desirable to do so within the limits of accuracy which would normally be considered quantitative.

MODEL FOR IMAGE ANALYSIS HALO AND SCRAPPING EFFECTS TABLE 3.20

	ICP Assays Recalculated Area%				Simulated IA Data from ICP Analysis				Image Analysis Assays Observed Area%			
Stream	Cp	Px	Gn	Sp	Cp	Px	Gn	Sp	Cp	Px	Gn	Sp
74A	4.2	36.2	20.8	38.8	2.8	36.6	28.0	32.6	2.5	38.0	27.3	32.1
74B	7.9	41.7	23.4	27.0	5.2	41.5	31.0	22.3	6.3	40.0	31.6	22.2
74C	9.7	47.0	21.5	21.8	6.5	46.9	28.5	18.1	9.8	46.8	29.6	15.7
76A	5.9	34.1	25.8	34.3	3.9	33.8	34.0	28.3	5.0	34.4	30.0	30.7
76B	9.5	39.3	27.4	23.7	6.2	38.5	35.8	19.4	7.5	37.6	35.8	19.2
76C	11.9	42.5	25.8	19.7	7.8	41.9	34.0	16.2	13.3	43.3	29.7	18.5
RTA	1.0	36.0	25.0	38.0	0.7	35.4	32.8	31.1	3.4	33.9	30.1	32.5
RTB	1.1	46.4	24.1	28.4	0.7	45.1	31.2	23.0	2.5	47.4	28.6	21.6
RTC	1.4	48.0	24.4	26.3	0.9	46.5	31.5	21.2	1.4	47.7	31.3	19.6
CFA	23.0	29.2	36.2	11.6	15.0	28.5	47.1	9.5	16.1	29.4	46.6	7.8
CFB	20.0	36.3	30.9	12.8	13.2	35.8	40.5	10.5	12.5	33.2	44.9	9.5
CFC	23.5	35.5	26.1	14.9	15.9	36.0	35.4	12.7	19.3	36.6	32.0	14.8
CTA	20.6	31.6	36.1	11.6	13.3	30.6	46.6	9.4	10.5	35.3	44.2	10.0
CTB	24.0	32.5	30.9	12.7	15.9	32.4	41.1	10.5	12.7	33.2	42.8	10.4
CTC	22.6	37.3	25.1	14.9	15.4	38.0	34.0	12.7	19.2	39.2	30.8	11.2
CNA	75.9	15.1	3.0	5.9	67.7	20.2	5.4	6.6	65.9	23.1	5.6	6.0
CNB	77.3	14.2	3.2	5.3	69.2	19.1	5.8	5.9	74.1	20.8	1.6	3.6
CNC	84.0	8.1	3.4	4.6	77.4	11.2	6.2	5.2	74.1	14.5	7.2	4.3

Cu Circuit Chalcopyrite Assays
(Model for IA Halo/Scrapping Effects)

Figure 3.6

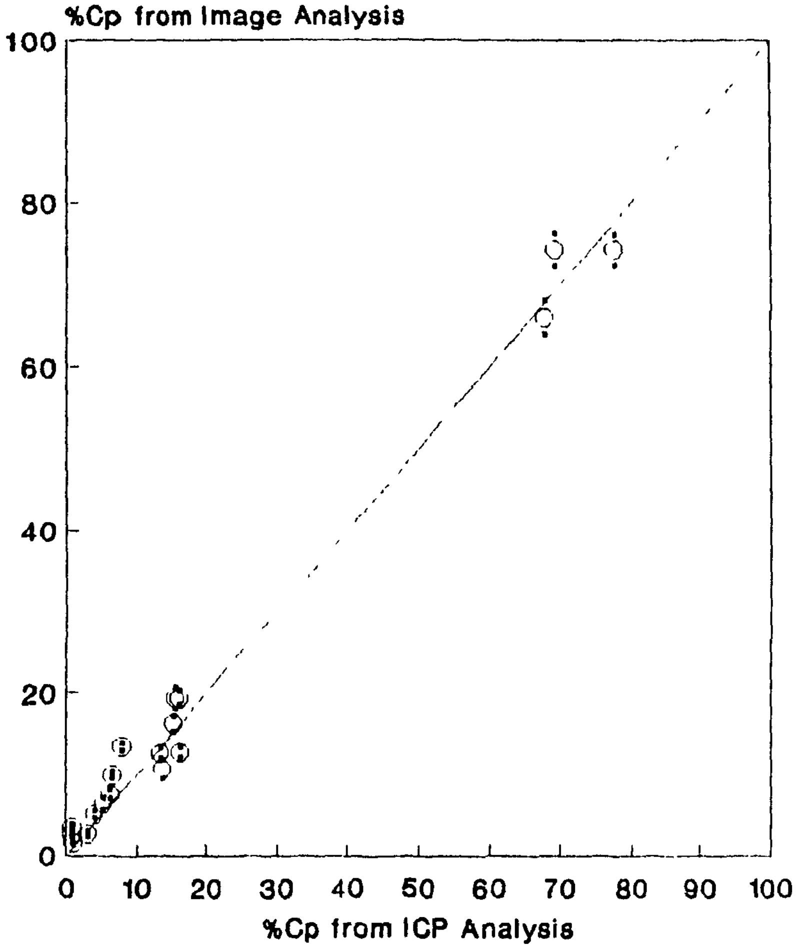

Cu Circuit Galena Assays
(Model for IA Halo/Scrapping Effects)

Figure 3 7

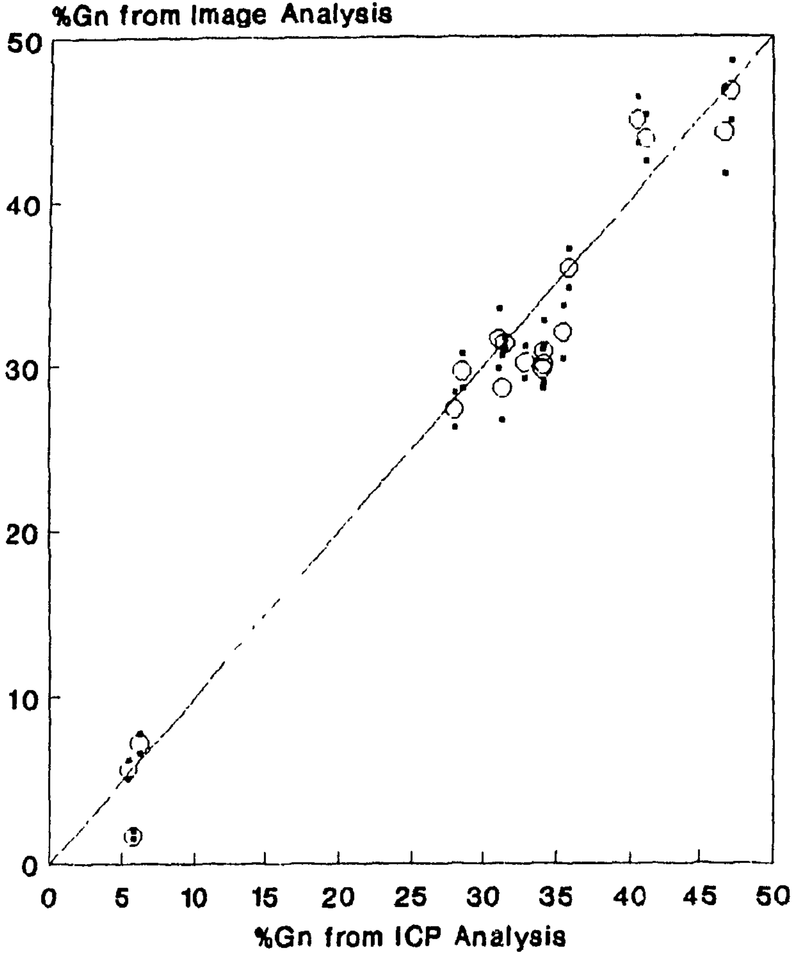

Cu Circuit Iron Mineral Assays
(Model for IA Halo/Scrapping Effects)

Figure 3.8

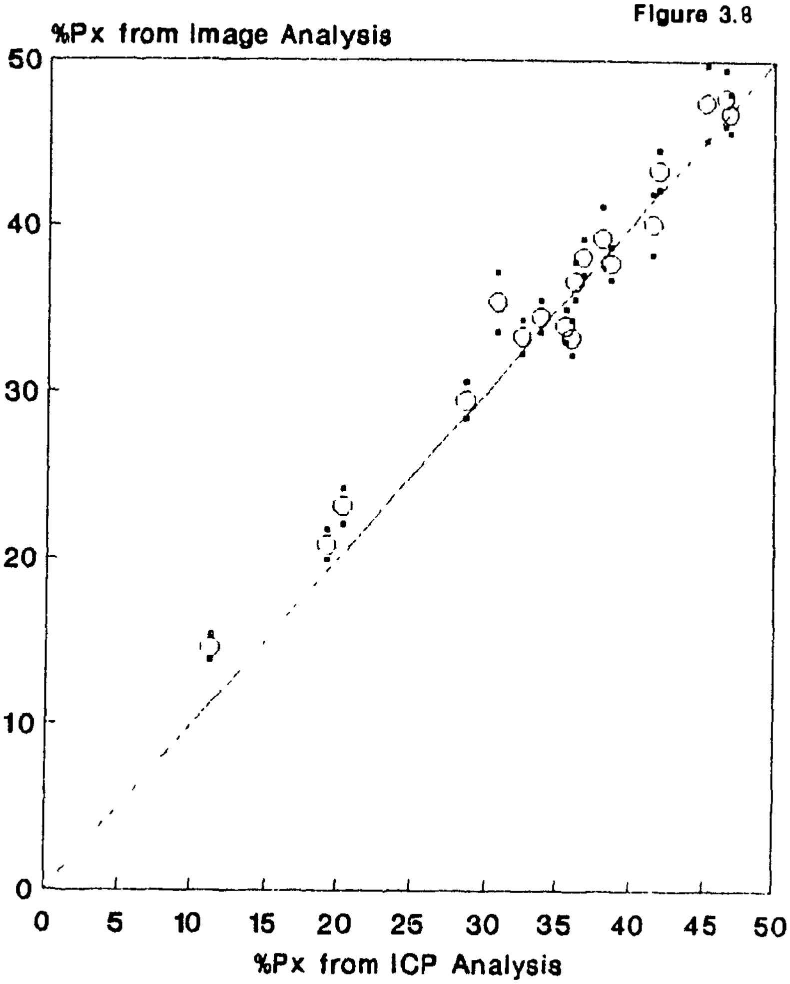

Cu Circuit Sphalerite Assays

(Model for IA Halo/Scrapping Effect)

Figure 3.9

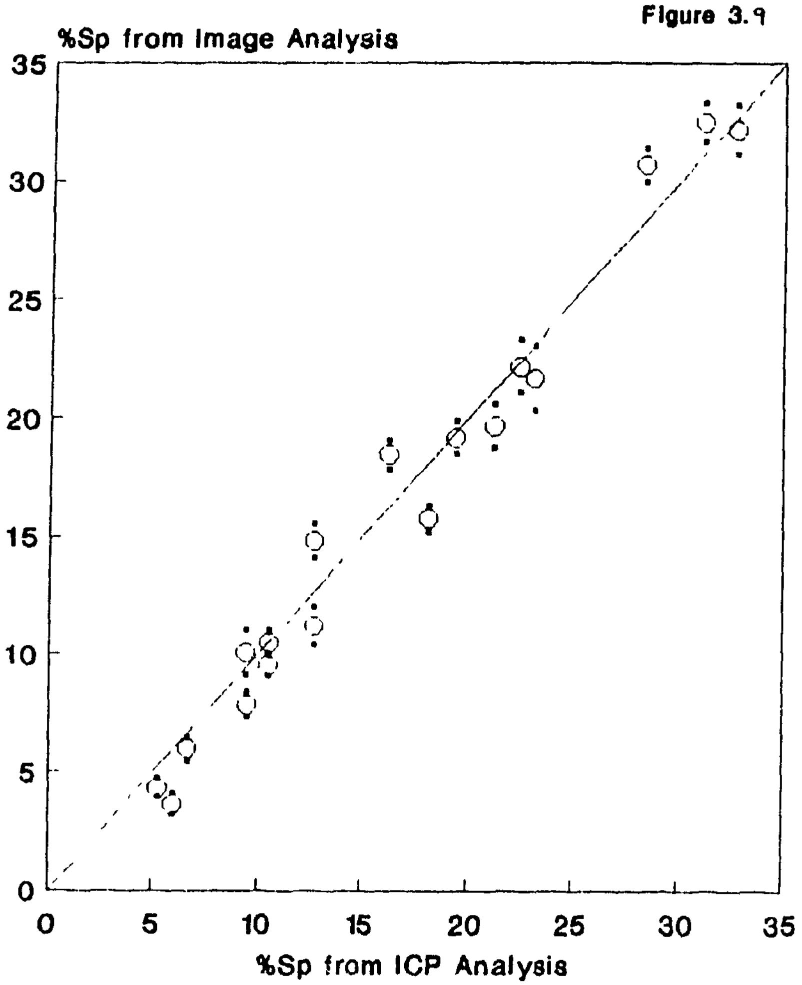

CHAPTER 4 : STEREOLOGICAL PROBLEMS IN LIBERATION STUDIES

4.0: Introduction

The goal of any microscopic study in mineral processing is to attempt to explain phenomena which are observed in plant practice in terms of the physical features of the ore. Typically the features of greatest interest would be size, liberation, and for flotation studies the degree of exposure of the flotable mineral at the surfaces of locked particles. Clearly these parameters are intended to describe three dimensional features; however, liberation studies employing micropscopy describe features in one dimension (linear intercepts) or in two dimensions (section areas). The data collected from microscopic studies is therefore subject to geometrical bias, usually referred to as stereological bias or stereological effects.

The simplest illustration of a locked particle is that of a sphere which contains two locked phases ("A" and "B"), both of which occupy half of the spherical volume and which are separated by a planar boundary (Figure 4.1). In three dimensional space the particle has a diameter "D" and a volumetric composition of 50% "A". However, it is clear that a line or a section through the particle will only rarely provide an accurate description of the particle size and composition.

For example, if a line was to be projected parallel to the X-axis through point "P" then the resultant intercept would describe the particle as having a diameter equal to chord length P-P' and a composition of 100% phase "A". The same line projected through point P but in a different orientation (eg. P-P") would describe the particle as having a diameter equal to chord length P-P" and a locked composition. Repeated sampling of the particle in one dimension would lead to a distribution of intercept sizes and compositions, whereas in reality the particle has only one size and composition. A similar phenomenon

Figure 4.1

Random Sectioning of a Sphere

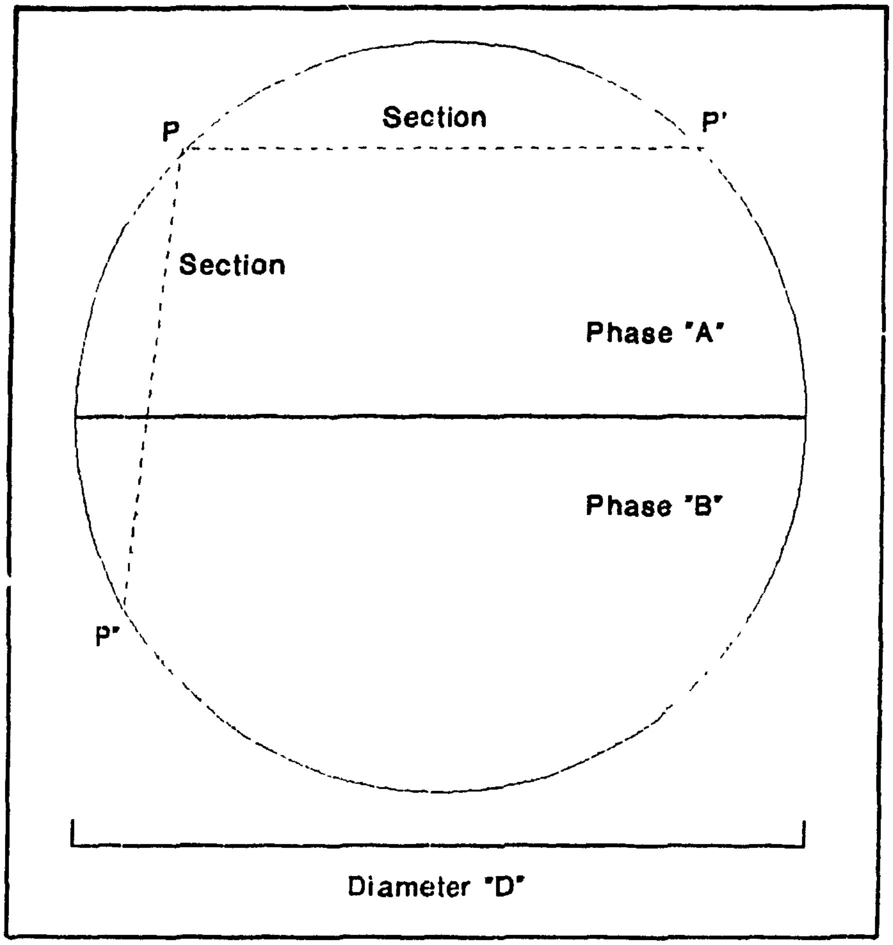

may be observed when the particle is sampled in two dimensions, since the chords P-P' and P-P" could just as easily be regarded as planar projections parallel to the Z axis (eg. standing out from the plane of the diagram). Repeated sectioning would result in a number of apparent sizes and compositions.

Two important points arise from the above. Repeated sampling of an individual locked particle in one or two dimensions results in a size distribution which is finer than the actual size, since a chord may be smaller than or equal to but not larger than the actual particle diameter. Repeated sampling will also yield a composition distribution which includes free observations of both phases. Liberation in a suite of particles will always be overestimated, since locked particles may generate free observations whereas free particles must always appear to be free. Thus, it is found that data from both one dimensional and two dimensional studies provides an incorrect description of the actual structural features present in the sample.

Quantitative description of stereological effects is a field of endeavor which has expanded simultaneously with the availability of computer hardware. Indeed, there is no unique quantitative solution to the problem, requiring that some model of particle sizes, shapes and textures be used to formulate a stereological correction. The need to apply stereological corrections to data severely limits the usefulness of image analysis as a descriptive tool, since the "correction" of the data requires complex mathematical transformations to be made, resulting in a considerable increase in the work involved. Moreover, there is no guarantee that the assumptions made in any particular mathematical model are strictly valid. Thus, one ends up with a corrected data set in which one has invested much time and effort and which may in fact be no better than or even worse than the uncorrected data.

Regardless of the fact that stereological phenomena present themselves in any image analysis data set, it is found that useful metallurgical interpretations can be and have been made from uncorrected data. This suggests that the magnitude of the stereological bias may not be great enough to overshadow the significance of the "real" information in the data set. Nonetheless, stereological phenomena cannot be discounted without making some attempt to estimate the type and magnitude of errors which are introduced.

One way to make such an estimation is to use a simple geometrical system which in some way emulates a particle assemblage but which is likely to produce a greater stereological bias than the assemblage itself. It follows that if the information from the artificial assemblage can be usefully interpreted then the same will be found for the real assemblage. It also follows that if a simple procedure is found for correcting data from the artificial assemblage then this same procedure will overcorrect data from the actual assemblage. The description of particles from the true assemblage will then lie somewhere between the description provided by the original observations and that provided by the overcorrected data. This allows original data to be retained in making metallurgical interpretations, and avoids the necessity of abiding by a single set of possibly incorrect assumptions in applying a correction model.

In this discussion spheres with planar boundaries are used as the simple geometrical model for estimating stereological errors. The stereological phenomena observed in real particle assemblages is expected to be qualitatively the same as and quantitatively less than the errors calculated for the spherical model. Corrections which restore sectional observations to a description of the particle assemblage are expected to overcorrect data from real assemblages.

The goal of this analysis is to devise the simplest possible method by which section information may be interpreted. Thus, the description of stereological phenomena for spherical particles starts off with a rigorous mathematical discussion of the phenomena and is subsequently simplified to an approximation which allows stereological correction to be made in a semi-quantitative way that requires little effort or data manipulation. It is believed that this is the optimum way in which the consideration of stereological phenomena may be incorporated into practical studies.

4.1: Effects of Stereology on Size Analysis

Using the example of spherical particles some quantitative estimation may be formulated concerning the distribution of section sizes which may be expected during random particle sampling. The description hinges upon a correct description of randomness, and is facilitated in the spherical model by the perfect symmetry of the particles.

A random plane through a particle must touch the surface of the particle at some point "P" (Fig. 4.2). The location of this point is arbitrary, since all locations on the spherical surface are considered to be equivalent.

Given that the plane includes point "P", a normal to the plane may be drawn through "P" to describe the orientation of the section. Sections with unique orientations have unique orientations of the normal vector. A hemisphere may be drawn around "P" (here pictured with a a radius R_t equal to 2, or twice the radius of the particle). If the plane is randomly oriented than the flux of normal vectors through the target hemisphere will be uniform. Thus, the proportion of planes with normals between height zero (height of "P") and height "H" will be equivalent to the proportion of the surface area of the target occurring between height zero and height "H". The proportion of target surface area is a linear function of "H", so that random planes have normals through "P" with random heights on the target.

Figure 4.2

Size/Frequency Function for Random Sections

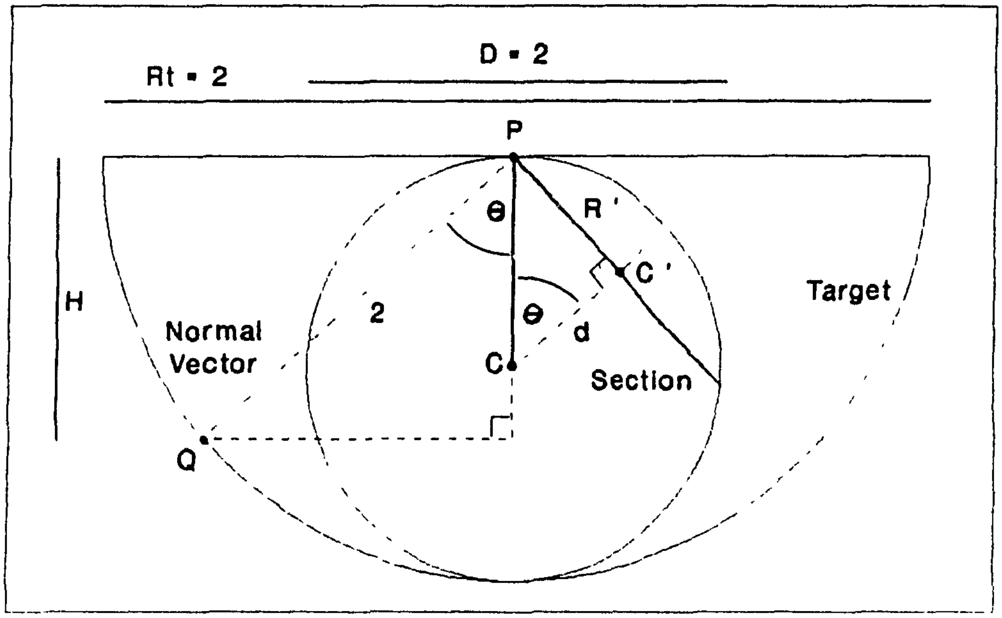

Figure 4.3

Size/Frequency Function for Random Intercepts

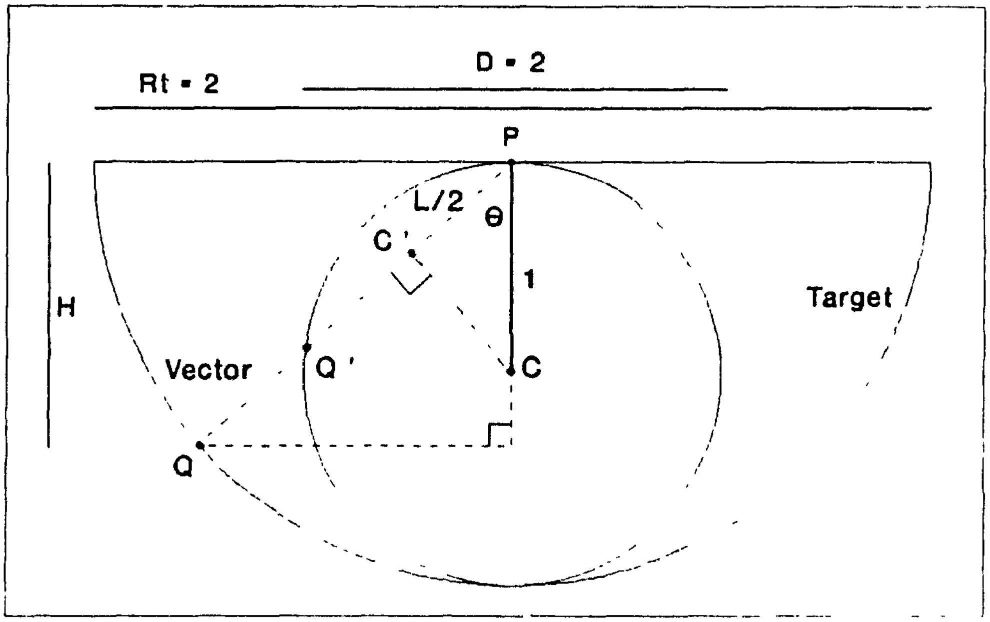

Figure 4.4

Comparison of Sections and Intercepts

Sampling of a Spherical Particle

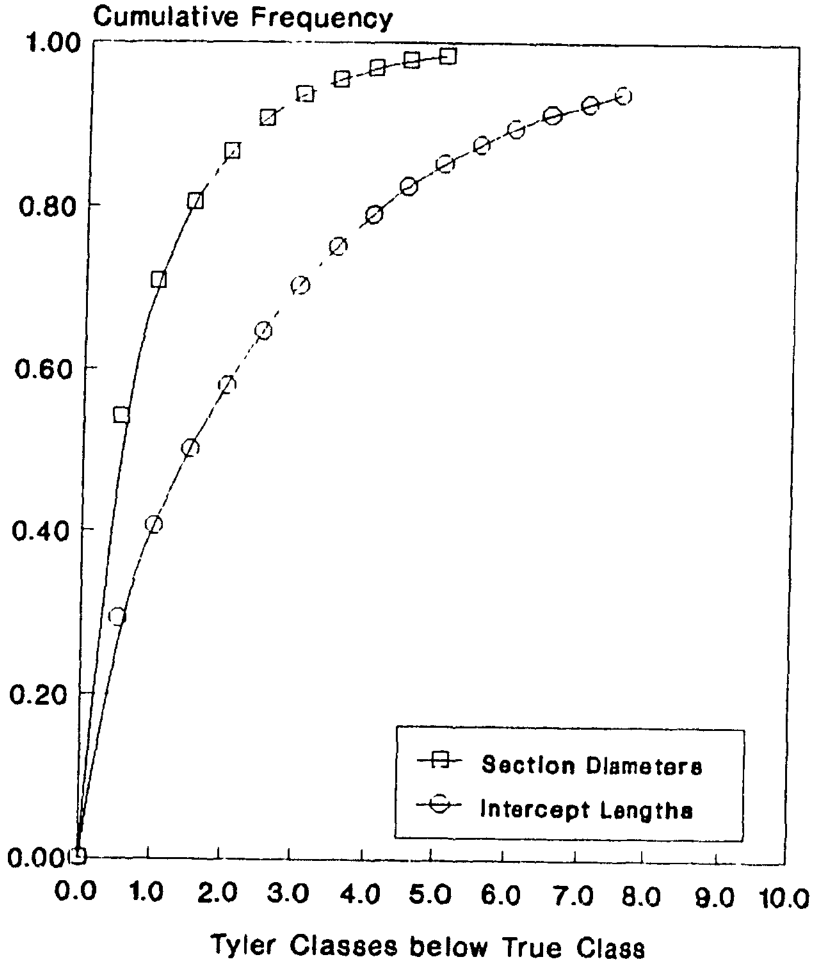

If a normal through a random plane happens to strike the target at point "Q" then the some angle "θ" will be subtended between the lines P-Q and P-C (C being the centre of the circle). If a normal to the section is drawn through "C" then it will have length "d" and describe an identical angle "θ" from the line P-C. The height of line P-Q will equal $R_t \cos(\theta)$, while the length "d" will equal $R \cos(\theta)$. Thus, $d = H/2$.

The radius of the section is described by length R', which is equal to $\sqrt{}(R^2 - d^2)$ or $\sqrt{}(1 - d^2)$. Thus, the radius of a section whose normal strikes the target at height "H" will be equal to $R' = \sqrt{}(1 - H^2/2R_t)$. The cumulative frequency function describing sections between radius zero ($H/R_t = 1$) and radius R' is therefore as follows:

$$F(R') = H / 2R_t = 1 - \sqrt{}(1 - R'^2)$$

A similar case may be laid out for linear intercepts. The particle of unit radius is redrawn, along with the hemispherical target (Figure 4.3). In this case it is the intercepts themselves which must have a uniform vector flux through the target. Thus, a random intercept will have a random height "H" on the target. An intercept striking the target at Q will have a length equal to the line P-Q'. The height on the target will equal $R_t \cos \theta$. If the intercept is bisected by a normal through the particle center (line C-C') then it may easily be verified that the length of the intercept is $L/2 = \cos(\theta)$, or $L = 2 \cos(\theta)$, or $L = 2H/R_t$. Thus, the cumulative frequency function for intercepts of between length zero and "L" will equal:

$$F(L) = L/2$$

Figure 4.4 illustrates the range of section and intercept sizes which would be expected during the sampling of spherical particles with unit diameter. The calculations are expressed as cumulative frequency vs. Tyler size classes below the true size. Numerical values are as follows:

Classes below True Size	Cumulative Frequency (Sections)	Cumulative Frequency (Intercepts)
1	70.7	29.3
2	86.6	50.0
3	93.5	64.6
4	96.8	75.0

It is observed that linear intercepts yield a more stereologically biased view of the particle size than do sections.

4.2: Example of Microscopic Size Analysis

It is seen that stereological bias alters the apparent size distribution of particles; however, the magnitude of the observed error is a function of both the particle shape and the number of size classes which are examined simultaneously.

Description of the size of a particle is, in itself, a difficult task. Typically a wide range of aspect ratios may be observed, with some minerals cleaving to form particles which are significantly elongated or even fibrous. The physical methods of size separation and measurement (screening, cyclosizing, sedimentation etc.) become less efficient as the aspect ratio increases. Cyclosizing or analysis by sedimentation have the additional limitation of being sensitive to particle density. Thus, it is expected that differences may exist between size analyses performed by various methods. One problem with examining stereological effects upon size is that there is no single method of unambiguously determining a "true" size.

Petruk[8] assessed the problem of differences between screen sizes and sizes observed in polished section, using samples which contained a fixed number of Tyler mesh sizes, ranging from 0.5 to 9.0 size classes per sample. Discrepancies between the true and observed sizes were used to calculate empirical "correction factors" which were proposed as a means by which subsequent microscopic analyses could be converted to screen analyses.

In actual fact the discrepancy between screen sizes and section sizes may be explained very well using the simple spherical model developed above. To simulate sectioning of a range of sizes one need simply add together the expected assemblages for a number of closely spaced individual sizes. For the purposes of this comparison assemblages of various particle size ranges were created by adding together increments of 0.05 Tyler classes, yielding simulated assemblages of particles with size ranges equivalent to those used by Petruk.

Petruk's data ("observed") has been interpolated from the published figures and is presented against data for spheres ("predicted") in Figures 4.5 to 4.8. The differences between the observed and predicted data are negligible. The only inconsistency arises in the sample containing 9 size classes. In this sample the observed distribution is actually coarser than the "true" distribution. This is a result of the assumptions made in this comparison concerning the composition of the sample. For modeling purposes the figures assume that each size class within the sample contains an equal number of particles. In actual fact the sample containing 9 size classes used in Petruk's work contained a disproportionate number of coarse particles.

In theory the spherical sectioning model can be used to reconstruct particle assemblages from sectioning data. If N designates a true size range and N' designates a size range observed under the microscope then an N' * N matrix can be formed, with each column showing the frequencies of various size observations (N') from a single particle size (N). If the inverse of this matrix is multiplied by the observed microscopic assemblage (a 1 * N' matrix) the result

Figure 4.5

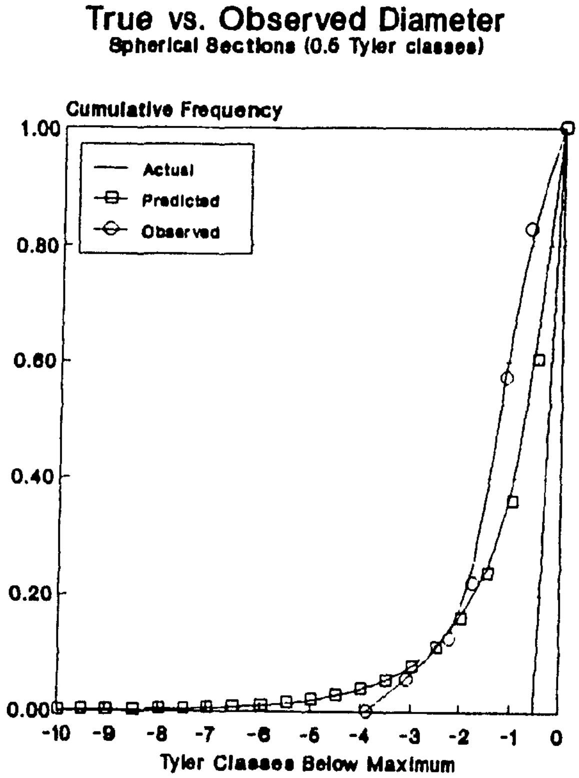

Figure 4.6

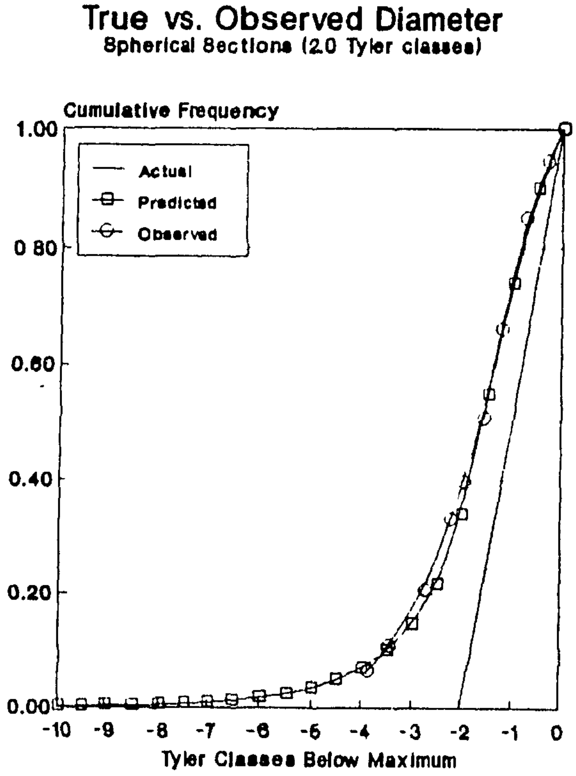

Figure 4.7

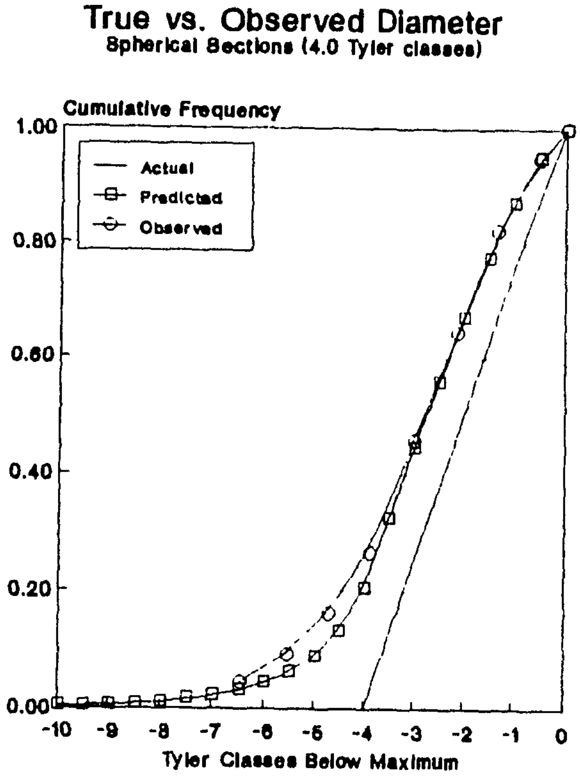
True vs. Observed Diameter
Spherical Sections (4.0 Tyler classes)

Figure 4.8

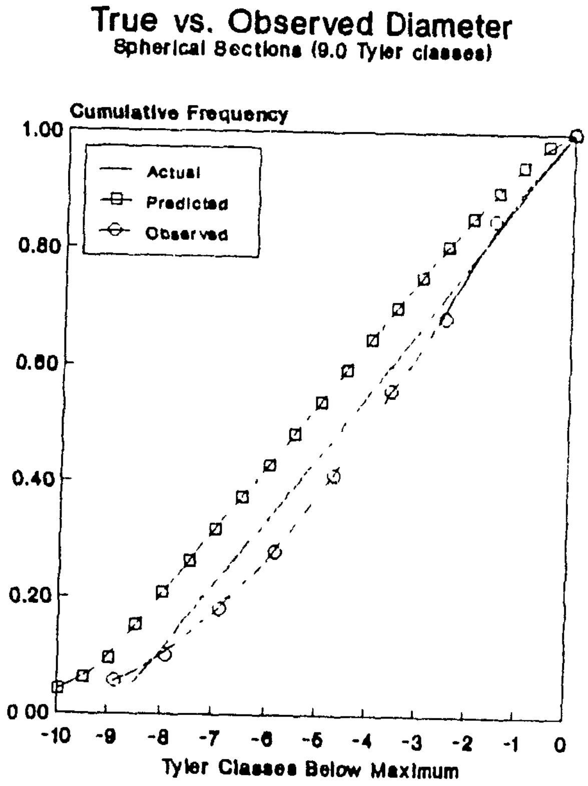
True vs. Observed Diameter
Spherical Sections (9.0 Tyler classes)

will be the true assemblage (a 1 * N matrix). While size reconstruction is not one of the goals of this work (since it has been maintained that sized samples should be used for liberation studies) it is proposed that the use of a spherical sectioning model could provide at least as good a reconstructive method as the use of empirical correction factors.

One interesting observation which may be made from Figures 4.5 to 4.8 is that the deviation between actual and observed sizes becomes less as more size intervals are included in the sample. This results from the fact that any size class other than the top size loses some observations to finer size classes but gains some from coarser classes. This manifests itself as a net cancellation of effects.

In summary, it is seen that stereological bias changes the apparent size distribution of particles. Data from one practical study correlates very well with model predictions derived from the simple system of spherical particles. The observed bias is a function of the number of size classes contained in the sample, and tends to be small if several size classes are present. It may be noted that Petruk's work involved sulphides, which tend to fracture into more or less equant particles. Particles with significant aspect ratios would not be described so well by the spherical model.

4.3: Qualitative Effects of Stereology upon Liberation

It is easy to give a phenomenological description of the effects of stereology upon liberation. Collection of one-dimensional or two-dimensional liberation data tends to "spread out" the composition distribution data, since particles with a unique composition may be sampled such as to make them appear to contain more or less of the phase of interest than they actually bear. Free observations will be generated from locked particles, so that liberation will be overestimated.

Stereological problems will be accentuated in particles of relatively simple mineralogical texture, and less important in particles of very intricate texture. The definition of "simple" or "intricate" texture is arbitrary, and relates largely to the ratio between mineral grain size and particle size. For example, if mineral crystals in an ore have a size of 1 mm and a large polished section is created from a single particle of 10 cm diameter there is little chance that only one mineral will be exposed. In fact, given a homogenous ore it is very likely that any polished section of this size would have a composition close to that of the ore sample as a whole.

Stereological problems are accentuated as the particle size approaches the grain size. For example, if the polished section from the above example contained particles of 1 mm diameter (about equal to the grain size) then the individual particles would be expected to contain one, two or perhaps three phases separated by relatively simple intercrystalline boundaries. Incidentally, it is this situation which is simulated by the spherical model. Sections through such particles do not necessarily reflect the true compositions of the particles.

At grind sizes much finer than the grain size stereology becomes less of a problem. For example, if the particle size in the above example was 0.1 mm (vs. a 1 mm crystal size) then most particles would be free. Of course, free particles cannot be sectioned to reveal anything but free particles.

In summary it is found that stereological problems are worst when the grind size is about equal to the grain size. This is the situation most commonly encountered in milling circuits. Liberation increases rapidly as the grind size approaches the grain size, then slows considerably once energy is expended in overgrinding particles which are already free. Expressed as energy input vs.

technical efficiency of downstream separation it is generaly found that the incremental benefit of additional energy input reaches a maximum at about the mineral grain size, beyond which large increments in energy are required for marginal gains in liberation. Since processing operations most commonly grind at or just beyond the point of largest marginal effect it is commonly found that process streams contain a fair number simple locked particles containing one or two interphase boundaries. (It should be noted that exceptions exist in the case of exceptionally fine textures and grinding, where progressively higher expenditure of energy is required to create progressively less size reduction. In such cases it is not uncommon to find that grinding fails to be feasible well before the crystal grain size is reached).

It is possible for minerals in an ore to differ in size one to another, and for individual minerals to possess a bimodal grain size distribution. One such case was seen in a study of Pine Point sphalerite [9] in which the ore texture showed sufficient bimodal characteristics to differentiate the textures into "simple" locking which could conceivably be removed by regrinding and "complex" locking which consisted of microfine inclusions, and could not be addressed by regrinding. (It was evident that the grinding strategy optimised liberation of the coarser texture but completely failed to address the finer texture). Stereological effects had to be considered in interpretation of the data for "simple" locking, but could be ignored in the interpretation of data for "complex" locking. Consideration of stereological bias must therefore include at least a cursory assessment of textural factors.

4.4: A Spherical Model for Quantitative Effects of Stereology

In order to properly interpret microscopic data it is necessary to have some idea as to the magnitude of stereological bias. The problem is studied here by referring back to the simple model of spheres with a planar boundary separating a major phase "A" from a minor phase "B".

It has already been determined that a random section through a sphere will have a random distance "d" from the centre of the sphere. Figure 4.9 presents a sphere with a section intersecting it at an arbitrary value of "d". The suite of sections which may be formed at this fixed distance may be simulated by allowing the section to assume a number of random orientations with respect to the A/B interface.

The approach is similar to that which was previously used for the prediction of size distributions. A normal to the section is drawn from the center of the particle to the perimeter, intersecting the perimeter at "P". If the orientation is random then the perimeter should have a uniform flux of intersections passing through it. Thus, a random section intersects the perimeter at a random height "H".

The reference direction in this model is a normal to the AB interface passing through the centre of the particle. The height "H" is measured in the direction of this normal. At any given value of "H" and "d" all sections are identical as a result of the symmetry of the particle.

An intersection at height "H" may be obtained by rotating the section θ_r from the reference normal. Thus, the height is equal to (1 - acos (θ_r)), with θ_r assuming values between 0 and π. Two other angles are used for the model, these being the angles subtended by the section boundary and the section normal (θ_d) and by the interface boundary and the interface normal (θ_i). The

Figure 4.9

Construction for Random Sectioning

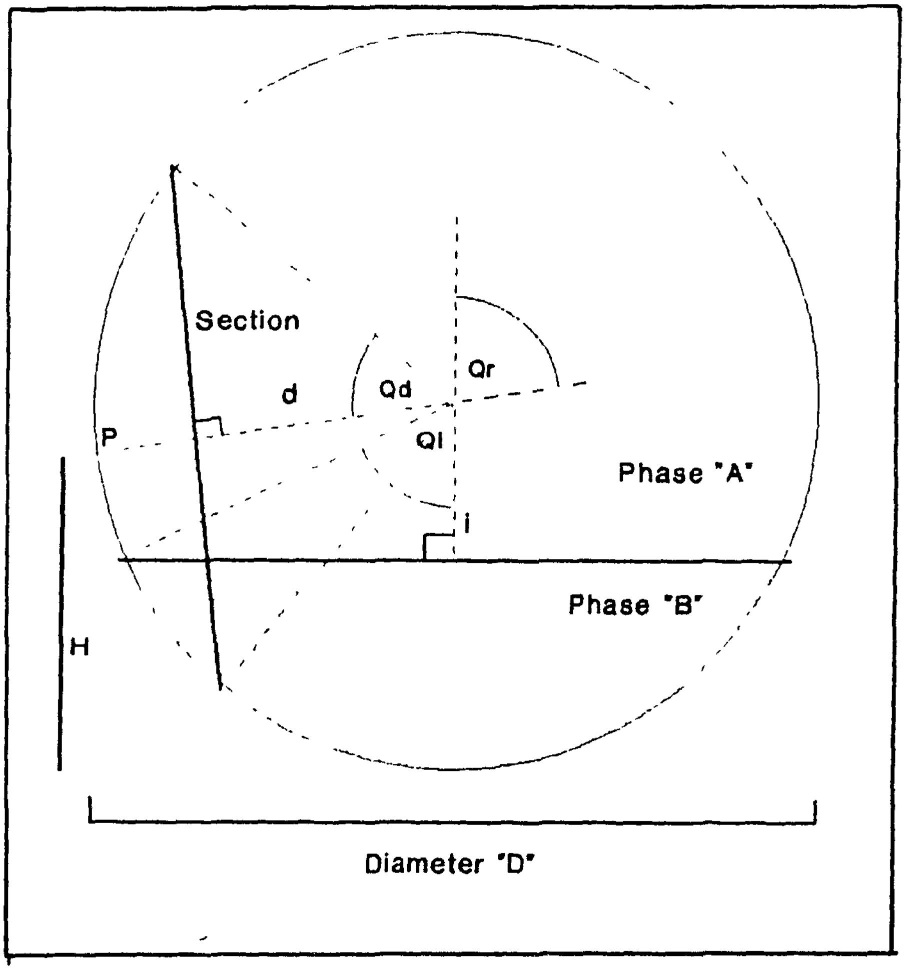

volumetric proportion of phase "B" may be calculated from distance "i" as follows:

$$V = (i^3 - 3i + 2) / 4$$

Some relationships may be observed between the angles θ_r, θ_i and θ_d:

$\theta_r < \theta_i - \theta_d$: Free "B" (occurs only when $d > i$)
$\theta_r < \theta_d - \theta_i$: Free "A" (occurs only when $i > d$)
$\theta_r > \theta_i + \theta_d$: Free "A"

$|\theta_i - \theta_d| < \theta_r > \theta_i + \theta_d$: Locked Section

The proportion of intercepts between any two values of θ_r is known exactly from the relationship between θ_r and H. Thus, the proportion of free and locked sections may be calculated exactly for any given particle composition (value of "i") and section distance "d". Since "d" is a random variable, the total number of locked and free sections may by obtained by a double integration through $(-1 <= \cos(Qr) <= 1)$ and $(0 <= d <= 1)$.

To complete the model, some means must be provided for estimating the composition (%A) of locked sections. Figure 4.10 shows a particle with a section intersecting both phases, and Figure 4.11 shows a view of the section oriented in the plane of the paper.

The co-ordinate system in Fig. 4.10 is set up such that the centre of the circle has height zero, with the interface at a height of $-i$. Since the interface is parallel to the x-axis any intersection with the interface must occur at $y = -i$.

A normal through the section passing through the centre of the particle intersects the section at point d', which is a distance "d" from the centre of the particle. The height of d' equals $(-d \cos \theta_r)$. The distance from d' to the interface (at point d") is designated by "x".

Figure 4.10

Evaluation of Locked Section Grade

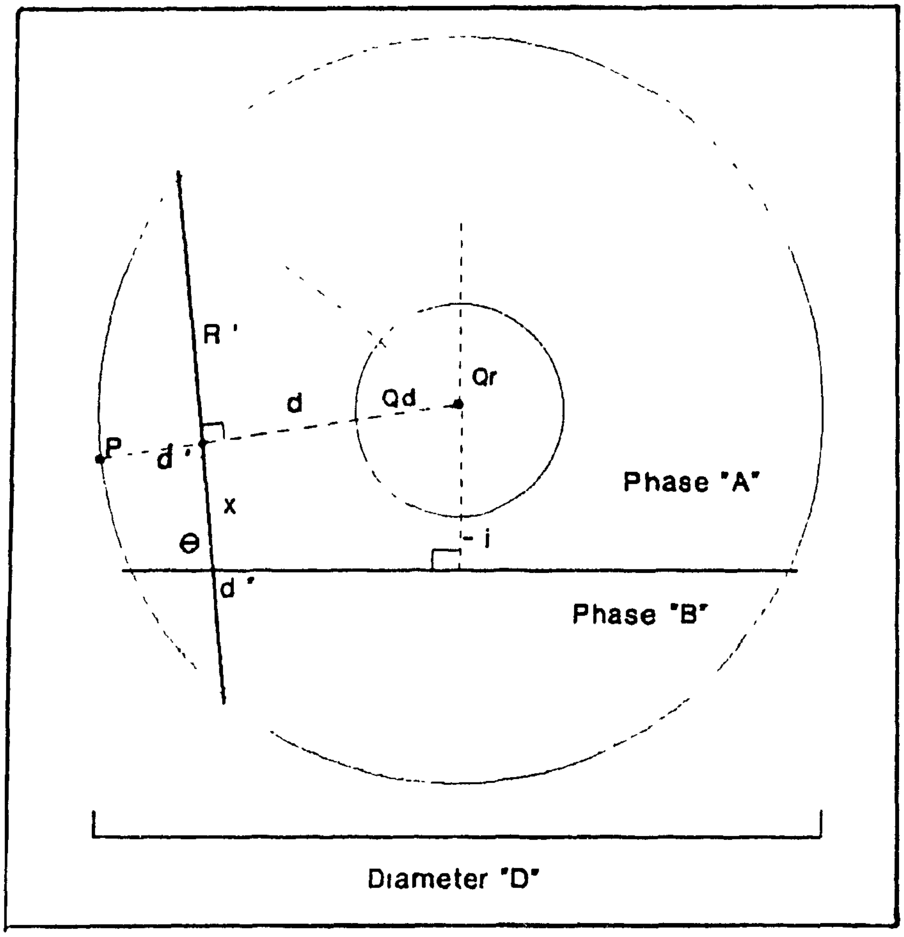

Figure 4.11

Projection of Locked Section

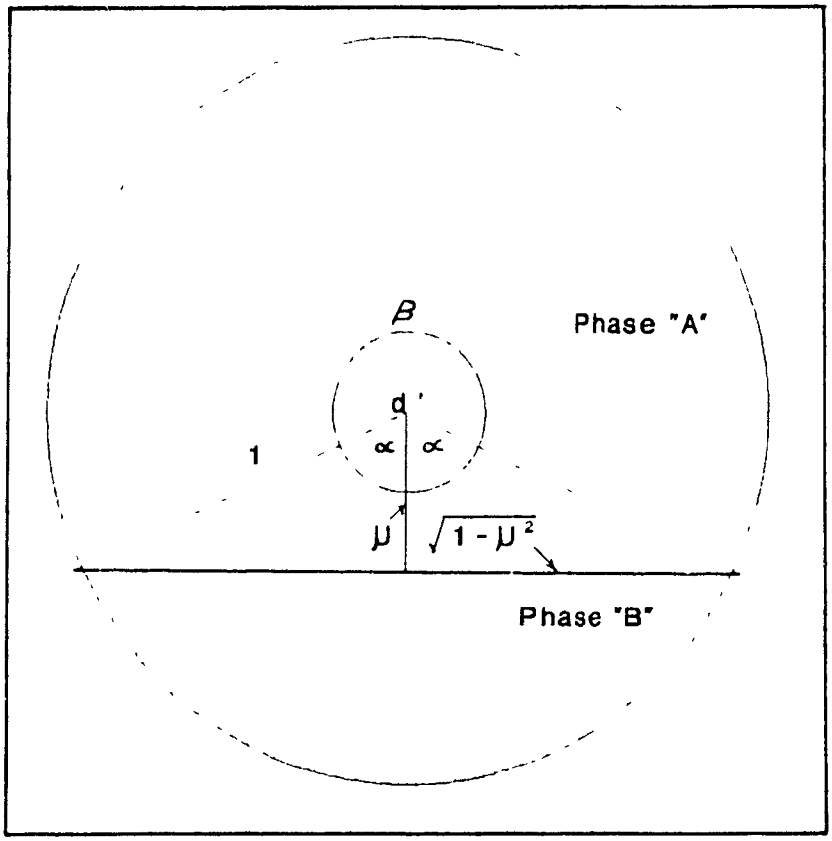

The height of d" equals the height of d' plus ($-x \sin \theta_r$). However, the height of d" is also equal to -i, so that:

$$-d \cos \theta_r - x \sin \theta_r = -i \qquad \text{or}$$

$$x = (i - d \cos \theta_r) / \sin \theta_r$$

The section has a radius R' equal to $\sqrt{(1 - d^2)}$. It is the ratio between x and R' which is needed to calculate the composition of the section. This ratio is called μ, where:

$$\mu = (i - d \cos \theta_r) / (\sin \theta_r \sqrt{(1 - d^2)})$$

Referring now to Figure 4.11, it may be seen that the angle (α) is equal to asin (μ), and the angle (β) is equal to ($\pi + 2$ asin (μ)). Thus, the segment of the circle subtended by (β) has a fractional area of ($\pi + 2$ asin (μ)) / 2π . The two triangles on the diagram have an area equal to ($\mu \sqrt{(1 - \mu^2)}$), or a fractional area of ($\mu - \sqrt{(1 - \mu^2)}$) / π. Thus, the fractional area occupied by phase "A" is equal to the fractional area of the segment plus the two triangles, as follows:

$$A = 0.5 + [\text{asin}(\mu) + \mu \sqrt{(1 - \mu^2)}] / \pi$$

A complete description of the section assemblage may therefore be obtained. The simplest method is to perform a stepwise approximation:

1) A value of "i" is selected, depending upon the particle composition to be simulated.
2) The value of "d" is set close to zero.
3) The value of "H" is varied between -1 and 1 in small increments, with a section composition (Free A, Free B or %A) and area recorded for each value of "H".
4) "d" is incremented by a small amount, and step (3) is repeated.

The procedure terminates when d=1.

The model was set up to increment "d" from 0.025 to 0.975 in increments of 0.050. The value of "H" was incremented from -0.99 to 0.99 in increments of 0.02. Thus, a total of 2000 observations were recorded per particle composition. Several particle compositions were simulated. The summed area of all observations should, of course, sum to 100 * (2π/3), which it did to within 0.2%. The recalculated particle composition from the summed sections should equal the particle composition, which it did to within 0.002%. Barbery and Pelletier [10] have published data for the number of locked sections expected from sectioning of a spherical particle with 50% "A". Their theoretical value is 0.7854, as compared with 0.7860 obtained here with the stepwise solution. An exact value of 0.7854 is obtained when 10,000 observations are recorded. There are therefore several pieces of corroborative evidence indicating the veracity of the model.

4.5: Stereological Artifacts in Observations from Spherical Particles

Data from the sectioning model is presented in Table 4.1. Jones [11] has performed a Monte Carlo simulation of sampling spherical particles with planar boundaries using linear intercepts. His data is presented in Table 4.2.

Figure 4.12 compares the number of observations recorded as a function of observed composition for sectional and linear data from a particle with 50% "A". The actual particle composition is represented by a vertical line through the 50% composition point. Both intercepts and sections produce numerous stereological artifacts; however, the bias is much worse for intercepts than it is for sections. A second comparison may be made in Figure 4.13 for sampling of a particle with 80% "A".

The parameter most commonly of interest in image analysis based liberation studies is the proportion of total measured area which constitutes locked or

Table 4.1

OBSERVATIONAL FREQUENCY OF VARIOUS SECTION COMPOSITIONS FROM KNOWN PARTICLE COMPOSITIONS

	(--------- ACTUAL PARTICLE COMPOSITION ---------)										
Observed	2.50	10.00	20.00	30.00	40.00	50.00	60.00	70.00	80.00	90.00	97.50
0	53.75	36.20	25.65	19.25	14.45	10.70	7.60	5.20	3.00	1.35	0.25
< 5	27.90	10.45	6.45	4.35	3.15	2.25	1.60	0.95	0.65	0.25	0.10
< 15	14 25	28.75	11.85	7.55	5.20	3.50	2.60	1.65	1.00	0.40	0.05
< 25	1.90	13.30	24.35	10.70	6.70	4.60	2.95	1.90	0.35	0.45	0.10
< 35	0.70	4.25	13.85	23.35	10.60	6.40	4.05	2.55	1.55	0.70	0.15
< 45	0.40	1.90	5.55	12.65	22.90	11.00	6.30	3.75	2.05	0.75	0.15
< 55	0.30	1.25	3.10	6.15	11.90	23.10	11.90	6.15	3.10	1.25	0.30
< 65	0.15	0.75	2.05	3.75	6.30	11.00	22.90	12.65	5.55	1.90	0.40
< 75	0.15	0.70	1.55	2.55	4.05	6.40	10.60	23.35	13.85	4.25	0.70
< 85	0.10	0.45	0.95	1.90	2.95	4.60	6.70	10.70	24.35	13.30	1.90
< 95	0.05	0.40	1.00	1.65	2.60	3.50	5.20	7.55	11.85	28.75	14.25
<100	0.10	0.25	0.65	0.95	1.60	2.25	3.15	4.35	6.45	10.45	27.90
100	0.25	1.35	3.00	5.20	7.60	10.70	14.45	19.25	25.65	36 20	53.75

CUMULATIVE OBSERVATIONAL FREQUENCY OF VARIOUS SECTION COMPOSITIONS FROM KNOWN PARTICLE COMPOSITIONS

Observed			(--------- ACTUAL PARTICLE COMPOSITION ---------)								
	2.50	10.00	20.00	30.00	40.00	50.00	60.00	70.00	80.00	90.00	97.50
0	53.75	36.20	25.65	19.25	14.45	10.70	7.60	5.20	3.00	1.35	0.25
5	81.65	46 65	32.10	23.60	17.60	12.95	9.20	6.15	3.65	1.60	0.35
15	95.90	75.40	43.95	31.15	22.80	16.45	11.80	7.80	4.65	2.00	0.40
25	97 90	88.70	68.30	41.85	29.50	21.05	14.75	9.70	5.60	2.45	0.50
35	98.50	92.95	82.15	65.20	40.10	27.45	18.80	12.25	7.15	3.15	0.65
45	98.90	94.85	87.70	77.85	63.00	38.45	25.10	16.00	9.20	3.90	0.80
55	99.20	96.10	90.80	84.00	74.90	61.55	37.00	22.15	12.30	5.15	1.10
65	99.35	96.85	92.85	87.75	81.20	72.55	59.90	34.80	17.85	7.05	1.50
75	99.50	97.55	94.40	90.30	85.25	78.95	70.50	58.15	31.70	11.30	2.20
85	99 60	98.00	95.35	92.20	88.20	83.55	77.20	68.85	56.05	24.60	4.10
95	99.65	98.40	96.35	93.85	90.80	87.05	82.40	76.40	67.90	53.35	18.35
100	99.75	98.65	97.00	94.80	92.40	89.30	85.55	80.75	74.35	63.80	46.25

Observation Frequency vs. Grade (Sectional Data)

Table 4.2

OBSERVATIONAL FREQUENCY OF VARIOUS INTERCEPT COMPOSITIONS FROM KNOWN PARTICLE COMPOSITIONS

	<--------- ACTUAL PARTICLE COMPOSITION --------->								
Observed	10.00	20.00	30.00	40.00	50.00	60.00	70.00	80.00	90.00
0	64.65	50.61	40.68	31.96	24.82	18.64	12.83	7.99	3.63
< 10	7.26	6.05	4.12	3.63	2.79	1.94	1.45	0.73	0.24
< 20	8.96	7.02	5.57	4.36	3.63	2.91	1.94	1.21	0.73
< 30	6.54	8.96	7.51	5.81	4.36	3.15	2.42	1.69	0.48
< 40	3.15	6.78	9.20	8.23	5.93	4.36	3.15	1.94	0.97
< 50	1.94	4.36	6.30	8.72	8.48	6.3	4.36	2.66	1.45
< 60	1.45	2.66	4.36	6.30	8.48	8.72	6.3	4.36	1.94
< 70	0.97	1.94	3.15	4.36	5.93	8.23	9.2	6.78	3.15
< 80	0.48	1.69	2.42	3.15	4.36	5.81	7.51	8.96	6.54
< 90	0.73	1.21	1.94	2.91	3.63	4.36	5.57	7.02	8.96
<100	0.24	0.73	1.45	1.94	2.79	3.63	4.12	6.05	7.26
100	3.63	7.99	12.83	18.64	24.82	31.96	40.88	50.61	64.65

OBSERVATIONAL FREQUENCY OF VARIOUS INTERCEPT COMPOSITIONS FROM KNOWN PARTICLE COMPOSITIONS

	<--------- ACTUAL PARTICLE COMPOSITION --------->								
Observed	10.00	20.00	30.00	40.00	50.00	60.00	70.00	80.00	90.00
0	64.65	50.61	40.68	31.96	24.82	18.64	12.83	7.99	3.63
10	71.91	56.66	44.80	35.59	27.61	20.58	14.28	8.72	3.87
20	80.87	63.68	50.37	39.95	31.23	23.49	16.22	9.93	4.60
30	87.41	72.64	57.88	45.76	35.59	26.64	18.64	11.62	5.08
40	90.56	79.42	67.08	53.99	41.52	31.00	21.79	13.56	6.05
50	92.50	83.78	73.38	62.71	50.00	37.30	26.15	16.22	7.50
60	93.95	86.44	77.74	69.01	58.48	46.02	32.45	20.58	9.44
70	94.92	88.38	80.89	73.37	64.41	54.25	41.65	27.36	12.59
80	95.40	90.07	83.31	76.52	68.77	60.06	49.16	36.32	19.13
90	96.13	91.28	85.25	79.43	72.39	64.42	54.73	43.34	28.09
100	96.37	92.01	86.70	81.37	75.18	68.05	58.85	49.39	35.35

Observation Frequency vs. Grade (Intercept Data)

(after Jones [11])

Figure 4.12

Comparison of Intercepts & Sections

(Particle = 50% Phase A)

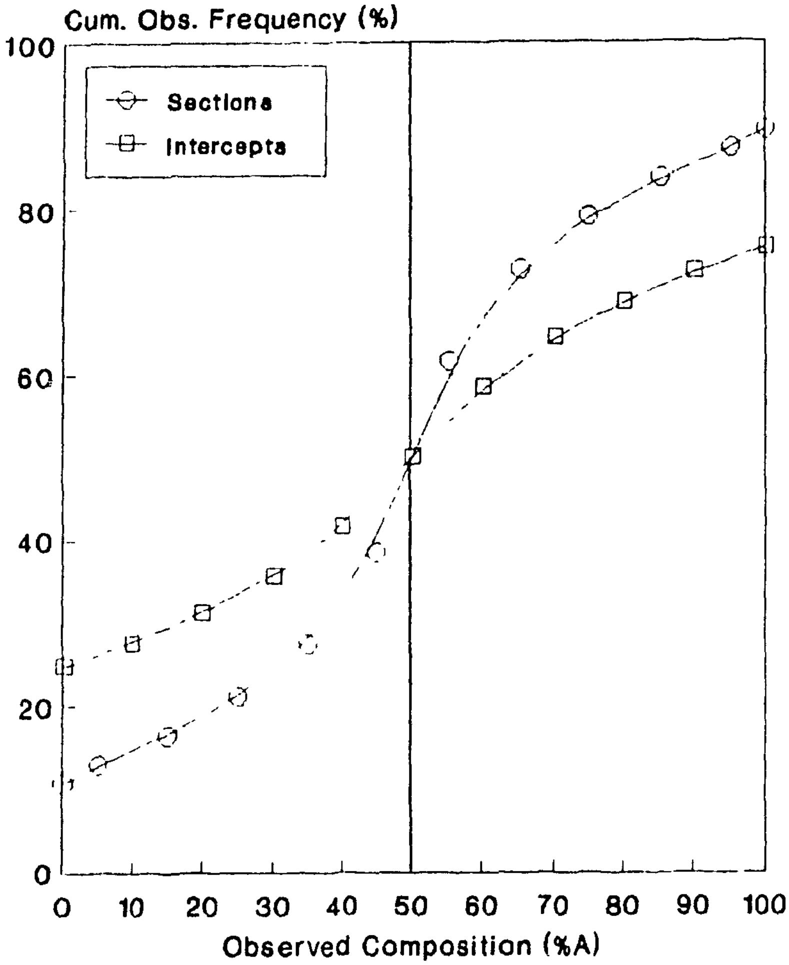

Figure 4.13

Comparison of Intercepts & Sections

(Particle = 80% Phase A)

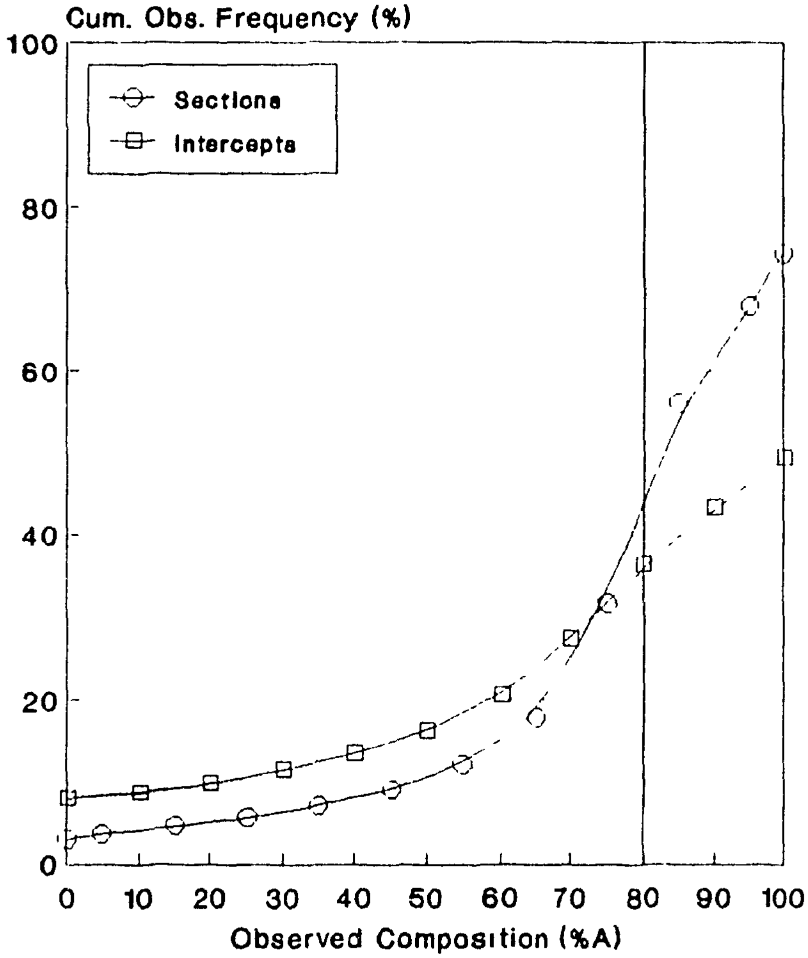

AREA FREQUENCY VS. GRADE - SECTIONING OF SPHERICAL PARTICLES

Table 4.3

MEASURED AREA FRACTION OF VARIOUS SECTION COMPOSITIONS FROM KNOWN PARTICLE COMPOSITIONS

(--------- ACTUAL PARTICLE COMPOSITION ---------)

Observed	2.50	10.00	20.00	30.00	40.00	50.00	60.00	70.00	80.00	90.00	97.50
0	48.39	29.54	18.89	12.97	8.78	5.83	3.67	2.14	0.97	0.30	0.03
< 5	35.57	11.92	6.69	4.11	2 78	1.74	1.06	0.54	0.30	0.09	0.01
< 15	14.43	37.21	13.60	7.93	4.94	3.00	1.93	1.07	0.53	0.14	0.02
< 25	0.97	14.61	31.96	12.35	7.09	4.35	2.47	1.31	0.53	0.19	0.01
< 35	0.29	3.43	16.37	31.02	12.41	6.73	3.80	2.08	0.98	0.31	0.03
< 45	0.13	1.19	5.20	15.01	30.38	12.99	6.50	3.28	1.46	0.37	0.03
< 55	0.08	0.69	2.51	6.20	14.19	30.71	14.19	6.20	2.51	0.69	0.08
< 65	0.03	0.37	1.46	3.28	6.50	12.99	30.38	15.01	5.20	1.19	0.13
< 75	0.03	0.31	0.98	2.08	3.80	6.73	12.41	31.02	16.37	3.43	0.29
< 85	0.01	0.19	0.53	1.31	2.47	4.35	7.09	12.35	31.96	14.61	0.97
< 95	0.02	0.14	0.53	1.07	1.93	3.00	4.94	7.93	13.60	37.21	14.43
<100	0.01	0.09	0.30	0.54	1.06	1.74	2.78	4.11	6.69	11.92	35.57
100	0.03	0.30	0.97	2.14	3.67	5.83	8.78	12.97	18.89	29.54	48.39

CUMULATIVE MEASURED AREA FRACTION OF VARIOUS SECTION COMPOSITIONS FROM KNOWN PARTICLE COMPOSITIONS

(--------- ACTUAL PARTICLE COMPOSITION ---------)

Observed	2.50	10.00	20.00	30.00	40.00	50.00	60.00	70.00	80.00	90.00	97.50
0	48.39	29.54	18.89	12.97	8.78	5.83	3.67	2.14	0.97	0.30	0.03
5	83.96	41.46	25.59	17.03	11.56	7.58	4.73	2.68	1.27	0.39	0.04
15	98.39	78.67	39.19	25.01	16.50	10.58	6.67	3.75	1.80	0.53	0.06
25	99.36	93.28	71.15	37.36	23.59	14.92	9.14	5.05	2.34	0.72	0.07
35	99.65	96.71	87.52	68.38	36.00	21.66	12.94	7.13	3.31	1.03	0.10
45	99.78	97.91	92.72	83.39	66.38	34.64	19.44	10.41	4.78	1.40	0.14
55	99.86	98.60	95.22	89.59	80.56	65.36	33.62	16.61	7.28	2.09	0.22
65	99.90	98.97	96.69	92.97	87.06	78.34	64.00	31.62	12.48	3.29	0.35
75	99.93	99.28	97.66	94.95	90.86	85.08	76.41	62.64	28.85	6.72	0.64
85	99.94	99.47	98.20	96.25	93.33	89.42	83.50	74.99	60.81	21.33	1.61
95	99.96	99.61	98.73	97.32	95.27	92.42	88.44	82.92	74.41	58.54	16.04
100	99.97	99.70	99.03	97.86	96.33	94.17	91.22	87.03	81.11	70.46	51.61

Figure 4.14

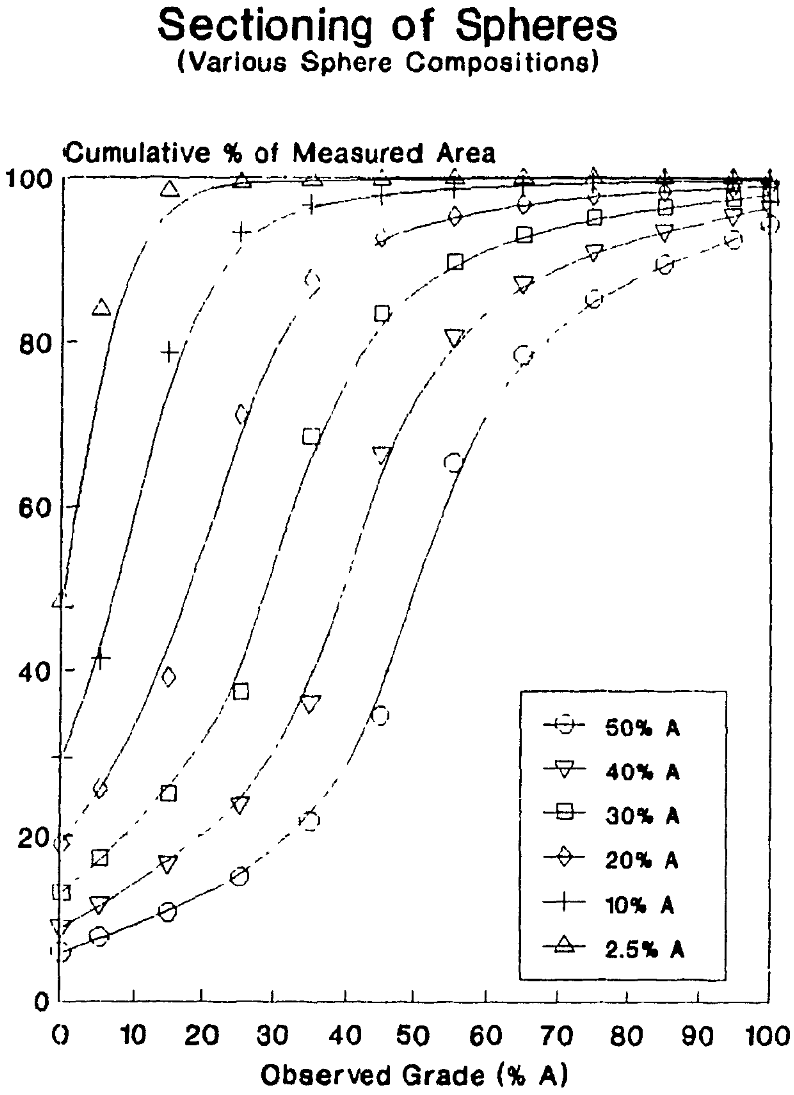
Sectioning of Spheres
(Various Sphere Compositions)
Cumulative % of Measured Area
100
80
60
40
20
0
0
10
20
30
40
50
60
70
80
90
100
Observed Grade (% A)
50% A
40% A
30% A
20% A
10% A
2.5% A

free observations. This differs from the observational frequency of free or locked sections, since observations must be weighted by their individual areas. The area frequency data from the sectioning model is presented in Table 4.3 and Figure 4.14.

At first sight it appears that sectional observations give only a very poor estimate of the compositions of particles in the "true" assemblage. However, it should also be recalled that actual assembages never consist of a single particle composition (with the exception of totally free assemblages, which do not suffer from stereological bias of this sort anyway). It was seen in the case of size related phenomena that addition of size classes resulted in a net cancellation of effects, so that the observed size assemblage came to approximate the true size assemblage. A similar phenomenon is observed when different particle compositions constitute a particle assemblage.

Table 4.4 provides three cases of what could be considered as idealized examples of particle assemblages. Assuming random breakage one might expect a feed to contain identical numbers of all locked particle compositions. A tailings from flotation of phase "A" would be heavily biased towards low grade particles and free "B", while a the concentrate would contain mostly high-grade and free "A" particles. A cleaner tailings might be expected to contain a large number of intermediate particles, since most particles on either extreme of the compositional spectrum would be either in the cleaner concentrate or the rougher tailings. The table shows the expected cumulative area vs. observation grade for the three types of assemblage (labeled as Observed: All).

When observations are collected from a particle assemblage it is not known whether or not the free observations are real or whether they are stereological artifacts. Thus, it is also of use to look at how sectioning alters the relative frequencies of various locked compositions, disregarding the free observations

Table 4.4

SIMULATION OF OBSERVATIONS FROM ASSEMBLAGES OF LOCKED PARTICLES

Cumulative Observed Composition	Simulated Feed			Simulated Con/Tails			Simulated Clnr Tails		
	Actual	Observed		Actual	Observed		Actual	Observed	
		All	Locked		All	Locked		All	Locked
0	0.00	10.73	0	0.00	25.43	0.00	0.00	7.82	0.00
5	5.00	15.43	5.99	20.00	38.44	17.75	0.00	10.42	3.08
15	15.00	23.19	15.87	50.00	57.05	43.13	5.00	16.03	9.73
25	25.00	30.73	25.46	70.00	70.80	61.89	12.50	23.09	18.11
35	35.00	38.45	35.30	85.00	81.39	76.34	22.50	32.00	29.67
45	45.00	46.10	45.04	95.00	88.75	86.38	37.50	43.19	41.93
55	55.00	53.90	54.96	100.00	93.36	92.67	62.50	56.81	58.07
65	65.00	61.55	64.70	100.00	95.56	95.68	77.50	68.00	71.33
75	75.00	69.27	74.54	100.00	96.88	97.48	87.50	76.91	81.89
85	85.00	76.81	94.13	100.00	97.71	98.61	95.00	83.97	90.27
95	95.00	84.57	94.01	100.00	98.37	99.50	100.00	89.58	96.92
100	100.00	89.27	100.00	100.00	98.73	100.00	100.00	92.18	100.00

Figure 4.15

Assemblages of Spheres

Sectioning of Simulated Feed

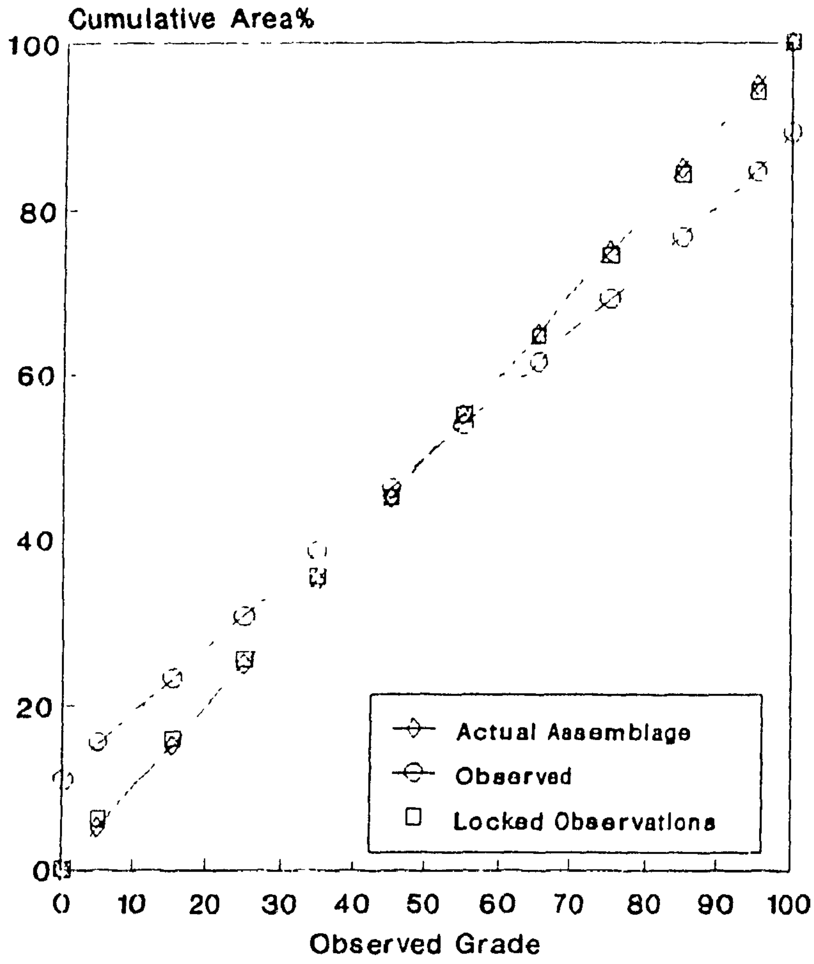

Figure 4.16

Assemblages of Spheres

Sectioning of Simulated Tails or Con

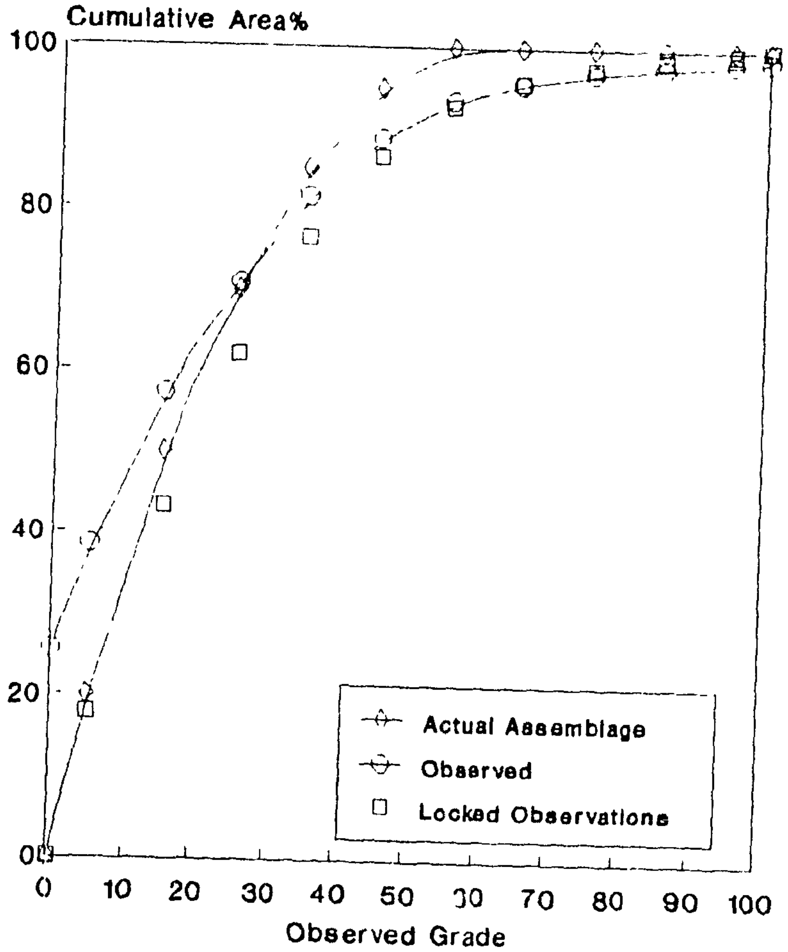

Figure 4.17

Assemblages of Spheres

Sectioning of Simulated Cleaner Tails

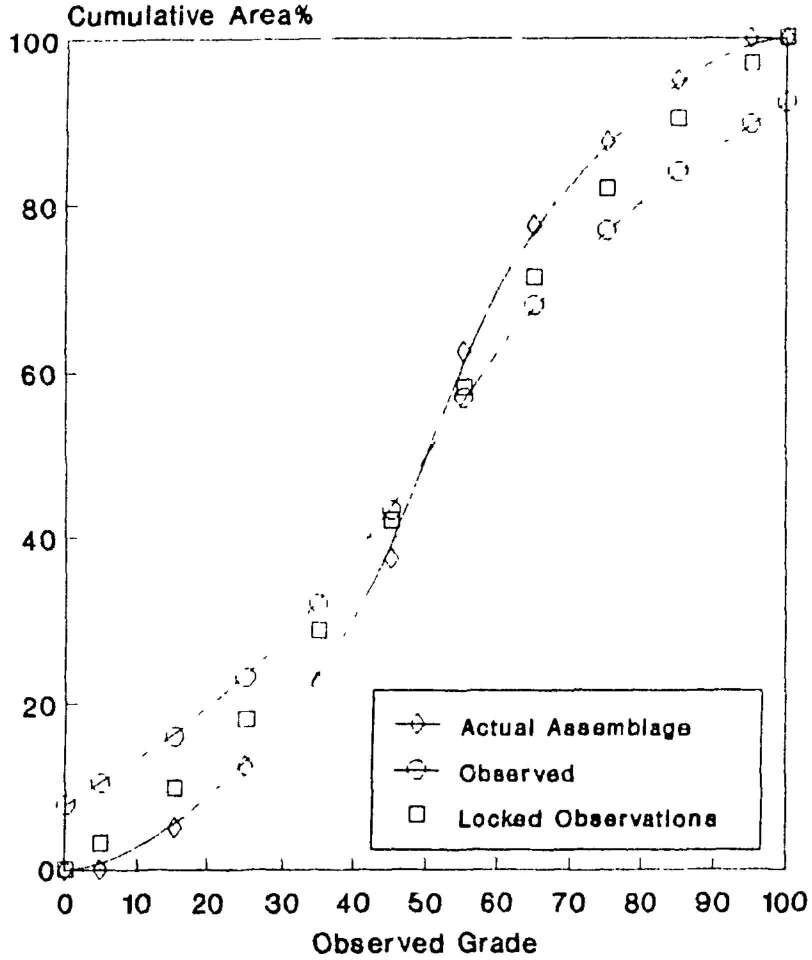

entirely (labeled as Observed: Locked).

Figures 4.15, 4.16 and 4.17 present the data graphically. The observed assemblage of locked sections provides a reasonable approximation of the true assemblage for all three cases. The data tends to be better when free observations are disregarded. For all intents and purposes an assemblage of locked sectional observations has the same distribution of measured area vs. grade as the parent assemblage of locked particles. The inaccuracies inherent in generating image analysis data outshadow the inaccuracies due to stereology.

4.6: Stereological Artifacts as a Function of Section Size

Comparison of Tables 4.1 and 4.3 shows that the stereological bias associated with measured area is less than that associated with observational frequency. This implies that small occurrences (which possess a smaller area) contain a greater amount of stereological bias than larger measurements.

Figure 4.18 presents the expected assemblage of measured observations from particles with 50% phase "A". The total assemblage of expected observations for such particles was presented in Figure 4.12; however, in Figure 4.18 the data is subdivided into observational frequencies for a number of section sizes.

It is seen that as the size of observations decreases the proportion of free observations increases. For example, (in this geometrical model), a section with the same size as the particle (size class #0) must always give an accurate assessment of the particle composition. A section of size class -0.5 yields about 20% free observations, increasing to about 35% for size class -1, 50% for size class -2, and about 70% for size class -3. Since both the frequency of observations and the area of observations decrease rapidly with diminishing size the net effect upon the overall area distribution is small. For example,

Figure 4.18

Effects of Section Size

Sectioning of Particles with 50% Phase A

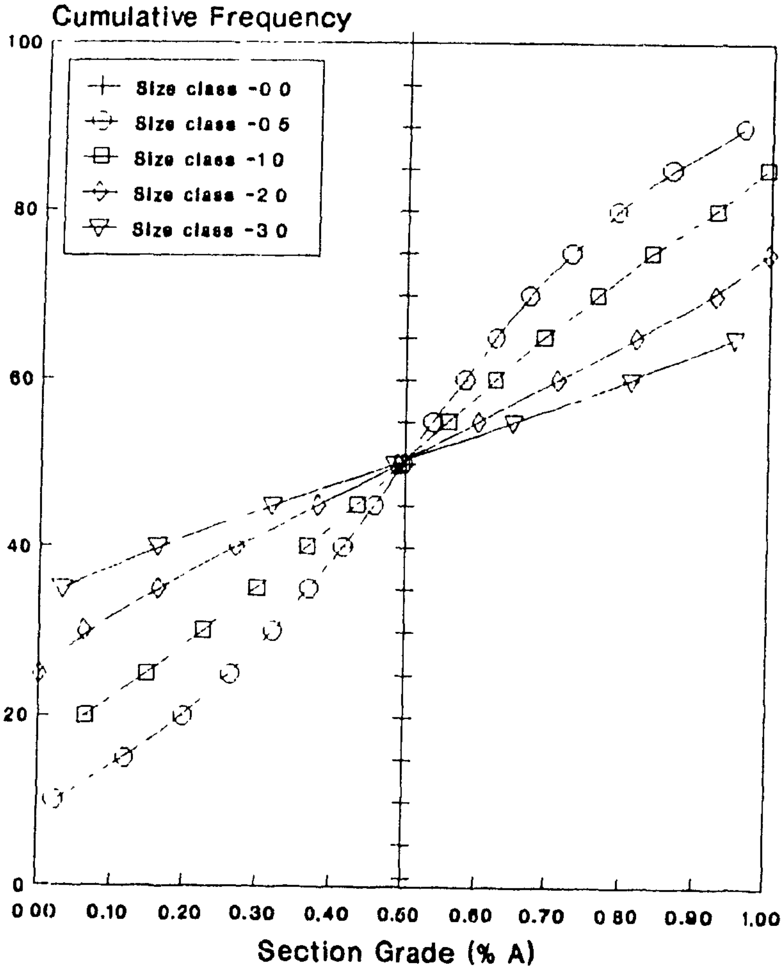

Table 4.3 showed that the expected area of free observations from a particle of 50% "A" would be only 11.6%.

The implications of the relationship between observed size and liberation become immediately apparent when one considers that unsized samples are sometimes used to describe size vs. liberation for a process stream. If Figure 4.18 was interpreted without any prior knowledge of the material making up the sample then it would appear that the sample consisted of various particle sizes ranging from coarse, locked material to fine, liberated material. Of course, such an observation would be consistent with what one would normally expect or even be looking for in a metallurgical process stream. In previous discussion it has been elaborated that due to a variety of analytical limitations liberation studies should employ only narrowly sized samples; however, it must also be considered that no size/liberation data could be reliably extracted from a single sample even if microscope conditions and processing algorithms could be established such that individual image analysis observations were correct.

4.7: Stereological Correction of Sectioning Data

Based upon the spherical sectioning it is possible to formulate a rigorous stereological correction or any one of a number of approximate solutions. Table 4.3 described the area fractions of various section compositions produced by particles of known composition. Each of the eleven columns of the table is an equation describing the sectioning products of an individual particle. (One could add to this the equations for free "A" and free "B" particles, which will of course, produce only free "A" or free "B" sections). Thus, thirteen equations are present to describe thirteen unknowns. the unknowns being the frequencies of particles in each composition class.

The rigorous solution is obtained by matrix algebra. When the sectioning data for free sections is included, Table 4.3 is a 13*13 square matrix. The observed frequency of sections in each composition class (a 1 * 13 matrix) is multiplied by the inverse of the sectioning data matrix to yield the true frequency of each particle type (a 1 * 13 matrix). This method has been previously described by the author [12].

The mathematically correct solution requires too many calculations to be consistent with the need to provide a simple stereological correction. A good approximation may be made as a substitute. As seen in the previous section the assemblage of locked sections provides a reasonable description of the assemblage of locked particles. The only reason why a correction would be needed, for most practical applications, is that there are fewer locked sections than locked particles. Stereological correction may therefore be simplified to the problem of distinguishing stereologically generated free sections from those which arise from actual free particles.

Figure 4.19 presents data from Table 4.3 and illustrates the area fraction of free "A" sections expected as particles with various amounts of phase "A" are observed. The data can be fit very well by the following empirical equation, labeled as "best fit equation" in Figure 4.19:

$$\text{Free A} = 10^{(2G-2)}/2 \qquad G = \text{Particle grade (\% A)}$$

It follows that the proportion of free "B" generated from the same particle will equal $10^{(2(1-G)-2)}/2$, or $10^{-2G}/2$.

The above equation allows data to be corrected in a simple manner. Table 4.5 illustrates the assemblage of sections derived from the "idealized feed" particle assemblage of Table 4.4. First, all free observations are disregarded and the total frequency of locked sections is summed up. Secondly, the above equation is applied to see how much free area would be expected from an

Figure 4.19

Sectioning of Spheres

Free Observations vs. Composition

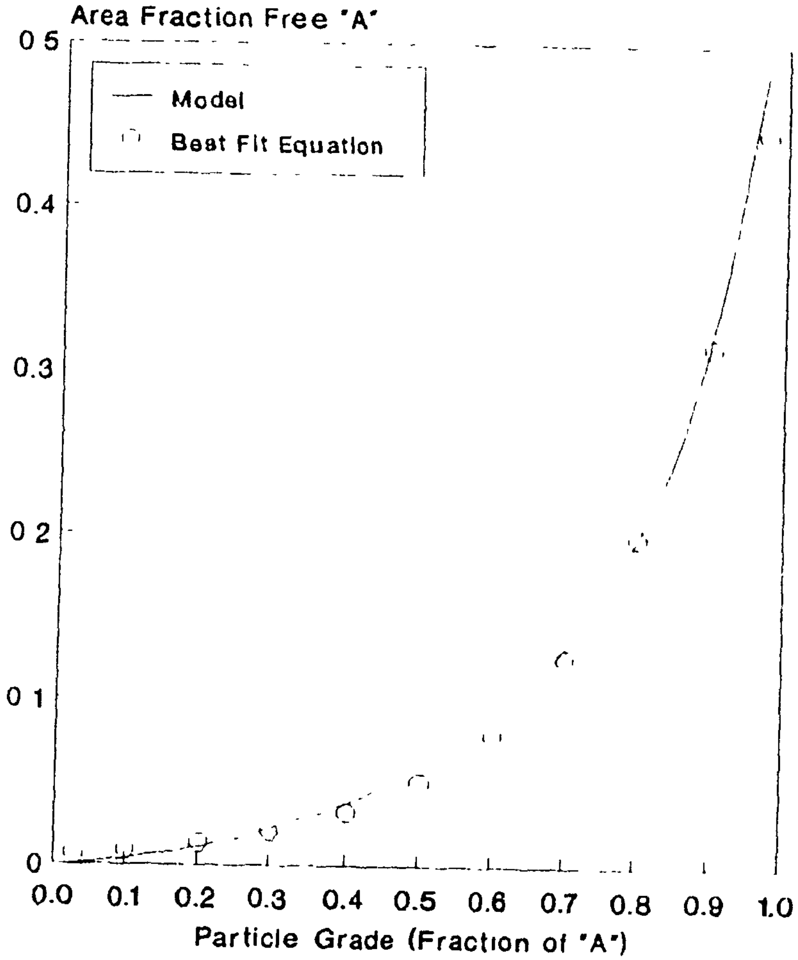

assemblage of particles identical to the observed assemblage of locked sections. For example, Table 4.5 reveals that 0.785 of the area consists of locked sections. If these were particles they would be expected to produce 0.614 locked sections, 0.086 free "A" and 0.086 free "B"". Thus, it follows that (0.785/0.614) locked particles would produce the observed assemblage of 0.785 locked sections. This ratio is 1.280, or the scaleup factor. All locked section values are multiplied by 1.280, the measured free "A" values are decremented by 1.280 * 0.086, and the number of free "B" values are decremented by 1.280 * 0.086. This yields the "corrected assemblage" in Table 4.5, which may be compared to the "actual frequency" of various particle types in the idealized assemblage (Figure 4.20). The procedure is repeated for the other two idealized assemblages in Tables 4.6 and 4.7 (Figures 4.21 and 4.22).

It may be observed that the approximation gives a reasonably close assessment of the original particle distribution. Remembering that the principal goal of the exercise was to estimate the true amount of free "A" and free "B" in the assemblages, the results of the correction may be compared to the "observed" sectioning data and the "actual" parent assemblage:

AREA% REPRESENTED BY FREE OBSERVATIONS

	Observed		Corrected		Actual	
Free Species:	A	B	A	B	A	B
Feed	11%	11%	0%	0%	0%	0%
Con/Tls	25%	1%	3%	-1%	0%	0%
Clnr Tails	8%	8%	-2%	-2%	0%	0%

Thus, a relatively simple method is proposed for reconstructing the particle distribution.

Perhaps the most useful way to conduct a liberation study is to simply interpret the data as collected, then to decide whether or not the free

Table 4.5

CONVERSION OF SECTIONAL AREA% OBSERVATIONS TO ORIGINAL ASSEMBLAGE
(ORIGINAL ASSEMBLAGE = IDEALIZED FEED)

Composition Interval	Interval Mean% A	All Obs.	Locked Obs.	PREDICTION Free A	 Locked	 Free B	Corrected Assemblage	Actual Frequency
0	0.000	0.107					-0.003	0.000
00-05	0.025	0.047	0.047	0.000	0.026	0.021	0.060	0.050
05-15	0.100	0.078	0.078	0.001	0.052	0.024	0.099	0.100
15-25	0.200	0.075	0.075	0.001	0.059	0.015	0.096	0.100
25-35	0.300	0.077	0.077	0.002	0.066	0.010	0.099	0.100
35-45	0.400	0.076	0.076	0.002	0.068	0.006	0.098	0.100
45-55	0.500	0.078	0.078	0.004	0.070	0.004	0.100	0.100
55-65	0.600	0.076	0.076	0.006	0.068	0.002	0.098	0.100
65-75	0.700	0.077	0.077	0.010	0.066	0.002	0.099	0.100
75-85	0.800	0.075	0.075	0.015	0.059	0.001	0.096	0.100
85-95	0.900	0.078	0.078	0.024	0.052	0.001	0.099	0.100
95-100	0.975	0.047	0.047	0.021	0.026	0.000	0.060	0.050
100	1.000	0.107					-0.003	0.000
		Total:	0.785	0.086	0.614	0.086	1.000	1.000
		Scaleup:	1.280	0.110	0.785	0.110		

CONVERSION OF SECTIONAL AREA% OBSERVATIONS TO ORIGINAL ASSEMBLAGE
(ORIGINAL ASSEMBLAGE = IDEALIZED CLEANER TAILS)

Composition Interval	Interval Mean% A	Obs. Freq.	Locked Obs.	PREDICTION			Corrected Assemblage	Actual Frequency
				Free A	Locked	Free B		
0	0.000	0.078					-0.016	0.000
00-05	0.025	0.026	0.026	0.000	0.014	0.012	0.032	0.000
05-15	0.100	0.056	0.056	0.000	0.038	0.018	0.069	0.050
15-25	0.200	0.071	0.071	0.001	0.056	0.014	0.086	0.075
25-35	0.300	0.089	0.089	0.002	0.076	0.011	0.109	0.100
35-45	0.400	0.112	0.112	0.004	0.099	0.009	0.137	0.150
45-55	0.500	0.136	0.136	0.007	0.123	0.007	0.167	0.250
55-65	0.600	0.112	0.112	0.009	0.099	0.004	0.137	0.150
65-75	0.700	0.089	0.089	0.011	0.076	0.002	0.109	0.100
75-85	0.800	0.071	0.071	0.014	0.056	0.001	0.086	0.075
85-95	0.900	0.056	0.056	0.018	0.038	0.000	0.069	0.050
95-100	0.975	0.026	0.026	0.012	0.014	0.000	0.032	0.000
100	1.000	0.078					-0.016	0.000
		Total:	0.844	0.077	0.690	0.077	1.000	1.000
		Scaleup:	1.223	0.094	0.844	0.094		

Table 4.7

CONVERSION OF SECTIONAL AREA% OBSERVATIONS TO ORIGINAL ASSEMBLAGE
(ORIGINAL ASSEMBLAGE = IDEALIZED CON/TAILS)

Composition Interval	Interval Mean% A	Obs. Freq.	Locked Obs.	PREDICTION Free A	PREDICTION Locked	PREDICTION Free B	Corrected Assemblage	Actual Frequency
0	0.000	0.254					0.031	0.000
00-05	0.025	0.130	0.130	0.001	0.071	0.058	0.174	0.200
05-15	0.100	0.186	0.186	0.001	0.126	0.059	0.249	0.300
15-25	0.200	0.137	0.137	0.002	0.108	0.027	0.184	0.200
25-35	0.300	0.106	0.106	0.002	0.090	0.013	0.142	0.150
35-45	0.400	0.074	0.074	0.002	0.065	0.006	0.099	0.100
45-55	0.500	0.046	0.046	0.002	0.041	0.002	0.062	0.050
55-65	0.600	0.022	0.022	0.002	0.020	0.001	0.030	0.000
65-75	0.700	0.013	0.013	0.002	0.011	0.000	0.018	0.000
75-85	0.800	0.008	0.008	0.002	0.007	0.000	0.011	0.000
85-95	0.900	0.007	0.007	0.002	0.004	0.000	0.009	0.000
95-100	0.975	0.004	0.004	0.002	0.002	0.000	0.005	0.000
100	1.000	0.013					-0.013	0.000
		Total:	0.733	0.019	0.547	0.167	1.000	1.000
		Scaleup:	1.340	0.026	0.733	0.223		

Figure 4.20

Reconstruction of Particle Assemblages

Sectioning of Simulated Feed

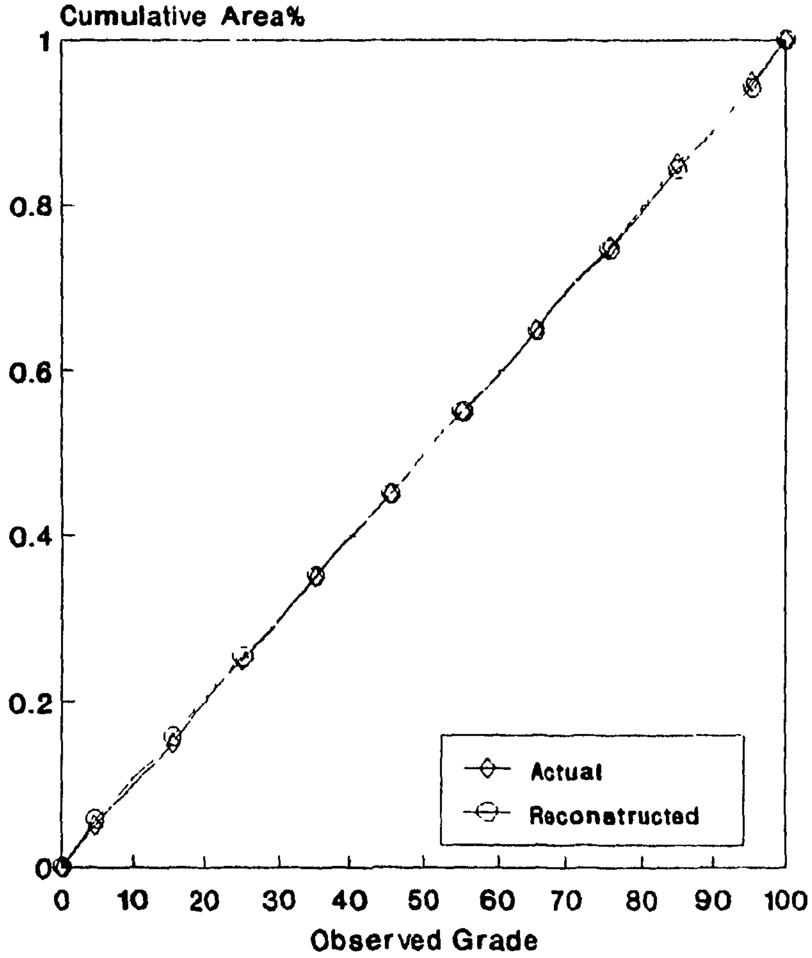

Figure 4.21

Reconstruction of Particle Assemblages

Sectioning of Simulated Tails or Con

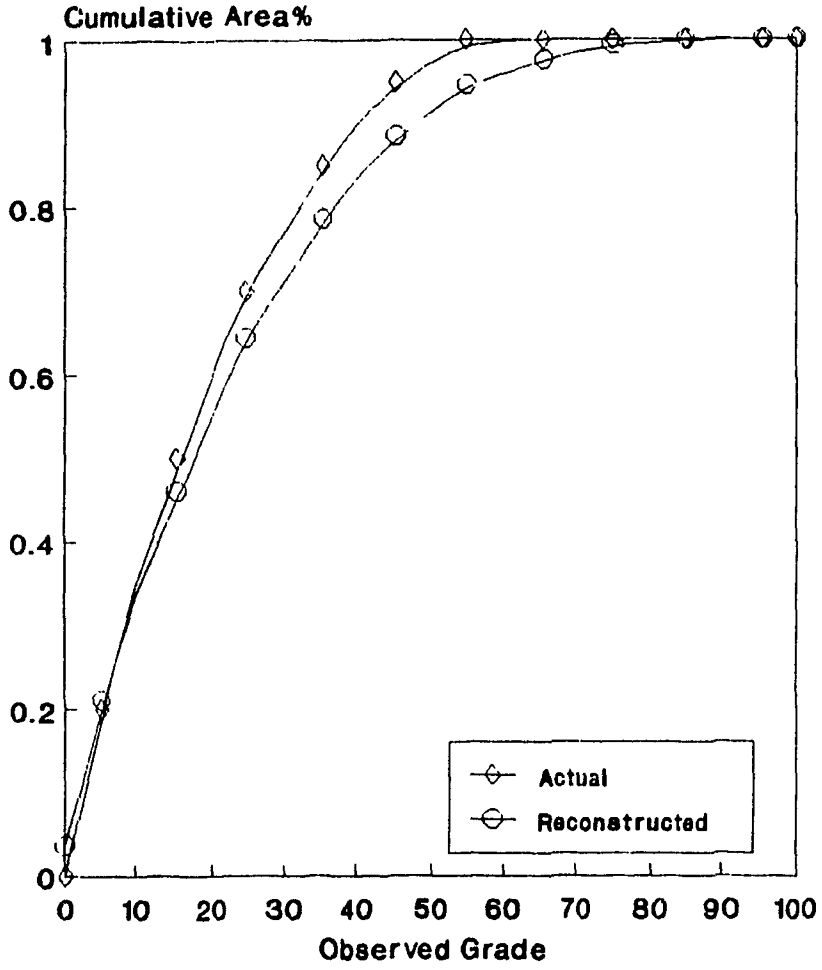

Figure 4.22

Reconstruction of Particle Assemblages

Sectioning of Simulated Cleaner Tails

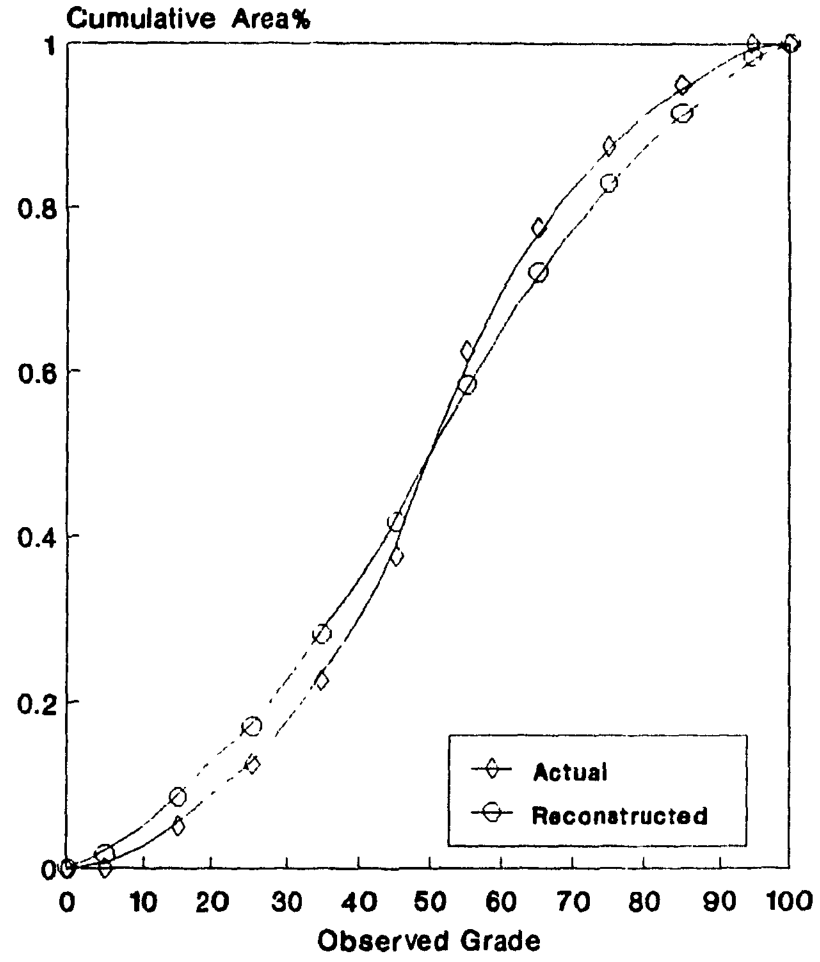

observations in any given stream are significant or not. The total measured area of free observations from sectioning of the idealized assemblages is relatively insensitive to the nature of the assemblage. Values (from Table 4.4) were 22% for the feed assemblage (11% A, 11% B), 26% for the con/tails assemblage (25% A, 1% B), and 16% for the cleaner tails assemblage (8% A, 8% B). Thus, for every unit of locked observations there are about 1/4 area units of free artifacts in the feed assemblage, 1/3 area units in the con/tails assemblage and 1/5 area units in the cleaner tails assemblage. The rule for making a semi-quantitative estimation of the original assemblage is as follows:

The area of free artifacts is about 1/4 the area of locked observations, and will generally lie within the limits 1/3 to 1/5, depending upon whether the locked section assemblage shows a composition distribution which is even, skewed towards low-grade/high-grade particles, or centralized around 50% composition.

In a uniform assemblage the free artifacts are evenly divided between the two phases; however, if the assemblage is biased towards particles of one phase (eg. average locked section grade less than 40% or greater than 50%) then almost all of the free artifacts will be of the predominant phase.

To recreate the true area of free observations, simply subtract about 1/5 to 1/3 of the locked observations then scale the locked and free frequencies back to a total of one.

The correction appears trivial, but provides a useful tool for making a fast assessment of whether free observations should be subjected to metallurgical interpretation or discounted as stereological artifacts. Interestingly, Petruk[13] has used an empirical correction factor where he estimates the number of free artifacts to be about 0.15 of the total measured area. This correlates reasonably well with the results of this modeling exercise, which suggests an average value of about 0.20. As previously mentioned, it is presumed that the model value of about 0.20 is an overcorrection.

Obviously the ease with which a "simple correction" may be applied relies upon the textural complexity of the ore. In cases where the locked particles contain several mineral nuclei, small inclusions, dendrites, or other features such that the particle size is significantly larger than the grain size it is usually unnecessary to apply a stereological correction at all. This model has been developed exclusively for the treatment of data from relatively simple locked particles where the particle size is less than the grain size, and therefore where only a few interphase boundaries are expected. Any increase in textural complexity will be accompanied by a decrease in the stereological bias; therefore, this discussion describes a limiting case, or a maximum correction which may be applied.

4.8: Errors in Recalculated Assay Contributions

There are a number of ways in which image analysis data may be presented. So far the discussion has included the number of observations vs. grade and the measured section area vs. grade. However, it is also common to express results in terms of recovery/grade relationships. In this case it is assay contribution vs. particle grade which is relevant. The assay contribution is equal to the measured area within a grade class weighted by the grade of the class, and is expressed as a proportion of the total area of the phase of interest.

It is evident that the contribution of free artifacts to the overall assay of a phase will exceed the contribution of free artifacts to the total measured section area, since free observations are given the highest weighting. Table 4.8 calculates the assay contributions of free sections to the overall observed grade. In theory the recalculated assay should equal the particle grade; however, in Table 4.4 rounding errors are introduced due to the use of only 13 grade classes. It may be observed that a particle with 50% "A" will have a

CONTRIBUTION OF VARIOUS TYPES OF MEASUREMENTS TO THE OVERALL "ASSAY" OF PHASE "A" Table 4.8

	(--------- ACTUAL PARTICLE COMPOSITION ---------)										
Observed --------	2.50	10.0	20.0	30.0	40.0	50.0	60.0	70.0	80.0	90.0	97.5
0.0	0.00	0.00	0.00	0.00	0.00	0.00	0.00	0.00	0.00	0.00	0.00
2.5	0.89	0.30	0.17	0.10	0.07	0.04	0.03	0.01	0.01	0.00	0.00
10.0	1.44	3.72	1.36	0.79	0.49	0.30	0.19	0.11	0.05	0.01	0.00
20.0	0.19	2.92	6.39	2.47	1.42	0.87	0.49	0.26	0.11	0.04	0.00
30.0	0.09	1.03	4.91	9.31	3.72	2.02	1.14	0.62	0.29	0.09	0.01
40.0	0.05	0.48	2.08	6.00	12.15	5.20	2.60	1.31	0.58	0.15	0.01
50.0	0.04	0.35	1.25	3.10	7.09	15.36	7.09	3.10	1.25	0.35	0.04
60.0	0.02	0.22	0.88	1.97	3.90	7.79	18.23	9.01	3.12	0.72	0.08
70.0	0.02	0.22	0.68	1.46	2.66	4.71	8.68	21.71	11.46	2.40	0.20
80.0	0.01	0.15	0.43	1.04	1.98	3.48	5.67	9.88	25.57	11.69	0.77
90.0	0.02	0.12	0.48	0.96	1.74	2.70	4.45	7.14	12.24	33.49	12.99
97.5	0.01	0.08	0.29	0.53	1.03	1.70	2.71	4.01	6.53	11.62	34.68
100.0	0.03	0.30	0.97	2.14	3.67	5.83	8.78	12.97	18.89	29.54	48.39
"Assay"	2.82	9.90	19.89	29.87	39.93	50.00	60.07	70.13	80.11	90.10	97.18
Free :	0.03	0.30	0.97	2.14	3.67	5.83	8.78	12.97	18.89	29.54	48.39
Free% ·	0.91	3.07	4.88	7.15	9.20	11.67	14.61	18.49	23.58	32.79	49.79

recalculated assay of 50% "A", 11.7% of which is in the form of free artifacts. In contrast, Table 5.3 shows that free "A" contributes only 5.8% of the measured section area. A particle with 90% "A" will present 32.8% of its "A" content as free artifacts, as opposed to 29.5% of its measured area, and so on.

In this work stereological corrections are not applied directly to assay contribution data. Adjustments are made to the measured areas, and the assay contributions calculated from the adjusted data set. However, it is worthwhile to note the magnitude of the stereological bias indicated by Table 4.8. In cases where any significant quantity of particles contain over about 40% of the phase of interest, large contributions to the overall assay of that phase will be made by free sections.

4.9: Summary of Stereological Phenomena and Corrections

A summary of the stereological phenomena relevant to image analysis based liberation studies is as follows:

1) Particle size is incorrectly estimated. A range of sizes at or under the true size is seen from a single particle size, with the bias much worse for linear intercepts than it is for sections.
2) Particle grade is incorrectly estimated, with a range of grades including free observations observed from a single particle composition. (Again the effect is much worse for linear intercepts than it is for sections). Small observations are more likely to appear free than large observations.
3) As a result of (1) and (2) it is found that a single particle composition will give rise to large locked observations and small free observations. Thus, it is very inadvisable to attempt to derive size vs. liberation data from a single unsized sample.
4) Measurements of cumulative area vs. grade are less affected by stereology than measurements of cumulative observational frequency vs. grade. This is a result of the fact that the greatest degree of stereological bias is seen in the smallest sections, which possess the smallest area.
5) When various particle compositions are combined together to simulate real particle assemblages it is found that some of the stereological effects cancel. An assemblage of locked sections tends to appear the same as the parent assemblage of locked particles. However, the production of free artifacts is cumulative.
6) Based upon (5) it is possible to make a simple stereological correction by estimating the area of free sections which would be expected due to stereology alone. This amounts to about 1/4 of the locked area in most

cases, with the split between the two possible phases determined by the average grade of locked sections.

The treatment of sectioning data is much easier than the treatment of intercept data. In essence, the results of the spherical model suggest that useful metallurgical interpretations may be made from sectioning data without an inordinate amount of consideration of stereological effects. Caution must simply be exercised in the metallurgical interpretation of free observations. The same cannot be said for linear intercept data. The magnitude of the stereological bias is such that the locked intercept grade distribution is significantly different from the locked particle grade distribution. Thus, one is obliged to convert the raw data by means of a mathematical model. A vast amount of work has been performed for the conversion of intercept data to volumetric data; however, the models all require a large amount of data manipulation and are very sensitive to any type of error in the data. Moreover, such models require a tradeoff between the collection of vast amounts of textural data or the use of simplistic assumptions. A review of the models and methodology for the correction of linear intercept data is not directly relevant to this discussion; however a list of pertinent references is included in the bibliography. Most importantly, it is only when working with section data that the raw information can provide reliable data of direct metallurgical interest without conducting studies specifically to define mineralogical texture. It is for this reason that collection of section data was considered to be the preferred method for this study.

The use of simplistic approximations to arrive at a stereological correction for particle sectioning is warranted by the fact that the original data appears to provide a reasonable description of the parent assemblage, with the singla exception that the number of free sections is overestimated. When it comes down to practice any comprehensive stereological correction must be applied "automatically", perhaps at the data compilation level, if it is to be used at all. However, the application of any type of correction or transformation leads to the inevitable possibility that useful data is obliterated by poor model assumptions. Thus, in cases where the raw data is usable (ie. in any case where a range of compositions are combined to form an assemblage) it is preferable to work directly with untransformed data and to use the simplest possible correction factor to semi-quantitatively assess the contributions of stereological bias to the observations. Comprehensive analysis of the spherical particle model suggests the use of a correction factor which is not at all dissimilar from the "locking factor" originally proposed by Gaudin[3].

CHAPTER 5: ANALYSIS OF COPPER CIRCUIT DATA

5.0 : Introduction

This chapter describes image analysis results for the BMS copper circuit. The work has the dual goals of interpreting the behaviour of the Brunswick copper circuit and demonstrating the quantitative analysis of image analysis data. ICP assays are used to construct a materials balance for the various mineral species in the circuit. Structural data from image analysis is then balanced against the mass flow data, allowing the path of locked and liberated particles to be described. Stereological factors are taken into account in the interpretation of results.

The copper circuit study employed six samples which were separated by cyclosizer to provide eighteen samples for image analysis. The sample points and mnemonics are shown in Figure 5.1. The size ranges prepared using the cyclosizer were the "A" or coarse fraction (+27 µm), the "B" or intermediate fraction (+13 µm) and the "C" or fine fraction (+9 µm). Samples for image analysis are identified by the stream mnemonic with the size range added as a suffix (eg. CF + "C" = CFC, or fine cleaner feed). The sizes reported above represent the theoretical cut-sizes based upon an S.G. of 5.0, and are appropriate for Cp and Px. Sphalerite is slightly coarser and galena finer than the numbers presented above. Particles reporting to the cyclosizer overflow (<9 µm) were not collected.

The original copper circuit samples were analysed at McGill University by means of atomic absorption (AA) for Cu, Zn and Pb. The sized fractions were sent to the N.B. Research and Productivity Council (RPC) where they were analysed by ICP for Cu, Zn, Pb, Fe and S. Assays and size analyses are reported in Table 5.1. The cyclosizer undersize masses and assays are calculated by difference. Pyrite could be reconstructed only for the sized

Brunswick Copper Circuit Sampling Points Figure 5.1

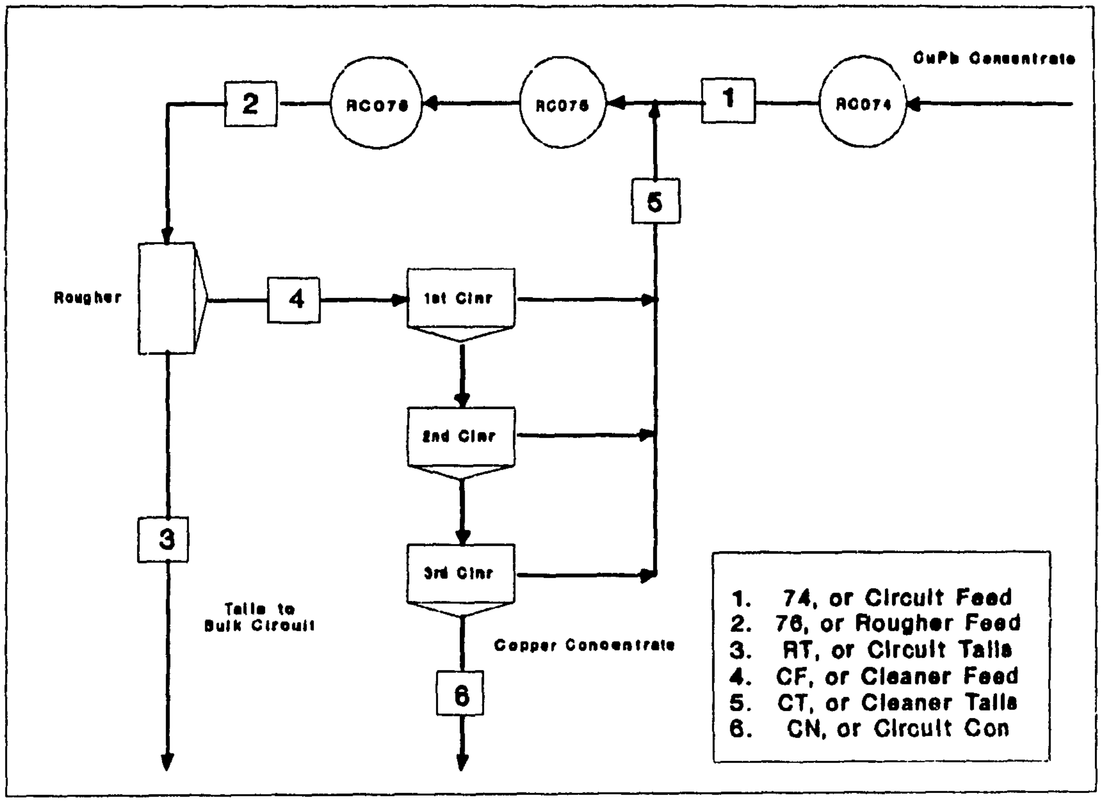

COPPER CIRCUIT SIZES, ASSAYS AND METALS DISTRIBUTIONS

Table 5.1

		ASSAY DATA						METALS DISTRIBUTION BETWEEN SIZES			
		Total	"A"	"B"	"C"	U/F		"A"	"B"	"C"	U/F
RC074	Mass	100.0	18.6	36.8	20.8	23.8					
	Cu	2.35	1.09	1.97	2.41	3.85	Cu	8.6	30.9	21.4	39.1
	Pb	27.08	24.02	26.16	23.70	33.86	Pb	16.5	35.5	18.2	29.8
	Zn	10.28	16.56	11.16	8.91	5.21	Zn	30.0	39.9	18.0	12.1
	Fe	----	18.36	21.95	23.80	----					
RC076	Mass	100.0	13.1	30.7	16.9	39.3					
	Cu	3.13	1.46	2.35	2.85	4.41	Cu	5.1	23.1	15.4	55.4
	Pb	30.78	28.69	30.17	27.60	33.32	Pb	12.2	30.1	15.2	42.5
	Zn	8.08	14.10	9.66	7 79	4.96	Zn	22.9	36.7	16.3	24.1
	Fe	----	18.23	20.76	21.92	----					
RT	Mass	100.0	21.0	40.2	21.7	17.1					
	Cu	0.33	0.24	0.26	0.34	0.57	Cu	15.5	32.0	22.6	29.9
	Pb	27.31	25.86	25.52	26.39	34.45	Pb	19.9	37.6	21.0	21.6
	Zn	11.04	14.52	11.14	10.51	7.21	Zn	27.6	40.6	20.7	11.2
	Fe	----	19.01	21.74	22.60	----					
CF	Mass	100.0	6.5	25.5	17.0	51.0					
	Cu	5.41	5.16	4.77	5.59	5.71	Cu	6.2	22.5	17.6	53.8
	Pb	32.81	36.23	32.79	27.75	34.08	Pb	7.2	25.5	14.4	53.0
	Zn	5.17	4.31	5.01	5.87	5.12	Zn	5.4	24.7	19.3	50.5
	Fe	----	18.09	20.48	21.37	----					
CT	Mass	100.0	4.9	23.8	13.4	57.9					
	Cu	5.55	4.65	5.44	5.35	5.72	Cu	4.1	23.3	12.9	59.7
	Pb	28.85	36.33	31.90	26.46	27.51	Pb	6.2	26.3	12.3	55.2
	Zn	4.77	4.33	4.83	5.82	4.54	Zn	4.4	24.1	16.3	55.1
	Fe	----	18.28	20.26	21.58	----					
CN	Mass	100.0	13.4	25.2	17.5	43.9					
	Cu	22.41	23.06	23.48	25.69	20.30	Cu	13.8	26.4	20.1	39.8
	Pb	5.91	4.12	4.39	4.60	7.85	Pb	9.3	18.7	13.6	58.3
	Zn	3.16	2.98	2.65	2.30	3.84	Zn	12.7	21.2	12.8	53.4
	Fe	----	29.28	28.82	27.75	----					

samples, since this calculation required the sulfur assay. The method for recalculating pyrite assays was described in Section 3.7.

5.1: Size-by-size Analysis

The data in Table 1 is typical of a set of data which might be collected for size-by-size circuit analysis. Thus, it is useful to see how much information may be derived from the wet chemical data before examining the additional information provided by the microscopic study. In practice it is best to use the wet chemical data to reconstruct mass flows through the circuit, since the wet chemical assays are superior to those which are recalculated from the image analysis study. The liberation data is then used to describe the characteristics of material at various points in the circuit.

5.1.1: Mass Balancing

In order to make use of the wet chemical data it is necessary to construct circuit balances. Data for all size ranges is balanced using the MATBAL program in Tables 5.2 through 5.7. All size fractions of the cleaner tailings required high adjustments to copper (about 30% of the measured assay). The fact that approximately the same adjustment is required in all size fractions indicates that the error lay in the sample and not in the assays. In the plant the cleaner tailings from the first, second and third copper cleaners are combined in a small sump which feeds by gravity into the RC075 conditioner. The stream had to be sampled from the sump itself, which contains an imperfectly mixed combination of the three sample streams. Thus, it was difficult to obtain a representative sample. Other than this, only small adjustments are required to balance the data.

The mass balanced data is used in Tables 5.7 to 5.11 to calculate the rougher and cleaner recoveries of the various species in the various size

MASS BALANCE OF COPPER CIRCUIT DATA - TOTAL SAMPLE

ATOMIC ABSORPTION ASSAY DATA				
	Mass	Cu	Pb	Zn
74	100.0	2.35	27.08	10.28
76		3.13	30.78	8.08
RT		0.33	27.31	11.04
CF		5.41	32.81	5.17
CT		5.55	28.85	4.77
CN		22.41	5.91	3.16
MATBAL BALANCED DATA				
74	100.0	2.34	27.49	10.42
7C	196.0	3.23	29.49	7.79
RT	90.9	0.33	29.64	11.14
CF	105.0	5.73	29.36	4.88
CT	96.0	4.15	31.57	5.04
CN	9.1	22.45	5.91	3.20
MAGNITUDE OF ASSAY ADJUSTMENT				
74		-0.01	0.41	0.14
76		0.10	-1.29	-0.29
RT		0.00	2.33	0.10
CF		0.32	-3.45	-0.29
CT		-1.40	2.72	0.27
CN		0.04	0.00	0.04
ADJUSTMENT AS % OF ORIGINAL ASSAY				
74		-1	5	-3
76		4	-3	-2
RT		1	-7	5
CF		10	-7	-3
CT		-29	6	2
CN		-2	0	1

Table 5.3

MASS BALANCE OF COPPER CIRCUIT DATA - COARSE FRACTION

	Mass	Cu	Pb	Zn	Py
	ICP ANALYSES (PYRITE CALCULATED)				
74	100.0	1.09	24.07	16.56	32.30
76		1.46	28.69	14.10	29.20
RT		0.24	25.86	14.52	28.60
CF		5.16	36.23	4.31	22.50
CT		4.65	36.33	4.33	24.50
CN		23.06	4.12	2.98	15.80
	MATBAL BALANCED DATA				
74	100.0	1.08	25.07	15.52	30.03
76	125.9	1.52	27.81	13.23	28.81
RT	96.3	0.24	25.88	16.00	30.59
CF	29.6	5.69	34.07	4.24	23.08
CT	25.9	3.24	38.37	4.41	24.11
CN	3.7	22.73	4.12	3.01	15.86
	MAGNITUDE OF ASSAY ADJUSTMENT				
74		-0.01	1.00	-1.04	-2.27
76		0.06	-0.88	-0.87	-0.39
RT		0.00	0.02	1.48	1.99
CF		0.53	-2.16	-0.07	0.58
CT		-1.41	2.04	0.08	-0.39
CN		-0.33	0.00	0.03	0.06
	ADJUSTMENT AS % OF ORIGINAL ASSAY				
74		-1	4	-6	-7
76		4	-3	-6	-1
RT		1	0	10	7
CF		10	-6	-2	3
CT		-30	6	2	-2
CN		-1	0	1	0

Table 5.4

MASS BALANCE OF COPPER CIRCUIT DATA - MEDIUM FRACTION

	Mass	Cu	Pb	Zn	Py
		ICP ANALYSES (PYRITE CALCULATED)			
74	100.0	1.97	26.16	11.16	35.90
76		2.35	30.17	9.66	33.30
RT		0.26	25.52	11.14	37.80
CF		4.77	32.79	5.01	29.70
CT		5.54	31.90	4.83	25.80
CN		23.48	4.39	2.65	14.90
		MATBAL BALANCED DATA			
74	100.0	1.95	26.26	11.17	36.16
76	168.4	2.46	29.29	8.69	32.90
RT	92.7	0.26	27.98	11.84	37.82
CF	75.7	5.16	30.90	4.84	26.86
CT	68.4	3.20	33.72	5.07	28.13
CN	7.3	23.44	4.39	2.68	14.97
		MAGNITUDE OF ASSAY ADJUSTMENT			
74		-0.02	0.10	0.01	0.26
76		0.11	-0.88	-0.97	-0.40
RT		0.00	2.46	0.70	0.02
CF		0.39	-1.89	-0.17	-2.84
CT		-2.34	1.82	0.24	2.33
CN		-0.04	0.00	0.03	0.07
		ADJUSTMENT AS % OF ORIGINAL ASSAY			
74		-1	0	0	1
76		5	-3	-10	-1
RT		0	10	6	0
CF		8	-6	-3	-10
CT		-42	6	5	9
CN		-0	0	1	0

Table 5.5

MASS BALANCE OF COPPER CIRCUIT DATA - FINE FRACTION

	Mass	Cu	Pb	Zn	Py
ICP ANALYSES (PYRITE CALCULATED)					
74	100.0	2.41	23.70	8.91	40.00
76		2.85	27.60	7.79	33.30
RT		0.34	26.39	10.51	37.80
CF		5.59	27.75	5.87	29.00
CT		5.35	26.46	5.82	30.30
CN		25.69	4.60	2.30	8.50
MATBAL BALANCED DATA					
74	100.0	2.39	24.79	9.31	37.13
76	176.9	2.98	26.27	7.87	34.08
RT	91.9	0.34	26.57	9.93	39.64
CF	85.0	5.84	25.96	5.65	28.06
CT	76.9	3.75	28.20	6.00	30.11
CN	8.1	25.72	4.60	2.30	8.54
MAGNITUDE OF ASSAY ADJUSTMENT					
74		-0.02	1.09	0.40	-2.88
76		0.13	-1.33	0.08	0.78
RT		0.00	0.18	-0.58	1.84
CF		0.25	-1.79	-0.22	-0.94
CT		-1.60	1.74	0.18	-0.19
CN		0.03	0.00	0.00	0.04
ADJUSTMENT AS % OF ORIGINAL ASSAY					
74		-1	5	4	-7
76		5	-5	1	2
RT		0	1	-6	5
CF		5	-6	-4	-3
CT		-30	7	3	-1
CN		0	0	0	0

Table 5.6

MASS BALANCE OF COPPER CIRCUIT DATA - UNDERSIZE

CALCULATED ASSAY DATA

	Mass	Cu	Pb	Zn
74	100.0	3.85	33.86	5.21
76		4.41	33.32	4.96
RT		0.57	34.45	7.21
CF		5.71	34.08	5.12
CT		5.72	27.51	4.54
CN		20.30	7.85	3.84
		MATBAL BALANCED DATA		
74	100.0	3.84	33.62	5.80
76	359.0	4.53	31.59	5.06
RT	83.4	0.57	38.77	6.22
CF	275.7	5.73	29.41	4.71
CT	259.0	4.79	30.80	4.78
CN	16.7	20.23	7.86	3.67
		MAGNITUDE OF ASSAY ADJUSTMENT		
74		-0.01	-0.24	0.59
76		0.12	-1.73	0.10
RT		0.00	4.32	-0.99
CF		0.02	-4.67	-0.41
CT		-0.93	3.29	0.24
CN		-0.07	0.01	-0.17
		ADJUSTMENT AS % OF ORIGINAL ASSAY		
74		-1	5	-3
76		4	-3	-2
RT		1	-7	5
CF		10	-7	-3
CT		-29	6	2
CN		-2	0	1

Table 5.7

COPPER CIRCUIT MASS FLOWS AND RECOVERIES - TOTAL SAMPLE

		Cu	Pb	Zn
		MATBAL BALANCED ASSAYS		
74	100.0	2.34	27.49	10.42
76	196.0	3.23	29.49	7.79
RT	90.9	0.33	29.64	11.14
CF	105.0	5.73	29.36	4.88
CT	96.0	4.15	31.57	5.04
CN	9.1	22.45	5.91	3.20
		MASS UNITS		
74		2.34	27.49	10.42
76		6.33	57.79	15.27
RT		0.30	26.95	10.13
CF		6.02	30.84	5.13
CT		3.98	30.29	4.84
CN		2.04	0.54	0.29
		STAGE RECOVERIES		
Rghr		95.1	53.4	33.6
Clnr		33.9	1.7	5.7
Circuit		87.1	2.0	2.8
Recirc Load		170.2	110.2	46.4

Table 5.8

COPPER CIRCUIT MASS FLOWS AND RECOVERIES - COARSE FRACTION

		Cu	Pb	Zn	Py
		MATBAL BALANCED ASSAYS			
74	100.0	1.1	25.1	15.5	30.0
76	125.9	1.5	27.8	13.2	28.8
RT	96.3	0.2	25.9	16.0	30.6
CF	29.6	5.7	34.1	4.2	23.1
CT	25.9	3.2	38.4	4.4	24.1
CN	3.7	22.7	4.1	3.0	15.9
		MASS UNITS			
74		1.08	25.07	15.52	30.03
76		1.92	35.02	16.66	36.27
RT		0.23	24.92	15.40	29.45
CF		1.69	10.09	1.26	6.84
CT		0.84	9.94	1.14	6.25
CN		0.85	0.15	0.11	0.59
		STAGE RECOVERIES			
Rghr		87.9	28.8	7.5	18.9
Clnr		50.2	1.5	8.9	8.6
Circuit		78.4	0.6	0.7	2.0
Recirc Load		77.8	39.7	7.4	20.8

Table 5.9

COPPER CIRCUIT MASS FLOWS AND RECOVERIES - MEDIUM FRACTION

		Cu	Pb	Zn	Py
		MATBAL BALANCED ASSAYS			
74	100.0	2.0	26.3	11.2	36.2
76	168.4	2.5	29.3	8.7	32.9
RT	92.7	0.3	28.0	11.8	37.8
CF	75.7	5.2	30.9	4.8	26.9
CT	68.4	3.2	33.7	5.1	28.1
CN	7.3	23.4	4.4	2.7	15.0
		MASS UNITS			
74		1.95	26.26	11.17	36.16
76		4.15	49.34	14.64	55.41
RT		0.24	25.94	10.97	35.06
CF		3.91	23.40	3.67	20.35
CT		2.19	23.08	3.47	19.25
CN		1.71	0.32	0.20	1.09
		STAGE RECOVERIES			
Rghr		94.2	47.4	25.0	36.7
Clnr		43.8	1.4	5.3	5.4
Circuit		87.6	1.2	1.8	3.0
Recirc Load		112.2	87.9	31.1	53.2

Table 5.10

COPPER CIRCUIT MASS FLOWS AND RECOVERIES - FINE FRACTION

		Cu	Pb	Zn	Py
		MATBAL BALANCED ASSAYS			
74	100.0	2.4	24.8	9.3	37.1
76	176.9	3.0	26.3	7.9	34.1
RT	91.9	0.3	26.6	9.9	39.6
CF	85.0	5.8	26.0	5.6	28.1
CT	76.9	3.8	28.2	6.0	30.1
CN	8.1	25.7	4.6	2.3	8.5
		MASS UNITS			
74		2.39	24.79	9.31	37.13
76		5.28	46.47	13.92	60.27
RT		0.31	24.42	9.12	36.43
CF		4.96	22.05	4.80	23.84
CT		2.88	21.68	4.61	23.15
CN		2.08	0.37	0.19	0.69
		STAGE RECOVERIES			
Rghr		94.1	47.5	34.5	39.6
Clnr		41.9	1.7	3.9	2.9
Circuit		86.9	1.5	2.0	1.9
Recirc Load		120.5	87.5	49.5	62.3

Table 5.11

COPPER CIRCUIT MASS FLOWS AND RECOVERIES - UNDERSIZE

		Cu	Pb	Zn
		MATBAL BALANCED ASSAYS		
74	100.0	3.84	33.62	5.80
76	359.0	4.53	31.59	5.06
RT	83.4	0.57	38.77	6.22
CF	275.7	5.73	29.41	4.71
CT	259.0	4.79	30.80	4.78
CN	16.7	20.23	7.86	3.67
		MASS UNITS		
74		3.84	33.62	5.80
76		16.26	113.41	18.17
RT		0.48	32.31	5.18
CF		15.79	81.07	12.98
CT		12.41	79.77	12.38
CN		3.37	1.31	0.61
		STAGE RECOVERIES		
Rghr		97.1	71.5	71.5
Clnr		21.3	1.6	4.7
Circuit		87.7	3.9	10.5
Recirc Load		323.1	237.3	213.5

CU / PB SEPARATION CIRCUIT: Table 5.12

SUMMARY OF CIRCUIT RECOVERIES AND RECIRCULATING LOADS

	Rougher	Cleaner	Total Circuit	Recirc Load
Copper	95.1	33.9	87.1	170
Coarse	87.9	50.2	78.4	78
Medium	94.2	43.8	87.6	112
Fine	94.1	41.9	86.9	121
U/F	97.1	21.3	87.7	323
Lead	53.4	1.7	2.0	110
Coarse	28.8	1.5	0.6	40
Medium	47.4	1.4	1.2	88
Fine	47.5	1.7	1.5	88
U/F	71.5	1.6	3.9	237
Zinc	33.6	5.7	2.8	46
Coarse	7.5	8.9	0.7	7
Medium	25.0	5.3	1.8	31
Fine	34.5	3.9	2.0	50
U/F	71.5	4.7	10.5	213
Pyrite	——	——	——	——
Coarse	18.9	8.6	2.0	21
Medium	36.7	5.4	3.0	53
Fine	39.6	2.9	1.9	62
U/F	——	——	——	——

classes, and to calculate recirculating loads. The recovery data from these Tables is summarized in Table 5.12.

Tables 5.2 to 5.7 balance the flows and assays of the various size classes, but calculate each size class on the basis of 100 feed units. Thus, it is not known from the balanced data how much of each size class is present at each sample point. As part of the overall interpretation of circuit performance it is necessary to assess the relative abundances of the different size classes through the circuit. Thus, the experimental size analyses must be somehow incorporated into the overall mass balance.

The incorporation of the various constraints into a mass balance is a task which is beyond the capacity of most microcomputer-based balancing programs. In effect, each sample point would have twenty assays (four species times five size classes, including the unsized sample) and the system would have eighteen nodes (unsized = sum of all size fractions for six sample points; four species balancing across three nodes, under which conditions the fifth species would have to balance). Thus, a simpler way of balancing the data must be devised.

The individual mass balances for the four size fractions and the unsized sample may be used to calculate the relative proportions of each size class present in the feed. Table 5.13 shows the experimental size analyses and the balanced mass flows for each of the size classes, with the flows calculated on the basis of 100 feed units. The individual sizes are combined together in proportions such that the recalculated screen analyses for the various sample points approach the experimental size analysis as closely as possible (ie. such that the sum of squared deviations between the recalculated and size analyses is minimized). In the case of this data the best fit occurs with a feed composition of 21.2% coarse, 39.0% medium, 21.0% fine, and 18.8% ultrafine. Using this combination it is found that the recalculated size abundances at any given sample point do not differ from the measured size analyses by more than about 3% for the majority of the data points.

Figure 5.2 shows the observed vs. calculated abundances of coarse, medium, fine and ultrafine material for all sample points, and shows that the recalculated size analyses from the individual mass balances tend to provide a good description of the measured screen analyses. Thus, only a slight error is introduced to the quantitative evaluation by treating the circuit as if it contains 21% coarse, 39% medium, 21% fine and 19% ultrafine material in the feed, each of which partitions according to its individual mass balance.

Using the above approximation it is possible to construct a table showing the quantitative flow of all size classes of each mineral through the circuit (Table 5.14). The total mass flows through the circuit are calculated by adding together the weighted mass flows for the individual size classes (as described above). The distributions of the individual mineral species between size classes are obtained using the mass balanced assays. To illustrate:

Cu in CF Coarse = 5.69 Mass = 29.6 feed units (Table 5.3)
Cu in CF Medium = 5.16 Mass = 75.7 feed units (Table 5.4)
Cu in CF Fine = 5.84 Mass = 85.0 feed units (Table 5.5)
Cu in CF U/F = 5.73 Mass = 275.7 feed units (Table 5.6)

Feed proportions are 21.2 Coarse, 39.0 Medium, 21.0 Fine, 18.8 U/F.

Total mass = .212(29.6) + .390(75.7) + .210(85.0) + .188(275.7)
= 266.0

Cu Assay = [.212(29.6)(5.69) + .390(75.7)(5.16) +
.210(85.0)(5.84) + .188(275.7)(5.73)] / 266.0
= 5.59%

Cu (Coarse) = .212(29.6)(5.69) / (266.0)(5.59) = .080
(Medium) = .390(75.7)(5.16) / (266.0)(5.59) = .386 etc...

Observed vs. Calculated Screen Analyses
(All Size Classes)

Figure 5.2

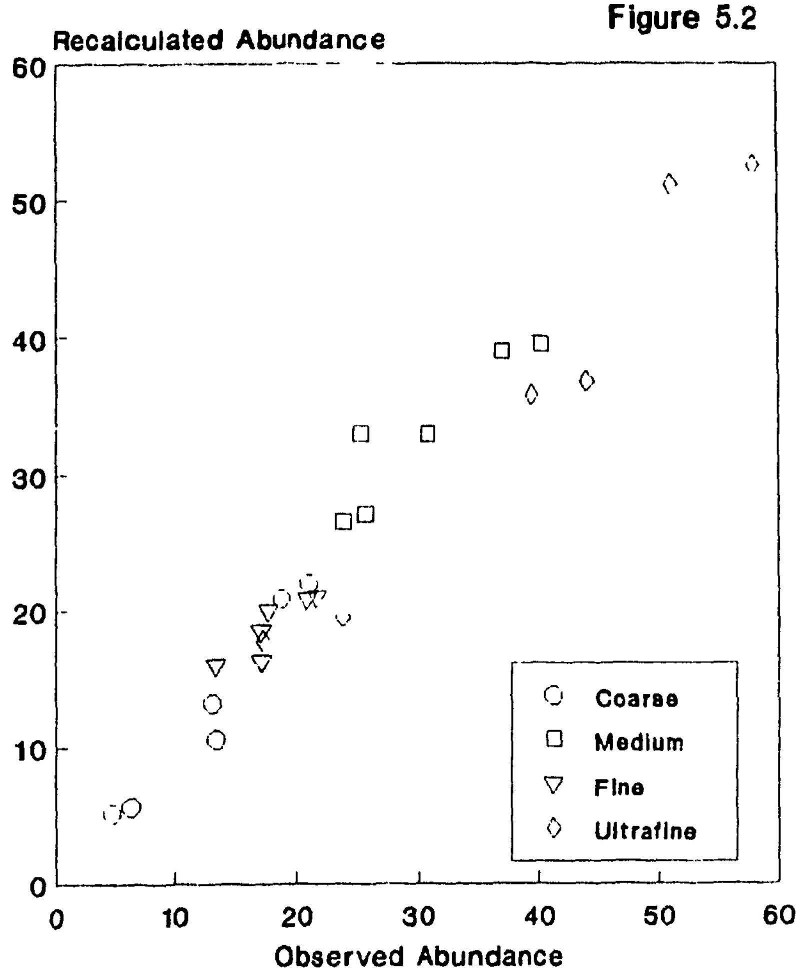

COMPARISON BETWEEN RECALCULATED AND MEASURED SCREEN ANALYSES   Table 5.13

MASS DISTRIBUTION WITHIN STREAM (SCREEN ANALYSIS)

	Total	Coarse	Medium	Fine	U/F
74	100.0	18.6	36.8	20.8	23.8
76	100.0	13.1	30.7	16.9	39.3
RT	100.0	21.0	40.2	21.7	17.1
CF	100.0	6.5	25.5	17.0	51.0
CT	100.0	4.9	23.8	13.4	57.9
CN	100.0	13.4	25.2	17.5	43.9

MASS BALANCE OF INDIVIDUAL STREAMS (USING ASSAY DATA)

	Total	Coarse	Medium	Fine	U/F
74	100.0	100.0	100.0	100.0	100.0
76	196.0	125.9	168.4	176.9	359.0
RT	90.9	96.3	92.7	91.9	83.4
CF	105.0	29.6	75.7	85.0	275.7
CT	96.0	25.9	68.4	76.9	259.0
CN	9.1	3.7	7.3	8.1	16.7

RECALCULATED SCREEN ANALYSIS (FROM MASS BALANCED FLOWS)

	Coarse	Medium	Fine	U/F
74	21.2	39.0	21.0	18.8
76	13.6	33.2	18.9	34.4
RT	22.2	39.4	21.2	17.2
CF	6.1	27.9	16.9	49.2
CT	5.6	27.2	16.6	50.6
CN	11.3	35.2	19.6	33.9

DIFFERENCE BETWEEN MEASURED AND RECALCULATED SCREEN ANALYSES

	Coarse	Medium	Fine	U/F
74	2.6	2.2	0.2	-5.0
76	0.5	2.5	2.0	-4.9
RT	1.2	-0.8	-0.5	0.1
CF	-0.4	2.4	-0.1	-1.8
CT	0.7	3.4	3.2	-7.3
CN	-2.1	10.0	2.1	-10.0

CALCULATED MASS DISTRIBUTIONS THROUGH THE COPPER CIRCUIT Table 5.14

			UNITS OF TOTAL FEED				
COPPER	Unsized Grade	Recalc Grade	Total	Coarse	Medium	Fine	U/F
74	2.34	2.21	100.0	10.3	34.4	22.7	32.6
76	3.23	3.14	279.5	18.4	73.0	50.0	138.0
RT	0.33	0.33	13.5	2.2	4.3	3.0	4.0
CF	5.73	5.59	266.0	16.1	68.8	47.1	134.1
CT	4.15	4.09	179.2	8.0	38.6	27.4	105.3
CN	22.45	22.64	86.5	8.1	30.1	19.8	28.6
Stage Recoveries		Rougher:	95.2	87.8	94.1	94.1	97.1
		Cleaner:	32.5	50.0	43.8	41.9	21.3
		Circuit:	86.5	78.0	87.6	87.0	87.7
		Recirc Load:	179	78	112	121	323
Product Grades		Feed	2.34	1.08	1.95	2.39	3.84
		Tails	0.33	0.24	0.26	0.34	0.57
		Rghr Con	5.73	5.69	5.16	5.84	5.73
		Circuit Con	22.45	22.73	23.44	25.69	20.30

			UNITS OF TOTAL FEED				
LEAD	Unsized Grade	Recalc Grade	Total	Coarse	Medium	Fine	U/F
74	27.49	27.08	100.0	19.6	37.8	19.2	23.3
76	29.49	29.31	213.2	27.4	71.0	36.0	78.7
RT	29.64	29.06	98.2	19.5	37.4	18.9	22.4
CF	29.36	29.52	115.0	7.9	33.7	17.1	56.3
CT	31.57	31.60	113.2	7.8	33.2	16.8	55.4
CN	5.91	5.69	1.8	0.1	0.5	0.3	0.9
Stage Recoveries		Rougher:	53.9	28.8	47.4	47.5	71.5
		Cleaner:	1.5	1.5	1.4	1.7	1.6
		Circuit:	1.8	0.6	1.2	1.5	3.9
		Recirc Load:	113	40	88	87	237
Product Grades		Feed	27.5	25.1	29.3	24.8	33.6
		Tails	29.6	25.9	28.0	26.6	38.8
		Rghr Con	29.4	34.1	30.9	26.0	29.4
		Circuit Con	5.9	4.1	4.4	4.6	7.9

CONTINUED ......

CALCULATED MASS DISTRIBUTIONS THROUGH THE COPPER CIRCUIT Table 5.14B

				UNITS OF TOTAL FEED			
ZINC	Unsized Grade	Recalc Grade	Total	Coarse	Medium	Fine	U/F
74	10.42	10.69	100.0	30.8	40.7	18.3	10.2
76	7.79	7.91	145.7	33.0	53.4	27.3	31.9
RT	11.14	11.40	97.6	30.6	40.0	17.9	9.1
CF	4.88	4.88	48.1	2.5	13.4	9.4	22.8
CT	5.04	5.04	45.8	2.3	12.7	9.1	21.8
CN	3.20	3.00	2.4	0.2	0.7	0.4	1.1
Stage Recoveries	Rougher:		33.0	7.5	25.0	34.5	71.5
	Cleaner:		4.9	8.9	5.3	3.9	4.7
	Circuit:		2.4	0.7	1.8	2.0	10.5
	Recirc Load:		46	7	31	50	213
Product Grades	Feed		10.42	15.52	11.17	9.31	5.80
	Tails		11.14	16.00	11.84	9.93	6.22
	Rghr Con		4.88	4.24	4.84	5.65	4.71
	Circuit Con		3.2	3.01	2.68	2.30	3.67

				UNITS OF TOTAL FEED			
PYRITE	Unsized Grade	Recalc Grade	Total	Coarse	Medium	Fine	U/F
74				22.5	49.9	27.6	
76				27.2	76.4	44.8	
RT				22.1	48.4	27.1	
CF				5.1	28.1	17.7	
CT				4.7	26.6	17.2	
CN				0.4	1.5	0.5	
Stage Recoveries	Rougher:			18.8	36.7	39.6	
	Cleaner:			8.6	5.4	2.9	
	Circuit:			2.0	3.0	1.9	
	Recirc Load:			21	53	62	
Product Grades	Feed			30.0	36.2	37.1	
	Tails			30.6	37.8	39.6	
	Rghr Con			23.1	26.9	28.1	
	Circuit Con			15.9	15.0	5.8	

Table 5.14 also contains data concerning stage recoveries and the grades of several of the streams, compiled from tables 5.2 through 5.12. This data is all that is usually required to conduct a comprehensive size-by-size circuit analysis.

Since the flows through the circuit are obtained by a "best fit" combination of the mass balances for the individual sizes there is not perfect correspondence between the mass-balanced assays for the unsized sample and the recalculated assays from balances of the sized material. For example, the recalculated grade of copper in the cleaner feed is 5.59 (above) as compared to 5.73 in Table 5.2. The mass-balanced assays for the unsized sample are shown as "Unsized Grade" in Table 5.14, and show a generally good correspondence with the recalculated stream assays.

5.1.2: Circuit Analysis: Copper/Lead Separation

The overall circuit recovery for copper is 86.5%, with a rougher recovery of 95.2% and a cleaner recovery of only 32.5%. Thus, a high recirculating load is seen (179%). Analysis of circuit recoveries on a size-by-size basis reveals that the highest recirculating loads originate in the ultrafine fraction. Rougher recoveries increase as the size decreases (from 88% in the coarse fraction to 97% in the ultrafines); however, cleaner recoveries are lower in the finer size fractions (decreasing from 50% for coarse particles to 21% for fine particles). This results in recirculating loads which increase from 78% in the coarse fraction to 121% in the fine fraction, and 323% in the ultrafines.

Copper in the circuit feed tends to be fine. While the overall grade of copper in the feed is 2.34%, the grade of the coarse fraction is only 1.08% while the grade of the ultrafines is 3.84%. Thus, despite the lower rougher recovery of coarse particles it is found that their contribution to the tailings is relatively low. Circuit recovery for coarse copper is only 78%, with a coarse rougher tailings grading 0.24% copper. In contrast, circuit recovery for ultrafines is 88%, with an ultrafine rougher tailings of 0.57% Cu. Certainly the high recirculating load of fine material must be held partly to blame for losses in the fines. The coarse fraction contains 10.3% of the feed copper, and contribute losses equivalent to 2.2% of the feed copper. In the absence of a recirculating load the coarse losses would be expected to lie somewhere around (1-.878)*10.3, or 1.3% of the feed copper. The ultrafines contain 32.6% of the feed copper, and contribute losses equivalent to 4% of the feed copper. In the absence of a recirculating load the ultrafine losses would be expected to lie somewhere around (1-.971)*32.6, or 0.9% of the feed copper. Thus, the rougher is less efficient at recovering coarse copper, but ends up rejecting high quantities of fine copper as a result of the high recirculating loads of fine material.

Upgrading in the rougher is not very efficient. The overall feed contains about 2.3% Cu, as opposed to only 5.7% in the rougher concentrate. The bulk of the upgrading is accomplished in the cleaners, where the grade is elevated to 22.5%. The grade of the concentrate does not vary excessively between size classes, but increases as the size decreases from coarse to fine. The ultrafine fraction produces the lowest concentrate grade. Copper behaviour is typical of a circuit in which locking impedes coarse recovery and mechanical entrainment lowers the concentrate grade.

5.1.3: Circuit Analysis: Lead

The overall circuit recovery for lead is 1.8%, with an overall rougher recovery of 53.9% and a cleaner recovery of 1.5%. Thus, a significant recirculating load exists (113%). Rougher recovery is strongly size-dependent, increasing from 29% in the coarse fraction to 72% in the fine fraction. Cleaner recoveries are 1.5-2.0% in all size fractions. The recirculating loads of lead vary from 40% for coarse lead to 237% for ultrafine lead.

Lead behaviour is dominated by the recovery of ultrafine material in the rougher. The lead grade of the final copper concentrate is about 4.1-4.6% for the coarse, medium and fine fractions but 7.9% for the ultrafine fraction. There is no obvious explanation for the relatively high levels of lead in the concentrate. The cleaner recoveries are not size dependent enough to suggest either a locking or a mechanical entrainment mechanism as being the dominant cause of lead contamination.

5.1.4: Circuit Analysis: Zinc and Pyrite

Zinc recoveries are 33% in the rougher and 4.9% in the cleaners, yielding an overall recovery of 2.4%. Rougher recovery is strongly size-dependent, increasing from 7.5% in the coarse fraction to 71.5% in the ultrafines. Cleaner recoveries appear to decrease in the finer sizes; however, overall circuit recovery of zinc is dominated by the high rougher recovery and high recirculating loads of ultrafines. Overall concentrate zinc levels decrease from 3.0% in the coarse fraction to 2.3% in the fine fraction, but jump to 3.7% in the ultrafines. Thus, both locking and entrainment could be factors in zinc recovery.

Less data is available for pyrite; however, pyrite behaviour appears to be similar to that of zinc. In the three sized fractions rougher recoveries increase from 18.8% (coarse) to 39.6% (fine). Cleaner recoveries appear to be strongly size dependent, with higher recoveries seen in the coarse fraction.

5.1.5: Overall Circuit Performance

Rougher recoveries are size-dependent for all species, with fine material showing higher recoveries than coarse material. While the ultrafine class is a recalculated class and must therefore be treated more skeptically than the coarse, medium and fine classes, it appears that recoveries are about 71% for Pb, Zn (and Py?) and about 97% for Cu. In order to explain the ultrafine Pb/Zn recoveries by mechanical entrainment the water recovery in the rougher would have to exceed 71%. It is estimated in Table 5.2 that the mass recovery in the rougher is just over 50% of the rougher feed. Thus, the rougher concentrate would have to have a considerably lower pulp density than the rougher feed. Although a water balance was not conducted, this is clearly not the case. It would appear, therefore, that Gn and Sp are at least partially flotable. Since lead shows greater rougher recoveries than zinc in all size fractions except the ultrafines it would appear either that lead is mineralogically associated with copper (eg. Cp/Gn locking) or that galena is more flotable than sphalerite. While the former is a distinct possibility, the latter also makes sense, since the feed to the copper circuit is CuPb concentrate, in which the lead is promoted.

Since ultrafine material is recovered strongly in the roughers it could be expected that ultrafines will constitute a high proportion of the circuit contamination. However, offsetting this is the fact that the cleaners aggressively reject a large proportion of all species. Under such conditions it would be expected both that mechanical entrainment would be minimal and that the highest levels of rejection would be seen in the ultrafine class, where flotation kinetics would be expected to be slow. In other words, given these contrasting expectations it is difficult to discern whether or not coarse contamination constitutes a locking phenomenon or not. It must also be recognized that the range of particle sizes is such that recovery in any of the size ranges may represent some degree of mechanical entrainment.

It is difficult, therefore, to assign specific mechanisms to the recoveries of Pb, Zn and Py in the copper circuit. Chalcopyrite losses to tailings carry a more distinct signature, and suggest a locking problem. The size range of "coarse" chalcopyrite is not high enough for coarse losses to be related to slow flotation kinetics.

Some general comments may be made regarding overall circuit performance. It is evident that the rougher is operated in an aggressive recovery-oriented mode. The amount of upgrading occurring in this stage is not spectacular, with circuit feeds ranging from 1.1% to 3.8% copper and rougher concentrates ranging from 5.2% to 5.8% copper. Since the target grade for the circuit is somewhere in the range of 25% copper a large amount of upgrading is required in the cleaners. It appears that the low grade of rougher concentrate is ultimately responsible for the high recirculating loads, which in turn reduce the effective retention time of the roughers and require more aggressive flotation, leading to increased mechanical entrainment, and so on. The circuit would probably benefit from lower recirculating loads, which could be achieved by moving towards less aggressive roughing. The cleaners could also be made to assume some of the recirculating load, perhaps by routing the third cleaner tailings to the rougher concentrate instead of the rougher feed.

In summary, the size-by-size data provides relatively little indication of the recovery mechanisms, but is useful in providing a broader perspective on circuit performance and problems. Liberation data is added in an attempt to explain some of the specific problems which result in the collection of a low-grade rougher concentrate and the passage of Gn, Sp and Py into the concentrate.

5.2: Liberation Data

The calculation of relevant parameters for the image analysis samples requires much data manipulation, and generates more tables than is practical to include with the data analysis. Thus, raw data and intermediate calculations are included as Appendix 1, and are described briefly as follows:

Tables A1.1 to A1.6 show the measured areas of various section types and grades. A given measured area (section) is classified by its type (eg. Cp/Px binary) and its grade (eg. 15% to 25% Cp). The data in these tables is processed through the algorithm described in section 3.3.2 to determine the proportion of free section area in the 00-05 and 95-100 grade classes. The processed data is converted into percentages of total observed area, and is presented in Tables A1.7 to A1.24.

Tables A1.25 to A1.42 show the frequency of observation of various section grades. Sections are classified as being free, high-grade (>85%), medium grade (15-85%) or low-grade (<15%). The principal behind the data reduction is to combine the information into as statistically relevant a description of the sample as possible, while retaining sufficient information to form a meaningful description of circuit performance. It was considered that the four descriptions of section grade given above could provide a useful description of circuit performance while minimizing the statistical error of the observations. The tables record the frequency of observation of each of the four section grades, with calculations carried out separately for each of the four measured mineral species.

Tables A1.43 to A1.60 calculate the distributions of various mineral observations into different section types and grades (eg. Area% of total Cp in the form of free Cp, or as Cp/Gn sections with 85-95% Cp). This data is further processed in Tables A1.61 to A1.78, in which the overall sample grade is recalculated and sectional grade/recovery data for the mineral species is presented.

The division of area observations into low-grade (00-15%), medium grade (15%-85%), high-grade (85%-100%) and free (100%) grade classes is shown in Tables 5.15 to 5.18. The data is presented as area distributions into the various section types, with all types summing to 100% for a given sample. Since locked sections contain less of the mineral of interest than do free sections it requires considerably more section observations to contribute a percentage point of area distribution. For example, low-grade Cp observations (0-15%) have an average grade of about 7.5% Cp, meaning that an average of 13.3 observations are required to contribute the same amount of Cp area as a single free section of equivalent size. Medium grade observations (15%-85%) have an average of 50% Cp, and thus require about two observations per percentage distribution, while high-grade particles (85%-100%) require only 1.1 observations to contribute as much Cp as a free section. Consequently, the low-grade observations tend to have a lower variance than the high-grade and free observations. This must be taken into account in the interpretation of the data.

It should be possible to balance the structural data around the various sample points in much the same way as the assay data was balanced. A balance can be conducted despite the fact that the observations are stereologically biased, since the suite of sections observed from a given particle type should not depend upon the number or types of other particles in the assemblage. However, in order to perform a meaningful balance it is necessary to assign a variance to each of the "structural assays".

The number of "mean events" recorded from the various samples was calculated in Section 3.5 (Table 3.14). The standard deviation of an assay is equal to the square root of the number of counts which are recorded. Table

5.19 illustrates the procedure by which the standard deviations of the structural assays are calculated, with chalcopyrite in the circuit feed (sample 74A) used here as an example. The sample assay (3.47% Cp) is multiplied by the number of mean events (5296) to yield a total number of "Cp events" (184, not shown on the table). The structural data for Cp in sample 74A shows that 2.62% of the measured Cp is low-grade, 25.21% is medium-grade, 12.03% is high-grade and 60.14% is free (Table 5.15). It takes 13.3 low-grade events to contribute one chalcopyrite event. Thus, the number of low-grade chalcopyrite events is approximately 184 (total events) * .0262 (amount low-grade) * 13.3 (events per Cp event), or 64 low-grade events. Similarly, the number of medium-grade events is 184 * .2521 * 2, or 93; the high-grade events number 184 * .1203 * 1.1, or 24. One free event is equivalent to one chalcopyrite event. Thus, the number of free events is equal to 184 * .6014, or 111 events.

Since the variance in the number of measured events is numerically equal to the number of measured events, the relative standard deviation of the "structural assay" can be calculated as $100/\sqrt{N}$, where N is the estimated number of mean events. Thus, the relative standard deviation of the assay for "low-grade Cp" is equal to $100/\sqrt{64}$, or 12.5, and so on. The relative standard deviations of the structural assays are calculated for the coarse, medium and fine samples in Tables 5.19, 5.20 and 5.21. It should be noted that the method is an approximation, since Poisson statistics are rigorously valid only when the events being measured are independent. The fact that the measured "structural assays" for the four structural types must add to 100% invalidates this requirement, although the calculated confidence intervals are good approximations for the purpose of mass balancing.

Using the structural assays and the estimated confidence limits for the assays it is possible to perform a mass balance for all section types around the circuit. The flows are obtained from the size-by-size data (Tables 5.8, 5.9 and 5.10) in which mass balances were conducted for the total flows of coarse, medium and fine minerals around the circuit. The data from these tables has been converted from assays into mineralogy, and the total sulfide content normalized to 100%. The balances are presented in Tables 5.22 to 5.33, with the flow data recorded as "Units" at the top of the tables. (The total units of sulfides in the circuit feed equals 100.00).

The balances are performed so as to minimize the weighted sum of squared adjustments which must be made to the structural data, with the variance of the structural assay used for weighting. (The assay variance is the square of assay standard deviation, which in turn is the product of the assay and the relative standard deviation. Only the relative standard deviations are shown in the tables). The tables show the original image analysis data, the balanced data, and the magnitude of the adjustments which had to be made. A summary of recoveries and recirculating loads through the rougher and cleaners is presented in Table 5.34.

LIBERATION DATA FOR CHALCOPYRITE

Table 5.15

DISTRIBUTION INTO VARIOUS PARTICLE TYPES

COARSE	74	76	RT	CF	CT	CN
00-15	2.62	2.20	3.67	4.10	6.81	0.79
15-85	25.21	30.66	23.30	35.41	26.59	17.03
85-100	12.03	17.28	42.30	12.64	11.66	17.41
Free	60.14	49.87	30.74	47.85	54.93	64.77
Total	100.00	100.01	100.01	100.00	99.99	100.00

MEDIUM	74	76	RT	CF	CT	CN
00-15	7.16	6.03	24.01	3.43	3.22	0.53
15-85	25.42	24.22	34.37	26.23	27.02	10.90
85-100	14.77	17.70	15.13	15.96	11.76	10.15
Free	52.65	52.05	26.49	54.38	58.00	78.42
Total	100.00	100.00	100.00	100.00	100.00	100.00

FINE	74	76	RT	CF	CT	CN
00-15	17.73	15.45	23.20	9.02	3.89	0.42
15-85	32.94	38.17	28.48	43.58	26.16	7.29
85-100	24.89	37.08	22.28	41.13	21.27	12.94
Free	24.43	9.31	26.04	6.27	48.67	79.35
Total	99.99	100.01	100.00	100.00	99.99	100.00

LIBERATION DATA FOR GALENA

Table 5.16

DISTRIBUTION INTO VARIOUS PARTICLE TYPES

COARSE	74	76	RT	CF	CT	CN
00-15	8.13	6.38	7.61	1.30	1.05	4.31
15-85	32.03	30.15	39.73	10.61	8.19	22.87
85-100	4.18	5.46	6.58	4.59	4.91	6.39
Free	55.65	58.00	46.08	83.51	85.84	66.43
Total	99.99	99.99	100.00	100.01	99.99	100.00

MEDIUM	74	76	RT	CF	CT	CN
00-15	5.48	2.73	4.28	0.88	0.70	9.51
15-85	22.11	13.98	15.29	6.83	5.55	40.68
85-100	5.62	3.95	4.77	2.99	2.41	17.08
Free	66.79	79.33	75.66	89.30	91.33	32.73
Total	100.00	99.99	100.00	100.00	99.99	100.00

FINE	74	76	RT	CF	CT	CN
00-15	3.49	2.61	2.83	1.93	2.03	2.19
15-85	17.96	13.97	11.94	13.52	9.20	8.44
85-100	5.87	6.62	3.04	5.34	4.65	5.72
Free	72.57	76.80	82.19	79.20	84.12	83.64
Total	99.89	100.00	100.00	99.99	100.00	99.99

LIBERATION DATA FOR SPHALERITE Table 5.17

DISTRIBUTION INTO VARIOUS PARTICLE TYPES

COARSE	74	76	RT	CF	CT	CN
00-15	2.07	1.86	3.26	4.35	3.15	9.79
15-85	31.81	36.38	40.59	51.76	36.55	52.14
85-100	36.21	36.16	36.55	20.49	18.06	15.42
Free	29.91	25.60	19.60	23.40	42.24	22.64
Total	100.00	100.00	100.00	100.00	100.00	99.99

MEDIUM	74	76	RT	CF	CT	CN
00-15	2.17	1.60	1.25	3.75	3.14	7.43
15-85	31.55	28.33	23.31	32.79	29.83	39.64
85-100	49.28	31.77	42.75	17.36	15.79	11.64
Free	17.00	38.30	32.69	46.10	51.25	41.29
Total	100.00	100.00	100.00	100.00	100.01	100.00

FINE	74	76	RT	CF	CT	CN
00-15	3.62	5.00	1.92	7.89	2.01	5.65
15-85	40.85	41.97	21.72	42.72	32.16	33.66
85-100	44.88	45.83	33.45	31.35	39.34	28.34
Free	10.65	7.20	42.91	18.04	26.49	32.35
Total	100.00	100.00	100.00	100.00	100.00	100.00

LIBERATION DATA FOR IRON MINERALS Table 5.18

DISTRIBUTION INTO VARIOUS PARTICLE TYPES

COARSE	74	76	RT	CF	CT	CN
00-15	0.80	0.99	1.08	1.09	0.57	3.39
15-85	31.68	33.45	41.18	33.56	19.11	41.81
85-100	37.40	35.76	40.58	30.58	32.39	24.72
Free	30.12	29.81	17.16	34.78	47.94	30.08
Total	100.00	100.01	100.00	100.01	100.01	100.00

MEDIUM	74	76	RT	CF	CT	CN
00-15	0.73	0.60	0.33	0.58	0.49	2.15
15-85	22.39	19.42	12.95	20.19	19.74	35.67
85-100	33.65	28.92	22.78	21.97	20.58	21.83
Free	43.23	51.07	63.93	57.26	59.20	40.35
Total	100.00	100.01	99.99	100.00	100.01	100.00

FINE	74	76	RT	CF	CT	CN
00-15	1.28	1.64	0.43	2.10	1.25	3.71
15-85	16.97	18.82	11.61	30.52	17.02	27.80
85-100	32.87	37.10	21.36	39.26	21.03	21.38
Free	48.88	42.44	66.60	28.12	60.69	47.11
Total	100.00	100.00	100.00	100.00	99.99	100.00

CALCULATION OF ASSAY STANDARD DEVIATIONS - COARSE FRACTION

Table 5.19

	Events per Assay% :		13.3	2.0	1.1	1.0				
	Events & Assays		# OF EVENTS				ASSAY STD DEV%			
			00-15	15-85	85-00	Free	00-15	15-85	85-00	Free
74	Events	5296								
	Cu	3.47	64	93	24	111	12.5	10.4	20.5	9.5
	Pb	30.57	1755	1037	73	901	2.4	3.1	11.7	3.3
	Zn	30.42	445	1025	631	482	4.7	3.1	4.0	4.6
	Fe	35.50	519	1196	736	562	4.4	2.9	3.7	4.2
76	Events	6107								
	Cu	4.68	84	175	53	143	10.9	7.6	13.7	8.4
	Pb	36.78	1911	1354	133	1303	2.3	2.7	8.7	2.8
	Zn	26.09	395	1159	623	408	5.0	2.9	4.0	5.0
	Fe	32.40	491	1440	773	507	4.5	2.6	3.6	4.4
RT	Events	6756								
	Cu	0.83	27	26	26	17	19.1	19.6	19.7	24.1
	Pb	35.80	2454	1922	172	1115	2.0	2.3	7.6	3.0
	Zn	29.02	852	1592	775	384	3.4	2.5	3.6	5.1
	Fe	34.40	1010	1887	918	456	3.1	2.3	3.3	4.7
CF	Events	4636								
	Cu	17.24	1043	833	133	181	3.1	3.5	8.7	7.4
	Pb	48.41	1227	1589	307	1074	2.9	2.5	5.7	3.1
	Zn	8.31	67	82	19	322	12.2	11.1	22.9	5.5
	Fe	26.04	700	1250	267	282	3.8	2.8	6.1	5.9
CT	Events	2159								
	Cu	15.42	302	177	42	183	5.8	7.5	15.4	7.4
	Pb	48.17	146	170	55	893	8.3	7.7	13.5	3.3
	Zn	8.29	104	185	40	42	9.8	7.3	15.9	15.5
	Fe	28.13	255	444	119	257	6.3	4.7	9.2	6.2
CN	Events	4823								
	Cu	72.31	367	1188	656	2259	5.2	2.9	3.9	2.1
	Pb	5.17	143	114	17	166	8.4	9.4	24.1	7.8
	Zn	5.39	109	190	51	110	9.6	7.3	14.0	9.5
	Fe	17.13	1078	862	138	187	3.0	3.4	8.5	7.3

CALCULATION OF ASSAY STANDARD DEVIATIONS - MEDIUM FRACTION Table 5.2o

Events per Assay% :			13.3	2.0	1.1	1.0				
Events & Assays			# OF EVENTS				ASSAY STD DEV%			
			00-15	15-85	85-00	Free	00-15	15-85	85-00	Free
74	Events	2542								
	Cu	1.97	5	32	20	15	43.3	17.8	22.2	25.7
	Pb	26.16	635	338	106	350	4.0	5.4	9.7	5.3
	Zn	11.16	207	125	17	189	6.9	8.9	24.1	7.3
	Fe	21.95	161	352	297	95	7.9	5.3	5.8	10.3
76	Events	7596								
	Cu	2.35	24	119	69	53	20.6	9.2	12.0	13.7
	Pb	30.17	1843	1110	439	1193	2.3	3.0	4.8	2.9
	Zn	9.66	267	205	31	582	6.1	7.0	17.9	4.1
	Fe	20.76	336	893	542	604	5.5	3.3	4.3	4.1
RT	Events	2253								
	Cu	0.26	1	5	3	1	108.9	45.5	62.4	99.7
	Pb	25.52	1841	395	94	152	2.3	5.0	10.3	8.1
	Zn	11.14	143	77	13	190	8.4	11.4	27.8	7.3
	Fe	21.74	82	228	226	160	11.1	6.6	6.6	7.9
CF	Events	7778								
	Cu	4.77	54	249	123	129	13.6	6.3	9.0	8.8
	Pb	32.79	1166	1338	440	1387	2.9	2.7	4.8	2.7
	Zn	5.01	46	53	13	348	14.8	13.7	28.2	5.4
	Fe	20.48	796	1045	299	734	3.5	3.1	5.8	3.7
CT	Events	7506								
	Cu	5.44	31	156	143	196	18.0	8.0	8.4	7.1
	Pb	31.90	1028	1294	304	1389	3.1	2.8	5.7	2.7
	Zn	4.83	34	40	9	331	17.2	15.8	32.5	5.5
	Fe	20.26	637	907	260	779	4.0	3.3	6.2	3.6
CN	Events	6197								
	Cu	23.48	658	1217	389	438	3.9	2.9	5.1	4.8
	Pb	4.39	19	59	30	213	22.8	13.0	18.3	6.8
	Zn	2.65	208	134	30	54	6.9	8.7	18.2	13.6
	Fe	28.82	1769	1416	225	737	2.4	2.7	6.7	3.7

CALCULATION OF ASSAY STANDARD DEVIATIONS - FINE FRACTION

Table 5.21

Events per Assay% : 13.3 2.0 1.1 1.0

	Events & Assays		# OF EVENTS				ASSAY STD DEV%			
			00-15	15-85	85-00	Free	00-15	15-85	85-00	Free
74	Events	8317								
	Cu	2.41	474	132	54	49	4.6	8.7	13.6	14.3
	Pb	23.70	917	708	125	1430	3.3	3.8	8.9	2.6
	Zn	8.91	358	605	360	79	5.3	4.1	5.3	11.3
	Fe	23.80	338	672	703	968	5.4	3.9	3.8	3.2
76	Events	7042								
	Cu	2.85	413	153	80	19	4.9	8.1	11.1	23.1
	Pb	27.60	676	543	139	1493	3.8	4.3	8.5	2.6
	Zn	7.79	366	460	272	39	5.2	4.7	6.1	15.9
	Fe	21.92	338	581	619	655	5.4	4.1	4.0	3.9
RT	Events	7988								
	Cu	0.34	84	15	7	7	10.9	25.4	39.1	37.6
	Pb	26.39	795	503	69	1733	3.5	4.5	12.0	2.4
	Zn	10.51	215	365	304	360	6.8	5.2	5.7	5.3
	Fe	22.60	104	419	417	1202	9.8	4.9	4.9	2.9
CF	Events	3800								
	Cu	5.59	255	185	94	13	6.3	7.3	10.3	27.4
	Pb	27.75	271	285	61	835	6.1	5.9	12.8	3.5
	Zn	5.87	235	191	76	40	6.5	7.2	11.5	15.8
	Fe	21.37	227	496	345	228	6.6	4.5	5.4	6.6
CT	Events	2850								
	Cu	5.35	79	80	35	74	11.2	11.2	16.9	11.6
	Pb	26.46	204	139	38	634	7.0	8.5	16.2	4.0
	Zn	5.82	44	107	71	44	15.0	9.7	11.9	15.1
	Fe	21.58	103	209	140	373	9.9	6.9	8.5	5.2
CH	Events	7551								
	Cu	25.69	109	283	271	1539	9.6	5.9	6.1	2.5
	Pb	4.60	101	59	21	291	9.9	13.1	21.6	5.9
	Zn	2.30	131	117	53	56	8.7	9.2	13.7	13.3
	Fe	27.75	1037	1165	484	987	3.1	2.9	4.5	3.2

LIEBERATION DATA FOR CHALCOPYRITE (COARSE FRACTION) Table 5.22

	74	76	RT	CF	CT	CN
Units	3.43	6.05	0.81	5.25	2.63	2.63
DISTRIBUTION INTO VARIOUS PARTICLE TYPES						
00-15	2.62	2.20	3.67	4.10	6.81	0.79
15-85	25.21	30.66	23.30	35.41	26.59	17.03
85-100	12.03	17.28	42.30	12.64	11.66	17.41
Free	60.14	49.87	30.74	47.85	54.93	64.77
RELATIVE STANDARD DEVIATION						
00-15	12.5	10.9	19.1	3.1	5.8	5.2
15-85	10.4	7.6	19.6	3.5	7.5	2.9
85-100	20.5	13.7	19.7	8.7	15.4	3.9
Free	9.5	8.4	24.1	7.4	7.4	2.1
MASS BALANCED DATA						
00-15	1.39	3.69	3.30	3.75	6.70	0.80
15-85	20.75	27.89	29.90	27.56	37.20	17.90
85-100	20.06	15.74	30.20	13.51	10.10	16.90
Free	57.99	52.80	36.60	55.24	46.00	64.40
MAGNITUDE OF CHANGE (ABSOLUTE)						
00-15	-1.2	1.5	-0.4	-0.4	-0.1	0.0
15-85	-4.5	-2.8	6.6	-7.9	10.6	0.9
85-100	8.0	-1.5	-12.1	0.9	-1.6	-0.5
Free	-2.2	2.9	5.9	7.4	-8.9	-0.4

STAGE RECOVERIES

	RGHR	CLNR	CIRCUIT	RECIRC LOAD
00-15	88	11	44	369
15-85	86	33	66	137
85-100	74	63	65	39
Free	91	58	85	61

LIBERATION DATA FOR GALENA (COARSE FRACTION) Table 5.23

	74	76	RT	CF	CT	CN
Units	32.14	44.47	31.94	12.52	12.32	0.19

DISTRIBUTION INTO VARIOUS PARTICLE TYPES

	74	76	RT	CF	CT	CN
00-15	8.13	6.38	7.61	1.30	1.05	4.31
15-85	32.03	30.15	39.73	10.61	8.19	22.87
85-100	4.18	5.46	6.58	4.59	4.91	6.39
Free	55.65	58.00	46.08	83.51	85.84	66.43

RELATIVE STANDARD DEVIATION

	74	76	RT	CF	CT	CN
00-15	4.4	4.5	3.1	3.8	6.3	3.0
15-85	2.9	2.6	2.3	2.8	4.7	3.4
85-100	3.7	3.6	3.3	6.1	9.2	8.5
Free	4.2	4.4	4.7	5.9	6.2	7.3

MASS BALANCED DATA

	74	76	RT	CF	CT	CN
00-15	7.88	6.03	7.90	1.25	1.20	4.30
15-85	36.51	29.05	36.60	9.80	9.60	23.00
85-100	5.10	5.02	5.10	4.82	4.80	6.10
Free	50.49	59.88	50.40	84.12	84.40	66.60

MAGNITUDE OF CHANGE (ABSOLUTE)

	74	76	RT	CF	CT	CN
00-15	-0.3	-0.4	0.3	-0.1	0.1	-0.0
15-85	4.5	-1.1	-3.1	-0.8	1.4	0.1
85-100	0.9	-0.4	-1.5	0.2	-0.1	-0.3
Free	-5.2	1.9	4.3	0.6	-1.4	0.2

STAGE RECOVERIES

	RGHR	CLNR	CIRCUIT	RECIRC LOAD
00-15	6	5	0	6
15-85	9	4	0	10
85-100	27	2	1	36
Free	40	1	1	64

LIBERATION DATA FOR SPHALERITE (COARSE FRACTION) Table 5.24

	74	76	RT	CF	CT	CN
Units	29.51	31.56	29.31	2.25	2.04	0.20

DISTRIBUTION INTO VARIOUS PARTICLE TYPES

	74	76	RT	CF	CT	CN
00-15	2.07	1.86	3.26	4.35	3.15	9.79
15-85	31.81	36.38	40.59	51.76	36.55	52.14
85-100	36.21	36.16	36.55	20.49	18.06	15.42
Free	29.91	25.60	19.60	23.40	42.24	22.64

RELATIVE STANDARD DEVIATION

	74	76	RT	CF	CT	CN
00-15	4.7	5.0	3.4	12.2	9.8	9.6
15-85	3.1	2.9	2.5	11.1	7.3	7.3
85-100	4.0	4.0	3.6	22.9	15.9	14.0
Free	4.6	5.0	5.1	5.6	15.5	9.5

MASS BALANCED DATA

	74	76	RT	CF	CT	CN
00-15	2.35	2.40	2.30	3.67	3.10	9.50
15-85	36.43	37.07	36.30	47.23	46.60	53.90
85-100	37.05	36.18	37.20	22.94	23.80	14.40
Free	24.19	24.33	24.20	26.10	26.50	22.20

MAGNITUDE OF CHANGE (ABSOLUTE)

	74	76	RT	CF	CT	CN
00-15	0.3	0.5	-1.0	-0.7	-0.0	-0.3
15-85	4.6	0.7	-4.3	-4.5	10.1	1.8
85-100	0.8	0.0	0.7	2.5	5.7	-1.0
Free	-5.7	-1.3	4.6	2.7	-15.7	-0.4

STAGE RECOVERIES

	RGHR	CLNR	CIRCUIT	RECIRC LOAD
00-15	11	23	3	9
15-85	9	10	1	9
85-100	5	6	0	4
Free	8	8	1	8

LIBERATION DATA FOR IRON MINERALS (COARSE FRACTION) Table 5.25

	74	76	RT	CF	CT	CN
Units	34.29	40.97	33.66	7.31	6.68	0.63
	DISTRIBUTION INTO VARIOUS PARTICLE TYPES					
00-15	0.80	0.99	1.08	1.09	0.57	3.39
15-85	31.68	33.45	41.18	33.56	19.11	41.81
85-100	37.40	35.76	40.58	30.58	32.39	24.72
Free	30.12	29.81	17.16	34.78	47.94	30.08
	RELATIVE STANDARD DEVIATION					
00-15	2.4	2.3	2.0	2.9	8.3	8.4
15-85	3.1	2.7	2.3	2.5	7.7	9.4
85-100	11.7	8.7	7.6	5.7	13.5	24.1
Free	3.3	2.8	3.0	3.1	3.3	7.8
	MASS BALANCED DATA					
00-15	0.96	0.93	0.91	1.01	0.78	3.43
15-85	36.90	35.56	36.80	29.87	28.70	42.30
85-100	40.83	39.03	41.10	29.52	29.80	26.60
Free	21.31	24.47	21.19	39.59	40.72	27.67
	MAGNITUDE OF CHANGE (ABSOLUTE)					
00-15	0.2	-0.1	-0.2	-0.1	0.2	0.0
15-85	5.2	2.1	-4.4	-3.7	9.6	0.5
85-100	3.4	3.3	0.5	-1.1	-2.6	1.9
Free	-8.8	-5.3	4.0	4.8	-7.2	-2.4

STAGE RECOVERIES

	RGHR	CLNR	CIRCUIT	RECIRC LOAD
00-15	19	29	7	16
15-85	15	12	2	15
85-100	13	8	1	14
Free	29	6	2	37

LIBERATION DATA FOR CHALCOPYRITE (MEDIUM FRACTION) Table 5.26

	74	76	RT	CF	CT	CN
Units	6.23	13.02	0.81	12.21	6.79	5.43
DISTRIBUTION INTO VARIOUS PARTICLE TYPES						
00-15	7.16	6.03	24.01	3.43	3.22	0.53
15-85	25.42	24.22	34.37	26.23	27.02	10.90
85-100	14.77	17.70	15.13	15.96	11.76	10.15
Free	52.65	52.05	26.49	54.38	58.00	78.42
RELATIVE STANDARD DEVIATION						
00-15	43.3	20.6	108.9	13.6	18.0	3.9
15-85	17.8	9.2	45.5	6.3	8.0	2.9
85-100	22.2	12.0	62.4	9.0	8.4	5.1
Free	25.7	13.7	99.7	8.8	7.1	4.8
MASS BALANCED DATA						
00-15	0.63	2.54	1.30	2.63	4.30	0.53
15-85	16.35	24.25	52.00	22.41	31.50	11.00
85-100	12.62	13.03	26.00	12.17	13.40	10.60
Free	70.56	60.26	20.70	62.88	50.80	77.87
MAGNITUDE OF CHANGE (ABSOLUTE)						
00-15	-6.5	-3.5	-22.7	-0.8	1.1	0.0
15-85	-9.1	0.0	17.6	-3.8	4.5	0.1
85-100	-2.2	-4.7	10.9	-3.8	1.6	0.4
Free	17.9	8.2	-5.8	8.5	-7.2	-0.5

STAGE RECOVERIES

	RGHR	CLNR	CIRCUIT	RECIRC LOAD
00-15	97	9	73	743
15-85	87	22	59	210
85-100	88	39	73	116
Free	98	55	96	78

LIBERATION DATA FOR GALENA (MEDIUM FRACTION) Table 5.27

	74	76	RT	CF	CT	CN
Units	33.44	62.83	33.03	29.78	29.38	0.41
			DISTRIBUTION INTO VARIOUS PARTICLE TYPES			
00-15	5.48	2.73	4.28	0.88	0.70	9.51
15-85	22.11	13.98	15.29	6.83	5.55	40.68
85-100	5.62	3.95	4.77	2.99	2.41	17.08
Free	66.79	79.33	75.66	89.30	91.33	32.73
			RELATIVE STANDARD DEVIATION			
00-15	7.9	5.5	11.1	3.5	4.0	2.4
15-85	5.3	3.3	6.6	3.1	3.3	2.7
85-100	5.8	4.3	6.6	5.8	6.2	6.7
Free	10.3	4.1	7.9	3.7	3.6	3.7
			MASS BALANCED DATA			
00-15	4.66	2.82	4.60	0.85	0.73	9.50
15-85	19.56	13.17	19.30	6.38	5.90	40.70
85-100	5.25	4.01	5.10	2.80	2.60	17.30
Free	70.53	79.98	71.00	90.00	90.77	32.50
			MAGNITUDE OF CHANGE (ABSOLUTE)			
00-15	-0.8	0.1	0.3	-0.0	0.0	-0.0
15-85	-2.5	-0.8	4.0	-0.4	0.4	0.0
85-100	-0.4	0.1	0.3	-0.2	0.2	0.2
Free	3.7	0.7	-4.7	0.7	-0.6	-0.2

STAGE RECOVERIES

	RGHR	CLNR	CIRCUIT	RECIRC LOAD
00-15	14	15	2	14
15-85	23	9	3	26
85-100	33	8	4	44
Free	53	0	1	113

LIBERATION DATA FOR SPHALERITE (MEDIUM FRACTION) Table 5.28

	74	76	RT	CF	CT	CN
Units	20.88	27.25	20.52	6.73	6.37	0.36

DISTRIBUTION INTO VARIOUS PARTICLE TYPES

	74	76	RT	CF	CT	CN
00-15	2.17	1.60	1.25	3.75	3.14	7.43
15-85	31.55	28.33	23.31	32.79	29.83	39.64
85-100	49.28	31.77	42.75	17.36	15.79	11.64
Free	17.00	38.30	32.69	46.10	51.25	41.29

RELATIVE STANDARD DEVIATION

	74	76	RT	CF	CT	CN
00-15	6.9	6.1	8.4	14.8	17.2	6.9
15-85	8.9	7.0	11.4	13.7	15.8	8.7
85-100	24.1	17.9	27.8	28.2	32.5	18.2
Free	7.3	4.1	7.3	5.4	5.5	13.6

MASS BALANCED DATA

	74	76	RT	CF	CT	CN
00-15	1.51	1.76	1.40	2.87	2.60	7.60
15-85	29.01	29.22	28.80	30.49	29.90	40.90
85-100	45.61	38.71	46.20	15.89	16.10	12.10
Free	23.87	30.31	23.60	50.76	51.40	39.40

MAGNITUDE OF CHANGE (ABSOLUTE)

	74	76	RT	CF	CT	CN
00-15	-0.7	0.2	0.1	-0.9	-0.5	0.2
15-85	-2.5	0.9	5.5	-2.3	0.1	1.3
85-100	-3.7	6.9	3.5	-1.5	0.3	0.5
Free	6.9	-8.0	-9.1	4.7	0.1	-1.9

STAGE RECOVERIES

	RGHR	CLNR	CIRCUIT	RECIRC LOAD
00-15	40	14	9	53
15-85	26	7	2	31
85-100	10	4	0	11
Free	41	4	3	66

LIBERATION DATA FOR IRON MINERALS (MEDIUM FRACTION) Table 5.29

	74	76	RT	CF	CT	CN
Units	40.54	61.51	39.34	22.17	20.97	1.20

DISTRIBUTION INTO VARIOUS PARTICLE TYPES

	74	76	RT	CF	CT	CN
00-15	0.73	0.60	0.33	0.58	0.49	2.15
15-85	22.39	19.42	12.95	20.19	19.74	35.67
85-100	33.65	28.92	22.78	21.97	20.58	21.83
Free	43.23	51.07	63.93	57.26	59.20	40.35

RELATIVE STANDARD DEVIATION

	74	76	RT	CF	CT	CN
00-15	4.0	2.3	2.3	2.9	3.1	22.8
15-85	5.4	3.0	5.0	2.7	2.8	13.0
85-100	9.7	4.8	10.3	4.8	5.7	18.3
Free	5.3	2.9	8.1	2.7	2.7	6.8

MASS BALANCED DATA

	74	76	RT	CF	CT	CN
00-15	0.47	0.47	0.37	0.66	0.49	3.60
15-85	16.81	17.83	16.20	20.73	19.80	36.90
85-100	32.65	28.78	33.00	21.29	21.30	21.10
Free	50.07	52.92	50.43	57.33	58.41	38.40

MAGNITUDE OF CHANGE (ABSOLUTE)

	74	76	RT	CF	CT	CN
00-15	-0.3	-0.1	0.0	0.1	0.0	1.5
15-85	-5.6	-1.6	3.3	0.5	0.1	1.2
85-100	-1.0	-0.1	10.2	-0.7	0.7	-0.7
Free	6.8	1.8	-13.5	0.1	-0.8	-1.9

STAGE RECOVERIES

	RGHR	CLNR	CIRCUIT	RECIRC LOAD
00-15	50	30	23	54
15-85	42	10	6	61
85-100	27	5	2	34
Free	39	4	2	60

LIBERATION DATA FOR CHALCOPYRITE (FINE FRACTION) Table 5.30

	74	76	RT	CF	CT	CN
Units	7.75	16.99	1.01	15.99	9.24	6.75
DISTRIBUTION INTO VARIOUS PARTICLE TYPES						
00-15	17.73	15.45	23.20	9.02	3.89	0.42
15-85	32.94	38.17	28.48	43.58	26.16	7.29
85-100	24.89	37.08	22.28	41.13	21.27	12.94
Free	24.43	9.31	26.04	6.27	48.67	79.35
RELATIVE STANDARD DEVIATION						
00-15	4.6	4.9	10.9	6.3	11.2	9.6
15-85	8.7	8.1	25.4	7.3	11.2	5.9
85-100	13.6	11.1	39.1	10.3	16.9	6.1
Free	14.3	23.1	37.6	27.4	11.6	2.5
MASS BALANCED DATA						
00-15	6.01	6.77	43.00	4.47	7.40	0.47
15-85	13.07	31.58	39.50	31.06	47.10	9.10
85-100	17.44	32.70	17.50	33.64	45.50	17.40
Free	63.61	29.01	0.00	30.83	0.00	73.03
MAGNITUDE OF CHANGE (ABSOLUTE)						
00-15	-11.7	-8.7	19.8	-4.5	3.5	0.0
15-85	-19.9	-6.6	11.0	-12.5	20.9	1.8
85-100	-7.5	-4.4	-4.8	-7.5	24.2	4.5
Free	39.2	19.7	-26.0	24.6	-48.7	-6.3

STAGE RECOVERIES

	RGHR	CLNR	CIRCUIT	RECIRC LOAD
00-15	62	4	7	147
15-85	93	12	61	430
85-100	97	22	87	311
Free	100	100	100	0

LIBERATION DATA FOR GALENA (FINE FRACTION) Table 5.31

	74	76	RT	CF	CT	CN
Units	31.58	59.48	31.09	28.38	27.91	0.48
			DISTRIBUTION INTO VARIOUS PARTICLE TYPES			
00-15	3.49	2.61	2.83	1.93	2.03	2.19
15-85	17.96	13.97	11.94	13.52	9.20	8.44
85-100	5.87	6.62	3.04	5.34	4.65	5.72
Free	72.57	76.80	82.19	79.20	84.12	83.64
			RELATIVE STANDARD DEVIATION			
00-15	5.4	5.4	9.8	6.6	9.9	3.1
15-85	3.9	4.1	4.9	4.5	6.9	2.9
85-100	3.8	4.0	4.9	5.4	8.5	4.5
Free	3.2	3.9	2.9	6.6	5.2	3.2
			MASS BALANCED DATA			
00-15	3.28	2.63	3.30	1.91	1.90	2.20
15-85	14.70	13.29	14.80	11.65	11.70	8.40
85-100	4.12	4.86	4.10	5.70	5.70	5.70
Free	77.87	79.21	77.80	80.78	80.70	83.70
			MAGNITUDE OF CHANGE (ABSOLUTE)			
00-15	-0.2	0.0	0.5	-0.0	-0.1	0.0
15-85	-3.3	-0.7	2.9	-1.9	2.5	-0.0
85-100	-1.7	-1.8	1.1	0.4	1.1	-0.0
Free	5.3	2.4	-4.4	1.6	-3.4	0.1

STAGE RECOVERIES

	RGHR	CLNR	CIRCUIT	RECIRC LOAD
00-15	35	2	1	51
15-85	42	1	1	70
85-100	56	2	2	122
Free	49	2	2	92

LIBERATION DATA FOR SPHALERITE (FINE FRACTION) Table 5.32

	74	76	RT	CF	CT	CN
Units	17.39	25.94	17.03	8.90	8.56	0.35
DISTRIBUTION INTO VARIOUS PARTICLE TYPES						
00-15	3.62	5.00	1.92	7.89	2.01	5.65
15-85	40.85	41.97	21.72	42.72	32.16	33.66
85-100	44.88	45.83	33.45	31.35	39.34	28.34
Free	10.65	7.20	42.91	18.04	26.49	32.35
RELATIVE STANDARD DEVIATION						
00-15	5.3	5.2	6.8	6.5	15.0	8.7
15-85	4.1	4.7	5.2	7.2	9.7	9.2
85-100	5.3	6.1	5.7	11.5	11.9	13.7
Free	11.3	15.9	5.3	15.8	15.1	13.3
MASS BALANCED DATA						
00-15	2.76	3.21	2.70	4.18	4.10	5.90
15-85	32.24	36.46	32.20	44.66	45.00	35.00
85-100	47.33	44.37	47.70	38.04	38.30	30.50
Free	17.62	15.97	17.40	13.24	12.60	28.60
MAGNITUDE OF CHANGE (ABSOLUTE)						
00-15	-0.9	-1.8	0.8	-3.7	2.1	0.3
15-85	-8.6	-5.5	10.5	1.9	12.8	1.3
85-100	2.4	-1.5	14.3	6.7	-1.0	2.2
Free	7.0	8.8	-25.5	-4.8	-13.9	-3.8

STAGE RECOVERIES

	RGHR	CLNR	CIRCUIT	RECIRC LOAD
00-15	45	6	4	73
15-85	42	3	2	69
85-100	29	3	1	40
Free	28	8	3	35

LIBERATION DATA FOR IRON MINERALS (FINE FRACTION) Table 5.33

	74	76	RT	CF	CT	CN
Units	43.17	69.54	42.40	27.15	26.37	0.78
	DISTRIBUTION INTO VARIOUS PARTICLE TYPES					
00-15	1.28	1.64	0.43	2.10	1.25	3.71
15-85	16.97	18.82	11.61	30.52	17.02	27.80
85-100	32.87	37.10	21.36	39.26	21.03	21.38
Free	48.88	42.44	66.60	28.12	60.69	47.11
	RELATIVE STANDARD DEVIATION					
00-15	3.3	3.8	3.5	6.1	7.0	9.9
15-85	3.8	4.3	4.5	5.9	8.5	13.1
85-100	8.9	8.5	12.0	12.8	16.2	21.6
Free	2.6	2.6	2.4	3.5	4.0	5.9
	MASS BALANCED DATA					
00-15	0.61	1.06	0.53	1.89	1.80	4.90
15-85	14.03	18.15	13.80	24.94	24.90	26.20
85-100	30.52	34.23	30.60	39.88	40.30	25.60
Free	54.87	46.58	55.07	33.30	33.00	43.30
	MAGNITUDE OF CHANGE (ABSOLUTE)					
00-15	-0.7	-0.6	0.1	-0.2	0.6	1.2
15-85	-2.9	-0.7	2.2	-5.6	7.9	-1.6
85-100	-2.4	-2.9	9.2	0.6	19.3	4.2
Free	6.0	4.1	-11.5	5.2	-27.7	-3.8

STAGE RECOVERIES

	RGHR	CLNR	CIRCUIT	RECIRC LOAD
00-15	70	7	15	181
15-85	54	3	3	108
85-100	45	2	2	81
Free	28	4	1	37

SUMMARY OF RECOVERIES AND RECIRCULATING LOADS FOR BALANCED DATA

Table 5.35

	ROUGHER				CLEANER				CIRCUIT				RECIRCULATING LOAD			
Cp	"A"	"B"	"C"	U/F	"A"	"B"	"C"	U/F	"A"	"B"	"C"	U/F	"A"	"B"	"C"	U/F
Total	87	94	94	97	50	44	42	21	77	87	87	88	77	109	119	323
00-15%	88	97	62		11	9	4		44	73	7		369	743	147	
15-85%	86	87	93		33	22	12		66	59	61		137	210	430	
85-00%	74	88	97		63	39	22		65	73	87		39	116	311	
Free	91	98	100		58	55	100		85	96	100		61	78	0	
Gn	"A"	"B"	"C"	U/F	"A"	"B"	"C"	U/F	"A"	"B"	"C"	U/F	"A"	"B"	"C"	U/F
Total	28	47	48	72	2	1	2	2	1	1	2	4	38	88	88	237
00-15%	6	14	35		5	15	2		0	2	1		6	14	51	
15-85%	9	23	42		4	9	1		0	3	1		10	26	70	
85-00%	27	33	56		2	8	2		1	4	2		36	44	122	
Free	40	53	49		1	0	2		1	1	2		64	113	92	
Sp	"A"	"B"	"C"	U/F	"A"	"B"	"C"	U/F	"A"	"B"	"C"	U/F	"A"	"B"	"C"	U/F
Total	7	25	34	72	9	5	4	5	1	2	2	11	7	31	49	214
00-15%	11	40	45		23	14	6		3	9	4		9	53	73	
15-85%	9	26	42		10	7	3		1	2	2		9	31	63	
85-00%	5	10	29		6	4	3		0	0	1		4	11	40	
Free	8	41	28		8	4	8		1	3	3		8	66	35	
Py	"A"	"B"	"C"	U/F	"A"	"B"	"C"	U/F	"A"	"B"	"C"	U/F	"A"	"B"	"C"	U/F
Total	18	36	39		9	5	3		2	3	2		20	52	61	
00-15%	19	50	70		29	30	7		7	23	15		16	54	181	
15-85%	15	42	54		12	10	3		2	6	3		15	61	108	
85-00%	13	27	45		8	5	2		1	2	2		14	34	81	
Free	29	39	28		6	4	4		2	2	1		37	60	37	

5.3 : Statistical Significance of Liberation Data

It was stated in Section 3.6 that verification of the accuracy of liberation data lies largely in the degree to which the data is internally consistent or useful in making meaningful metallurgical interpretations. It is desirable to use this test to see whether or not useful information may be detected in the data set; however, by subjecting the data to mass balancing internal consistency is assured. Thus, it is necessary to assess the consistency of the unbalanced data independently from the usefulness of the balanced data.

The assignment of a quantitative test parameter to describe the quality of the structural data is not an easy task. Adjustments will be needed under all circumstances, since no analytical method is perfect. However, some method must be established to determine whether the required adjustments are acceptable or unacceptable. This discussion provides an approximate statistical method which may be used to arrive at a numerical description of the usefulness of the data set.

For the purpose of this exercise it is assumed that the wet chemical data is essentially accurate, and that the mass units of each mineral flowing through each sample point have been estimated with a fair degree of precision (or at least with more precision than that with which structural information may be collected). Thus, the mass balanced flow units in Tables 5.3 to 5.5 are considered to be "true" data, against which the structural data must be adjusted. This is a simplifying assumption which assigns all error in sampling and assaying to the image analysis data.

Sources of error in the structural information may be resolved into statistical error (scatter due to sampling statistics) and actual inaccuracy or imprecision of the structural information. The test of the image analyser is whether the useful information in the data set (information which aids in achieving a balance) outweighs the useless information (information which must be altered to achieve a balance).

If one imagined an image analyser which collected no useful structural information at all but simply responded randomly to the presence of a sample, one would find that the best materials balance would be one in which it was assumed that there was no structural difference from sample point to sample point. All variations between individual samples would be construed as "error". All analyses would be adjusted to a single "mean analysis" in order to create a balance.

One test of the image analysis data is a comparison of the variance which is eliminated from the structural balance by including the structural data (ie. how much the balanced data varies from a "mean analysis") as compared to how large an adjustment must be made to create the balance. In other words, in a suite of samples with structural variations the image analysis data should be able to detect the structural variations, allowing a balance to be formed by making smaller adjustments than those which would be made by assuming all structural data to be constant.

It goes without saying that in order for the image analyser to successfully detect differences between samples, some real difference must exist. One could imagine a case in which no structural partitioning occurs within a processing circuit (eg. all Cp floats regardless of particle grade). In such a case it would be impossible to test the image analysis data, since one would not know whether there were real differences between sample points which the image analyser failed to distinguish or whether there actually were no differences from point to point. However, even in such a data set one would still detect scatter in the image analysis results, requiring some adjustment to be made to correct the data back to the mean analysis. Thus, the magnitude of required adjustments is a measure of the error of the method, while the magnitude of non-required adjustments (ie. differences which persist after balancing) is a measure of the accuracy of the method.

The method which is used to test the data is ANOVA, or analysis of variance. For each size class of each mineral four structural types (00-15%, 15-85%, 85-100%, Free) have been measured across six sample points, yielding 24 pieces of data. Since the sum of all structural types must be 100% the data for one of the structural types is redundant. The data set can therefore be completely described by three mean analyses (for three of the structural types) and fifteen pieces of data (three types over five sample points). The data set therefore contains 15 degrees of freedom.

For any given set of samples there is an "average composition" which may be used at all sample points to minimize the sum of squared adjustments made to the data set. In cases where the assays all have equal variance this average composition is equal to the mean composition, with the total sum of squared adjustments being equal to NS^2 (where N is the number of sample points and S^2 is the variance of the data set). In this example the variances of the assays differ and the assays are not completely independent (since they must sum to 100%). The best average composition was determined by an iterative method. The sum of squared adjustments (weighted by the assay variance) required to fit the data to a constant composition is designated (SS_{total}), and is a measure of the variation of data from point to point in the circuit.

When the data is adjusted to create the optimum balance the sum of squared changes which must be made to the data is some number between zero and (SS_{total}). The required changes are attributed to error, and are designated (SS_{error}). Any variation between sample points which did not have to be eliminated in the balanced data is an indication of real sample differences after data adjustment, designated (SS_{data}). This sum of squares is numerically equal to (SS_{total} - SS_{error}). The statistical significance of data variations from point to point in the circuit is measured by the degree to which (SS_{data}) exceeds (SS_{err}).

The degrees of freedom associated with the balanced data set may be calculated by considering the additional constraints which are imposed upon the balanced data as compared to the raw data. The data must satisfy three nodal constraints:

76 = RT + CF (Rougher Feed = Rougher Tails + Cleaner Feed)
CF = CN + CT (Cleaner Feed = Cleaner Con + Cleaner Tails)
76 = 74 + CT (Rougher Feed = Circuit Feed + Cleaner Tails)

from which it also follows that:

74 = RT + CN (Circuit Feed = Rougher Feed + Cleaner Concentrate)

Thus, three non-redundant balancing equations exist for each of three structural types (under which conditions the fourth type will have to balance, and so is redundant). Nine degrees of freedom are used by the balancing constraints, leaving six degrees of freedom with which to account for error. (SS_{data}) is therefore distributed among the nine degrees of freedom (DF_{data} = 9) while (SS_{error}) is distributed among six degrees of freedom (DF_{error} = 6).

The significance of the structural data is evaluated by comparing the reduction of variance attributable to balancing constraints (SS_{data} / DF_{data}), or (MS_{data}) to the residual error (SS_{error} / DF_{error}), or (MS_{error}). The ratio of (MS_{data} / MS_{error}), or F*, may be compared to the standard one-tailed F-test for significance. For example, the 90% significance level for F(9,6) is equal to 2.9. A ratio of over 2.9 indicates that the data is more significant than the data adjustments with 90% probability.

Statistical interpretation of the data must be carried out cautiously, since calculated parameters less than the critical F-ratio indicate simply that the sum total of statistical sampling error and measurement error were not significantly smaller than the real differences from sample point to sample point. This could mean any of the following:

1) The variations in real structural makeup of the sample from point to point did not change enough to be detected, given the number of events which were measured.
2) The data reduction ratio was not sufficiently high.
3) The image analyser collected incorrect data.

Statistical data for the copper circuit samples is presented in Tables 5.35 to 5.38 for the four different minerals. The values of SS_{total}, SS_{data} and SS_{error} are given, along with the best average composition (Comp*) for the calculation of SS_{total}, the degrees of freedom and the values of F*.

As an approximation to determine the more significant elements of the data set the F-ratios for the individual structural types is included, assuming five degrees of freedom for the raw data and two for the balanced data. Three degrees of freedom are used by the nodal constraints. This approach is not strictly correct, since the balanced data optimises the total sum of squared adjustments rather than the sum for any individual compositional type; moreover, the distribution of material into any one of the compositional types is not totally independent of the amount in the other types (since they must add to 100%). However, the calculated F* ratios for the individual structural types provide a broad indication of which types retain significant differences between sample points in the balanced data. A "significant" ratio at the 90% level is somewhere around nine for the individual compositional types. As with any statistical comparison, the larger the sample size the lower the detection limit for significant events. Thus it is found that the mineralogical analyses, which are divided into four possible structural types over six sample points, require

STATISTICAL SIGNIFICANCE OF STRUCTURAL DATA - CHALCOPYRITE

Table 5.35

Cp Coarse		SS(Total)	SS(Err)	SS(Data)	DF(Total)	DF(Err)	DF(Data)	F*
Total	Comp*	1186.1	165.1	1020.9	15	6	9	4.1
00-15%	1.2	874.6	60.8	813.8	5	2	3	8.9
15-85%	20.7	229.5	78.7	150.7	5	2	3	1.3
85-00%	16.1	32.6	15.1	17.5	5	2	3	0.8
Free	62.0	49.3	10.5	38.9	5	2	3	2.5

Cp Medium		SS(Total)	SS(Err)	SS(Data)	DF(Total)	DF(Err)	DF(Data)	F*
Total	Comp*	342.4	60.9	281.6	15	6	9	3.1
00-15%	0.5	84.9	19.5	65.4	5	2	3	2.2
15-85%	12.3	176.0	15.0	161.0	5	2	3	7.2
85-00%	11.8	27.2	17.0	10.2	5	2	3	0.4
Free	75.4	54.3	9.3	45.0	5	2	3	3.2

Cp Fine		SS(Total)	SS(Err)	SS(Data)	DF(Total)	DF(Err)	DF(Data)	F*
Total	Comp*	3643.6	1260.4	2383.3	15	6	9	1.3
00-15%	0.6	1203.9	529.5	674.4	5	2	3	0.8
15-85%	13.9	446.0	138.8	307.3	5	2	3	1.5
85-00%	28.6	416.3	87.1	329.2	5	2	3	2.5
Free	56.9	1577.4	505.0	1072.4	5	2	3	1.4

STATISTICAL SIGNIFICANCE OF STRUCTURAL DATA - GALENA + SULFARSENIDES Table 5.36

Gn Coarse		SS(Total)	SS(Err)	SS(Data)	DF(Total)	DF(Err)	DF(Data)	F*
Total	Comp*	4284.0	165.3	4118.7	15	6	9	16.6
00-15%	1.8	1755.7	9.8	1745.9	5	2	3	118.3
15-85%	15.3	2062.1	57.4	2004.7	5	2	3	23.3
85-00%	5.2	95.9	88.5	7.4	5	2	3	0.1
Free	77.7	370.3	9.5	360.8	5	2	3	25.4

Gn Medium		SS(Total)	SS(Err)	SS(Data)	DF(Total)	DF(Err)	DF(Data)	F*
Total	Comp*	5649.5	44.4	5605.2	15	6	9	84.2
00-15%	0.9	1818.0	6.5	1811.6	5	2	3	186.2
15-85%	8.2	1492.7	31.5	1461.2	5	2	3	30.9
85-00%	3.7	277.4	5.3	272.1	5	2	3	34.1
Free	87.2	2061.4	1.1	2060.3	5	2	3	1300.8

Gn Fine		SS(Total)	SS(Err)	SS(Data)	DF(Total)	DF(Err)	DF(Data)	F*
Total	Comp*	563.3	252.3	311.0	15	6	9	0.8
00-15%	2.3	60.5	4.6	55.9	5	2	3	8.2
15-85%	10.6	256.2	72.6	183.6	5	2	3	1.7
85-00%	4.7	224.7	165.3	59.4	5	2	3	0.2
Free	82.4	22.0	9.9	12.1	5	2	3	0.8

STATISTICAL SIGNIFICANCE OF STRUCTURAL DATA - SPHALERITE

Table 5.31

Sp Coarse		SS(Total)	SS(Err)	SS(Data)	DF(Total)	DF(Err)	DF(Data)	F*
Total	Comp*	430.5	226.4	204.1	15	6	9	0.6
00-15%	2.4	185.4	116.7	68.7	5	2	3	0.4
15-85%	38.0	67.6	54.6	13.0	5	2	3	0.2
85-00%	34.4	123.9	5.1	118.8	5	2	3	15.6
Free	25.2	53.5	49.9	3.6	5	2	3	0.0

Sp Medium		SS(Total)	SS(Err)	SS(Data)	DF(Total)	DF(Err)	DF(Data)	F*
Total	Comp*	555.5	110.0	445.5	15	6	9	2.7
00-15%	1.7	174.0	27.8	146.1	5	2	3	3.5
15-85%	36.3	46.4	5.7	40.7	5	2	3	4.8
85-00%	28.5	79.8	1.8	77.9	5	2	3	28.6
Free	33.5	255.4	74.7	180.7	5	2	3	1.6

Sp Fine		SS(Total)	SS(Err)	SS(Data)	DF(Total)	DF(Err)	DF(Data)	F*
Total	Comp*	756.5	635.9	120.6	15	6	9	0.1
00-15%	3.1	267.6	203.0	64.6	5	2	3	0.2
15-85%	34.7	165.3	137.3	27.9	5	2	3	0.1
85-00%	45.1	71.6	60.2	11.3	5	2	3	0 1
Free	17.1	252.1	235.3	16.7	5	2	3	0.0

STATISTICAL SIGNIFICANCE OF STRUCTURAL DATA - IRON MINERALS Table 5.38

Px Coarse		SS(Total)	SS(Err)	SS(Data)	DF(Total)	DF(Err)	DF(Data)	F*
Total	Comp*	1055.2	504.2	551.1	15	6	9	0.7
00-15%	0.9	259.3	162.0	97.3	5	2	3	0.4
15-85%	34.3	173.7	117.4	56.3	5	2	3	0.3
85-00%	39.1	33.5	2.6	31.0	5	2	3	8.0
Free	25.7	588.7	222.2	366.5	5	2	3	1.1

Px Medium		SS(Total)	SS(Err)	SS(Data)	DF(Total)	DF(Err)	DF(Data)	F*
Total	Comp*	756.6	313.8	442.9	15	6	9	0.9
00-15%	0.4	526.6	221.7	304.9	5	2	3	0.9
15-85%	19.0	114.0	54.3	59.6	5	2	3	0.7
85-00%	25.1	39.8	19.9	19.9	5	2	3	0.7
Free	55.5	76.3	17.9	58.5	5	2	3	2.2

Px Fine		SS(Total)	SS(Err)	SS(Data)	DF(Total)	DF(Err)	DF(Data)	F*
Total	Comp*	1707.1	808.4	898.7	15	6	9	0.7
00-15%	0.6	917.8	432.1	485.7	5	2	3	0.7
15-85%	16.2	164.0	79.4	84.6	5	2	3	0.7
85-00%	38.4	87.3	47.1	40.2	5	2	3	0.6
Free	44.8	538.0	249.8	288.2	5	2	3	0.8

a lower F ratio for significance than the individual structural types, which consist of only one measurement per sample point.

The calculations indicate that significant partitioning of structural types was observed for Cp and Gn in the coarse samples, for Cp, Gn and probably Sp in the medium samples, and for none of the minerals in the fine samples. Thus, of the twelve mineral analyses (four minerals over three sizes) it is found that four or probably five contain data variations which cannot be attributed to chance.

The converse case is one in which it can be proven that the variations observed between samples are random. This condition is indicated by F-ratio which is sufficiently low to say that data inconsistencies are significantly higher than the variations between data measurements. In this case the critical F-ratio for the mineral analyses is 0.2, revealing that no inferences may be made about the behaviour of fine sphalerite. This does not necessarily mean that anything went wrong with the analysis, since this is exactly the result that one would expect if sphalerite grains did not partition differentially in the circuit according to their composition. The result simply reveals that the balanced data for fine sphalerite contains no useful information, so that all compositional types of fine sphalerite should be considered to behave identically.

The results of this statistical analysis are quite positive, since they indicate that the analyser recorded data which, in the cases of several of the analyses, showed internally consistent and statistically significant variations in the relative abundances of the different structural types through the circuit. There are definite limits to this type of data analysis, since it does not prove, for example, whether the data is "good" or "bad". However, the observation of systematic variations which cannot be attributed to chance provides a positive affirmation that the image analyser collected structural data in a non-random manner which helped to explain the behaviour of locked particles through the circuit.

5.4: Circuit Interpretation using Liberation Data

The mass flows of coarse, medium and fine mineral species through the copper circuit has previously been discussed in Section 5.1. However, it was found in the size-by-size analysis that the mechanisms for the recoveries of the various species could not be adequately explained. This discussion focuses upon interpretation of mechanistic phenomena.

Data for the coarse and medium size classes is considered to be good. Data for the fine size class was pushing the analytical limits of the equipment (particle size 9-13 µm), and there are indications from the recalculated grades of the ternary/quaternary sections (Table 3.17) that samples 76C and CFC may have undergone overly aggressive processing. Thus, calculated rougher and cleaner recoveries for this size class may not be correct. Furthermore, none of the fine samples contained structural variations large enough and consistent enough to pass the F-test for data significance. It is expected that the fine fraction contains useful structural data, but that the variance of this data is high. Consequently, most of the interpretation rests upon data from the coarse and medium size classes.

The balanced liberation data for Cp is presented in Table 5.39, with stereologically corrected data in Table 5.40. Similarly, data for galena is found in Tables 5.41 and 5.42, sphalerite in Tables 5.43 and 5.44, and iron minerals (pyrite) in Tables 5.45 and 5.46.

The methodology for stereological correction is illustrated in Table 5.47 for coarse chalcopyrite in sample 74A, and follows the simplified procedure previously outlined in Chapter 4 (section 4.7). The adjustment proceeds as follows:

1) The structural assays (area units) are converted back into events by dividing them by their mean grade. The total number of locked events (ie. 81.72) is recorded.

2) Using the equation developed in Section 4.7 the expected proportions of free Cp, other free, and locked section area are calculated for particles of grade 7.5%, 50.0% and 92.5%.

3) The events are treated as if they represent a particle assemblage. The expected number of locked sections is calculated from the recorded number of events and the expected proportion of locked sections. A total of 63.0 locked sections would be expected from the assemblage of 81.7 events. Thus, the scaling factor is calculated as being 81.7/63.0, or 1.296.

4) The events are multiplied by the scaling factor to estimate the number of locked particles. The expected amount of free Cp artifacts is calculated by multiplying the particle counts by the expected proportion of free Cp. The total artifacts are subtracted from the observed free particles to yield the corrected particle suite.

5) Particles are multiplied by their grade to reconstruct the area distribution. If this was an exact correction then the summed area distribution would exactly equal 100%. Since this is only an approximation the recalculated grade falls (typically) between 99% and 101%, and is scaled back to 100%.

In general the uncorrected data is used to make circuit interpretations. The corrected data is used only to determine the range of interpretations which may be made for the behaviour of free particles. In cases where a range of values is given for the distribution into free particles the range corresponds to the uncorrected and corrected values. It is known that the uncorrected value is too high (since some stereological artifacts are present) and that the corrected values is too low (since the stereological correction overcorrects the data). For example, free Cp in sample 74A is 57.99% (uncorrected) and 45.24% (corrected). Thus, the true amount of free Cp in sample 74A is 45-58%.

BALANCED LIBERATION DATA FOR CHALCOPYRITE (ALL FRACTIONS) Table 5.39

COARSE	74	76	RT	CF	CT	CN	Recoveries			Recirc Load
							Rghr	Clnr	Total	
Units	3.43	6.05	0.81	5.25	2.63	2.63				
00-15	1.39	3.69	3.30	3.75	6.70	0.80	88	11	44	369
15-85	20.75	27.89	29.90	27.56	37.20	17.90	86	33	66	137
85-100	20.06	15.74	30.20	13.51	10.10	16.90	74	63	65	39
Free	57.99	52.80	36.60	55.24	46.00	64.40	91	58	85	61

MEDIUM	74	76	RT	CF	CT	CN	Recoveries			Recirc Load
							Rghr	Clnr	Total	
Units	6.23	13.02	0.81	12.21	6.79	5.43				
00-15	0.63	2.54	1.30	2.63	4.30	0.53	97	9	73	743
15-85	16 35	24.25	52.00	22.41	31.50	11.00	87	22	59	210
85-100	12 62	13 03	26.00	12.17	13.40	10.60	88	39	73	116
Free	70.56	60.26	20.70	62.88	50.80	77.87	98	55	96	78

FINE	74	76	RT	CF	CT	CN	Recoveries			Recirc Load
							Rghr	Clnr	Total	
Units	7.75	16.99	1.01	15.99	9.24	6.75				
00-15	6.01	6 77	43.00	4.47	7.40	0.47	62	4	7	147
15-85	13.07	31 58	39.50	31.06	47.10	9.10	93	12	61	430
85-100	17.44	32.70	17.50	33.64	45.50	17.40	97	22	87	311
Free	63.61	29.01	0.00	30.83	0.00	73.03	100	100	100	0

STEREOLOGICALLY CORRECTED DATA FOR CHALCOPYRITE (ALL FRACTIONS) Table 5.40

COARSE	74	76	RT	CF	CT	CN	Recoveries			Recirc
							Rghr	Clnr	Total	Load
Units	3.43	6.05	0.81	5.25	2.63	2.63				
00-15	1.80	4.72	4.34	4.78	8.34	1.03	88	11	44	355
15-85	26.93	35.66	39.28	35.12	46.33	2 .03	85	33	66	132
85-100	26.03	20.13	39.68	17.22	12.58	21.75	74	63	64	37
Free	45.24	39.48	16.71	42.89	32.75	54.19	94	63	92	55

MEDIUM	74	76	RT	CF	CT	CN	Recoveries			Recirc
							Rghr	Clnr	Total	Load
Units	6.23	13.02	0.81	12.21	6.79	5.43				
00-15	0.80	3.24	1.60	3.36	5.43	0.68	97	9	75	743
15-85	20.65	30.86	64.19	28.68	39 79	14.15	87	22	60	210
85-100	15.94	16.58	32.09	15.57	16.92	13.64	88	39	75	116
Free	62.61	49.32	2.12	52 39	37 86	71 52	100	61	100	66

FINE	74	76	RT	CF	CT	CN	Recoveries			Recirc
							Rghr	Clnr	Total	Load
	7 75	16.99	1.01	15 99	9.24	6.75				
00-15	8 34	8.93	43 00	5.92	7 40	0 63	62	5	7	106
15-85	18.14	41.66	39.50	41.07	47.10	12 29	93	13	59	310
85-100	24 19	43 13	17.50	44 48	45.50	23.50	97	22	85	224
Free	49.34	6.29	0.00	8.54	0.00	63.57	128	314	112	0

BALANCED LIBERATION DATA FOR GALENA (ALL FRACTIONS) Table 5.41

COARSE	74	76	RT	CF	CT	CN	Recoveries Rghr	 Clnr	 Total	Recirc Load
Units	32.14	44.47	31.94	12.52	12.32	0.19				
00-15	7.88	6.03	7.90	1.25	1.20	4.30	6	5	0	6
15-85	36.51	29.05	36.60	9.80	9.60	23.00	9	4	0	10
85-100	5.10	5.02	5.10	4.82	4.80	6.10	27	2	1	36
Free	50.49	59 88	50.40	84.12	84.40	66.60	40	1	1	64

MEDIUM	74	76	RT	CF	CT	CN	Recoveries Rghr	 Clnr	 Total	Recirc Load
Units	33.44	62.83	33.03	29.78	29.38	0.41				
00-15	4.66	2.82	4.60	0.85	0.73	9.50	14	15	2	14
15-85	19.56	13.17	19.30	6.38	5.90	40.70	23	9	3	26
85-100	5 25	4.01	5.10	2 80	2.60	17.30	33	8	4	44
Free	70 53	79.98	71.00	90 00	90.77	32.50	53	0	1	113

FINE	74	76	RT	CF	CT	CN	Recoveries Rghr	 Clnr	 Total	Recirc Load
Units	31.58	59.48	31.09	28.38	27.91	0.48				
00-15	3.28	2 63	3.30	1.91	1 90	2.20	35	2	1	51
15-85	14.70	13.29	14.80	11.65	11.70	8.40	42	1	1	70
85-100	4 12	4.86	4.10	5.70	5.70	5.70	56	2	2	122
Free	77.87	79.21	77.80	80.78	80.70	83.70	49	2	2	92

STEREOLOGICALLY CORRECTED DATA FOR GALENA (ALL FRACTIONS) Table 5.42

COARSE	74	76	RT	CF	CT	CN	Recoveries			Recirc Load
							Rghr	Clnr	Total	
Units	32.14	44.47	31.94	12.52	12.32	0.19				
00-15	9.77	7.60	9.79	1.62	1.56	5.50	6	5	0	6
15-85	45.27	36.64	45.36	12.72	12.45	29.42	10	4	0	11
85-100	6.33	6.33	6.32	6.25	6.23	7.80	28	2	1	38
Free	38.63	49.42	38.52	79.41	79.76	57.28	45	1	1	79

MEDIUM	74	76	RT	CF	CT	CN	Recoveries			Recirc Load
							Rghr	Clnr	Total	
Units	33.44	62.83	33.03	29.78	29.38	0.41				
00-15	6.06	3.71	5.99	1.11	0.95	11.92	14	15	2	14
15-85	25.45	17.32	25.12	8.31	7.66	51.05	23	8	2	26
85-100	6.83	5.27	6.64	3.65	3.37	21.70	33	8	4	43
Free	61.66	73.70	62.26	86.93	88.02	15.34	56	0	0	125

FINE	74	76	RT	CF	CT	CN	Recoveries			Recirc Load
							Rghr	Clnr	Total	
Units	31.58	59.48	31.09	28.38	27.91	0.48				
00-15	4.31	3.46	4.33	2.50	2.49	2.99	34	2	1	51
15-85	19.29	17.45	19.41	15.27	15.33	11.42	42	1	1	70
85-100	5.41	6.39	5.38	7.47	7.47	7.75	56	2	2	122
Free	70.99	72.70	70.89	74.76	74.71	77.84	49	2	2	93

BALANCED LIBERATION DATA FOR SPHALERITE (ALL FRACTIONS) Table 5.43

COARSE	74	76	RT	CF	CT	CN	Recoveries			Recirc Load
							Rghr	Clnr	Total	
Units	29.51	31.56	29.31	2.25	2.04	0.20				
00-15	2.35	2.40	2.30	3.67	3.10	9.50	11	23	3	9
15-85	36.43	37.07	36.30	47.23	46.60	53.90	9	10	1	9
85-100	37.05	36.18	37.20	22.94	23.80	14.40	5	6	0	4
Free	24.19	24.33	24.20	26.10	26.50	22.20	8	8	1	8

MEDIUM	74	76	RT	CF	CT	CN	Recoveries			Recirc Load
							Rghr	Clnr	Total	
Units	20.88	27.25	20.52	6.73	6.37	0.36				
00-15	1.51	1.76	1.40	2.87	2.60	7 60	40	14	9	53
15-85	29.01	29 22	28.80	30.49	29.90	40.90	26	7	2	31
85-100	45 61	38.71	46.20	15.89	16.10	12.10	10	4	0	11
Free	23.87	30.31	23 60	50.76	51.40	39.40	41	4	3	66

FINE	74	76	RT	CF	CT	CN	Recoveries			Recirc Load
							Rghr	Clnr	Total	
Units	17.39	25.94	17.03	8 90	8.56	0.35				
00-15	2.76	3.21	2.70	4.18	4.10	5.90	45	6	4	73
15-85	32.24	36 46	32.20	44.66	45.00	35.00	42	3	2	69
85-100	47.33	44 37	47.70	38.04	38 30	30.50	29	3	1	40
Free	17.62	15.97	17.40	13.24	12.60	28.60	28	8	3	35

STEREOLOGICALLY CORRECTED DATA FOR SPHALERITE (ALL FRACTIONS)

Table 5.44

COARSE	74	76	RT	CF	CT	CN	Recoveries			Recirc Load
							Rghr	Clnr	Total	
Units	29.51	31.56	29.31	2.25	2.04	0.20				
00-15	3.07	3.13	3.01	4.56	3.86	11.49	10	23	3	9
15-85	47.66	48.36	47.53	58.67	57.96	65.18	9	10	1	8
85-100	48.48	47.19	48.71	28.50	29.60	17.41	4	5	0	4
Free	0.79	1.32	0.76	8.27	8.58	5.91				

MEDIUM	74	76	RT	CF	CT	CN	Recoveries			Recirc Load
							Rghr	Clnr	Total	
Units	20.88	27.25	20.52	6.73	6.37	0.36				
00-15	1.98	2.35	1.83	3.62	3.28	9.43	38	14	8	51
15-85	38.11	39.01	37.70	38.49	37.74	50.73	24	7	2	30
85-100	59.92	51.69	60.47	20.05	20.32	15 01	10	4	0	10
Free	0.00	6.94	0.00	37.84	38 65	24.84				

FINE	74	76	RT	CF	CT	CN	Recoveries			Recirc Load
							Rghr	Clnr	Total	
Units	17.39	25.94	17.03	8.90	8.56	0.35				
00-15	3.36	3.81	3.27	4 81	4.69	7.68				
15-85	39.16	43.39	38.98	51.41	51 49	45.56				
85-100	57 49	52.80	57.75	43.79	43.82	39 70				
Free	0.00	0.00	0.00	0.00	0 00	7.06				

BALANCED LIBERATION DATA FOR IRON MINERALS (ALL FRACTIONS) Table 5.45

COARSE	74	76	RT	CF	CT	CN	Recoveries			Recirc
							Rghr	Clnr	Total	Load
Units	34.29	40.97	33.66	7.31	6.68	0.63				
00-15	0.96	0.93	0.91	1.01	0.78	3.43	19	29	7	16
15-85	36.90	35.56	36.80	29.87	28.70	42.30	15	12	2	15
85-100	40 83	39.03	41.10	29.52	29.80	26.60	13	8	1	14
Free	21.31	24.47	21.19	39.59	40.72	27.67	29	6	2	37

MEDIUM	74	76	RT	CF	CT	CN	Recoveries			Recirc
							Rghr	Clnr	Total	Load
Units	40.54	61.51	39.34	22.17	20.97	1.20				
00-15	0.47	0.47	0.37	0.66	0.49	3.60	50	30	23	54
15-85	16.81	17.83	16.20	20.73	19.80	36.90	42	10	6	61
85-100	32.65	28 78	33.00	21.29	21.30	21.10	27	5	2	34
Free	50.07	52.92	50.43	57 33	58.41	38.40	39	4	2	60

FINE	74	76	RT	CF	CT	CN	Recoveries			Recirc
							Rghr	Clnr	Total	Load
Units	43.17	69.54	42.40	27.15	26.37	0.78				
00-15	0.61	1.06	0.53	1.89	1.80	4 90	70	7	15	181
15-85	14.03	18 15	13.80	24.94	24.90	26.20	54	3	3	108
85-100	30.52	34 23	30.60	39 88	40.30	25.60	45	2	2	81
Free	54 87	46.58	55.07	33.30	33.00	43.30	28	4	1	37

STEREOLOGICALLY CORRECTED DATA FOR IRON MINERALS (ALL FRACTIONS) Table 5.46

COARSE	74	76	RT	CF	CT	CN	Recoveries			Recirc Load
							Rghr	Clnr	Total	
Units	34.29	40.97	33.66	7.31	6.68	0.63				
00-15	1.22	1.22	1.15	1.31	1.01	4.34	19	29	7	16
15-85	46.89	46.67	46.69	38.70	37.25	53.46	15	12	2	15
85-100	51.89	51.23	52.15	38.24	38.68	33.62	13	8	1	15
Free	0.00	0.88	0.00	21.75	23.06	8.58				

MEDIUM	74	76	RT	CF	CT	CN	Recoveries			Recirc Load
							Rghr	Clnr	Total	
Units	40.54	61.51	39.34	22.17	20.97	1.20				
00-15	0.63	0.63	0.50	0.85	0.63	4.55	48	29	21	52
15-85	22.86	23.84	22.09	26.75	25.56	46.62	40	9	6	58
85-100	44.39	38.48	44.99	27.47	27.50	26.66	26	5	2	32
Free	32.12	37.05	32.42	44.93	46.31	22.17	44	3	2	75

FINE	74	76	RT	CF	CT	CN	Recoveries			Recirc Load
							Rghr	Clnr	Total	
Units	43.17	69.54	42.40	27.15	26.37	0.78				
00-15	0.84	1.45	0.73	2.56	2.44	6.48	69	7	14	179
15-85	19.25	24.78	18.95	33.83	33.80	34.67	53	3	3	107
85-100	41.87	46.74	42.01	54.10	54.71	33.88	45	2	1	80
Free	38.05	27.03	38.31	9.51	9.04	24.96	14	8	1	15

EXAMPLE OF STEREOLOGICAL CORRECTION FOR CP IN SAMPLE 74A Table 5.47

	AREA UNITS	MEAN GRADE	MEAN EVENTS PER UNIT	EVENTS	Free Cp 10^(2G-2)/2	Other Free 10^(-2G)/2	Locked
00-15	1.39	7.5%	13.33	18.53	0.0071	0.3540	0.639
15-85	20.75	50.0%	2.00	41.50	0.0500	0.0500	0.900
85-100	20.06	92.5%	1.08	21.69	0.3540	0.0071	0.639
Free	57.99	100.0%	1.00	57.99			
			Locked :	81.72			

	EXPECTED SECTIONS	LOCKED PARTICLES	EXPECTED ARTIFACTS	FREE CP	PARTICLE SUITE	RECALC AREA	SCALED AREA
00-15	11.8	24.0	0.2		24.0	1.8	1.80
15-85	37.3	53.8	2.7		53.8	26.9	26.93
85-100	13.9	28.1	9.9		28.1	26.0	26.03
FREE				58.0	45.2	45.2	45.24
	63.0	105.9	12.8	45.2	151.1	99.9	100.00

SCALEUP: 1.296

5.4.1: Chalcopyrite

It was found in Section 5.1 that chalcopyrite rougher recoveries increased as a function of diminishing size, but that the cleaner recovery was lower in the fine size fractions. Table 5.39 shows the structural information for chalcopyrite in the copper circuit, with the stereologically corrected data presented in Table 5.40. Data for fine chalcopyrite must be interpreted cautiously since this mineral was the most difficult to properly identify, especially in the fine samples.

Chalcopyrite in the circuit feed is imperfectly liberated. Free observations make up 45-58% of the coarse Cp and 63-71% of the medium Cp (49-64% of the fine Cp). Composites have a tendency to be high-grade. For example, the 85%-100% class contains approximately the same quantity of material as the 15%-85% class. Low-grade material makes up only a small fraction of the feed.

All grades of chalcopyrite-bearing sections show good recovery in the rougher, with the highest recovery seen for free sections. Some free chalcopyrite may be lost in the coarse fraction; however, almost all of the free chalcopyrite in the medium size fraction and all of the chalcopyrite in the fine fraction of the rougher tailings may be accounted for by stereology. The only type of chalcopyrite which appears to be recovered poorly is the low-grade component of the fine material.

In the cleaners recovery is strongly dependent upon composition. Free chalcopyrite shows recoveries of 58-63% (coarse) and 55-61% (medium). No free Cp is seen in the fine rougher tailings. While the latter finding may not be trusted, it certainly suggests that the amount of free Cp in the fine rougher tailings is low. In contrast, the lowest grade of locked particle (0-15% Cp) shows circuit recoveries of only 11% (coarse), 9% (medium) and 4% (fine). The intermediate grades show intermediate recoveries. Consequently, the recirculating load is composed largely of locked particles.

Cleaner recoveries of locked particles decrease both as a function of lower grade and finer size. Thus, it is seen that coarse, free Cp exhibits recoveries of 58-63% while fine, low-grade Cp shows only 4-5% recovery. Both size and grade seem to have approximately equal effect. This certainly impedes separation efficiency, since (for example) a fine particle with 85-100% Cp has a cleaner recovery of 22%, somewhere between that of a coarse particle with 15-85% Cp (33%) and that of a coarse particle with 0-15% Cp (11%). Thus, grade control in the cleaners results in the inevitable recirculation of large amounts of high-grade fines.

Total circuit recoveries are highest for free chalcopyrite, at 85-92% (coarse), 96-100% (medium) and 100% (fine). Locked particles over 15% grade have recoveries of about 60-80%, with size appearing to affect the magnitude of the recirculating load more than it effects the final recovery. Low-grade particles (15% Cp) appear to have size-dependent recoveries, with losses experienced in both coarse and fine particles, but especially in the fines.

In summary it is found that the rougher recovers more or less all of the free chalcopyrite, and about 75-95% of the locked chalcopyrite. In the cleaners the recoveries are low, since even coarse, free chalcopyrite exhibits only about a 60% recovery. Recoveries of fine particles and locked particles in the cleaners are even lower, ranging from about 4% to 40%. The combination of high rougher recovery and low cleaner recovery results in the buildup of high recirculating loads of locked Cp-bearing particles and fine Cp particles of all grade, which contribute to overall tailings losses.

5.4.2: Galena

Table 5.41 summarizes the liberation data for galena, while Table 5.42 presents the stereologically corrected data. Since galena was the easiest mineral to identify, data for galena does not show as high a variance in the fine fraction as the data for chalcopyrite. Consequently, all fractions may be interpreted with approximately the same confidence. It should be remembered that "galena" as defined for the image analysis study includes sulfarsenide species. Thus, a small leakage of free material into the concentrate may represent the recovery of tetrahedrite and other accessory minerals. However, the assay of lead in the final concentrate is 4-5% in all image analysis size fractions, so that the majority of "galena" observations must actually be lead sulfide.

Galena in the feed shows a reasonable degree of liberation, ranging from 39-51% free in the coarse fraction to 62-71% free in the medium fraction and 71-78% free in the fine fraction. The locked observations are spread approximately evenly over the spectrum of possible grades.

Galena behaviour in the rougher indicates beyond any doubt that galena is recovered by flotation. The recoveries of free galena are 40-45% (coarse), 53-56% (medium) and 49% (fine). This may be compared with composites of 15-85% galena, which exhibit recoveries of 9-10% (coarse), 23% (medium) and 42% (fine). Composites with low galena content exhibit very low flotation recoveries of 6% (coarse), 14% (medium) and 34-35% (fine).

The fact that recovery is positively linked to galena content in all size classes shows that galena is recovered by flotation. However, the tendency of fine particles to be recovered more strongly than coarse particles is opposite to that which would be expected from a flotation mechanism (at least in this range of particle sizes), and shows that at least part of the galena recovery is attributable to mechanical entrainment. This is reinforced by the fact that the selectivity of recovery as a function of composition diminishes as the size becomes finer.

Cleaner recoveries follow an opposite trend to those of the rougher. In the cleaners the recoveries of all grades of lead are low, but in the case of both coarse and medium galena are maximized in low-grade locked particles. This indicates a predominantly passive recovery mechanism in the cleaners, presumably by locking to chalcopyrite. The differential flotation recovery of low-grade vs. high-grade particles is not seen in the fine fraction, indicating that in this fraction mechanical entrainment probably contributes more to lead contamination than locking.

The recovery of free galena in the rougher leads to the buildup of a recirculating load of 64-79% (coarse), 113-125% (medium) and 92-93% (fine). Thus, the cleaner has a throughput of galena mass which is approximately equal to the galena content of the feed. Since the majority of the cleaner feed consists of free galena it is free galena which predominates as the source of concentrate contamination. In the final copper concentrate a total of 57-67% of the coarse galena is free, versus 15-33% of the medium galena and 78-84% of the fine galena. This is more than can be accounted for by sulfarsenides. However, in the coarse and medium fractions of the concentrate the proportion of galena which is free is lower than that that of the cleaner tailings, showing that coarse galena is selectively rejected. This suggests that galena flotability is slight or negligible at this point, and that the predominant recovery mechanism is mechanical entrainment, with some recovery also attributable to locking.

The recovery of galena to the final concentrate can be directly attributed to the flotation of galena in the roughers. Since galena has only moderate rougher flotability relative to chalcopyrite it is hard to determine whether the change in galena recovery between the rougher and the cleaners is attributable to the non-aggressive flotation in the cleaning circuits or due to some chemical change which occurs between roughing and cleaning.

A number of mechanisms could be invoked to explain differential flotability of galena between the rougher and the cleaners. However, one interesting possibility is that the depression of galena with sulfur dioxide requires aerative conditions. Sulfur dioxide is a reducing agent in the absence of oxygen but a powerful catalyst to oxidation when oxygen is present. It is possible that galena is almost totally flotable in the roughers, but interacts with SO_2 following the introduction of oxygen in flotation, laundering, and pumping of concentrate to the cleaners. Under such circumstances the rougher recoveries of free galena would be expected to be about 50%, since fresh material would be almost totally recovered while recirculating material would be almost totally rejected. This correlates well with the experimental observations, and suggests that some test work should be carried out concerning the response of galena to increased conditioning time prior to flotation and/or aeration following SO_2 addition.

In summary, it appears that galena is recovered in the roughers as a result of flotation and mechanical entrainment. Liberation is a minor factor in the recovery of galena in the cleaners, but is overshadowed by the probable entrainment or possible flotation of free galena. Attempts to reject galena from the concentrate should focus upon reasons for the flotation of free galena in the rougher, and possible differential flotability of galena between the rougher and the cleaners.

5.4.3: Sphalerite

Liberation data for sphalerite is presented in Table 5.43, with the stereologically corrected data presented in Table 5.44. It should be recalled from the F-tests that the data adjustments required to create a balance for fine sphalerite were significantly larger than the measured differences between samples. Thus, no interpretation can be made from the fine sphalerite data. It must be assumed that all grades of fine sphalerite behave identically. In other words, the recoveries of all types are considered to be equal to 34% in the rougher and 4% in the cleaners, as indicated by the wet chemical balance.

Sphalerite in the feed is predominantly locked. The stereological corrections applied to the data reveals that all free sphalerite in the circuit feed may be explained by stereology. This is not surprising, since the copper circuit feed is a cleaned concentrate from the CuPb circuit, in which sphalerite was not supposed to be flotable. In most of the copper circuit streams the observed free sphalerite may be explained by stereology alone, with the exception of the coarse and medium cleaner streams. Since these are the streams in which sphalerite is the least abundant they are also the streams in which the variance of the sphalerite observations is the greatest. Thus, it is considered that free sphalerite does rot contribute significantly to overall contamination of the copper concentrate. The interpretation of sphalerite behaviour will focus exclusively upon the behaviour of locked particles.

Recovery of sphalerite in the rougher is both size-dependent and grade-dependent. Low-grade particles are recovered at the highest rate, showing that a locking mechanism is partially responsible for recovery. The recoveries of low-grade particles are 10-11% (Coarse) and 40-41% (Medium), as opposed to the recoveries of high-grade particles, which equal 4-5% (Coarse) and 10% (Medium).

As an approximation, one might assume that the recoveries of high-grade sphalerite particles are a measure of sphalerite entrainment/flotation. Thus, the amount of mechanical entrainment or flotation recovery in the rougher could be estimated as about 5% (coarse) and 10% (fine). If this is the case then the considerably higher recoveries of low-grade and medium-grade sphalerite particles must be attributed to passive recovery by locking. In other words, locking appears to be a major cause of sphalerite recovery in the coarse and medium size fractions.

The size dependence of sphalerite recovery also targets mechanical entrainment as a rougher recovery mechanism. The wet chemical data indicates overall rougher recoveries of 7% (coarse), 25% (medium) and 34% (fine). Thus, mechanical entrainment may be considered to be as predominant a rougher recovery mechanism as locking.

A similar flotation response is seen in the cleaners. The recovery of low-grade sphalerite is about 23% (coarse) and 14% (medium), while medium-grade sphalerite shows recoveries of 10% (coarse) and 7% (medium). High-grade sphalerite shows recoveries of only 6% (coarse) and 4% (medium). Thus, locking is the predominant recovery mechanism in the coarse and medium size fractions, although mechanical entrainment is probably predominant in the fine fraction.

In summary, sphalerite in the feed is almost totally locked. Recovery in both the roughers and the cleaners may be attributed to a combination of locking and mechanical entrainment, with locking providing the dominant recovery mechanism in the coarse and possibly the medium fractions, and mechanical entrainment providing the dominant recovery mechanism in the fine fraction. There is no indication of sphalerite flotability.

5.4.4: Iron Minerals (Pyrite)

Liberation data for pyrite is shown in Table 5.45, with stereologically corrected data shown in Table 5.46.

Pyrite appears not to be significantly liberated in the coarse feed, since all free observations in 74A, 76A and RTA can be accounted for by stereology. However, liberated pyrite is seen in the medium fraction (32-50%) and in the fine fraction (38-55%). The behaviour of pyrite in the rougher and in the cleaners is more or less identical to that of sphalerite, and is interpreted in the same manner. Thus, only a brief description of pyrite behaviour is given.

Pyrite recoveries in the rougher vary as a function of particle grade and particle size, with particle size representing the dominant factor. Within a given size class recoveries are higher in the low-grade particle types. Thus, recoveries of locked pyrite range from 13-19% (coarse), 27%-50% (medium) and 45-70% (fine). While the effects of locking may clearly be seen, there is little doubt that mechanical entrainment is the dominant recovery mechanism. There is no indication of pyrite flotability.

In the cleaners recovery varies as a function of composition more than as a function of size. Recoveries are 8-29% (coarse), 5-30% (medium) and 2-7% (fine). Thus, it is found that locking is the dominant recovery mechanism in the cleaners. However, it is also found that free pyrite accounts for 8-28% of the concentrate pyrite contamination in the coarse fraction, 22-38% in the medium fraction and 25-43% in the fine fraction. This is a result of the large abundance of free pyrite in the rougher concentrate, and shows the persistence of mechanical entrainment in the cleaners. Again there is no indication of pyrite flotability.

5.5: Overall Circuit Interpretation

Gathering all of the above information, it is found that the rougher recovers a huge quantity of material by mechanical entrainment. This is revealed by the strongly size-dependent recoveries of all species calculated from the wet chemical assays. Entrainment in the ultrafines is calculated as being about 70%. This is not a reasonable number for mechanical entrainment; however, liberation data for the coarse, medium and fine size fractions is consistent with mechanical entrainment as a fine recovery mechanism. It is possible that the materials balance for ultrafines exaggerates the ultrafine recirculating load, since data for the ultrafines is recalculated. It is also possible that sliming is an accessory mechanism.

Copper appears to float well in the rougher, although open-circuit recoveries are obscured by the high magnitude of the recirculating load. It appears that in an open circuit losses would be predominantly in the form of low-grade composites; however, the huge amount of recirculating fines leads to losses of all grades of fine Cp under the current operating mode. Thus, copper losses in the current operation must be attributed largely to the fines.

Galena floats in the roughers. Again the open-circuit recoveries are hard to predict, since there is evidence suggesting that the recirculating load may have a significantly lower flotability than the fresh feed material. However, the recovery of free feed galena as a result of true flotation is at least 40%, and may even approach 100%. It is found that the mass of galena in the rougher concentrate is about the same as the mass of galena in the feed.

There is no evidence that pyrite or sphalerite float in the rougher, although significant quantities are recovered by mechanical entrainment and locking.

The cleaners assume the burden of rejecting the large quantities of entrained material in the rougher concentrate. The liberation data shows that recovery of locked gangue (Gn,Sp,Py) is significantly higher than the recovery of free gangue, indicating that flotation is not the predominant gangue recovery mechanism. However, mechanical entrainment is still significant. Concentrate contamination appears to be a mixture of fine entrainment and locked recovery.

The flotability of galena seen in the rougher disappears in the cleaners. It cannot be determined with certainty whether this is a result of the less aggressive flotation in cleaning, or whether this reflects an actual change in galena flotability. The fact that locked galena is recovered at a significantly higher rate than free galena suggests the latter.

One thing which has not been established is that locked particles are locked to chalcopyrite. For example, sphalerite and pyrite are known to associate closely in the ore, and could be expected to account for a significant number of locked sphalerite and locked pyrite particles. Tables A1.43 to A1.60 include calculations of the percentage of binary area in Cp binaries. These values are summarized in Table 5.48. (For example, in the "A" fraction of the final concentrate a total of 52% of the binary Gn area was in the form of Gn/Cp binaries). This data is not mass balanced, and is presented as calculated from the raw image analyser data.

In reference to Table 5.48 it is seen that locked galena in the feed is not predominantly associated with chalcopyrite. In the cleaner feed and tailings the degree of association with Cp is only marginally higher. However, in the cleaner concentrate about 50% of the locked galena is locked to chalcopyrite. Thus, about half of the locked galena in the concentrate is present as a result of flotation of the chalcopyrite component.

Binary sphalerite in the flotation feed is not associated with chalcopyrite in

PERCENTAGE OF BINARY AREA IN CP BINARIES Table 5.48

		STREAM					
	Size	74	76	RT	CF	CT	CN
Galena	"A"	3	3	1	8	7	52
	"B"	10	5	10	6	7	47
	"C"	5	20	4	17	19	46
Sphal.	"A"	1	3	7	17	19	73
	"B"	15	22	36	17	19	69
	"C"	59	88	18	58	41	80
Pyrite	"A"	2	9	4	65	60	89
	"B"	7	23	10	51	57	89
	"C"	45	95	9	84	46	88

the coarse fraction, but is 59% associated with chalcopyrite in the fine fraction. (This probably reflects more non-Cp locking in the coarse fraction, as opposed to more Cp-locking in the fine fraction. It is likely that most of the Sp/Cp associations in the coarse fraction are ternary Sp/Py/Cp, which is not counted here). In the cleaner concentrate the sphalerite binaries are about 70-80% Sp/Cp, showing that most of the locked Sp in the concentrate is recovered due to locking with chalcopyrite.

Pyrite in the feed is not associated with chalcopyrite in the coarse fraction, but is 45% associated with chalcopyrite in the fine fraction. (This phenomenon is explained the same way as for sphalerite, above). In the cleaner feed, cleaner tailings and rougher concentrate the majority of the locked pyrite is associated with chalcopyrite. In the cleaner concentrate about 85-90% of the locked pyrite contamination may be explained by locking to chalcopyrite.

It is difficult to assign precise quantitative figures to the relative importance of locking and mechanical entrainment as mechanisms for concentrate contamination, since in an environment where material is mechanically entrained at least some of the locked recovery (and even some of the free Cp recovery) may be attributed to mechanical entrainment. However, an estimation may be made, based upon the mass distributions calculated in Table 5.14 and the liberation data in Tables 5.39 to 5.46. In Table 5.14 it was found that about half of the lead contamination and sphalerite contamination (and presumably half of the pyrite contamination) originated from the ultrafines. This material may be considered to be liberated, and is presumably recovered by mechanical entrainment. Of the remaining contamination, about half originates in the medium size class, which may be used to evaluate recovery mechanisms.

Table 5.42 reveals that about 85% of the galena in the "B" fraction of the concentrate is locked. Table 5.48 shows that of this, about 50% is associated with Cp. Thus it is estimated that 50% of the Gn contamination is ultrafine, 20% locked to Cp, and 30% unassociated with Cp (entrained/floated).

Table 5.44 shows that about 75% of the sphalerite in the "B" fraction of the concentrate is locked. Of this, about 75% is locked to Cp. Thus, it is estimated that 50% of the sphalerite is ultrafine, 30% locked to Cp, and 20% unassociated with Cp (entrained).

Table 5.46 shows that about 80% of the pyrite in the "B" fraction of the concentrate is locked. Of this, about 90% is associated with Cp. Thus, about 50% of the pyrite is ultrafine, 35% associated with Cp, and 15% unassociated with Cp (entrained).

Thus, it is found that in the measured size classes (ie. down to 9μm) locking is slightly more important than mechanical entrainment as a contamination mechanism. However, since about half of the total concentrate contamination occurs in the ultrafines the overall contribution of mechanical entrainment to contamination is more in the order of 65-80%.

5.6: Suggested Process Modifications

Although the principal goal of this work is to demonstrate the process by which liberation data may be collected, compiled and interpreted, it is also of interest to continue the analysis to the point where process recommendations are made.

It is evident from the analysis that several problems present themselves in the copper circuit. Gangue is recovered primarily by mechanical entrainment, with some contribution due to locking. The ultrafines are especially responsible for entrained contamination. Locking is a second problem, responsible for about 30-35% of the Sp/Py contamination and about 20% of the Gn contamination. The greater relative contribution of entrainment to lead contamination is caused by the fact that free galena floats in the roughers, and is therefore present in considerable quantities in the cleaners. There is no indication that any of the mineral species show significant flotation response in the cleaners. It is predicted that in an open circuit copper would be lost predominantly in the form of low-grade coarse composites; however, due to high recirculating loads it is found that losses of fine Cp predominate.

The major problems in the copper circuit may be summarized as follows:

1) Presence of ultrafines in the feed, which are below the required liberation size and hinder separation due to their slow flotation kinetics and tendency towards high mechanical entrainment.

2) Over-aggressive rougher flotation, which results in the entrainment of massive quantities of fine, free gangue and which is ultimately responsible for the high recirculating loads of fine material from the cleaners.

3) Flotation of galena in the rougher, which results in a need for high levels of lead rejection in the cleaners. Not only does this result in lead contamination of the concentrate, but it also leads inevitably to increased recirculation of fine copper in the cleaner tailings, resulting in fine copper losses.

Possible solutions for the circuit problems are as follows:

1) In the absence of any circuit modifications, benefits could be derived from lowering the recirculating loads of free gangue and fine copper. It is possible that lowering the aggressiveness of rougher flotation could be beneficial. Less gangue would pass into the cleaners, requiring less upgrading and a lower recirculating load of copper. The increased retention time and lower copper load of the roughers could very well offset the effects of less aggressive flotation, and result in overall improvements.

2) The differential flotation behaviour of galena in the rougher and the cleaners should be investigated, as previously discussed. If the depression of galena requires SO_2/air, as opposed to SO_2 by itself, it is possible that the RC076 conditioner could be used for aeration prior to flotation.

3) Better size control in the CuPb cleaners would send less ultrafines to the copper circuit. Perhaps two-stage cycloning would be beneficial. If this is not possible then a coarser grind might be warranted, since liberation is considerably less of a problem than entrainment.

4) The cleaners should be carefully monitored to be sure that their stage efficiencies are approximately equal. Since the cleaners are sequential, the high recirculating loads of fine copper could originate from any one of the cleaners if too much upgrading was attempted in a single bank of flotation cells.

5) The cleaners could be arranged in countercurrent mode (ie. recirculation of cleaner tails to the feed of the preceding cleaner). This might be especially beneficial in combination with (1).

5.7: Copper Circuit Analysis - Conclusions

It has been demonstrated that the use of liberation data to describe circuit performance has resulted in the production of a much more useful analysis of circuit performance than that which can be obtained from size-by-size analysis alone. Certainly this would not always be the case, since under certain circumstances the particle size distribution of the feed would be coarse enough for locking and mechanical entrainment to carry characteristic size signatures. However, in the case of the BMS circuit it impossible to eliminate mechanical entrainment as a recovery mechanism even for the coarser size classes, while locking may persist even in the fines.

One of the major criteria for successful data interpretation is that it be possible to formulate some type of quantitative description of circuit performance. This does not necessarily mean that a quantitative interpretation has to be made; however, interpretation of unbalanced liberation data is no easier than interpretation of unbalanced assay data. A lot of useful information may be lost simply due to superimposed data scatter.

In summary, the copper circuit liberation data provides a coherent and logical description of circuit performance which has been used to formulate a number of fixed suggestions concerning how circuit performance could be improved. The combination of wet assay data and liberation data provides a powerful tool for circuit analysis, each providing information which may not be obtained from the other. The success of the study is largely attributable to the use of a quantitative approach. Several tests were made in the course of analysis to reaffirm as well as possible that the data was correct, and data adjustments were all made on the basis of statistical confidence intervals. The data was combined sufficiently to provide statistically useful information, while still extracting enough information to make a comprehensive circuit interpretation.

CHAPTER 6 : DISCUSSION

6.1 : Facilities and Methods for Image Analysis Based Liberation Studies

Despite the large number of image analysis based liberation studies which have been conducted there is almost no published data concerning equipment setup parameters or measurement algorithms. This is surprising, since these factors have great bearing upon the quality of the results which are obtained.

In its original conception this work was intended to be an analysis of the Brunswick copper and zinc circuits, with image analysis used as a principal analytical method. It was assumed that since image analysis based liberation studies appear commonly in literature the technology had already been developed, and that the level of sophistication required to conduct a liberation study was little more than to prepare the samples and "turn the machine on". However, soon after commencement of the work at RPC it was discovered that the existing methodologies were inadequate for fine particle analysis, and that alternatives had to be devised. This led to a shift in the focus of this work from the Brunswick circuit itself to the analysis of and methodologies for liberation work.

Image analysis data acquisition is accomplished by means of an interplay between equipment, unit operations such as the IPS instructions "BTHINN" or "DELIN" (as described in Chapter 2), and the sequence of unit operations required to collect accurate liberation data. These may be respectively referred to as "hardware", "firmware" and "software". Image analysis studies almost universally refer to the hardware which is employed, and sometimes give a description of one or more of the firmware operations. However, these are of no use if the sequence of processing operations does not lead to the acquisition of correct liberation data.

The limitations of image analysis studies have been discussed in detail in

Chapter 2, and arise from a number of factors ranging from the physics of the process (eg. resolution loss due to beam penetration, minimum image acquisition times) to limitations of the hardware (eg. limits imposed by pixel or gray level resolution) to limitations of the discriminatory algorithms (eg. false locking vs. false liberation, or grade preservation vs. structural preservation). These impose a number of constraints upon the types of samples which may be used and the types of data which may be collected from a given sample. Thus, it is inadequate simply to describe the hardware and the image analysis results unless the methodologies have been clearly described and the inherent problems recognized and accounted for.

The following discussion summarizes the major research groups involved in two-dimensional liberation work and reviews published information concerning their methodologies for conducting liberation studies. Stereological correction methods are discussed where applicable.

6.1.1 : CANMET, (Canada), W. Petruk

The CANMET group headed by W. Petruk is unquestionably one of the most productive and prolific mineralogical research groups in the mineral processing industry. Initial work was conducted on a Quantimet 720 image analyser, which was a hard-wired optical system which provided a wide variety of unit operations but relatively little capacity for the development of advanced algorithms. In the mid-80's the group acquired an SEM-based Kontron (IBAS II) system, identical to the one employed in this study.

Apparently, the original Quantimet studies were highly labour intensive. Petruk states that "whenever a mineral cannot be properly detected, an operator interactive image editor, which is an integral part of all large image analysers, can be used ..."[13]. However, this mode of semi-automated operation does not even come close to exploiting the capabilities of the Kontron system, and is presumably no longer used for routine work. The discriminatory algorithms used on the Kontron system have never been published.

Petruk has published a methodology for presenting image analysis data [14]. It is stated that "in some instances the mill products can be analysed directly without screening into fractions, but in other instances, particularly if the mill product is coarse grained, it has to be screened". It appears that early liberation work on the Quantimet 720 was conducted predominantly upon unsized samples, presumably in an attempt to reduce total analytical time.

In a subsequent publication [15] work was carried out to assess the difference in observed liberation between screened fractions and composite samples. The apparent liberation (area% free) of sphalerite, chalcopyrite and galena was measured in unsized samples (-10µm to -37µm, and +37µm to -208µm) and reassessed by mathematically combining data from closely sized fractions. The proportion of the area in locked sections may be presented as follows:

Area Percentage in Locked Particles

	Unsized			Sized		
	Sp	Cp	Gn	Sp	Cp	Gn
-37µm	29	27	37	15	12	9
37-208µm	67	57	74	69	62	65

adapted from Petruk [15]

It was explained in Chapter 2 that the use of unsized samples increases the effective packing density of the sample, leading to an increased number of point contacts and the production of false locking. In the fine fraction all three mineral species show at least twice as much locking when an unsized sample is used, leading one to assume that the sample data contains at least as many false locked observations as true locked observations. This is not as great a problem in the coarse size ranges, since the equipment does not operate as close to its resolution limit and locked vs. touching sections can be more readily discriminated. In the coarser size ranges stereological effects predominate, with the apparent liberation in the top-sizes decreasing (as shown previously in Fig 4.18). Petruk states that "the reason for the discrepancy between results obtained by measuring narrow size range fractions and wide size range fractions is not readily apparent ...", but attributes the error to sample preparation. He rightly concludes that only narrow size range samples are representative enough for image analysis studies of mill products, but still advocates the use of wide size range screen fractions for collecting semi-quantitative data.

Petruk has also investigated stereological phenomena. Tests were carried out with samples of sized, unliberated particles produced by heavy liquid fractionation.[13] The results showed that about 10-15% of the area of unliberated grains appeared as free grains. An empirical correction of factor of 15% was suggested. It appears that this correction has rarely been applied; however, as mentioned in Section 4.7, Petruk's correction agrees quite well with the correction suggested by the spherical sectioning model.

Petruk claims that the best materials balances are obtained by using the raw apparent mineral liberation data[16]. It was explained in Section 5.1.1 that a an exact balance should be possible using uncorrected data. In cases where the correction is inexact (ie. probably all cases) the application of a stereological correction will add variance to the balance instead of reducing variance. (It was for this reason that stereological correction was applied after mass balancing in Chapter 5). Nonetheless, Petruk's correction factor is correct in principle and appears to be correct in magnitude, and could be beneficially applied to the balanced data.

One area in which Petruk's work is difficult to understand is his lower size limit for analysis. In several of his studies liberation data is presented right down to a size of 3μm, even where analysis involves optical light microscopy.[17] This implies the ability to discriminate features a fraction of a micrometer in size, as well as the ability to perform image processing without obliterating any features above this fractional size. Such an ability was judged in this work to be clearly beyond the capability of even the IBAS II system. In fact, in this study even the "fine" size range (9-13 μm) was more or less at the analytical limits of the equipment for all minerals except galena when using a practical set of operating conditions and image acquisition time.

6.1.2 : Mintek, (S. Africa), Oosthuyzen

Oosthuyzen appears to be the only researcher to have published his discriminatory algorithm.[18] The equipment is a Leitz TAS image analyser, which is essentially a Leitz optical microscope interfaced to a digitizer and a computer. The discriminatory algorithm is illustrated in Figure 6.1, and proceeds as follows:

a) An image is acquired, containing "ore" (light) and "gangue" (dark).
b) A binary image is stored, containing all gangue-bearing particles.
c) A binary image is stored, containing all ore-bearing particles.
d) The gangue image is dilated.
e,f) The dilated gangue image is combined with the ore image using the Boolean [AND] operator. The resultant "marker" image is stored. This marker image consists of all ore pixels adjacent to gangue pixels.
g,h) All ore particles which contain at least one marked pixel are called locked particles.

While the algorithm is logically correct, it is susceptible to even the most trivial of data errors. For example, there is no provision whatsoever for the

Image Analysis Processing Algorithm (Oosthuyzen)[18] Figure 6.1

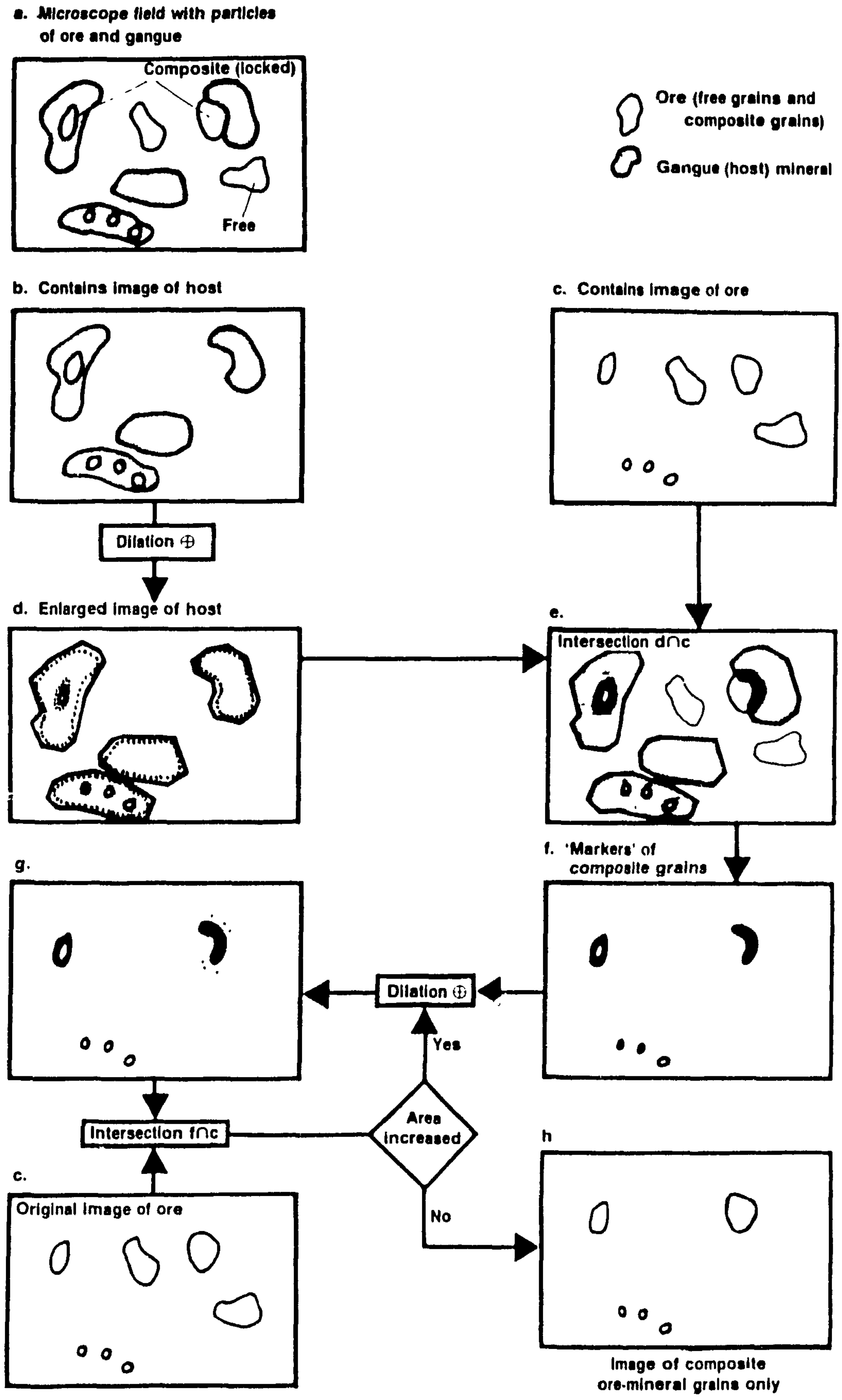

discrimination of locked from touching particles, and there is no allowance for any type of relief effect. (Halo effects are not seen in optical microscopy; however, optical studies are much more susceptible to problems generated by relief and surface defects). The presence of a single misidentified pixel at the boundary of the particle is sufficient to categorize the particle as locked. The algorithm may be applicable to perfect samples which are perfectly prepared and analysed at a size well above the resolution limit of the microscope, it is far too simplistic to be of any use for BEI or fine particle work.

6.1.3 : GIPSY, Virginia Polytechnical Institute, Yoon et. al.

The general image processing system (GYPSY) is based upon a Leitx optical microscope which collects images on a television camera[19]. The images are transmitted to a VAX 11/780 computer. The linear resolution of the digitized image is 100-5000 pixels, making this one of the highest resolution systems in use.

Images are divided into discrete segments by looking for edges. Thus, in contrast to systems which identify each pixel the Gypsy system assumes that any group of pixels without a distinct boundary region constitutes a particle. In the most simple of terms, boundaries are found by looking for areas in the sample where the pixel gray level undergoes an "S-shaped" change - ie. the gray level drops off from one gray level and stabilizes at another. The individual segments are then identified.

It does not appear that this system is currently being used to perform liberation studies; however, it is worth mentioning simply due to the resolution of the system and the edge discrimination algorithm.

6.1.4 : GRAAIM, (Laval University, Canada), Bérubé et. al.

The system is a modular image analyser consisting of a Leitz microscope, a video scanner, a digitizer, and a PDP 11-03 computer.[20] The system has a relatively good resolution of 307,200 pixels, or a linear resolution in excess of 500 pixels.

Most of the software for the system is custom designed. Initial processing is by the use of digital filters, which include two filters for the reduction of halo effects and crack effects. Liberation measurements are carried out upon samples which may contain particles of a single or of several size classes. The definition of "several" is not elaborated upon; however, in the absence of specifications delineating the number of size classes which may be treated simultaneously it is assumed that unsized samples are sometimes analysed.

The objective lens is chosen such that 100-150 particles are displayed in each image field. The sampling grid of the image is then chosen such that the smallest particles occupy about 100 pixels. The image filters are set interactively, depending upon the effective magnification being employed. A "liberation" filter is used so that a particle must contain some specified area proportion of the minor phase before being classified as locked. The suggested value is 5%, but it is acknowledged that this is too high for studies including base metal sulfides. Liberation measurements are conducted using the "LIBER" algorithm, which quantifies the particle grades and tabulates the image analysis results. No mention is made of the procedures whereby touched sections are differentiated from locked sections.

6.1.5 : QEM*SEM, CSIRO, (Australia) Reid et. al.

The QEM*SEM system consists of a computer-controlled SEM with an energy dispersive X-ray detector and a backscattered electron detector. In backscatter studies it is quoted that particles may range in size from 5μm to 500μm, and that typically the speed of analysis is about 500 particles in the 53-106μm size range per hour.[21] Liberation measurements are made by use of linear intercepts or by use of area data. No information is published concerning the algorithm for processing the area data. Consideration is given to the correspondence between image analysis assays and chemical assays, and to the reproducibility of liberation measurements. However, there is no indication that any method has been devised for verifying the accuracy (as opposed to precision) of the structural information.

6.1.6 : Summary

Unfortunately there are few facilities conducting image analysis based liberation studies, and even fewer conducting such studies using scanning electron microscopy. Thus, there is not a wealth of published information upon which to draw. Several groups are not mentioned in the above discussion, among whom are B.R.G.M. (France), Barbery et. al.; Imperial College (England), Jones et. al.; MINTEK (S. Africa), King et. al. These researchers conduct liberation studies using linear intercepts, which are changed to volumetric abundances by means of relatively complex mathematical transformations.

While numerous descriptions of equipment and transformation methodologies are presented for facilities performing linear liberation analysis it would appear that the facilities have not been widely used for applied studies. The major application appears to be in the formulation of integrated comminution/liberation models, in which (typically) drill core samples are characterized by means of linear intercepts, and the data used to predict grinding requirements. This field of endeavour is only indirectly related to this research, and is therefore not reviewed. A list of publications is included in the bibliography.

6.2 : Stereological Correction

In general stereological corrections are not applied to two-dimensional liberation data. None of the aforementioned groups indicate that they routinely correct sectioning data in any manner. This is largely due to the reasonable interpretability of the uncorrected data. In contrast, linear intercept data must always be transformed before interpretation. Thus it is found that although the literature abounds with stereological corrections the vast majority are applicable only to linear studies; a number of these are referenced in the bibliography.

In the case of sectioning data it appears that few liberation solutions have been proposed. The only corrections of which the author is aware are the solutions proposed by Gaudin[3] (ie. the original "locking factor"), the approximation provided by Petruk [8], the spherical sectioning model presented in the current work, and a recent attempt by Lin et. al. [22].

The work by Lin et. al. is particularly interesting, since it attempts to generate random complex particles on a purely mathematical basis, then to simulate their random sectioning. The simulation of particle growth is named PARGEN, and allows the used to determine (for example) tendencies towards elongation, rates of growth (and therefore particle size) of the various minerals, tendencies of various species to nucleate (ie. to form particles with several mineral nuclei), etcetera. This allows a sectioning matrix to be constructed which in theory should closely simulate the actual expected assemblage of sections from a given assemblage of particles. The actual transformation of data is similar to the matrix approach which has been described here for the spherical sectioning model.

The use of a random particle generator to provide the sectioning matrix is an inherently more useful approach than the use of spherical particles with planar boundaries, and may actually provide a much more definitive solution to the problem of two dimensional data transformation. However, the simulation requires some type of textural evaluation of each ore which is to be modeled, in order to assure that the simulated particle assemblage closely emulates the particles in the actual sample. Thus, no single solution can be proposed. The transformation of the data therefore becomes labour intensive and reliant upon the availability of the particle generator for every application.

In contrast, the spherical model used here is not intended to provide an absolute transformation, but rather a set of general guidelines for determining the range of values which the particle assemblage might assume. Since the spherical correction is known and intended to be an overcorrection, the methodology is expected to be applicable in a very simple manner to a wide variety of mineral assemblages. The models of Lin et. al. and Hill et. al may be considered to be complementary, and attempt to satisfy slightly different objectives.

The models of Lin et. al. and Hill et. al have both been criticized by Barbery[10]. In the former case it appeared that the calculated particle volumes were not consistent with theoretical values calculated from the simulated section areas. Thus, the model may still require refinement. In the latter case the spherical sectioning model was published[12] with cumulative area frequencies misleadingly compared to Jones' model for linear intercept observation frequencies[11]. Barbery concluded that the sectioning model failed to correctly predict cumulative observation frequencies for particle sectioning, and presented a solution for the simple case of spheres with 50% composition. In actual fact the data of Hill et. al. agreed perfectly with Barbery's solution for the 50% case. The criticism arose from a misunderstanding which has been subsequently corrected.[23]

6.3 : Independent Study of the Brunswick Copper Circuit

Petruk has conducted several liberation studies upon the Brunswick Mining and Smelting circuit. While the majority of this work focuses upon the zinc circuit, one study was conducted in which data was included for the feed, concentrate and tailings of the copper/lead separation circuit.[17] This work was conducted using the Quantimet 720 image analyser, and it appears that unsized samples were used for the analysis.

The copper circuit followed a slightly different flowsheet at the time that Petruk's survey was conducted. A conditioner was located in between the rougher and the first cleaner, and tailings from the second and third copper cleaners entered this conditioner (instead of being routed back to the rougher feed, as per current practice). The screen analysis of the copper concentrate was 2.8% "A", 47.7% "B", 16.9% "C" and 32.5% "ultrafines", using the size definitions employed in Chapter 5. In comparison, the screen analysis obtained for the copper concentrate in this study was 13.4% "A", 25.2% "B", 17.5% "C" and 43.9% "ultrafines". It would appear that the screen size distribution is not quite as narrow at the present time as it was in past years, although the mean size is perhaps a little finer.

Circulating loads in the rougher (ie. 1st cleaner tailings) and in the cleaner (2nd and 3rd cleaner tailings) were about 7% and 89%, respectively. This compares to a total recirculating load of 96% calculated in this study. In the circuit concentrate is was estimated that free particles accounted for 35% of the sphalerite, 90% of the galena and 90% of the chalcopyrite. In comparison, it was estimated in Section 5.5 that free sections accounted for about 70% of the sphalerite and 80% of the galena. Chalcopyrite was not calculated, but is somewhere in excess of 90%.

Petruk's study and the current study were conducted upon different circuit arrangements separated by a wide time lapse. Thus, it is difficult to make any conclusions concerning the similarities or differences between liberation results. However, it is interesting to note that the recirculating loads are about the same, and that in both studies substantial amounts of free material enter the copper concentrate. It appears that roughly similar phenomena were observed. One point of interest is the conditioner between the rougher and the cleaners. The function of this conditioner is not mentioned in Petruk's study; however, the circuit arrangement is very similar to the proposed circuit modification made in Section 5.6, in which it was postulated that a conditioner might be needed for lead depression in the rougher, and that the third cleaner tailings might be routed to the first cleaner feed. It would be interesting to know why this conditioner was incorporated into the original circuit design.

6.4: Project Summary

The analysis conducted in this study has been detailed, and goes well beyond the scope of most liberation studies. Most of the work has been geared towards demonstrating the validity of various procedures and approximations, and elaborating upon the several pitfalls that may be encountered when conducting liberation work. It is relevant, therefore, to summarize the factors which are considered to be essential for the collection of useful liberation data:

1) The sample should be prepared according to a proper procedure which minimizes differential settling, fractionation and inclusion of air bubbles. The use of an inert filler material is recommended. The sample should be polished carefully so as to minimize relief and surface imperfections.

2) Samples should always be sized, with no more than about four screen classes per sample.

3) The SEM should be operated at the lowest practical accelerating voltage, depending upon the available analytical time. A value of 10 kV is suggested, with a maximum suggested value of 15 kV. The beam current must be maintained at a constant level.

4) The magnification should be chosen such that about 50-100 sections are visible in each frame, or such that the largest section has a diameter no more than about 1/10 of the image diameter.

5) Gray levels should be chosen such that no minerals which are to be quantified go off scale.

6) Some image filtering is advantageous and aids in subsequent image processing by the liberation algorithm.

7) The processing algorithm must be developed according to sound principles. There should be an efficient method for distinguishing between locked and touching sections; however, alterations must be as slight as possible.

8) If it is possible to classify particles with less than about 5% contamination as being "free", then free sections may be identified at the machine level. However, if it is important to distinguish between low-grade locked particles and zero-grade particles then this is best accomplished by extrapolation of the data set. Limited confidence may be placed in the interpretation of any single pixel.

9) Data should be reduced by a ratio of at least about 300-400 to one if quantitative data is to be analysed.

10) If the data is to be balanced the statistical precision of the various measurements must be taken into account.

11) Stereological correction is not strictly necessary; however, if the data is left uncorrected then it must be remembered that (usually) about 20% of the locked particle area may be expected to appear as free section area. The data interpretation should be modified accordingly.

The data verification procedures and statistical tests conducted in this study cannot be considered essential to routine mineralogical analysis. They have been included simply to test the integrity of the processing algorithm to as great an extent as possible. A subsequent study would not require so rigorous an error analysis. Similarly, there are cases in which the data analysis may be a lot more comparative than quantitative, in which case mass balancing may not be necessary and the calculation of data confidence intervals may not be required. The author has published such a study, using the same equipment and image processing algorithm as used in this work.[24]

In conclusion, it is found that the image analyser is a useful tool which allows quantitative data to be collected on a scale which has never before been possible. However, the methodologies are still developmental. The high precision of image analysis results must not be mistaken for high accuracy; nor must simple data tests such as recalculated grades be taken as indications that structural data is correct. Nonetheless, it is possible by the careful and judicious design of image analysis software to collect data which is useful, and which may be made to extract circuit data which is unavailable from size-by-size analysis or from less quantitative manual microscopic methods.

CHAPTER 7 : CONCLUSIONS

The procedures for conducting two dimensional image analysis studies by means of image analysis have been critically appraised. It has been found that such liberation studies are very dependent upon the sample type, the equipment operating parameters, and the processing algorithms which are used. Some accepted procedures, such as the use of widely sized samples or attempts to extract size-by-size liberation data from a single sample, are shown to be fundamentally unsound.

Most research operations do not publish their processing algorithms; however, in one published example it was found that while the processing algorithm was logically correct, in actual fact it would not be appropriate for fine particle analysis. An algorithm had to be custom developed in this thesis for fine particle work.

Conventional tests for the quality of image analysis data (eg. recalculated grade, data reproducibility) are inadequate. In fact, the construction of an image analysis algorithm to rigorously preserve grade relationships may, in some cases, lead to the collection of poorer structural data. Thus, it is impossible to tell from existing data sets whether or not structural information is correct. A number of tests have been devised to verify integrity, although no single, authoritative test can be formulated.

In practical studies operating under economic constraints a balance must be achieved between processing time and data quality. Processing time is usually dictated by cost, and the required number of particle counts is usually dictated by statistics. It is therefore necessary to optimize the analytical procedure as much as possible so that high quality data may be assembled within fixed time constraints. Guidelines have been developed for maximizing the speed of image acquisition and for balancing analytical time between image acquisition and image processing. The processing algorithm is streamlined to operate as efficiently as possible.

Data must be reduced appropriately so that observations have a reasonable precision. It is demonstrated that when observations are weighted by their variance it is possible to conduct a materials balance which bears statistically relevant information and which is compatible with mass balanced data from wet chemical analyses. This greatly expedites the interpretation of data, and allows the greatest possible amount of quantitative information to be extracted from the study.

It has been found that uncorrected sectioning data provides an acceptable description of the parent particle assemblage, with the single exception that the amount of free material is overestimated. A simple model has been used to estimate the magnitude of the bias, and easily applicable procedures have been developed to compensate for it.

In an analysis of the Brunswick copper circuit it was found that size-by-size data did not provide a very good description of circuit performance, since the observed phenomena could not be conclusively interpreted. The addition of quantitative liberation data allowed a useful interpretation of circuit performance to be made, leading to recommendations for circuit improvement.

It has been found, therefore that image analysis provides a useful tool for circuit analysis, but that the technique is still in its developmental stage. This work has developed and demonstrated procedures for the collection of image analysis data in an accurate, quantitative and cost effective manner.

REFERENCES

1. Luff, W.; "Geology of Brunswick No.12 Mine"; CIM Bull., June, 1977.
2. Anonymous, "The Brunswick Mining and Smelting concentrator"; unpublished, internal publication of Brunswick Mining and Smelting Ltd., 1984.
3. Gaudin, A.M.; "Principals of Mineral Dressing"; McGraw-Hill, New York, 1939.
4. Jackson, R.; "Rapid production of high-quality polished sections for automated image analysis of minerals"; Proc. Australas. Inst. Min. Metall., No.289, March, 1984, pp. 93-97.
5. Gomez, C.P., McGill University, personal communication.
6. Rowlands, N.; "Electron beam techniques for the analysis of fine particles in the minerals industry"; Journal of Metals, June, 1985, pp. 16-19.
7. Kimoto, S.; "The scanning microscope as a system"; JEOL News, V.10e, No.2, 1972, pp. 1-31.
8. Petruk, W.; "Correlation between grain sizes in polished section with sieving data and investigation of mineral liberation measurements from polished sections"; Trans. IMM Sect. C, December, 1978, pp. C272-C277.
9. Hill, G., Rowlands, N., and Finch, J.; "Ore texture and magnesium contamination in ores from Pine Point, NWT"; IJMP, 1987.
10. Barbery, G., and Pelletier, R.; "Simulation techniques in mineral liberation analysis"; in Computer Applications in the Minerals Industry (Eds. Fytas, Collins, Singhal), Balkema, 1988, Rotterdam, pp. 251-256.
11. Jones, M.P., and Horton, R.; "Recent developments in the stereological assessment of composite (middling) particles by linear measurements"; in Proc. XIth Commonwealth Min. and Metal. Conf., ed. M.J. Jones, IMM, London, 1979, pp. 113-122.
12. Hill, G., Rowlands, N., and Finch, J.; "Data correction in two-dimensional liberation studies"; in Process Mineralogy VII (Eds. A. Vassiliou, D. Hausen and D. Carbon) TMS, 1987, pp.617-632.
13. Petruk, W.; "Image analysis in process mineralogy"; in Process Mineralogy II, AIME, 1982, pp. 39-53.
14. Petruk, W.; "Image analysis measurements and data presentation for mineral dressing applications"; in Applied Mineralogy, Proc. 2nd Intl. Cong. on Applied Mineralogy in the Minerals Industry, AIME, Los Angeles, 1984, pp. 127-141.
15. Petruk, W.; "Relationship between observed mineral liberations in screened fractions and in composite samples"; Min. and Metall. Processing, Feb. 1986, pp. 60-62.
16. Petruk, W.; "Predicting and measuring mineral liberations in ores and mill products and effect of mineral textures and grinding methods on mineral liberations"; in Process Mineralogy VII, AIME, 1986, pp. 393-403.
17. Petruk, W., and J. Schnarr; "An evaluation of the recovery of free and unliberated mineral grains, metals and trace elements in the concentrator of Brunswick Mining and Smelting Corp. Ltd."; CIM Bulletin, Sept. 1981, pp.132-159.

REFERENCES .... continued

18. Oosthuyzen, E.J.; "The application of automatic image analysis to mineralogy and extractive metallurgy"; Spec. Pub. Geol. Soc. S. Africa, V.7, 1983, pp. 449-464
19. Craig, J.R., et. al.; "The application of the general image processing system (GYPSY) to mineral benefication studies"; in Process Mineralogy II, AIME, 1982, pp. 55-67.
20. Berube, M.A., J.C. Marchand and B. Champagne; "Mineral liberation measurements using a modular image analyser"; in Applied Mineralogy, Proc. 2nd Intl. Cong. on Applied Mineralogy in the Minerals Industry, AIME, Los Angeles, 1984, pp. 259-275.
21. Reid, A.F., et.al.; "QEM*SEM image analysis of ore minerals : volume fraction, liberation and observational variances"; in Applied Mineralogy, Proc. 2nd Intl. Cong. on Applied Mineralogy in the Minerals Industry, AIME, Los Angeles, 1984, pp. 191-194.
22. Lin, C.L., J.D. Miller and J.A. Herbst; "Solutions to the transformation equation for volumetric grade distribution from linear and/or areal grade distributions"; Powder Technology, V.50, No.1, 1987, pp.55-63.
23. Hill, G.S., Rowlands, N. and Finch, J; "Verification of a Particle Sectioning Model"; Canadian Metallurgical Quarterly, 1990, in press.
24. Hill, G.S., Rowlands, N., and Finch, J.; "Circuit analysis and flotation kinetics at Brunswick Mining and Smelting Ltd."; in Fine Particles '88, Proc. 27th Conf. Metall., CIM, 1988.

BIBLIOGRAPHY

Austin, L.G., and P.T. Luckie; "An assessment of the problems of quantifying mineral liberation"; in Process Mineralogy VI, AIME, 1986, pp. 3-24.

Barbery, G., G. Huyet and C. Gateau; "Liberation analysis by means of image analysers: theory and applications"; Proc. XIIIth IMPC, Warsaw, 1979, pp. 568-595.

Barbery, G.; "Mineral liberation analysis using stereological methods: a review of concepts and problems"; in Applied Mineralogy, Proc. 2nd Intl. Cong. on Applied Mineralogy in the Minerals Industry, AIME, Los Angeles, 1984, pp. 171-191.

Barbery, G., and D. Leroux; "Prediction of particle composition after fragmentation of heterogenous materials: influence of texture"; in Process Mineralogy VI, AIME, 1986, pp. 415-427.

Barbery, G.; "Random sets and integral geometry in comminution and liberation of minerals"; Minerals and Metall. Processing, May, 1987, pp. 96-101.

Barbery, G., and D. Leroux; "Prediction of particle composition distribution after fragmentation of heterogenous materials"; IJMP, V.22, 1988, pp. 9-24.

Belardi, G., G. Bonifazi and P. Massacci; "Particle breakage and liberation modelling"; Chem. Eng. Res Des, V.64, Sept, 1986, pp. 381-391.

Beattie, M.J.V., and D.J. Barratt; "Applied Mineralogy in Flowsheet Development"; in Applied Mineralogy, Proc. 2nd Intl. Cong. on Applied Mineralogy in the Minerals Industry, AIME, Los Angeles, 1984, pp. 331-353.

Bodziony, J. and W. Kraj; "Stereological analysis as a method im modern granulometry"; Proc. XIIIth IMPC, Warsaw, 1979, pp. 600-624.

Bodziony, J. and W. Kraj; "Some remarks on the problem of mineral liberation"; Bull. Polish Academy of Sci., V.34, 1986, pp. 163-170.

Choi, W.Z., G.T. Adel and R.H. Yoon; "Size reduction/liberation model of grinding including multiple classes of composite particles"; Min. and Metall. Proces., May, 1987, pp. 102-108.

Choi, W.Z., G.T. Adel and R.H. Yoon; "Liberation modeling using automated image analysis"; IJMP, V.22, 1988, pp.59-73.

Dobby, G.S., and D.I. Castillo; "Characterizing and cleaning of zinc concentrates"; Final report for MISP project, unpublished, 1989.

Finch, J.A., and W. Petruk; "Testing a solution to the King liberation model"; IJMP V.12, 1984, pp. 305-311.

Gomez, C.O., "Quantifying mineral liberation using image analysis"; unpublished, presented in McGill University Professional Development Seminar (Mineral separation systems and column flotation), May, 1986.

Hagni, R.D.; "The utilization of quantitative microscopic techniques in the study of ore minerals"; in Process Mineralogy, AIME, 1981, pp. 51-62.

Hausen, D.M., "Gross-count method of microscopic quantification"; SME/AIME Trans., V.252, Sept, 1972, pp. 328-332.

Hennessy, J.A.; "The importance of geology in process design"; in Applied Mineralogy, Proc. 2nd Intl. Cong. on Applied Mineralogy in the Minerals Industry, AIME, Los Angeles, 1984, pp. 291-296.

Hockings, W.A.; "Measurement of liberation of finely ground iron ores"; in Process Mineralogy, AIME, 1981, pp. 245-253.

BIBLIOGRAPHY ... continued

Holland-Batt, A.B.; "Liberation analysis"; Trans. IMM Sect. C, V.92, Sept, 1983, pp. 129-137.

Holmgren, C., and M. Marti; "Applied mineralogy and metallurgical forecasting"; in Applied Mineralogy, Proc. 2nd Intl. Cong. on Applied Mineralogy in the Minerals Industry, AIME, Los Angeles, 1984, pp. 407-419.

Johnson, N.W.; "Application of kinetics and liberation data to analysis of an industrial flotation process"; CIM Bull., March, 1987, pp. 112-117.

Jones, M.P.; "Automatic mineralogical measurements in mineral processing"; Proc. 13th IMPC, Warsaw, 1979, pp. 533-564.

Jones, M.P., "Designing an X-ray image analyser for measuring mineralogical data"; Proc. XIVth IMPC, Toronto, 1982, paper #VIII.4.

Jones, M.P., and G.J. Warren, "Automation of Mineralogical Measuring Procedures"; Proc. 4th IFAC Symp., IFAC, Helsinki, 1983, pp. 511-518.

Jones, M.P.; "Recent developments in the rapid collection of quantitative mineralogical data"; in Applied Mineralogy , Proc. 2nd Intl. Cong. on Applied Mineralogy in the Minerals Industry, AIME, Los Angeles, 1984, pp. 141-155.

Jones, M.P.; "Assessment of particle compositions by automated linear analysis"; Trans. IMM Sect. C, V.94, Dec, 1985, pp. 224-229.

Khnagonkar, P.R. and C. Satyanarayana; "Liberation analysis and release analysis"; Trans. IMM Sect. C., V.90, Sept, 1981, pp.113-114.

King, R.P.; "Prediction of mineral liberation from mineralogical texture"; Proc. XIVth IMPC, Toronto, 1982, Paper #VIII-1.

King, R.P.; "A quantitative morphological model for the microstructure of two-component solids"; Advances in Mineral and Coal Processing using Flotation, Engineering Foundation Conference, Florida, 1989.

Klimpel, R.R.; "Some practical approaches to analyzing liberation from a binary system"; in Process Mineralogy III, AIME, 1983, pp. 65-81.

Klimpel, R.R., "A preliminary model of liberation from a binary system"; Powder Technology, V.34, 1983, pp. 121-130.

Klimpel, R.R., "Applications of a model for the analysis of liberation from a binary system"; Powder Technology, V.39, 1984, pp. 117-128.

Lin, C.L., J.D. Miller and J.A. Herbst; "Prediction of volumetric abundance from two-dimensional mineral images"; in Applied Mineralogy, Proc. 2nd Intl. Cong. on Applied Mineralogy in the Minerals Industry, AIME, Los Angeles, 1984, pp. 157-171.

Lin, C.L. and J.D. Miller; "Effect of grain size distribution and grain type on linear and areal grade distributions"; in Process Mineralogy VII, AIME, 1986, pp. 405-413.

Malvik, T.; "An empirical model to establish the liberation properties of minerals"; Proc. XIVth ICMP, Toronto, 1982, Paper #VIII-2.

McKee, D.J.; "The use of scanning electron microscopy in evaluating metallurgical plant performance"; in Applied Mineralogy, Proc. 2nd Intl. Cong. on Applied Mineralogy in the Minerals Industry, AIME, Los Angeles, 1984, pp. 103-116.

Meloy, T.P., and K. Gotoh; "Liberation in a homogenous two-phase ore"; IJMP, V.14, 1985, pp.45-55.

Meloy, T.P., and N. Clark; "Theoretical study of locked particle comminution"; Proc. XVth IMPC, Cannes, 1985, pp. 12-19.

BIBLIOGRAPHY ... continued

Meloy, T.P., U. Prett and G. Ferrara; "Liberation - volume and mass lockedness profiles derived - theoretical and practical conclusions"; IJMP V.20, 1987, pp. 17-34.

Miller, J.D., and C.L. Lin; "Treatment of polished section data for detailed liberation analysis"; IJMP V.22, 1988, pp. 41-58.

Miller, P.R., A.F. Reid and M.A. Zuiderwyk; "QEM*SEM image analysis in the determination of modal assays, mineral associations and mineral liberation"; Proc. XIVth IMPC, Toronto, 1982, Paper #VIII.3.

Moore, S.W., and M.P. Jones; "Random linear probes through composite spheres that have multiple planar boundaries"; Trans IMM Sect. C, Dec., 1980, pp. 190-193.

Moore, S.W., and M.P. Jones; "Mathematical methods for estimating particle compositions from the results of image analysis"; Proc. XVth IMPC, Cannes, 1985, pp. 3-11.

Naruk, S.; "Quantitative microscopic analysis of a sulfide flotation circuit - an example"; TMS Paper A80-46, TMS-AIME, 1980, 44 pp.

Petruk, W., and R.G. Pinard; "Image analysis studies of tailings from the mill of Brunswick Mining and Smelting Corporation in New Brunswick"; CANMET Report MRP-MSL 77-8, January, 1977.

Petruk, W.; "Image analysis study of mill products from batch tests on Brunswick Mining and Smelting mill tailings"; CANMET report 78-23, 1978.

Petruk, W.; "The behaviour of sphalerite during flotation of a base metal ore from the Brunswick No.12 deposit in New Brunswick"; Proc. ICAM 81, Johannesburg, S.A., June, 1981.

Petruk, W.; "The behaviour of galena, chalcopyrite and tetrahedrite during flotation of a fine-grained base metal ore in the concentrator of Brunswick Mining and Smelting Limited"; Process Mineralogy, ed. D. Hausen and W.C. Park, AIME, 1981, pp. 201-213.

Petruk, W.; "Image analysis study of the minerals in the secondary zinc circuit of the BMS concentrator'; CANMET report 84-7E, 1983.

Petruk, W.; "Applied mineralogy in ore dressing of volcanogenic massive sulfide ores"; in Applied Mineralogy, Proc. 2nd Intl. Cong. on Applied Mineralogy in the Minerals Industry, AIME, Los Angeles, 1984, pp. 279-291.

Petruk, W.; "Image analysis studies to determine liberations of sphalerite, chalcopyrite and galena during grinding of fine grained pyritic Zn-Pb-Cu-Ag ores"; in Complex Ores: New Mineralogical Methods and Techniques, Proc. XVth IMPC, Cannes, 1985, pp.77-87.

Petruk, W.; "Image analysis - an overview of developments"; CANMET report 86-4e, 1986, 5 pp.

Pillai, K.J., et.al.; "Applications of mineralogical factors in the benefication of complex sulfides - a case history"; in Applied Mineralogy, Proc. 2nd Intl. Cong. on Applied Mineralogy in the Minerals Industry, AIME, Los Angeles, 1984, pp. 421-439.

Sepulveda, J.E., J.D. Miller and C.L. Lin; "Generation of irregularly shaped multiphase particles for liberation analysis"; Proc. XVth IMPC, Cannes, 1985, pp 120-133.

Wiegel, R.L., and K. Li; "A random model for mineral liberation by size reduction"; SME/AIME Trans., June, 1967, pp. 179-191.

APPENDIX I

IMAGE ANALYSIS DATA AND IMTERMEDIATE CALCULATIONS

SAMPLE 74: MEASURED AREA (100's of μm^2) AS A FUNCTION OF SECTION TYPE AND GRADE TABLE A1.1

Section Grade (% of first-mentioned type) Eg. %Cp in Cp/Px Binaries

COARSE	00-05	05-15	15-25	25-35	35-45	45-55	55-65	65-75	75-85	85-95	95-00
Cp/Px	5160	39	72	26	26	6	43	38	64	39	760
Cp/Gn	285	45	7	5	12	13	0	32	33	34	93
Cp/Sp	133	15	7	8	15	24	11	26	13	7	89
Gn/Sp	5790	1700	750	596	362	287	350	264	306	237	7980
Px/Sp	1180	179	27	43	40	85	39	87	132	366	347
Px/Gn	912	38	181	297	292	443	585	881	1420	3370	4050
Px/TQ	7390	1300	800	859	800	1080	1360	1200	1680	2240	554
Cp/TQ	18600	248	118	59	38	69	15	24	11	58	37
Gn/TQ	6030	6170	2640	1480	911	658	510	323	245	204	110
Sp/TQ	3760	2740	1210	1480	1050	1160	992	1110	1490	2560	1730

MEDIUM	00-05	05-15	15-25	25-35	35-45	45-55	55-65	65-75	75-85	85-95	95-00
Cp/Px	991	22	15	4	5	6	6	6	9	20	160
Cp/Gn	62	15	2	3	3	1	1	1	5	15	41
Cp/Sp	79	41	16	4	2	0	1	0	3	5	49
Gn/Sp	335	177	37	45	24	27	28	14	27	22	1520
Px/Sp	46	20	3	3	5	1	0	2	7	24	61
Px/Gn	40	28	24	18	28	32	64	95	119	313	497
Px/TQ	914	122	100	111	89	105	103	103	164	293	216
Cp/TQ	1860	215	82	34	25	16	18	14	20	10	29
Gn/TQ	913	589	243	200	92	80	67	33	47	41	15
Sp/TQ	827	255	94	115	114	73	104	101	157	276	204

FINE	00-05	05-15	15-25	25-35	35-45	45-55	55-65	65-75	75-85	85-95	95-00
Cp/Px	1580	108	21	10	7	5	3	3	6	20	63
Cp/Gn	13	4	0	0	0	0	0	0	0	2	23
Cp/Sp	65	43	8	6	2	1	1	0	2	9	46
Gn/Sp	97	17	8	9	8	6	6	6	6	10	1290
Px/Sp	8	4	1	0	0	0	0	0	1	5	58
Px/Gn	143	17	8	14	20	19	17	35	33	100	103
Px/TQ	900	311	141	93	100	97	104	125	168	425	338
Cp/TQ	1260	831	240	98	57	46	44	26	29	69	108
Gn/TQ	1470	484	213	138	125	82	60	52	43	45	90
Sp/TQ	1360	302	96	85	73	88	98	112	185	276	131

SAMPLE 76: MEASURED AREA (100's of μm^2) AS A FUNCTION OF SECTION TYPE AND GRADE

TABLE A1.2

Section Grade (% of first-mentioned type) Eg. %Cp in Cp/Px Binaries

COARSE	00-05	05-15	15-25	25-35	35-45	45-55	55-65	65-75	75-85	85-95	95-00
Cp/Px	6660	324	306	113	152	70	75	160	101	90	1660
Cp/Gn	48	15	40	19	46	47	29	42	36	188	142
Cp/Sp	338	107	47	46	31	17	73	27	14	13	131
Gn/Sp	7720	4090	2090	1250	876	633	678	518	505	467	12200
Px/Sp	183	211	116	81	145	151	146	231	314	680	602
Px/Gn	136	324	275	372	325	448	616	1050	1500	3040	2470
Px/TQ	2080	1410	970	1080	825	1110	1100	1300	1190	1970	577
Cp/TQ	12400	254	239	79	155	125	84	92	78	125	0
Gn/TQ	4540	4070	1950	891	878	554	355	210	105	47	17
Sp/TQ	3440	2200	1200	1320	1270	821	647	820	820	716	348

MEDIUM	00-05	05-15	15-25	25-35	35-45	45-55	55-65	65-75	75-85	85-95	95-00
Cp/Px	4530	308	126	85	63	41	36	41	37	96	895
Cp/Gn	26	13	7	9	20	1	14	1	18	47	52
Cp/Sp	191	165	29	19	15	16	14	8	9	23	59
Gn/Sp	1880	412	206	156	156	87	64	60	65	69	6420
Px/Sp	32	20	24	22	20	17	47	43	68	155	135
Px/Gn	101	93	74	69	95	113	141	225	342	899	702
Px/TQ	990	224	124	158	163	186	123	230	194	234	59
Cp/TQ	1910	362	104	84	49	59	55	21	9	22	6
Gn/TQ	1120	541	326	188	113	134	83	70	38	54	20
Sp/TQ	631	361	242	151	172	163	174	112	218	385	75

FINE	00-05	05-15	15-25	25-35	35-45	45-55	55-65	65-75	75-85	85-95	95-00
Cp/Px	1230	192	28	9	9	3	4	4	10	20	15
Cp/Gn	12	4	1	0	0	0	0	0	0	3	8
Cp/Sp	60	65	16	6	3	2	0	1	1	16	64
Gn/Sp	59	2	1	1	1	2	1	3	1	7	1020
Px/Sp	12	5	1	0	0	0	0	0	0	5	14
Px/Gn	138	3	1	2	1	1	1	3	3	2	4
Px/TQ	1010	321	125	99	70	77	101	129	196	412	225
Cp/TQ	1050	735	288	180	87	52	39	30	51	136	115
Gn/TQ	1550	378	165	114	82	57	62	42	45	60	213
Sp/TQ	997	434	237	156	118	76	76	94	169	262	144

SAMPLE RT: MEASURED AREA (100's of μm^2) AS A FUNCTION OF SECTION TYPE AND GRADE

TABLE A1.3

Section Grade (% of first-mentioned type) Eg. %Cp in Cp/Px Binaries

COARSE	00-05	05-15	15-25	25-35	35-45	45-55	55-65	65-75	75-85	85-95	95-00
Cp/Px	4010	96	17	22	15	4	3	2	2	3	33
Cp/Gn	39	2	18	4	13	1	9	3	6	14	34
Cp/Sp	855	135	109	36	68	102	136	74	170	633	1250
Gn/Sp	5870	3050	1770	1060	843	655	417	441	552	558	10600
Px/Sp	2	0	4	2	1	0	0	0	8	0	1
Px/Gn	260	300	334	215	342	395	457	524	1110	2210	1900
Px/TQ	9070	2230	2100	1730	1580	1930	2170	2660	3690	5440	2210
Cp/TQ	33600	596	253	97	87	36	54	19	8	23	4
Gn/TQ	9340	10000	5780	2980	2150	1400	1080	975	558	396	92
Sp/TQ	11000	5760	2850	1930	1430	1590	1750	1730	1990	3320	1460

MEDIUM	00-05	05-15	15-25	25-35	35-45	45-55	55-65	65-75	75-85	85-95	95-00
Cp/Px	1740	40	11	3	7	1	1	4	1	2	24
Cp/Gn	8	15	1	2	2	2	2	6	10	14	23
Cp/Sp	134	79	19	5	3	2	7	2	0	0	2
Gn/Sp	458	90	48	21	21	14	28	11	17	19	1460
Px/Sp	11	17	5	7	2	5	7	11	23	32	44
Px/Gn	13	27	20	19	22	29	44	51	116	300	509
Px/TQ	560	43	20	41	32	28	47	49	83	108	55
Cp/TQ	807	197	31	9	3	4	5	1	2	0	6
Gn/TQ	491	295	94	45	39	38	15	15	20	10	2
Sp/TQ	221	108	56	38	36	61	51	56	80	208	150

FINE	00-05	05-15	15-25	25-35	35-45	45-55	55-65	65-75	75-85	85-95	95-00
Cp/Px	2050	33	7	3	2	3	1	1	2	1	19
Cp/Gn	8	3	1	1	2	1	1	1	2	9	12
Cp/Sp	40	43	8	3	2	0	1	0	0	2	3
Gn/Sp	623	122	58	31	21	16	14	10	14	16	1670
Px/Sp	39	29	6	10	9	10	13	19	29	96	160
Px/Gn	44	21	19	17	21	30	34	48	79	194	131
Px/TQ	217	63	22	24	30	26	33	49	73	137	33
Cp/TQ	572	101	17	5	3	1	3	1	2	1	0
Gn/TQ	301	175	77	59	25	21	24	11	6	5	3
Sp/TQ	225	96	41	32	32	29	30	41	52	89	41

SAMPLE CF. MEASURED AREA (100's of μm^2) AS A FUNCTION OF SECTION TYPE AND GRADE

TABLE A1.4

Section Grade (% of first-mentioned type) Eg. %Cp in Cp/Px Binaries

COARSE	00-05	05-15	15-25	25-35	35-45	45-55	55-65	65-75	75-85	85-95	95-00
Cp/Px	5520	1340	886	588	439	295	214	235	164	366	4080
Cp/Gn	196	50	17	21	15	24	29	32	22	48	167
Cp/Sp	161	48	26	32	16	51	41	28	49	37	48
Gn/Sp	784	236	179	122	176	121	162	176	160	190	19500
Px/Sp	96	27	23	8	6	12	11	22	49	51	42
Px/Gn	1070	266	189	143	147	167	175	223	313	677	1060
Px/TQ	3100	776	627	748	439	749	596	867	1000	1230	575
Cp/TQ	4790	1560	951	837	473	557	383	307	399	291	153
Gn/TQ	5420	1750	813	561	403	428	352	285	291	273	123
Sp/TQ	5990	1240	507	432	433	400	453	354	366	313	209

MEDIUM	00-05	05-15	15-25	25-35	35-45	45-55	55-65	65-75	75-85	85-95	95-00
Cp/Px	4280	452	246	135	100	68	50	38	35	66	1060
Cp/Gn	17	14	11	14	6	4	4	4	13	29	66
Cp/Sp	48	37	29	9	17	34	21	21	24	88	600
Gn/Sp	1050	152	124	78	79	82	64	64	74	88	9340
Px/Sp	16	30	18	14	19	18	21	43	44	137	258
Px/Gn	70	91	59	58	49	50	66	105	169	273	370
Px/TQ	493	199	134	119	133	159	187	239	296	300	183
Cp/TQ	884	367	273	240	136	105	109	95	56	114	60
Gn/TQ	1610	342	139	79	61	59	48	22	45	27	6
Sp/TQ	1330	386	155	99	100	86	48	79	55	83	19

FINE	00-05	05-15	15-25	25-35	35-45	45-55	55-65	65-75	75-85	85-95	95-00
Cp/Px	459	196	70	20	23	10	11	15	14	18	43
Cp/Gn	12	7	1	1	1	1	0	1	5	7	9
Cp/Sp	24	36	12	7	7	4	2	5	15	73	14
Gn/Sp	87	16	9	6	5	4	6	5	6	7	757
Px/Sp	13	7	1	0	1	0	3	1	5	13	10
Px/Gn	47	16	6	4	4	9	10	9	12	16	6
Px/TQ	243	163	64	49	47	46	60	63	81	99	15
Cp/TQ	164	228	112	74	43	40	37	32	54	113	33
Gn/TQ	564	130	66	42	37	29	28	11	12	6	4
Sp/TQ	275	235	133	57	38	29	33	25	46	49	10

SAMPLE CT: MEASURED AREA (100's of μm^2) AS A FUNCTION OF SECTION TYPE AND GRADE

TABLE A1.5

Section Grade (% of first-mentioned type) Eg. %Cp in Cp/Px Binaries

COARSE	00-05	05-15	15-25	25-35	35-45	45-55	55-65	65-75	75-85	85-95	95-00
Cp/Px	4540	868	273	206	136	129	51	55	61	80	1390
Cp/Gn	54	14	12	9	13	17	10	19	22	53	57
Cp/Sp	51	60	47	15	37	9	20	9	20	34	70
Gn/Sp	961	156	169	103	85	50	53	79	66	158	9110
Px/Sp	102	40	33	23	12	43	28	31	83	167	272
Px/Gn	284	108	100	56	42	45	83	119	111	365	449
Px/TQ	574	192	105	190	108	134	196	163	292	365	136
Cp/TQ	1280	529	208	147	91	79	54	15	3	43	8
Gn/TQ	1180	401	208	131	119	67	107	59	62	75	43
Sp/TQ	1230	304	159	89	150	82	116	89	83	119	31

MEDIUM	00-05	05-15	15-25	25-35	35-45	45-55	55-65	65-75	75-85	85-95	95-00
Cp/Px	4630	528	356	198	116	108	96	63	57	68	1610
Cp/Gn	18	11	1	7	3	11	8	7	12	42	42
Cp/Sp	2	47	29	36	23	24	41	30	14	51	115
Gn/Sp	1230	132	103	74	82	55	62	43	70	55	6970
Px/Sp	54	50	42	22	30	31	34	41	65	191	204
Px/Gn	62	87	44	69	43	48	49	82	134	226	106
Px/TQ	328	113	94	86	118	99	102	153	175	159	32
Cp/TQ	495	226	185	160	71	64	93	41	45	47	30
Gn/TQ	993	201	70	45	40	31	21	25	7	14	7
Sp/TQ	568	318	102	108	83	47	48	53	45	59	26

FINE	00-05	05-15	15-25	25-35	35-45	45-55	55-65	65-75	75-85	85-95	95-00
Cp/Px	547	37	18	15	17	14	14	13	21	36	'87
Cp/Gn	7	5	2	2	1	1	2	1	3	8	17
Cp/Sp	7	20	8	7	1	3	4	2	2	3	36
Gn/Sp	78	14	7	5	5	3	2	1	2	1	609
Px/Sp	8	8	3	3	1	1	1	1	3	8	17
Px/Gn	10	12	5	5	5	8	9	12	25	52	64
Px/TQ	121	43	17	16	10	8	18	13	22	45	4
Cp/TQ	85	89	32	16	13	10	10	12	12	17	21
Gn/TQ	195	53	24	10	4	15	4	3	4	5	0
Sp/TQ	141	34	19	12	8	10	12	14	18	41	7

SAMPLE CN: MEASURED AREA (100's of μm^2) AS A FUNCTION OF SECTION TYPE AND GRADE

TABLE A1.6

Section Grade (% of first-mentioned type) Eg. %Cp in Cp/Px Binaries

COARSE	00-05	05-15	15-25	25-35	35-45	45-55	55-65	65-75	75-85	85-95	95-00
Cp/Px	4130	1440	1010	602	755	717	513	514	822	1730	19100
Cp/Gn	44	69	27	31	35	49	28	112	110	165	278
Cp/Sp	69	112	154	204	208	116	157	197	298	553	5600
Gn/Sp	750	46	25	24	7	36	18	4	3	37	2000
Px/Sp	25	32	29	30	26	18	20	32	97	124	281
Px/Gn	71	12	38	30	27	32	18	34	60	107	175
Px/TQ	2520	1890	1070	813	689	674	618	551	752	670	234
Cp/TQ	1320	893	777	879	701	773	668	869	919	1580	1090
Gn/TQ	8660	796	276	200	250	131	60	57	33	13	0
Sp/TQ	5820	2030	934	356	397	269	168	126	135	173	66

MEDIUM	00-05	05-15	15-25	25-35	35-45	45-55	55-65	65-75	75-85	85-95	95-00
Cp/Px	1760	470	336	270	288	239	226	241	344	561	10900
Cp/Gn	15	11	13	11	7	14	11	22	25	80	144
Cp/Sp	33	37	53	28	31	30	45	54	76	156	238
Gn/Sp	250	13	6	4	3	3	4	5	1	6	84
Px/Sp	4	8	5	5	8	12	21	16	22	38	44
Px/Gn	19	11	4	4	10	5	8	16	31	43	46
Px/TQ	230	139	107	89	58	53	74	84	109	43	15
Cp/TQ	66	124	108	83	101	57	70	103	94	148	47
Gn/TQ	787	106	42	23	11	7	4	8	6	5	2
Sp/TQ	590	219	65	37	12	14	12	20	16	10	6

FINE	00-05	05-15	15-25	25-35	35-45	45-55	55-65	65-75	75-85	85-95	95-00
Cp/Px	459	99	64	53	40	46	43	38	65	173	3250
Cp/Gn	6	4	1	2	4	5	3	4	8	25	45
Cp/Sp	23	33	11	12	12	17	15	9	22	66	519
Gn/Sp	89	6	1	2	1	1	1	1	1	2	370
Px/Sp	3	4	1	1	1	2	1	0	2	8	33
Px/Gn	7	4	2	4	1	3	2	4	3	11	14
Px/TQ	243	104	37	20	26	22	12	16	11	13	1
Cp/TQ	28	34	28	22	23	24	29	25	38	106	148
Gn/TQ	427	39	8	6	3	4	3	2	5	6	3
Sp/TQ	363	53	22	10	6	10	7	10	13	7	4

Sample: RC074 COARSE FREQUENCY OF VARIOUS OBSERVATIONS AS A PERCENTAGE (SAMPLE = 100%) Table 41.7

Particle Grade (% of First Mentioned Phase - eg. Cp in Cp/Px Binaries)

	0.0000	0.0250	0.1000	0.2000	0.3000	0.4000	0.5000	0.6000	0.7000	0.8000	0.9000	0.9750	1.0000
Cp/Px		0.00	0.06	0.12	0.04	0.04	0.01	0.07	0.06	0.11	0.06	0.00	
Cp/Gn		0.07	0.07	0.01	0.01	0.02	0.02	0.00	0.05	0.05	0.06	0.03	
Cp/Sp		0.02	0.02	0.01	0.01	0.02	0.04	0.02	0.04	0.02	0.01	0.01	
Cp/TQ		0.27	0.41	0.20	0.10	0.06	0.11	0.02	0.04	0.02	0.10	0.06	
Cp/All	95.85	0.35	0.58	0.34	0.16	0.15	0.19	0.11	0.20	0.20	0.23	0.10	1.53
Px/Cp		0.00	0.06	0.11	0.06	0.07	0.01	0.04	0.04	0.12	0.06	0.00	
Px/Gn		0.01	0.06	0.30	0.49	0.49	0.74	0.97	1.47	2.36	5.61	3.98	
Px/Sp		0.29	0.30	0.04	0.07	0.07	0.14	0.06	0.14	0.22	0.61	0.46	
Px/TQ		1.55	2.16	1.33	1.43	1.33	1.80	2.26	2.00	2.80	3.73	0.92	
Px/All	47.74	1.84	2.59	1.78	2.06	1.96	2.69	3.35	3.65	5.50	10.01	5.36	11.47
Gn/Cp		0.03	0.06	0.05	0.05	0.00	0.02	0.02	0.01	0.01	0.07	0.07	
Gn/Px		3.98	5.61	2.36	1.47	0.97	0.74	0.49	0.49	0.30	0.06	0.01	
Gn/Sp		2.08	2.83	1.25	0.99	0.60	0.48	0.58	0.44	0.51	0.39	0.10	
Gn/TQ		7.11	10.27	4.39	2.46	1.52	1.10	0.85	0.54	0.41	0.34	0.18	
Gn/All	28.60	13.19	18.77	8.06	4.98	3.09	2.33	1.94	1.48	1.23	0.87	0.36	15.10
Sp/Cp		0.01	0.01	0.02	0.04	0.02	0.04	0.02	0.01	0.01	0.02	0.02	
Sp/Px		0.46	0.61	0.22	0.14	0.06	0.14	0.07	0.07	0.04	0.30	0.29	
Sp/Gn		0.10	0.39	0.51	0.44	0.58	0.48	0.60	0.99	1.25	2.83	2.08	
Sp/TQ		3.78	4.56	2.01	2.46	1.75	1.93	1.65	1.85	2.48	4.26	2.71	
Sp/All	48.03	4.36	5.58	2.77	3.09	2.41	2.59	2.35	2.92	3.79	7.41	5.09	9.61

Sample: RC074 MEDIUM FREQUENCY OF VARIOUS OBSERVATIONS AS A PERCENTAGE (SAMPLE = 100%) Table A1.8

	Particle Grade (% of First Mentioned Phase - eg. Cp in Cp/Px Binaries)												
	0.0000	0.0250	0.1000	0.2000	0.3000	0.4000	0.5000	0.6000	0.7000	0.8000	0.9000	0.9750	1.0000
Cp/Px		0.12	0.29	0.20	0.05	0.07	0.08	0.08	0.08	0.12	0.26	0.18	
Cp/Gn		0.19	0.20	0.03	0.04	0.04	0.01	0.01	0.01	0.07	0.20	0.14	
Cp/Sp		0.36	0.54	0.21	0.05	0.03	0.00	0.01	0.00	0.04	0.07	0.03	
Cp/TQ		1.97	2.83	1.08	0.45	0.33	0.21	0.24	0.18	0.26	0.13	0.00	
Cp/All	85.20	2.64	3.86	1.51	0.59	0.46	0.30	0.34	0.28	0.49	0.66	0.35	3.32
Px/Cp		0.18	0.26	0.12	0.08	0.08	0.08	0.07	0.05	0.20	0.29	0.12	
Px/Gn		0.17	0.37	0.32	0.24	0.37	0.42	0.84	1.25	1.57	4.12	3.18	
Px/Sp		0.24	0.26	0.04	0.04	0.07	0.01	0.00	0.03	0.09	0.32	0.24	
Px/TQ		1.02	1.61	1.32	1.46	1.17	1.38	1.36	1.36	2.16	3.86	2.38	
Px/All	47.93	1.62	2.50	1.79	1.82	1.68	1.89	2.26	2.68	4.01	8.58	5.91	17.32
Gn/Cp		0.14	0.20	0.07	0.01	0.01	0.01	0.04	0.04	0.03	0.20	0.19	
Gn/Px		3.18	4.12	1.57	1.25	0.84	0.42	0.37	0.24	0.32	0.37	0.17	
Gn/Sp		2.14	2.33	0.49	0.59	0.32	0.36	0.37	0.18	0.36	0.29	0.03	
Gn/TQ		5.87	7.75	3.20	2.63	1.21	1.05	0.88	0.43	0.62	0.54	0.14	
Gn/All	33.45	11.32	14.40	5.32	4.49	2.38	1.84	1.66	0.89	1.32	1.39	0.53	21.01
Sp/Cp		0.03	0.07	0.04	0.00	0.01	0.00	0.03	0.05	0.21	0.54	0.36	
Sp/Px		0.24	0.32	0.09	0.03	0.00	0.01	0.07	0.04	0.04	0.26	0.24	
Sp/Gn		0.03	0.29	0.36	0.18	0.37	0.36	0.32	0.59	0.49	2.33	2.14	
Sp/TQ		2.88	3.36	1.24	1.51	1.50	0.96	1.37	1.33	2.07	3.63	2.23	
Sp/All	64.06	3.16	4.03	1.72	1.72	1.88	1.33	1.78	2.01	2.80	6.76	4.97	3.77

Sample: RC074 FINE FREQUENCY OF VARIOUS OBSERVATIONS AS A PERCENTAGE (SAMPLE = 100%) Table A1.9

	Particle Grade (% of First Mentioned Phase - eg. Cp in Cp/Px Binaries)												
	0.0000	0.0250	0.1000	0.2000	0.3000	0.4000	0.5000	0.6000	0.7000	0.8000	0.9000	0.9750	1.0000
Cp/Px		1.33	1.56	0.30	0.14	0.10	0.07	0.04	0.04	0.09	0.29	0.22	
Cp/Gn		0.06	0.06	0.00	0.00	0.00	0.00	0.00	0.00	0.00	0.03	0.03	
Cp/Sp		0.55	0.62	0.12	0.09	0.03	0.01	0.01	0.00	0.03	0.13	0.10	
Cp/TQ		9.27	12.04	3.48	1.42	0.83	0.67	0.64	0.38	0.42	1.00	0.77	
Cp/All	60.68	11.21	14.28	3.90	1.65	0.96	0.75	0.70	0.42	0.54	1.45	1.12	2.35
Px/Cp		0.22	0.29	0.09	0.04	0.04	0.07	0.10	0.14	0.30	1.56	1.33	
Px/Gn		0.23	0.25	0.12	0.20	0.29	0.28	0.25	0.51	0.48	1.45	1.22	
Px/Sp		0.04	0.06	0.01	0.00	0.00	0.00	0.00	0.00	0.01	0.07	0.06	
Px/TQ		3.14	4.50	2.04	1.35	1.45	1.40	1.51	1.81	2.43	6.16	4.63	
Px/All	36.98	3.64	5.10	2.26	1.59	1.78	1.75	1.85	2.46	3.23	9.24	7.24	22.87
Gn/Cp		0.03	0.03	0.00	0.00	0.00	0.00	0.00	0.00	0.00	0.06	0.06	
Gn/Px		1.22	1.45	0.48	0.51	0.25	0.28	0.29	0.20	0.12	0.25	0.23	
Gn/Sp		0.20	0.25	0.12	0.13	0.12	0.09	0.09	0.09	0.09	0.14	0.10	
Gn/TQ		4.92	7.01	3.08	2.00	1.81	1.19	0.87	0.75	0.62	0.65	0.41	
Gn/All	48.40	6.37	8.73	3.68	2.64	2.17	1.55	1.25	1.04	0.83	1.10	0.80	21.45
Sp/Cp		0.10	0.13	0.03	0.00	0.01	0.01	0.03	0.09	0.12	0.62	0.55	
Sp/Px		0.06	0.07	0.01	0.00	0.00	0.00	0.00	0.00	0.01	0.06	0.04	
Sp/Gn		0.10	0.14	0.09	0.09	0.09	0.09	0.12	0.13	0.12	0.25	0.20	
Sp/TQ		3.60	4.37	1.39	1.23	1.06	1.27	1.42	1.62	2.68	4.00	1.90	
Sp/All	70.43	3.86	4.72	1.52	1.32	1.16	1.38	1.56	1.84	2.93	4.92	2.69	1.67

Sample: RC076 COARSE FREQUENCY OF VARIOUS OBSERVATIONS AS A PERCENTAGE (SAMPLE = 100%) Table A1.10

	Particle Grade (% of First Mentioned Phase - eg. Cp in Cp/Px Binaries)												
	0.0000	0.0250	0.1000	0.2000	0.3000	0.4000	0.5000	0.6000	0.7000	0.8000	0.9000	0.9750	1.0000
Cp/Px		0.11	0.47	0.44	0.16	0.22	0.10	0.11	0.23	0.15	0.13	0.10	
Cp/Gn		0.00	0.02	0.06	0.03	0.07	0.07	0.04	0.06	0.05	0.27	0.21	
Cp/Sp		0.12	0.15	0.07	0.07	0.04	0.02	0.11	0.04	0.02	0.02	0.02	
Cp/TQ		0.08	0.37	0.35	0.11	0.22	0.18	0.12	0.13	0.11	0.18	0.00	
Cp/All	91.91	0.31	1.01	0.91	0.37	0.55	0.37	0.38	0.46	0.33	0.60	0.32	2.47
Px/Cp		0.10	0.13	0.15	0.23	0.11	0.10	0.22	0.16	0.44	0.47	0.11	
Px/Gn		0.20	0.47	0.40	0.54	0.47	0.65	0.89	1.52	2.17	4.39	2.98	
Px/Sp		0.20	0.30	0.17	0.12	0.21	0.22	0.21	0.33	0.45	0.98	0.70	
Px/TQ		1.41	2.04	1.40	1.56	1.19	1.60	1.59	1.88	1.72	2.84	0.83	
Px/All	50.91	1.91	2.94	2.11	2.44	1.98	2.57	2.91	3.89	4.78	8.68	4.62	10.27
Gn/Cp		0.21	0.27	0.05	0.06	0.04	0.07	0.07	0.03	0.06	0.02	0.00	
Gn/Px		2.98	4.39	2.17	1.52	0.89	0.65	0.47	0.54	0.40	0.47	0.20	
Gn/Sp		3.79	5.90	3.02	1.80	1.26	0.91	0.98	0.75	0.73	0.67	0.32	
Gn/TQ		3.70	5.88	2.82	1.29	1.27	0.80	0.51	0.30	0.15	0.07	0.02	
Gn/All	30.16	10.68	16.44	8.05	4.67	3.46	2.43	2.03	1.62	1.34	1.23	0.54	17.36
Sp/Cp		0.02	0.02	0.02	0.04	0.11	0.02	0.04	0.07	0.07	0.15	0.12	
Sp/Px		0.70	0.98	0.45	0.33	0.21	0.22	0.21	0.12	0.17	0.30	0.20	
Sp/Gn		0.32	0.67	0.73	0.75	0.98	0.91	1.26	1.80	3.02	5.90	3.79	
Sp/TQ		2.40	3.18	1.73	1.91	1.83	1.19	0.93	1.18	1.18	1.03	0.44	
Sp/All	50.43	3.43	4.85	2.94	3.03	3.13	2.34	2.45	3.17	4.44	7.40	4.55	7.85

Sample: RC076 MEDIUM FREQUENCY OF VARIOUS OBSERVATIONS AS A PERCENTAGE (SAMPLE = 100%) Table A1.11

	Particle Grade (% of First Mentioned Phase - eg. Cp in Cp/Px Binaries)												
	0.0000	0.0250	0.1000	0.2000	0.3000	0.4000	0.5000	0.6000	0.7000	0.8000	0.9000	0.9750	1.0000
Cp/Px		0.99	1.36	0.55	0.37	0.28	0.18	0.16	0.18	0.16	0.42	0.35	
Cp/Gn		0.05	0.06	0.03	0.04	0.09	0.00	0.06	0.00	0.08	0.21	0.13	
Cp/Sp		0.64	0.73	0.13	0.08	0.07	0.07	0.06	0.04	0.04	0.10	0.08	
Cp/TQ		1.32	1.59	0.46	0.37	0.22	0.26	0.24	0.09	0.04	0.10	0.03	
Cp/All	83.63	3.00	3.73	1.17	0.87	0.65	0.52	0.52	0.31	0.32	0.83	0.59	3.87
Px/Cp		0.35	0.42	0.16	0.18	0.16	0.18	0.28	0.37	0.55	1.36	0.99	
Px/Gn		0.24	0.41	0.33	0.30	0.42	0.50	0.62	0.99	1.51	3.96	2.95	
Px/Sp		0.03	0.09	0.11	0.10	0.09	0.07	0.21	0.19	0.30	0.68	0.48	
Px/TQ		0.79	0.99	0.55	0.70	0.72	0.82	0.54	1.01	0.85	1.03	0.26	
Px/All	52.97	1.40	1.91	1.14	1.28	1.38	1.57	1.65	2.57	3.21	7.03	4.67	19.22
Gn/Cp		0.13	0.21	0.08	0.00	0.06	0.00	0.09	0.04	0.03	0.06	0.05	
Gn/Px		2.95	3.96	1.51	0.99	0.62	0.50	0.42	0.30	0.33	0.41	0.24	
Gn/Sp		1.25	1.81	0.91	0.69	0.69	0.38	0.28	0.26	0.29	0.30	0.15	
Gn/TQ		1.36	2.38	1.44	0.83	0.50	0.59	0.37	0.31	0.17	0.24	0.09	
Gn/All	43.36	5.69	8.36	3.93	2.51	1.87	1.48	1.15	0.92	0.81	1.01	0.52	28.40
Sp/Cp		0.08	0.10	0.04	0.04	0.06	0.07	0.07	0.08	0.13	0.73	0.64	
Sp/Px		0.48	0.68	0.30	0.19	0.21	0.07	0.09	0.10	0.11	0.09	0.03	
Sp/Gn		0.15	0.30	0.29	0.26	0.28	0.38	0.69	0.69	0.91	1.81	1.25	
Sp/TQ		0.86	1.59	1.07	0.66	0.76	0.72	0.77	0.49	0.96	1.70	0.33	
Sp/All	71.38	1.56	2.68	1.69	1.15	1.31	1.25	1.61	1.36	2.10	4.32	2.25	7.34

Sample: RC076 FINE FREQUENCY OF VARIOUS OBSERVATIONS AS A PERCENTAGE (SAMPLE = 100%) Table A1.12

Particle Grade (% of First Mentioned Phase - eg. Cp in Cp/Px Binaries)

	0.0000	0.0250	0.1000	0.2000	0.3000	0.4000	0.5000	0.6000	0.7000	0.8000	0.9000	0.9750	1.0000
Cp/Px		2.88	3.28	0.48	0.15	0.15	0.05	0.07	0.07	0.17	0.34	0.21	
Cp/Gn		0.05	0.07	0.02	0.00	0.00	0.00	0.00	0.00	0.00	0.05	0.05	
Cp/Sp		0.89	1.11	0.27	0.10	0.05	0.03	0.00	0.02	0.02	0.27	0.27	
Cp/TQ		9.19	12.58	4.93	3.08	1.49	0.89	0.67	0.51	0.87	2.33	1.71	
Cp/All	49.40	13.01	17.04	5.70	3.34	1.69	0.98	0.74	0.60	1.06	2.99	2.23	1.22
Px/Cp		0.21	0.34	0.17	0.07	0.07	0.05	0.15	0.15	0.48	3.28	2.88	
Px/Gn		0.05	0.05	0.02	0.03	0.02	0.02	0.02	0.05	0.05	0.03	0.01	
Px/Sp		0.07	0.09	0.02	0.00	0.00	0.00	0.00	0.00	0.00	0.09	0.09	
Px/TQ		4.20	5.49	2.14	1.69	1.20	1.32	1.73	2.21	3.35	7.05	3.85	
Px/All	38.84	4.53	5.97	2.34	1.80	1.28	1.39	1.90	2.41	3.88	10.45	6.83	18.38
Gn/Cp		0.05	0.05	0.00	0.00	0.00	0.00	0.00	0.00	0.02	0.07	0.05	
Gn/Px		0.01	0.03	0.05	0.05	0.02	0.02	0.02	0.03	0.02	0.05	0.05	
Gn/Sp		0.03	0.03	0.02	0.02	0.02	0.03	0.02	0.05	0.02	0.12	0.13	
Gn/TQ		4.62	6.47	2.82	1.95	1.40	0.98	1.06	0.72	0.77	1.03	0.62	
Gn/All	53.68	4.71	6.59	2.89	2.02	1.44	1.03	1.09	0.80	0.82	1.27	0.85	22.82
Sp/Cp		0.27	0.27	0.02	0.02	0.09	0.03	0.05	0.10	0.27	1.11	0.89	
Sp/Px		0.09	0.09	0.00	0.00	0.00	0.00	0.00	0.00	0.02	0.09	0.07	
Sp/Gn		0.13	0.12	0.02	0.05	0.02	0.03	0.02	0.02	0.02	0.03	0.03	
Sp/TQ		4.71	7.43	4.05	2.67	2.02	1.30	1.30	1.61	2.89	4.48	2.40	
Sp/All	59.96	5.18	7.90	4.09	2.74	2.04	1.37	1.37	1.73	3.20	5.71	3.38	1.33

Sample: RGHR TLS COARSE FREQUENCY OF VARIOUS OBSERVATIONS AS A PERCENTAGE (SAMPLE = 100%) Table A1.13

Particle Grade (% of First Mentioned Phase - eg. Cp in Cp/Px Binaries)

	0.0000	0.0250	0.1000	0.2000	0.3000	0.4000	0.5000	0.6000	0.7000	0.8000	0.9000	0.9750	1.0000
Cp/Px		0.12	0.13	0.02	0.03	0.02	0.01	0.00	0.00	0.00	0.00	0.00	
Cp/Gn		0.00	0.00	0.02	0.01	0.02	0.00	0.01	0.00	0.01	0.02	0.01	
Cp/Sp		0.06	0.18	0.14	0.05	0.09	0.13	0.18	0.10	0.22	0.83	0.65	
Cp/TQ		0.51	0.78	0.33	0.13	0.11	0.05	0.07	0.02	0.01	0.03	0.01	
Cp/All	93.84	0.69	1.08	0.52	0.21	0.24	0.19	0.26	0.13	0.24	0.88	0.67	1.05
Px/Cp		0.00	0.00	0.00	0.00	0.00	0.01	0.02	0.03	0.02	0.13	0.12	
Px/Gn		0.10	0.39	0.44	0.28	0.45	0.52	0.60	0.68	1.45	2.89	1.78	
Px/Sp		0.00	0.00	0.01	0.00	0.00	0.00	0.00	0.00	0.01	0.00	0.00	
Px/TQ		1.30	2.91	2.74	2.26	2.06	2.52	2.83	3.47	4.82	7.10	2.89	
Px/All	49.35	1.40	3.31	3.19	2.54	2.51	3.04	3.45	4.19	6.30	10.11	4.78	5.82
Gn/Cp		0.01	0.02	0.01	0.00	0.01	0.00	0.02	0.01	0.02	0.00	0.00	
Gn/Px		1.78	2.89	1.45	0.68	0.60	0.52	0.45	0.28	0.44	0.39	0.10	
Gn/Sp		2.36	3.98	2.31	1.38	1.10	0.86	0.54	0.58	0.72	0.73	0.30	
Gn/TQ		7.46	13.06	7.55	3.89	2.81	1.83	1.41	1.27	0.73	0.52	0.12	
Gn/All	21.00	11.61	19.94	11.32	5.96	4.52	3.20	2.42	2.13	1.91	1.64	0.51	13.84
Sp/Cp		0.65	0.83	0.22	0.10	0.18	0.13	0.09	0.05	0.14	0.18	0.06	
Sp/Px		0.00	0.00	0.01	0.00	0.00	0.00	0.00	0.00	0.01	0.00	0.00	
Sp/Gn		0.30	0.73	0.72	0.58	0.54	0.86	1.10	1.38	2.31	3.98	2.36	
Sp/TQ		5.06	7.52	3.72	2.52	1.87	2.08	2.29	2.26	2.60	4.33	1.91	
Sp/All	39.99	6.01	9.08	4.67	3.19	2.59	3.06	3.48	3.69	5.06	8.49	4.33	6.36

Sample. RGHR TLS MEDIUM FREQUENCY OF VARIOUS OBSERVATIONS AS A PERCENTAGE (SAMPLE : 100%) Table A1.14

	Particle Grade (% of First Mentioned Phase - eg. Cp in Cp/Px Binaries)												
	0.0000	0.0250	0.1000	0.2000	0.3000	0.4000	0.5000	0.6000	0.7000	0.8000	0.9000	0.9750	1.0000
Cp/Px		0.45	0.59	0.16	0.04	0.10	0.01	0.01	0.06	0.01	0.03	0.04	
Cp/Gn		0.12	0.22	0.01	0.03	0.03	0.03	0.03	0.09	0.15	0.21	0.10	
Cp/Sp		0.93	1.17	0.28	0.07	0.04	0.03	0.10	0.03	0.00	0.00	0.01	
Cp/TQ		2.53	2.92	0.46	0.13	0.04	0.06	0.07	0.01	0.03	0.00	0.00	
Cp/All	87.84	4.03	4.91	0.92	0.28	0.22	0.13	0.22	0.19	0.19	0.24	0.16	0.65
Px/Cp		0.04	0.03	0.01	0.06	0.01	0.01	0.10	0.04	0.16	0.59	0.45	
Px/Gn		0.19	0.40	0.30	0.28	0.33	0.43	0.65	0.76	1.72	4.45	3.11	
Px/Sp		0.16	0.25	0.07	0.10	0.03	0.07	0.10	0.16	0.34	0.47	0.22	
Px/TQ		0.65	0.64	0.30	0.61	0.47	0.42	0.70	0.73	1.23	1.60	0.73	
Px/All	45.44	1.05	1.32	0.68	1.05	0.85	0.93	1.56	1.69	3.46	7.12	4.51	30.34
Gn/Cp		0.10	0.21	0.15	0.09	0.03	0.03	0.03	0.03	0.01	0.22	0.12	
Gn/Px		3.11	4.45	1.72	0.76	0.65	0.43	0.33	0.28	0.30	0.40	0.19	
Gn/Sp		0.78	1.34	0.71	0.31	0.31	0.21	0.42	0.16	0.25	0.28	0.11	
Gn/TQ		3.32	4.38	1.40	0.67	0.58	0.56	0.22	0.22	0.30	0.15	0.00	
Gn/All	48.09	7.31	10.37	3.98	1.83	1.57	1.23	0.99	0.70	0.86	1.05	0.42	21.59
Sp/Cp		0.01	0.00	0.00	0.03	0.10	0.03	0.04	0.07	0.28	1.17	0.93	
Sp/Px		0.22	0.47	0.34	0.15	0.10	0.07	0.03	0.10	0.07	0.25	0.16	
Sp/Gn		0.11	0.28	0.25	0.16	0.42	0.21	0.31	0.31	0.71	1.34	0.78	
Sp/TQ		1.05	1.60	0.83	0.56	0.53	0.91	0.76	0.83	1.19	3.09	2.23	
Sp/All	69.78	1.40	2.36	1.42	0.92	1.16	1.22	1.14	1.32	2.26	5.85	4.10	7.08

Sample: RGHR TLS FINE FREQUENCY OF VARIOUS OBSERVATIONS AS A PERCENTAGE (SAMPLE = 100%) Table A1.15

Particle Grade (% of First Mentioned Phase - eg. Cp in Cp/Px Binaries)

	0.0000	0.0250	0.1000	0.2000	0.3000	0.4000	0.5000	0.6000	0.7000	0.8000	0.9000	0.9750	1.0000
Cp/Px		0.42	0.50	0.11	0.05	0.03	0.05	0.02	0.02	0.03	0.02	0.00	
Cp/Gn		0.04	0.05	0.02	0.02	0.03	0.02	0.02	0.02	0.03	0.14	0.11	
Cp/Sp		0.55	0.65	0.12	0.05	0.03	0.00	0.02	0.00	0.00	0.03	0.03	
Cp/TQ		1.31	1.52	0.26	0.08	0.05	0.02	0.05	0.02	0.03	0.02	0.00	
Cp/All	93.15	2.31	2.72	0.50	0.18	0.14	0.08	0.09	0.05	0.09	0.20	0.14	0.37
Px/Cp		0.00	0.02	0.03	0.02	0.02	0.05	0.03	0.05	0.11	0.50	0.42	
Px/Gn		0.16	0.32	0.29	0.26	0.32	0.45	0.51	0.72	1.19	2.93	1.98	
Px/Sp		0.42	0.44	0.09	0.15	0.14	0.15	0.20	0.29	0.44	1.45	1.15	
Px/TQ		0.80	0.95	0.33	0.36	0.45	0.39	0.50	0.74	1.10	2.07	0.50	
Px/All	44.76	1.38	1.72	0.74	0.78	0.92	1.04	1.24	1.80	2.84	6.94	4.05	31.79
Gn/Cp		0.11	0.14	0.03	0.02	0.02	0.02	0.03	0.02	0.02	0.05	0.04	
Gn/Px		1.98	2.93	1.19	0.72	0.51	0.45	0.32	0.26	0.29	0.32	0.16	
Gn/Sp		1.20	1.84	0.88	0.47	0.32	0.24	0.21	0.15	0.21	0.24	0.11	
Gn/TQ		1.92	2.64	1.16	0.89	0.38	0.32	0.36	0.17	0.09	0.08	0.05	
Gn/All	50.80	5.22	7.55	3.26	2.10	1.22	1.03	0.92	0.59	0.60	0.68	0.35	25.69
Sp/Cp		0.03	0.03	0.00	0.00	0.02	0.00	0.03	0.05	0.12	0.65	0.55	
Sp/Px		1.15	1.45	0.44	0.29	0.20	0.15	0.14	0.15	0.09	0.44	0.42	
Sp/Gn		0.11	0.24	0.21	0.15	0.21	0.24	0.32	0.47	0.88	1.84	1.20	
Sp/TQ		1.07	1.45	0.62	0.48	0.48	0.44	0.45	0.62	0.78	1.34	0.62	
Sp/All	70.97	2.36	3.17	1.27	0.92	0.91	0.83	0.94	1.28	1.87	4.27	2.79	8.42

Sample: RGHR CON COARSE FREQUENCY OF VARIOUS OBSERVATIONS AS A PERCENTAGE (SAMPLE = 100%) Table A1.16

	Particle Grade (% of First Mentioned Phase - eg. Cp in Cp/Px Binaries)												
	0.0000	0.0250	0.1000	0.2000	0.3000	0.4000	0.5000	0.6000	0.7000	0.8000	0.9000	0.9750	1.0000
Cp/Px		1.42	2.55	1.69	1.12	0.84	0.56	0.41	0.45	0.31	0.70	0.61	
Cp/Gn		0.08	0.10	0.03	0.04	0.03	0.05	0.06	0.06	0.04	0.09	0.08	
Cp/Sp		0.07	0.09	0.05	0.06	0.03	0.10	0.08	0.05	0.09	0.07	0.00	
Cp/TQ		1.95	2.97	1.81	1.59	0.90	1.06	0.73	0.58	0.76	0.55	0.09	
Cp/All	67.33	3.53	5.70	3.58	2.81	1.79	1.76	1.27	1.15	1.21	1.41	0.78	7.68
Px/Cp		0.61	0.70	0.31	0.45	0.41	0.56	0.84	1.12	1.69	2.55	1.42	
Px/Gn		0.28	0.51	0.36	0.27	0.28	0.32	0.33	0.42	0.60	1.29	0.90	
Px/Sp		0.02	0.05	0.04	0.02	0.01	0.02	0.02	0.04	0.09	0.10	0.02	
Px/TQ		0.99	1.48	1.19	1.42	0.84	1.42	1.13	1.65	1.90	2.34	1.09	
Px/All	57.65	1.90	2.73	1.91	2.16	1.53	2.33	2.32	3.23	4.28	6.27	3.45	10.24
Gn/Cp		0.08	0.09	0.04	0.06	0.06	0.05	0.03	0.04	0.03	0.10	0.08	
Gn/Px		0.90	1.29	0.60	0.42	0.33	0.32	0.28	0.27	0.36	0.51	0.28	
Gn/Sp		0.22	0.45	0.34	0.23	0.33	0.23	0.31	0.33	0.30	0.36	0.22	
Gn/TQ		2.32	3.33	1.55	1.07	0.77	0.81	0.67	0.54	0.55	0.52	0.23	
Gn/All	39.17	3.52	5.16	2.52	1.78	1.49	1.41	1.29	1.19	1.25	1.48	0.82	38.91
Sp/Cp		0.00	0.07	0.09	0.05	0.08	0.10	0.03	0.06	0.05	0.09	0.07	
Sp/Px		0.02	0.10	0.09	0.04	0.02	0.02	0.01	0.02	0.04	0.05	0.02	
Sp/Gn		0.22	0.36	0.30	0.33	0.31	0.23	0.33	0.23	0.34	0.45	0.22	
Sp/TQ		1.81	2.36	0.96	0.82	0.82	0.76	0.86	0.67	0.70	0.60	0.24	
Sp/All	83.09	2.06	2.89	1.46	1.25	1.23	1.11	1.24	0.98	1.13	1.19	0.55	1.83

Sample: RGHR CON MEDIUM FREQUENCY OF VARIOUS OBSERVATIONS AS A PERCENTAGE (SAMPLE = 100%) Table A1.17

	Particle Grade (% of First Mentioned Phase - eg. Cp in Cp/Px Binaries)												
	0.0000	0.0250	0.1000	0.2000	0.3000	0.4000	0.5000	0.6000	0.7000	0.8000	0.9000	0.9750	1.0000
Cp/Px		1.18	1.94	1.06	0.58	0.43	0.29	0.22	0.16	0.15	0.28	0.22	
Cp/Gn		0.04	0.06	0.05	0.06	0.03	0.02	0.02	0.02	0.06	0.12	0.08	
Cp/Sp		0.05	0.16	0.12	0.04	0.07	0.15	0.09	0.09	0.10	0.38	0.32	
Cp/TQ		0.92	1.58	1.17	1.03	0.58	0.45	0.47	0.41	0.24	0.49	0.26	
Cp/All	76.95	2.19	3.74	2.40	1.71	1.11	0.91	0.79	0.68	0.55	1.28	0.87	6.81
Px/Cp		0.22	0.28	0.15	0.16	0.22	0.29	0.43	0.58	1.06	1.94	1.18	
Px/Gn		0.26	0.39	0.25	0.25	0.21	0.22	0.28	0.45	0.73	1.17	0.67	
Px/Sp		0.07	0.13	0.08	0.06	0.08	0.08	0.09	0.18	0.19	0.59	0.49	
Px/TQ		0.54	0.86	0.58	0.51	0.57	0.68	0.80	1.03	1.27	1.29	0.53	
Px/All	58.88	1.08	1.66	1.06	0.98	1.08	1.27	1.61	2.24	3.25	5.00	2.87	19.02
Gn/Cp		0.08	0.12	0.06	0.02	0.02	0.02	0.03	0.06	0.05	0.06	0.04	
Gn/Px		0.67	1.17	0.73	0.45	0.28	0.22	0.21	0.25	0.25	0.39	0.26	
Gn/Sp		0.29	0.65	0.53	0.34	0.34	0.35	0.28	0.28	0.32	0.38	0.20	
Gn/TQ		1.04	1.47	0.60	0.34	0.26	0.25	0.21	0.09	0.19	0.12	0.00	
Gn/All	45.97	2.08	3.42	1.91	1.14	0.90	0.84	0.72	0.68	0.81	0.95	0.50	40.06
Sp/Cp		0.32	0.38	0.10	0.09	0.09	0.15	0.07	0.04	0.12	0.16	0.05	
Sp/Px		0.49	0.59	0.19	0.18	0.09	0.08	0.08	0.06	0.08	0.13	0.07	
Sp/Gn		0.20	0.38	0.32	0.28	0.28	0.35	0.34	0.34	0.53	0.65	0.29	
Sp/TQ		1.21	1.66	0.67	0.43	0.43	0.37	0.21	0.34	0.24	0.36	0.08	
Sp/All	82.07	2.22	3.01	1.28	0.98	0.89	0.95	0.70	0.77	0.97	1.30	0.49	4.38

Sample: RGHR CON FINE FREQUENCY OF VARIOUS OBSERVATIONS AS A PERCENTAGE (SAMPLE = 100%) Table A1.18

	Particle Grade (% of First Mentioned Phase - eg. Cp in Cp/Px Binaries)												
	0.0000	0.0250	0.1000	0.2000	0.3000	0.4000	0.5000	0.6000	0.7000	0.8000	0.9000	0.9750	1.0000
Cp/Px		4.31	6.21	2.22	0.63	0.73	0.32	0.35	0.48	0.44	0.57	0.36	
Cp/Gn		0.21	0.22	0.03	0.03	0.03	0.03	0.00	0.03	0.16	0.22	0.08	
Cp/Sp		0.76	1.14	0.38	0.22	0.22	0.13	0.06	0.16	0.48	2.31	0.44	
Cp/TQ		4.85	7.23	3.55	2.35	1.36	1.27	1.17	1.01	1.71	3.58	1.05	
Cp/All	45.67	10.13	14.81	6.18	3.23	2.35	1.74	1.59	1.68	2.79	6.69	1.93	1.20
Px/Cp		0.36	0.57	0.44	0.48	0.35	0.32	0.73	0.63	2.22	6.21	4.31	
Px/Gn		0.38	0.51	0.19	0.13	0.13	0.29	0.32	0.29	0.38	0.51	0.19	
Px/Sp		0.19	0.22	0.03	0.00	0.03	0.00	0.10	0.03	0.16	0.41	0.27	
Px/TQ		3.92	5.17	2.03	1.55	1.49	1.46	1.90	2.00	2.57	3.14	0.48	
Px/All	42.64	4.85	6.47	2.70	2.16	2.00	2.06	3.04	2.95	5.33	10.27	5.25	10.29
Gn/Cp		0.08	0.22	0.16	0.03	0.00	0.03	0.03	0.03	0 03	0.22	0.21	
Gn/Px		0.19	0.51	0.38	0.29	0.32	0.29	0.13	0.13	0.19	0.51	0.38	
Gn/Sp		0.32	0.51	0.29	0.19	0.16	0.13	0.19	0.16	0.19	0.22	0.11	
Gn/TQ		2.70	4.12	2.09	1.33	1.17	0.92	0.89	0.35	0.38	0.19	0.00	
Gn/All	53.75	3.28	5.36	2.92	1.84	1.65	1.36	1.24	0.67	0.79	1.14	0.70	25.30
Sp/Cp		0.44	2.31	0.48	0.16	0.06	0.13	0.22	0.22	0.38	1.14	0.76	
Sp/Px		0.27	0.41	0.16	0.03	0.10	0.00	0.03	0.00	0.03	0.22	0.19	
Sp/Gn		0.11	0.22	0.19	0.16	0.19	0.13	0.16	0.19	0.29	0.51	0.32	
Sp/TQ		4.14	7.45	4.22	1.81	1.20	0.92	1.05	0.79	1.46	1.55	0.32	
Sp/All	62.22	4.96	10.40	5.04	2.16	1.55	1.17	1.46	1.20	2.16	3.42	1.59	2.66

Sample: CLNR TLS COARSE FREQUENCY OF VARIOUS OBSERVATIONS AS A PERCENTAGE (SAMPLE = 100%) Table A1.19

	Particle Grade (% of First Mentioned Phase - eg. Cp in Cp/Px Binaries)												
	0.0000	0.0250	0.1000	0.2000	0.3000	0.4000	0.5000	0.6000	0.7000	0.8000	0.9000	0.9750	1.0000
Cp/Px		2.85	3.55	1.12	0.84	0.56	0.53	0.21	0.22	0.25	0.33	0.19	
Cp/Gn		0.03	0.06	0.05	0.04	0.05	0.07	0.04	0.08	0.09	0.22	0.17	
Cp/Sp		0.08	0.25	0.19	0.06	0.15	0.04	0.08	0.04	0.08	0.14	0.08	
Cp/TQ		1.61	2.16	0.85	0.60	0.37	0.32	0.22	0.06	0.01	0.18	0.03	
Cp/All	75.11	4.57	6.01	2.21	1.54	1.13	0.96	0.55	0.40	0.43	0.86	0.46	5.77
Px/Cp		0.19	0.33	0.25	0.22	0.21	0.53	0.56	0.84	1.12	3.55	2.85	
Px/Gn		0.15	0.44	0.41	0.23	0.17	0.18	0.34	0.49	0.45	1.49	1.28	
Px/Sp		0.08	0.16	0.13	0.09	0.05	0.18	0.11	0.13	0.34	0.68	0.41	
Px/TQ		0.74	0.78	0.43	0.78	0.44	0.55	0.80	0.67	1.19	1.49	0.56	
Px/All	55.99	1.16	1.72	1.22	1.32	0.87	1.43	1.81	2.12	3.10	7.21	5.09	16.95
Gn/Cp		0.17	0.22	0.09	0.08	0.04	0.07	0.05	0.04	0.05	0.06	0.03	
Gn/Px		1.28	1.49	0.45	0.49	0.34	0.18	0.17	0.23	0.41	0.44	0.15	
Gn/Sp		0.16	0.64	0.69	0.42	0.35	0.20	0.22	0.32	0.27	0.65	0.54	
Gn/TQ		1.06	1.64	0.85	0.54	0.49	0.27	0.44	0.24	0.25	0.31	0.17	
Gn/All	44.90	2.66	3.98	2.08	1.52	1.21	0.73	0.88	0.83	0.98	1.45	0.88	37.88
Sp/Cp		0.08	0.14	0.08	0.04	0.08	0.04	0.15	0.06	0.19	0.25	0.08	
Sp/Px		0.41	0.68	0.34	0.13	0.11	0.18	0.05	0.09	0.13	0.16	0.08	
Sp/Gn		0.54	0.65	0.27	0.32	0.22	0.20	0.35	0.42	0.69	0.64	0.16	
Sp/TQ		0.77	1.24	0.65	0.36	0.61	0.33	0.47	0.36	0.34	0.49	0.13	
Sp/All	82.01	1.79	2.71	1.34	0.85	1.03	0.75	1.02	0.94	1.36	1.53	0.44	4.23

Sample: CLNR TLS MEDIUM FREQUENCY OF VARIOUS OBSERVATIONS AS A PERCENTAGE (SAMPLE = 100%) Table A1.20

	Particle Grade (% of First Mentioned Phase - eg. Cp in Cp/Px Binaries)												
	0.0000	0.0250	0.1000	0.2000	0.3000	0.4000	0.5000	0.6000	0.7000	0.8000	0.9000	0.9750	1.0000
Cp/Px		1.21	2.35	1.59	0.88	0.52	0.48	0.43	0.28	0.25	0.30	0.19	
Cp/Gn		0.06	0.35	0.00	0.03	0.01	0.05	0.04	0.03	0.05	0.19	0.15	
Cp/Sp		0.01	0.21	0.13	0.16	0.10	0.11	0.18	0.13	0.06	0.23	0.23	
Cp/TQ		0.54	1.01	0.82	0.71	0.32	0.29	0.41	0.18	0.20	0.21	0.10	
Cp/All	77.18	1.82	3.62	2.54	1.79	0.95	0.92	1.06	0.63	0.57	0.93	0.67	7.33
Px/Cp		0.19	0.30	0.25	0.28	0.43	0.48	0.52	0.88	1.59	2.35	1.21	
Px/Gn		0.28	0.39	0.20	0.31	0.19	0.20	0.22	0.37	0.60	1.01	0.47	
Px/Sp		0.08	0.22	0.19	0.10	0.13	0.14	0.15	0.18	0.29	0.85	0.65	
Px/TQ		0.28	0.50	0.42	0.38	0.53	0.44	0.45	0.68	0.78	0.71	0.14	
Px/All	59.32	0.83	1.42	1.06	1.07	1.28	1.27	1.34	2.11	3.25	4.92	2.47	19.67
Gn/Cp		0.15	0.19	0.05	0.03	0.04	0.05	0.01	0.03	0.00	0.05	0.06	
Gn/Px		0.47	1.01	0.60	0.37	0.22	0.20	0.19	0.31	0.20	0.39	0.28	
Gn/Sp		0.29	0.59	0.46	0.33	0.37	0.25	0.28	0.19	0.31	0.25	0.03	
Gn/TQ		0.68	0.90	0.31	0.20	0.18	0.14	0.09	0.11	0.03	0.06	0.03	
Gn/All	49.09	1.60	2.68	1.42	0.93	0.80	0.64	0.57	0.64	0.54	0.74	0.40	39.95
Sp/Cp		0.23	0.23	0.06	0.13	0.18	0.11	0.10	0.16	0.13	0.21	0.01	
Sp/Px		0.65	0.85	0.29	0.18	0.15	0.14	0.13	0.10	0.19	0.22	0.08	
Sp/Gn		0.03	0.25	0.31	0.19	0.28	0.25	0.37	0.33	0.46	0.59	0.29	
Sp/TQ		1.20	1.42	0.45	0.48	0.37	0.21	0.21	0.24	0.20	0.26	0.12	
Sp/All	81.62	2.12	2.74	1.12	0.99	0.98	0.70	0.82	0.82	0.98	1.28	0.50	5.34

Sample: CLNR 1LS FINE FREQUENCY OF VARIOUS OBSERVATIONS AS A PERCENTAGE (SAMPLE = 100%) Table A1.21

	Particle Grade (% of First Mentioned Phase - eg. Cp in Cp/Px Binaries)												
	0.0000	0.0250	0.1000	0.2000	0.3000	0.4000	0.5000	0.6000	0.7000	0.8000	0.9000	0.9750	1.0000
Cp/Px		1.12	1.56	0.76	0.63	0.72	0.59	0.59	0.55	0.89	1.52	0.91	
Cp/Gn		0.17	0.21	0.08	0.08	0.04	0.04	0.08	0.04	0.13	0.34	0.23	
Cp/Sp		0.30	0.85	0.34	0.30	0.04	0.13	0.17	0.08	0.08	0.13	0.08	
Cp/TQ		2.75	3.76	1.35	0.68	0.55	0.42	0.42	0.51	0.51	0.72	0.46	
Cp/All	64.73	4.33	6.38	2.54	1.69	1.35	1.18	1.27	1.18	1.61	2.71	1.69	9.34
Px/Cp		0.91	1.52	0.89	0.55	0.59	0.59	0.72	0.63	0.76	1.56	1.12	
Px/Gn		0.40	0.51	0.21	0.21	0.21	0.34	0.38	0.51	1.06	2.20	1.39	
Px/Sp		0.27	0.34	0.13	0.13	0.04	0.04	0.04	0.04	0.13	0.34	0.23	
Px/TQ		1.44	1.82	0.72	0.68	0.42	0.34	0.76	0.55	0.93	1.90	0.17	
Px/All	47.48	3.02	4.18	1.94	1.56	1.27	1.31	1.90	1.73	2.87	6.00	2.92	23.80
Gn/Cp		0.23	0.34	0.13	0.04	0.08	0.04	0.04	0.08	0.08	0.21	0.17	
Gn/Px		1.39	2.20	1.06	0.51	0.38	0.34	0.21	0.21	0.21	0.51	0.40	
Gn/Sp		0.40	0.59	0.30	0.21	0.21	0.13	0.08	0.04	0.08	0.04	0.00	
Gn/TQ		1.44	2.24	1.01	0.42	0.17	0.63	0.17	0.13	0.17	0.21	0.00	
Gn/All	56.55	3.47	5.37	2.49	1.18	0.85	1.14	0.51	0.46	0.55	0.97	0.57	25.89
Sp/Cp		0.08	0.13	0.08	0.08	0.17	0.13	0.04	0.30	0.34	0.85	0.30	
Sp/Px		0.23	0.34	0.13	0.04	0.04	0.04	0.04	0.13	0.13	0.34	0.27	
Sp/Gn		0.00	0.04	0.08	0.04	0.08	0.13	0.21	0.21	0.30	0.59	0.40	
Sp/TQ		0.89	1.44	0.80	0.51	0.34	0.42	0.51	0.59	0.76	1.73	0.30	
Sp/All	82.44	1.20	1.94	1.10	0.68	0.63	0.72	0.80	1.23	1.52	3.51	1.27	2.96

Sample: CLNR CON COARSE FREQUENCY OF VARIOUS OBSERVATIONS AS A PERCENTAGE (SAMPLE = 100%) Table A1.22

Particle Grade (% of First Mentioned Phase - eg. Cp in Cp/Px Binaries)

	0.0000	0.0250	0.1000	0.2000	0.3000	0.4000	0.5000	0.6000	0.7000	0.8000	0.9000	0.9750	1.0000
Cp/Px		1.34	2.63	1.85	1.10	1.38	1.31	0.94	0.94	1.50	3.16	2.13	
Cp/Gn		0.08	0.13	0.05	0.06	0.06	0.09	0.05	0.20	0.20	0.30	0.20	
Cp/Sp		0.11	0.20	0.28	0.37	0.38	0.21	0.29	0.36	0.54	1.01	0.65	
Cp/TQ		1.02	1.63	1.42	1.61	1.28	1.41	1.22	1.59	1.68	2.89	1.93	
Cp/All	15.44	2.54	4.60	3.60	3.14	3.11	3.03	2.50	3.09	3.93	7.36	4.97	42.69
Px/Cp		2.13	3.16	1.50	0.94	0.94	1.31	1.38	1.10	1.85	2.63	1.34	
Px/Gn		0.00	0.02	0.07	0.05	0.05	0.06	0.03	0.06	0.11	0.20	0.12	
Px/Sp		0.03	0.06	0.05	0.05	0.05	0.03	0.04	0.06	0.18	0.23	0.08	
Px/TQ		2.24	3.46	1.96	1.49	1.26	1.23	1.13	1.01	1.37	1.23	0.35	
Px/All	56.44	4.41	6.70	3.58	2.54	2.29	2.63	2.58	2.23	3.51	4.28	1.89	6.93
Gn/Cp		0.20	0.30	0.20	0.20	0.05	0.09	0.06	0.06	0.05	0.13	0.08	
Gn/Px		0.12	0.20	0.11	0.06	0.03	0.06	0.05	0.05	0.07	0.02	0.00	
Gn/Sp		0.06	0.08	0.05	0.04	0.01	0.07	0.03	0.01	0.01	0.07	0.07	
Gn/TQ		1.13	1.46	0.50	0.37	0.46	0.24	0.11	0.10	0.06	0.02	0.00	
Gn/All	89.13	1.51	2.04	0.86	0.68	0.55	0.45	0.26	0.22	0.18	0.24	0.15	3.72
Sp/Cp		0.65	1.01	0.54	0.36	0.29	0.21	0.38	0.37	0.28	0.20	0.11	
Sp/Px		0.08	0.23	0.18	0.06	0.04	0.03	0.05	0.05	0.05	0.06	0.03	
Sp/Gn		0.07	0.07	0.01	0.01	0.03	0.07	0.01	0.04	0.05	0.08	0.06	
Sp/TQ		2.33	3.71	1.71	0.65	0.73	0.49	0.31	0.23	0.25	0.32	0.12	
Sp/All	82.06	3.12	5.02	2.44	1.08	1.08	0.80	0.75	0.70	0.63	0.66	0.32	1.34

Sample: CLNR CON MEDIUM FREQUENCY OF VARIOUS OBSERVATIONS AS A PERCENTAGE (SAMPLE = 100%) Table A1.23

	Particle Grade (% of First Mentioned Phase - eg. Cp in Cp/Px Binaries)												
	0.0000	0.0250	0.1000	0.2000	0.3000	0.4000	0.5000	0.6000	0.7000	0.8000	0.9000	0.9750	1.0000
Cp/Px		1.45	2.54	1.81	1.46	1.55	1.29	1.22	1.30	1.86	3.03	1.82	
Cp/Gn		0.02	0.06	0.07	0.06	0.04	0.08	0.06	0.12	0.13	0.43	0.36	
Cp/Sp		0.00	0.20	0.29	0.15	0.17	0.16	0.24	0.29	0.41	0.84	0.58	
Cp/TQ		0.31	0.67	0.58	0.45	0.55	0.31	0.38	0.56	0.51	0.80	0.25	
Cp/All	12.43	1.78	3.46	2.75	2.12	2.30	1.83	1.90	2.27	2.91	5.10	3.01	58.13
Px/Cp		1.82	3.03	1.86	1.30	1.22	1.29	1.55	1.46	1.81	2.54	1.45	
Px/Gn		0.05	0.06	0.02	0.02	0.05	0.03	0.04	0.09	0.17	0.23	0.11	
Px/Sp		0.02	0.04	0.03	0.03	0.04	0.06	0.11	0.09	0.12	0.21	0.13	
Px/TQ		0.41	0.75	0.58	0.48	0.31	0.29	0.40	0.45	0.59	0.23	0.00	
Px/All	66.05	2.30	3.88	2.48	1.83	1.63	1.67	2.11	2.08	2.69	3.21	1.69	8.38
Gn/Cp		0.36	0.43	0.13	0.12	0.06	0.08	0.04	0.06	0.07	0.06	0.02	
Gn/Px		0.11	0.23	0.17	0.09	0.04	0.03	0.05	0.02	0.02	0.06	0.05	
Gn/Sp		0.05	0.07	0.03	0.02	0.02	0.02	0.02	0.03	0.01	0.03	0.04	
Gn/TQ		0.41	0.57	0.23	0.12	0.06	0.04	0.02	0.04	0.03	0.03	0.01	
Gn/All	95.29	0.92	1.31	0.56	0.35	0.18	0.16	0.13	0.15	0.13	0.18	0.12	0.53
Sp/Cp		0.58	0.84	0.41	0.29	0.24	0.16	0.17	0.15	0.29	0.20	0.00	
Sp/Px		0.13	0.21	0.12	0.09	0.11	0.06	0.04	0.03	0.03	0.04	0.02	
Sp/Gn		0.04	0.03	0.01	0.03	0.02	0.02	0.02	0.02	0.03	0.07	0.05	
Sp/TQ		0.93	1.18	0.35	0.20	0.06	0.08	0.06	0.11	0.09	0.05	0.02	
Sp/All	90.83	1.68	2.26	0.89	0.60	0.44	0.32	0.29	0.31	0.43	0.37	0.09	1.49

Sample: CLNR CON FINE FREQUENCY OF VARIOUS OBSERVATIONS AS A PERCENTAGE (SAMPLE = 100%) Table A1.24

	Particle Grade (% of First Mentioned Phase - eg. Cp in Cp/Px Binaries)												
	0.0000	0.0250	0.1000	0.2000	0.3000	0.4000	0.5000	0.6000	0.7000	0.8000	0.9000	0.9750	1.0000
Cp/Px		0.98	1.58	1.02	0.85	0.64	0.73	0.69	0.61	1.04	2.76	2.03	
Cp/Gn		0.06	0.06	0.02	0.03	0.06	0.08	0.05	0.06	0.13	0.40	0.30	
Cp/Sp		0.37	0.53	0.18	0.19	0.19	0.27	0.24	0.14	0.35	1.05	0.77	
Cp/TQ		0.27	0.54	0.45	0.35	0.37	0.38	0.46	0.40	0.61	1.69	1.28	
Cp/All	15.90	1.68	2.71	1.66	1.42	1.26	1.47	1.44	1.21	2.12	5.90	4.39	58.83
Px/Cp		2.03	2.76	1.04	0.61	0.69	0.73	0.64	0.85	1.02	1.58	0.98	
Px/Gn		0.06	0.06	0.03	0.06	0.02	0.05	0.03	0.06	0.05	0.18	0.16	
Px/Sp		0.05	0.06	0.02	0.02	0.02	0.03	0.02	0.00	0.03	0.13	0.10	
Px/TQ		1.23	1.66	0.59	0.32	0.41	0.35	0.19	0.26	0.18	0.21	0.02	
Px/All	73.61	3.37	4.55	1.68	1.01	1.13	1.16	0.88	1.16	1.28	2.09	1.25	6.84
Gn/Cp		0.30	0.40	0.13	0.06	0.05	0.08	0.06	0.03	0.02	0.06	0.06	
Gn/Px		0.16	0.18	0.05	0.06	0.03	0.05	0.02	0.06	0.03	0.06	0.06	
Gn/Sp		0.10	0.10	0.02	0.03	0.02	0.02	0.02	0.02	0.02	0.03	0.02	
Gn/TQ		0.54	0.62	0.13	0.10	0.05	0.06	0.05	0.03	0.08	0.10	0.03	
Gn/All	89.84	1.10	1.29	0.32	0.26	0.14	0.21	0.14	0.14	0.14	0.26	0.18	5.98
Sp/Cp		0.77	1.05	0.35	0.14	0.24	0.27	0.19	0.19	0.18	0.53	0.37	
Sp/Px		0.10	0.13	0.03	0.00	0.02	0.03	0.02	0.02	0.02	0.06	0.05	
Sp/Gn		0.02	0.03	0.02	0.02	0.02	0.02	0.02	0.03	0.02	0.10	0.10	
Sp/TQ		0.57	0.85	0.35	0.16	0.10	0.16	0.11	0.16	0.21	0.11	0.00	
Sp/All	90.71	1.47	2.06	0.75	0.32	0.37	0.48	0.34	0.40	0.41	0.80	0.51	1.39

Sample: RC074 COARSE FREQUENCY OF VARIOUS OBSERVATIONS Table A1.25

Chalcopyrite	Sample%	Cp Observations%		
Free Occurrences	1.53	36.9		
High Grade (85-100)	0.33	8.0		
Med. Grade (15-85)	1.36	32.7		
Low Grade (00-15)	0.93	22.4		
Iron Minerals	Sample%	Px Observations%		Binary Px %
Free Occurrences	11.47	21.9	With High Cp (85-100)	0.33
High Grade (85-100)	15.38	29.4	With Med. Cp (15-85)	2.35
Med. Grade (15-85)	20.99	40.2	With Low Cp (00-15)	0.33
Low Grade (00-15)	4.43	8.5	With No Cp	96.98
Galena + Arsenides	Sample%	Gn Observations%		Binary Gn %
Free Occurrences	15.10	21.1	With High Cp (85-100)	0.31
High Grade (85-100)	1.23	1.7	With Med. Cp (15-85)	0.63
Med. Grade (15-85)	23.11	32.4	With Low Cp (00-15)	0.52
Low Grade (00-15)	31.96	44.8	With No Cp	98.54
Sphalerite	Sample%	Sp Observations%		Binary Sp %
Free Occurrences	9.61	18.5	With High Cp (85-100)	0.18
High Grade (85-100)	12.51	24.1	With Med. Cp (15-85)	1.34
Med. Grade (15-85)	19.92	38.3	With Low Cp (00-15)	0.35
Low Grade (00-15)	9.93	19.1	With No Cp	98.13

Sample. RC074 MEDIUM FREQUENCY OF VARIOUS OBSERVATIONS Table A1.26

Chalcopyrite	Sample%	Cp Observations%
Free Occurrences	3.32	22.5
High Grade (85-100)	1.01	6.8
Med. Grade (15-85)	3.97	26.9
Low Grade (00-15)	6.49	43.9

Iron Minerals	Sample%	Px Observations%		Binary Px %
Free Occurrences	17.32	33.3	With High Cp (85-100)	2.85
High Grade (85-100)	14.49	27.8	With Med. Cp (15-85)	4.27
Med. Grade (15-85)	16.15	31.0	With Low Cp (00-15)	2.60
Low Grade (00-15)	4.12	7.9	With No Cp	90.28

Galena + Arsenides	Sample%	Gn Observations%		Binary Gn %
Free Occurrences	21.01	31.6	With High Cp (85-100)	1.58
High Grade (85-100)	1.92	2.9	With Med. Cp (15-85)	0.99
Med. Grade (15-85)	17.90	26.9	With Low Cp (00-15)	1.83
Low Grade (00-15)	25.72	38.6	With No Cp	95.60

Sphalerite	Sample%	Sp Observations%		Binary Sp %
Free Occurrences	3.77	10.5	With High Cp (85-100)	0.91
High Grade (85-100)	11.73	32.6	With Med. Cp (15-85)	3.39
Med. Grade (15-85)	13.25	36.9	With Low Cp (00-15)	8.85
Low Grade (00-15)	7.19	20.0	With No Cp	86.85

Sample: RC074 FINE FREQUENCY OF VARIOUS OBSERVATIONS Table A1.27

Chalcopyrite	Sample%	Cp Observations%		
Free Occurrences	2.35	6.0		
High Grade (85-100)	2.57	6.5		
Med. Grade (15-85)	8.91	22.7		
Low Grade (00-15)	25.49	64.8		
Iron Minerals	**Sample%**	**Px Observations%**		**Binary Px %**
Free Occurrences	22.87	36.3	With High Cp (85-100)	5.28
High Grade (85-100)	16.48	26.2	With Med. Cp (15-85)	8.18
Med. Grade (15-85)	14.93	23.7	With Low Cp (00-15)	29.76
Low Grade (00-15)	8.73	13.9	With No Cp	56.77
Galena + Arsenides	**Sample%**	**Gn Observations%**		**Binary Gn %**
Free Occurrences	21.45	41.6	With High Cp (85-100)	0.85
High Grade (85-100)	1.90	3.7	With Med. Cp (15-85)	0.00
Med. Grade (15-85)	13.15	25.5	With Low Cp (00-15)	1.69
Low Grade (00-15)	15.11	29.3	With No Cp	97.46
Sphalerite	**Sample%**	**Sp Observations%**		**Binary Sp %**
Free Occurrences	1.67	5.7	With High Cp (85-100)	6.91
High Grade (85-100)	7.61	25.7	With Med. Cp (15-85)	8.64
Med. Grade (15-85)	11.70	39.6	With Low Cp (00-15)	34.99
Low Grade (00-15)	8.58	29.0	With No Cp	49.46

Sample: RC076 COARSE FREQUENCY OF VARIOUS OBSERVATIONS Table A1.28

Chalcopyrite	Sample%	Cp Observations%
Free Occurrences	2.47	30.5
High Grade (85-100)	0.92	11.4
Med. Grade (15-85)	3.38	41.8
Low Grade (00-15)	1.32	16.3

Iron Minerals	Sample%	Px Observations%		Binary Px %
Free Occurrences	10.27	20.9	With High Cp (85-100)	1.11
High Grade (85-100)	13.30	27.1	With Med. Cp (15-85)	6.80
Med. Grade (15-85)	20.68	42.1	With Low Cp (00-15)	2.77
Low Grade (00-15)	4.84	9.9	With No Cp	89.33

Galena + Arsenides	Sample%	Gn Observations%		Binary Gn %
Free Occurrences	17.36	24.9	With High Cp (85-100)	1.34
High Grade (85-100)	1.77	2.5	With Med. Cp (15-85)	1.05
Med. Grade (15-85)	23.59	33.8	With Low Cp (00-15)	0.06
Low Grade (00-15)	27.12	38.8	With No Cp	97.56

Sphalerite	Sample%	Sp Observations%		Binary Sp %
Free Occurrences	7.85	15.8	With High Cp (85-100)	0.15
High Grade (85-100)	11.94	24.1	With Med. Cp (15-85)	1.49
Med. Grade (15-85)	21.49	43.4	With Low Cp (00-15)	1.11
Low Grade (00-15)	8.28	16.7	With No Cp	97.25

Sample: RC076 MEDIUM FREQUENCY OF VARIOUS OBSERVATIONS Table A1.29

Chalcopyrite	Sample%	Cp Observations%		
Free Occurrences	3.87	23.6		
High Grade (85-100)	1.41	8.6		
Med. Grade (15-85)	4.36	26.6		
Low Grade (00-15)	6.73	41.1		
Iron Minerals	**Sample%**	**Px Observations%**		**Binary Px %**
Free Occurrences	19.22	40.9	With High Cp (85-100)	3.95
High Grade (85-100)	11.70	24.9	With Med. Cp (15-85)	9.66
Med. Grade (15-85)	12.80	27.2	With Low Cp (00-15)	11.99
Low Grade (00-15)	3.31	7.0	With No Cp	74.41
Galena + Arsenides	**Sample%**	**Gn Observations%**		**Binary Gn %**
Free Occurrences	28.40	50.1	With High Cp (85-100)	1.69
High Grade (85-100)	1.53	2.7	With Med. Cp (15-85)	1.54
Med. Grade (15-85)	12.66	22.4	With Low Cp (00-15)	0.52
Low Grade (00-15)	14.05	24.8	With No Cp	96.25
Sphalerite	**Sample%**	**Sp Observations%**		**Binary Sp %**
Free Occurrences	7.34	25.6	With High Cp (85-100)	1.59
High Grade (85-100)	6.58	23.0	With Med. Cp (15-85)	4.25
Med. Grade (15-85)	10.47	36.6	With Low Cp (00-15)	12.01
Low Grade (00-15)	4.24	14.8	With No Cp	82.15

Sample: RC076 FINE FREQUENCY OF VARIOUS OBSERVATIONS Table A1.30

Chalcopyrite	Sample%	Cp Observations%
Free Occurrences	1.22	2.4
High Grade (85-100)	5.23	10.3
Med. Grade (15-85)	14.10	27.9
Low Grade (00-15)	30.05	59.4

Iron Minerals	Sample%	Px Observations%		Binary Px %
Free Occurrences	18.38	30.0	With High Cp (85-100)	6.40
High Grade (85-100)	17.28	28.3	With Med. Cp (15-85)	13.40
Med. Grade (15-85)	15.00	24.5	With Low Cp (00-15)	72.10
Low Grade (00-15)	10.50	17.2	With No Cp	8.10

Galena + Arsenides	Sample%	Gn Observations%		Binary Gn %
Free Occurrences	22.82	49.3	With High Cp (85-100)	9.60
High Grade (85-100)	2.11	4.6	With Med. Cp (15-85)	1.60
Med. Grade (15-85)	10.09	21.8	With Low Cp (00-15)	11.20
Low Grade (00-15)	11.29	24.4	With No Cp	77.60

Sphalerite	Sample%	Sp Observations%		Binary Sp %
Free Occurrences	1.33	3.3	With High Cp (85-100)	13.97
High Grade (85-100)	9.09	22.7	With Med. Cp (15-85)	12.86
Med. Grade (15-85)	16.53	41.3	With Low Cp (00-15)	51.88
Low Grade (00-15)	13.09	32.7	With No Cp	21.29

Sample: RGHR TLS COARSE FREQUENCY OF VARIOUS OBSERVATIONS Table A1.31

Chalcopyrite	Sample%	Cp Observations%
Free Occurrences	1.05	17.1
High Grade (85-100)	1.55	25.2
Med. Grade (15-85)	1.79	29.0
Low Grade (00-15)	1.77	28.7

Iron Minerals	Sample%	Px Observations%		Binary Px %
Free Occurrences	5.82	11.5	With High Cp (85-100)	0.07
High Grade (85-100)	14.90	29.4	With Med. Cp (15-85)	0.86
Med. Grade (15-85)	25.22	49.8	With Low Cp (00-15)	2.45
Low Grade (00-15)	4.71	9.3	With No Cp	96.53

Galena + Arsenides	Sample%	Gn Observations%		Binary Gn %
Free Occurrences	13.84	17.5	With High Cp (85-100)	0.13
High Grade (85-100)	2.15	2.7	With Med. Cp (15-85)	0.29
Med. Grade (15-85)	31.46	39.8	With Low Cp (00-15)	0.01
Low Grade (00-15)	31.55	39.9	With No Cp	99.58

Sphalerite	Sample%	Sp Observations%		Binary Sp %
Free Occurrences	6.36	10.6	With High Cp (85-100)	8.45
High Grade (85-100)	12.82	21.4	With Med. Cp (15-85)	5.18
Med. Grade (15-85)	25.75	42.9	With Low Cp (00-15)	1.34
Low Grade (00-15)	15.08	25.1	With No Cp	85.03

Sample: RGHR TLS MEDIUM FREQUENCY OF VARIOUS OBSERVATIONS Table A1.32

Chalcopyrite	Sample%	Cp Observations%
Free Occurrences	0.65	5.4
High Grade (85-100)	0.40	3.3
Med. Grade (15-85)	2.17	17.8
Low Grade (00-15)	8.94	73.5

Iron Minerals	Sample%	Px Observations%		Binary Px %
Free Occurrences	30.34	55.6	With High Cp (85-100)	0.46
High Grade (85-100)	11.64	21.3	With Med. Cp (15-85)	2.57
Med. Grade (15-85)	10.23	18.7	With Low Cp (00-15)	6.48
Low Grade (00-15)	2.37	4.3	With No Cp	90.49

Galena + Arsenides	Sample%	Gn Observations%		Binary Gn %
Free Occurrences	21.59	41.6	With High Cp (85-100)	1.68
High Grade (85-100)	1.48	2.8	With Med. Cp (15-85)	2.00
Med. Grade (15-85)	11.16	21.5	With Low Cp (00-15)	1.84
Low Grade (00-15)	17.68	34.1	With No Cp	94.47

Sphalerite	Sample%	Sp Observations%		Binary Sp %
Free Occurrences	7.08	23.4	With High Cp (85-100)	0.16
High Grade (85-100)	9.94	32.9	With Med. Cp (15-85)	5.90
Med. Grade (15-85)	9.44	31.2	With Low Cp (00-15)	21.97
Low Grade (00-15)	3.75	12.4	With No Cp	71.97

Sample: RGHR TLS FINE FREQUENCY OF VARIOUS OBSERVATIONS Table A1.33

Chalcopyrite	Sample%	Cp Observations%
Free Occurrences	0.37	5.4
High Grade (85-100)	0.34	5.0
Med. Grade (15-85)	1.12	16.3
Low Grade (00-15)	5.03	73.3

Iron Minerals	Sample%	Px Observations%		Binary Px %
Free Occurrences	31.79	57.5	With High Cp (85-100)	0.10
High Grade (85-100)	10.99	19.9	With Med. Cp (15-85)	1.88
Med. Grade (15-85)	9.36	16.9	With Low Cp (00-15)	5.99
Low Grade (00-15)	3.10	5.6	With No Cp	92.03

Galena + Arsenides	Sample%	Gn Observations%		Binary Gn %
Free Occurrences	25.69	52.2	With High Cp (85-100)	1.61
High Grade (85-100)	1.03	2.1	With Med. Cp (15-85)	0.88
Med. Grade (15-85)	9.72	19.8	With Low Cp (00-15)	0.54
Low Grade (00-15)	12.76	25.9	With No Cp	96.97

Sphalerite	Sample%	Sp Observations%		Binary Sp %
Free Occurrences	8.42	29.0	With High Cp (85-100)	0.49
High Grade (85-100)	7.06	24.3	With Med. Cp (15-85)	1.73
Med. Grade (15-85)	8.02	27.6	With Low Cp (00-15)	9.80
Low Grade (00-15)	5.53	19.1	With No Cp	87.99

Sample: RGHR CON COARSE FREQUENCY OF VARIOUS OBSERVATIONS Table A1.34

Chalcopyrite	Sample%	Cp Observations%
Free Occurrences	7.68	23.5
High Grade (85-100)	2.19	6.7
Med. Grade (15-85)	13.57	41.5
Low Grade (00-15)	9.24	28.3

Iron Minerals	Sample%	Px Observations%		Binary Px %
Free Occurrences	10.24	24.2	With High Cp (85-100)	7.84
High Grade (85-100)	9.72	22.9	With Med. Cp (15-85)	32.25
Med. Grade (15-85)	17.76	41.9	With Low Cp (00-15)	23.87
Low Grade (00-15)	4.63	10.9	With No Cp	36.05

Galena + Arsenides	Sample%	Gn Observations%		Binary Gn %
Free Occurrences	38.91	64.0	With High Cp (85-100)	1.79
High Grade (85-100)	2.31	3.8	With Med. Cp (15-85)	3.18
Med. Grade (15-85)	10.93	18.0	With Low Cp (00-15)	1.86
Low Grade (00-15)	8.68	14.3	With No Cp	93.16

Sphalerite	Sample%	Sp Observations%		Binary Sp %
Free Occurrences	1.83	10.8	With High Cp (85-100)	1.66
High Grade (85-100)	1.73	10.3	With Med. Cp (15-85)	10.31
Med. Grade (15-85)	8.40	49.7	With Low Cp (00-15)	3.65
Low Grade (00-15)	4.95	29.2	With No Cp	84.38

Sample: RGHR CON MEDIUM FREQUENCY OF VARIOUS OBSERVATIONS Table A1.35

Chalcopyrite	Sample%	Cp Observations%
Free Occurrences	6.81	29.5
High Grade (85-100)	2.15	9.3
Med. Grade (15-85)	8.16	35.4
Low Grade (00-15)	5.93	25.7

Iron Minerals	Sample%	Px Observations%		Binary Px %
Free Occurrences	19.02	46.3	With High Cp (85-100)	3.71
High Grade (85-100)	7.87	19.1	With Med. Cp (15-85)	21.50
Med. Grade (15-85)	11.49	27.9	With Low Cp (00-15)	23.21
Low Grade (00-15)	2.74	6.7	With No Cp	51.58

Galena + Arsenides	Sample%	Gn Observations%		Binary Gn %
Free Occurrences	40.06	74.2	With High Cp (85-100)	2.15
High Grade (85-100)	1.45	2.7	With Med. Cp (15-85)	2.57
Med. Grade (15-85)	7.01	13.0	With Low Cp (00-15)	1.10
Low Grade (00-15)	5.50	10.2	With No Cp	94.18

Sphalerite	Sample%	Sp Observations%		Binary Sp %
Free Occurrences	4.38	24.4	With High Cp (85-100)	9.24
High Grade (85-100)	1.79	10.0	With Med. Cp (15-85)	8.81
Med. Grade (15-85)	6.53	36.4	With Low Cp (00-15)	2.81
Low Grade (00-15)	5.22	29.1	With No Cp	79.14

Sample: RGHR CON FINE FREQUENCY OF VARIOUS OBSERVATIONS Table A1.36

Chalcopyrite	Sample%	Cp Observations%
Free Occurrences	1.20	2.2
High Grade (85-100)	8.62	15.9
Med. Grade (15-85)	19.56	36.0
Low Grade (00-15)	24.94	45.9

Iron Minerals	Sample%	Px Observations%		Binary Px %
Free Occurrences	10.29	17.9	With High Cp (85-100)	4.38
High Grade (85-100)	15.52	27.1	With Med. Cp (15-85)	24.18
Med. Grade (15-85)	20.23	35.3	With Low Cp (00-15)	49.26
Low Grade (00-15)	11.32	19.7	With No Cp	22.18

Galena + Arsenides	Sample%	Gn Observations%		Binary Gn %
Free Occurrences	25.30	54.7	With High Cp (85-100)	4.43
High Grade (85-100)	1.84	4.0	With Med. Cp (15-85)	4.66
Med. Grade (15-85)	10.46	22.6	With Low Cp (00-15)	6.29
Low Grade (00-15)	8.64	18.7	With No Cp	84.62

Sphalerite	Sample%	Sp Observations%		Binary Sp %
Free Occurrences	2.66	7.0	With High Cp (85-100)	27.02
High Grade (85-100)	5.01	13.3	With Med. Cp (15-85)	16.15
Med. Grade (15-85)	14.74	39.0	With Low Cp (00-15)	18.63
Low Grade (00-15)	15.36	40.7	With No Cp	38.20

Sample: CLNR TLS COARSE FREQUENCY OF VARIOUS OBSERVATIONS Table A1.37

Chalcopyrite	Sample%	Cp Observations%
Free Occurrences	5.77	23.2
High Grade (85-100)	1.32	5.3
Med. Grade (15-85)	7.22	29.0
Low Grade (00-15)	10.58	42.5

Iron Minerals	Sample%	Px Observations%		Binary Px %
Free Occurrences	16.95	38.5	With High Cp (85-100)	2.77
High Grade (85-100)	12.30	28.0	With Med. Cp (15-85)	19.98
Med. Grade (15-85)	11.88	27.0	With Low Cp (00-15)	34.34
Low Grade (00-15)	2.87	6.5	With No Cp	42.91

Galena + Arsenides	Sample%	Gn Observations%		Binary Gn %
Free Occurrences	37.88	68.8	With High Cp (85-100)	3.48
High Grade (85-100)	2.33	4.2	With Med. Cp (15-85)	3.80
Med. Grade (15-85)	8.23	14.9	With Low Cp (00-15)	0.76
Low Grade (00-15)	6.64	12.1	With No Cp	91.95

Sphalerite	Sample%	Sp Observations%		Binary Sp %
Free Occurrences	4.23	23.5	With High Cp (85-100)	2.68
High Grade (85-100)	1.98	11.0	With Med. Cp (15-85)	8.02
Med. Grade (15-85)	7.28	40.5	With Low Cp (00-15)	4.11
Low Grade (00-15)	4.50	25.0	With No Cp	85.18

Sample: CLNR TLS MEDIUM FREQUENCY OF VARIOUS OBSERVATIONS Table A1.38

Chalcopyrite	Sample%	Cp Observations%
Free Occurrences	7.33	32.1
High Grade (85-100)	1.60	7.0
Med. Grade (15-85)	8.46	37.1
Low Grade (00-15)	5.43	23.8

Iron Minerals	Sample%	Px Observations%		Binary Px %
Free Occurrences	19.67	48.4	With High Cp (85-100)	3.14
High Grade (85-100)	7.39	18.2	With Med. Cp (15-85)	28.21
Med. Grade (15-85)	11.37	28.0	With Low Cp (00-15)	22.68
Low Grade (00-15)	2.24	5.5	With No Cp	45.97

Galena + Arsenides	Sample%	Gn Observations%		Binary Gn %
Free Occurrences	39.95	78.5	With High Cp (85-100)	4.09
High Grade (85-100)	1.14	2.2	With Med. Cp (15-85)	2.66
Med. Grade (15-85)	5.54	10.9	With Low Cp (00-15)	1.33
Low Grade (00-15)	4.28	8.4	With No Cp	91.93

Sphalerite	Sample%	Sp Observations%		Binary Sp %
Free Occurrences	5.34	29.1	With High Cp (85-100)	5.82
High Grade (85-100)	1.79	9.7	With Med. Cp (15-85)	11.14
Med. Grade (15-85)	6.40	34.8	With Low Cp (00-15)	2.77
Low Grade (00-15)	4.86	26.4	With No Cp	80.27

Sample: CLNR TLS FINE FREQUENCY OF VARIOUS OBSERVATIONS Table A1.39

Chalcopyrite	Sample%	Cp Observations%
Free Occurrences	9.34	26.5
High Grade (85-100)	4.40	12.5
Med. Grade (15-85)	10.82	30.7
Low Grade (00-15)	10.72	30.4

Iron Minerals	Sample%	Px Observations%		Binary Px %
Free Occurrences	23.80	45.3	With High Cp (85-100)	12.79
High Grade (85-100)	8.92	17.0	With Med. Cp (15-85)	24.92
Med. Grade (15-85)	12.60	24.0	With Low Cp (00-15)	14.13
Low Grade (00-15)	7.21	13.7	With No Cp	48.16

Galena + Arsenides	Sample%	Gn Observations%		Binary Gn %
Free Occurrences	25.89	59.6	With High Cp (85-100)	5.20
High Grade (85-100)	1.54	3.6	With Med. Cp (15-85)	4.62
Med. Grade (15-85)	7.19	16.5	With Low Cp (00-15)	3.47
Low Grade (00-15)	8.83	20.3	With No Cp	86.71

Sphalerite	Sample%	Sp Observations%		Binary Sp %
Free Occurrences	2.96	16.8	With High Cp (85-100)	3.34
High Grade (85-100)	4.78	27.2	With Med. Cp (15-85)	18.06
Med. Grade (15-85)	6.68	38.0	With Low Cp (00-15)	18.06
Low Grade (00-15)	3.15	17.3	With No Cp	60.54

Sample: CLNR CON COARSE FREQUENCY OF VARIOUS OBSERVATIONS Table A1.40

Chalcopyrite	Sample%	Cp Observations%
Free Occurrences	42.69	50.5
High Grade (85-100)	12.34	14.6
Med. Grade (15-85)	22.39	26.5
Low Grade (00-15)	7.14	8.4

Iron Minerals	Sample%	Px Observations%		Binary Px %
Free Occurrences	6.93	15.9	With High Cp (85-100)	26.58
High Grade (85-100)	6.17	14.2	With Med. Cp (15-85)	45.30
Med. Grade (15-85)	19.36	44.5	With Low Cp (00-15)	19.94
Low Grade (00-15)	11.10	25.5	With No Cp	8.18

Galena + Arsenides	Sample%	Gn Observations%		Binary Gn %
Free Occurrences	3.72	34.2	With High Cp (85-100)	18.75
High Grade (85-100)	0.39	3.6	With Med. Cp (15-85)	26.63
Med. Grade (15-85)	3.21	29.5	With Low Cp (00-15)	7.68
Low Grade (00-15)	3.55	32.7	With No Cp	46.94

Sphalerite	Sample%	Sp Observations%		Binary Sp %
Free Occurrences	1.34	7.5	With High Cp (85-100)	28.77
High Grade (85-100)	0.99	5.5	With Med. Cp (15-85)	42.34
Med. Grade (15-85)	7.47	41.7	With Low Cp (00-15)	5.46
Low Grade (00-15)	8.14	45.4	With No Cp	23.42

Sample: CLNR CON MEDIUM FREQUENCY OF VARIOUS OBSERVATIONS Table A1.41

Chalcopyrite	Sample%	Cp Observations%
Free Occurrences	58.13	66.4
High Grade (85-100)	8.11	9.3
Med. Grade (15-85)	16.08	18.4
Low Grade (00-15)	5.25	6.0

Iron Minerals	Sample%	Px Observations%		Binary Px %
Free Occurrences	8.38	24.7	With High Cp (85-100)	23.01
High Grade (85-100)	4.90	14.4	With Med. Cp (15-85)	49.78
Med. Grade (15-85)	14.49	42.7	With Low Cp (00-15)	18.92
Low Grade (00-15)	6.18	18.2	With No Cp	8.30

Galena + Arsenides	Sample%	Gn Observations%		Binary Gn %
Free Occurrences	0.53	11.2	With High Cp (85-100)	30.04
High Grade (85-100)	0.30	6.3	With Med. Cp (15-85)	21.19
Med. Grade (15-85)	1.66	35.3	With Low Cp (00-15)	2.98
Low Grade (00-15)	2.23	47.2	With No Cp	45.78

Sphalerite	Sample%	Sp Observations%		Binary Sp %
Free Occurrences	1.49	16.2	With High Cp (85-100)	31.25
High Grade (85-100)	0.46	5.0	With Med. Cp (15-85)	37.67
Med. Grade (15-85)	3.28	35.8	With Low Cp (00-15)	4.40
Low Grade (00-15)	3.94	43.0	With No Cp	26.68

Sample: CLNR CON FINE FREQUENCY OF VARIOUS OBSERVATIONS Table A1.42

Chalcopyrite	Sample%	Cp Observations%
Free Occurrences	58.83	70.0
High Grade (85-100)	10.29	12.2
Med. Grade (15-85)	10.58	12.6
Low Grade (00-15)	4.40	5.2

Iron Minerals	Sample%	Px Observations%		Binary Px %
Free Occurrences	6.84	25.9	With High Cp (85-100)	33.84
High Grade (85-100)	3.34	12.7	With Med. Cp (15-85)	39.37
Med. Grade (15-85)	8.30	31.4	With Low Cp (00-15)	18.10
Low Grade (00-15)	7.91	30.0	With No Cp	8.69

Galena + Arsenides	Sample%	Gn Observations%		Binary Gn %
Free Occurrences	5.98	58.8	With High Cp (85-100)	29.24
High Grade (85-100)	0.44	4.3	With Med. Cp (15-85)	17.94
Med. Grade (15-85)	1.36	13.3	With Low Cp (00-15)	5.32
Low Grade (00-15)	2.39	23.5	With No Cp	47.51

Sphalerite	Sample%	Sp Observations%		Binary Sp %
Free Occurrences	1.39	14.9	With High Cp (85-100)	35.67
High Grade (85-100)	1.31	14.1	With Med. Cp (15-85)	30.53
Med. Grade (15-85)	3.06	33.0	With Low Cp (00-15)	17.45
Low Grade (00-15)	3.53	38.0	With No Cp	16.36

Sample: RC074 COARSE AREA % DISTRIBUTION OF TOTAL MINERAL AS PARTICLES OF A GIVEN GRADE AND TYPE Table A1.43

		Particle Grade (% of First Mentioned Phase - eg. Cp in Cp/Px Binaries)											
Type	Total	0.0250	0.1000	0.2000	0.3000	0.4000	0.5000	0.6000	0.7000	0.8000	0.9000	0.9750	1.0000
Cp/Px	11.67	0.00	0.26	0.94	0.51	0.68	0.20	1.69	1.74	3.35	2.30	0.00	
Cp/Gn	7.58	0.07	0.29	0.09	0.10	0.31	0.43	0.00	1.47	1.73	2.00	1.09	
Cp/Sp	4.71	0.02	0.10	0.09	0.16	0.39	0.79	0.43	1.19	0.68	0.41	0.45	
Cp/TQ	15.90	0.26	1.62	1.55	1.16	1.00	2.26	0.59	1.10	0.58	3.42	2.36	
Cp/All	100.00	0.35	2.27	2.67	1.93	2.38	3.67	2.71	5.50	6.34	8.14	3.90	60.14
Px/Cp	0.76	0.00	0.02	0.06	0.05	0.08	0.01	0.07	0.08	0.25	0.15	0.00	
Px/Gn	34.69	0.00	0.02	0.16	0.39	0.51	0.97	1.53	2.70	4.97	13.26	10.19	
Px/Sp	3.89	0.02	0.08	0.02	0.06	0.07	0.19	0.10	0.27	0.46	1.44	1.18	
Px/TQ	30.55	0.10	0.57	0.70	1.13	1.40	2.36	3.57	3.67	5.88	8.81	2.36	
Px/All	100.00	0.12	0.68	0.94	1.62	2.05	3.53	5.27	6.71	11.56	23.67	13.73	30.12
Gn/Cp	0.75	0.00	0.02	0.04	0.06	0.00	0.04	0.04	0.02	0.03	0.25	0.24	
Gn/Px	12.05	0.37	2.07	1.74	1.62	1.44	1.36	1.07	1.28	0.89	0.20	0.02	
Gn/Sp	10.63	0.19	1.04	0.92	1.10	0.89	0.88	1.29	1.13	1.50	1.31	0.38	
Gn/TQ	20.91	0.65	3.79	3.24	2.72	2.24	2.02	1.88	1.39	1.20	1.13	0.66	
Gn/All	100.00	1.22	6.92	5.94	5.50	4.56	4.30	4.29	3.82	3.63	2.88	1.30	55.65
Sp/Cp	0.38	0.00	0.00	0.01	0.04	0.02	0.06	0.05	0.03	0.03	0.07	0.06	
Sp/Px	2.90	0.04	0.19	0.14	0.14	0.08	0.22	0.12	0.16	0.11	0.83	0.88	
Sp/Gn	22.95	0.01	0.12	0.32	0.41	0.73	0.74	1.12	2.16	3.11	7.92	6.30	
Sp/TQ	43.87	0.29	1.42	1.25	2.30	2.18	3.00	3.08	4.02	6.17	11.93	8.21	
Sp/All	100.00	0.34	1.74	1.72	2.89	3.00	4.03	4.38	6.37	9.42	20.76	15.45	29.91

Sample. RC074 MEDIUM AREA % DISTRIBUTION OF TOTAL MINERAL AS PARTICLES OF A GIVEN GRADE AND TYPE Table A1.44

		Particle Grade (% of First Mentioned Phase - eg. Cp in Cp/Px Binaries)											
Type	Total	0.0250	0.1000	0.2000	0.3000	0.4000	0.5000	0.6000	0.7000	0.8000	0.9000	0.9750	1.0000
Cp/Px	12.15	0.05	0.46	0.63	0.25	0.42	0.63	0.75	0.88	1.50	3.75	2.85	
Cp/Gn	7.07	0.08	0.31	0.08	0.19	0.25	0.10	0.13	0.15	0.83	2.82	2.13	
Cp/Sp	4.05	0.14	0.85	0.67	0.25	0.17	0.00	0.13	0.00	0.50	0.94	0.41	
Cp/TQ	24.07	0.78	4.48	3.42	2.13	2.09	1.67	2.25	2.04	3.34	1.88	0.00	
Cp/All	100.00	1.05	6.11	4.80	2.82	2.92	2.40	3.25	3.07	6.17	9.38	5.39	52.65
Px/Cp	1.90	0.01	0.07	0.06	0.06	0.08	0.10	0.10	0.09	0.39	0.65	0.29	
Px/Gn	24.89	0.01	0.09	0.16	0.18	0.37	0.53	1.26	2.18	3.13	9.25	7.73	
Px/Sp	1.73	0.02	0.07	0.02	0.03	0.07	0.02	0.00	0.05	0.18	0.71	0.58	
Px/TQ	28.26	0.06	0.40	0.66	1.09	1.17	1.72	2.03	2.37	4.31	8.66	5.78	
Px/All	100.00	0.10	0.62	0.89	1.36	1.68	2.36	3.39	4.69	8.01	19.27	14.38	43.23
Gn/Cp	1.55	0.01	0.06	0.04	0.01	0.02	0.02	0.08	0.09	0.07	0.56	0.59	
Gn/Px	9.11	0.25	1.31	1.00	1.19	1.07	0.67	0.70	0.53	0.80	1.05	0.53	
Gn/Sp	5.68	0.17	0.74	0.31	0.56	0.40	0.56	0.70	0.41	0.90	0.83	0.08	
Gn/TQ	16.88	0.47	2.46	2.03	2.51	1.54	1.67	1.68	0.97	1.57	1.54	0.43	
Gn/All	100.00	0.90	4.58	3.38	4.28	3.03	2.93	3.16	1.99	3.35	3.99	1.63	66.79
Sp/Cp	4.84	0.00	0.03	0.04	0.00	0.02	0.00	0.07	0.17	0.76	2.19	1.56	
Sp/Px	2.90	0.03	0.14	0.08	0.04	0.00	0.03	0.18	0.12	0.14	1.07	1.07	
Sp/Gn	25.50	0.00	0.13	0.32	0.25	0.66	0.80	0.85	1.87	1.76	9.45	9.40	
Sp/TQ	49.76	0.32	1.51	1.12	2.05	2.71	2.17	3.70	4.19	7.45	14.74	9.81	
Sp/All	100.00	0.36	1.82	1.55	2.33	3.39	3.00	4.81	6.35	10.11	27.45	21.84	17.00

Sample: RC074 FINE AREA % DISTRIBUTION OF TOTAL MINERAL AS PARTICLES OF A GIVEN GRADE AND TYPE Table A1.45

		Particle Grade (% of First Mentioned Phase - eg. Cp in Cp/Px Binaries)											
Type	Total	0.0250	0.1000	0.2000	0.3000	0.4000	0.5000	0.6000	0.7000	0.8000	0.9000	0.9750	1.0000
Cp/Px	10.14	0.35	1.62	0.63	0.45	0.42	0.38	0.27	0.32	0.72	2.71	2.27	
Cp/Gn	0.64	0.02	0.06	0.00	0.00	0.00	0.00	0.00	0.00	0.00	0.27	0.29	
Cp/Sp	4.07	0.14	0.65	0.24	0.27	0.12	0.08	0.09	0.00	0.24	1.22	1.03	
Cp/TQ	60.72	2.41	12.49	7.22	4.42	3.43	3.46	3.97	2.74	3.49	9.34	7.77	
Cp/All	100.00	2.91	14.82	8.09	5.14	3.97	3.91	4.33	3.05	4.45	13.53	11.36	24.43
Px/Cp	6.91	0.01	0.06	0.04	0.03	0.04	0.08	0.13	0.22	0.52	3.01	2.78	
Px/Gn	8.01	0.01	0.05	0.05	0.13	0.25	0.29	0.32	0.76	0.82	2.79	2.55	
Px/Sp	0.31	0.00	0.01	0.01	0.00	0.00	0.00	0.00	0.00	0.02	0.14	0.12	
Px/TQ	35.89	0.17	0.96	0.87	0.86	1.24	1.50	1.93	2.71	4.16	11.84	9.64	
Px/All	100.00	0.19	1.09	0.97	1.02	1.52	1.87	2.38	3.68	5.52	17.78	15.09	48.88
Gn/Cp	0.38	0.00	0.01	0.00	0.00	0.00	0.00	0.00	0.00	0.00	0.18	0.19	
Gn/Px	5.13	0.10	0.49	0.32	0.51	0.33	0.47	0.59	0.48	0.31	0.75	0.76	
Gn/Sp	2.01	0.02	0.08	0.08	0.13	0.16	0.15	0.18	0.21	0.24	0.44	0.33	
Gn/TQ	19.92	0.42	2.37	2.09	2.03	2.45	2.01	1.76	1.78	1.69	1.98	1.34	
Gn/All	100.00	0.54	2.95	2.49	2.68	2.94	2.62	2.53	2.47	2.23	3.35	2.63	72.57
Sp/Cp	8.29	0.02	0.08	0.04	0.00	0.04	0.05	0.11	0.39	0.59	3.57	3.42	
Sp/Px	0.75	0.01	0.05	0.02	0.00	0.00	0.00	0.00	0.00	0.07	0.33	0.27	
Sp/Gn	5.12	0.02	0.09	0.11	0.17	0.22	0.28	0.44	0.58	0.59	1.41	1.21	
Sp/TQ	75.19	0.57	2.78	1.77	2.35	2.69	4.06	5.42	7.23	13.64	22.90	11.77	
Sp/All	100.00	0.61	3.01	1.94	2.52	2.95	4.38	5.97	8.20	14.90	28.21	16.67	10.65

Sample: RC076 COARSE AREA % DISTRIBUTION OF TOTAL MINERAL AS PARTICLES OF A GIVEN GRADE AND TYPE Table A1.46

		Particle Grade (% of First Mentioned Phase - eg. Cp in Cp/Px Binaries)											
Type	Total	0.0250	0.1000	0.2000	0.3000	0.4000	0.5000	0.6000	0.7000	0.8000	0.9000	0.9750	1.0000
Cp/Px	17.83	0.05	0.95	1.79	0.99	1.77	1.02	1.31	3.27	2.36	2.36	1.96	
Cp/Gn	12.84	0.00	0.04	0.23	0.17	0.54	0.69	0.51	0.86	0.84	4.94	4.04	
Cp/Sp	4.51	0.06	0.31	0.27	0.40	0.36	0.25	1.28	0.55	0.33	0.34	0.36	
Cp/TQ	14.95	0.04	0.74	1.39	0.69	1.81	1.82	1.47	1.88	1.82	3.28	0.00	
Cp/All	100.00	0.15	2.04	3.69	2.25	4.48	3.78	4.57	6.55	5.34	10.92	6.36	49.87
Px/Cp	3.87	0.01	0.04	0.08	0.20	0.13	0.15	0.38	0.33	1.03	1.22	0.30	
Px/Gn	31.90	0.01	0.14	0.23	0.47	0.54	0.94	1.55	3.08	5.03	11.47	8.44	
Px/Sp	7.49	0.01	0.09	0.10	0.10	0.24	0.32	0.37	0.68	1.05	2.57	1.97	
Px/TQ	26.93	0.10	0.59	0.81	1.36	1.38	2.33	2.77	3.81	3.99	7.43	2.36	
Px/All	100.00	0.14	0.85	1.23	2.13	2.30	3.73	5.06	7.90	11.10	22.69	13.07	29.81
Gn/Cp	0.79	0.02	0.09	0.03	0.06	0.06	0.11	0.13	0.06	0.15	0.07	0.00	
Gn/Px	12.25	0.25	1.47	1.45	1.52	1.19	1.08	0.94	1.26	1.06	1.41	0.64	
Gn/Sp	18.06	0.32	1.97	2.02	1.81	1.69	1.53	1.96	1.75	1.95	2.03	1.04	
Gn/TQ	10.90	0.31	1.96	1.88	1.29	1.69	1.34	1.03	0.71	0.41	0.20	0.08	
Gn/All	100.00	0.89	5.49	5.38	4.68	4.63	4.06	4.06	3.78	3.57	3.70	1.76	58.00
Sp/Cp	1.49	0.00	0.01	0.01	0.04	0.14	0.04	0.09	0.15	0.18	0.45	0.38	
Sp/Px	4.26	0.06	0.32	0.30	0.33	0.27	0.36	0.41	0.27	0.44	0.89	0.62	
Sp/Gn	48.05	0.03	0.22	0.48	0.73	1.28	1.49	2.47	4.12	7.87	17.33	12.05	
Sp/TQ	20.60	0.20	1.04	1.13	1.86	2.39	1.93	1.83	2.70	3.09	3.03	1.40	
Sp/All	100.00	0.28	1.58	1.91	2.96	4.08	3.82	4.80	7.24	11.57	21.71	14.45	25.60

Sample: RC076 MEDIUM AREA % DISTRIBUTION OF TOTAL MINERAL AS PARTICLES OF A GIVEN GRADE AND TYPE Table A1.47

		Particle Grade (% of First Mentioned Phase - eg. Cp in Cp/Px Binaries)											
Type	Total	0.0250	0.1000	0.2000	0.3000	0.4000	0.5000	0.6000	0.7000	0.8000	0.9000	0.9750	1.0000
Cp/Px	22.30	0.33	1.82	1.49	1.51	1.49	1.21	1.28	1.70	1.75	5.12	4.59	
Cp/Gn	6.44	0.02	0.08	0.08	0.16	0.47	0.03	0.50	0.04	0.85	2.50	1.70	
Cp/Sp	6.22	0.22	0.98	0.34	0.34	0.36	0.47	0.50	0.33	0.43	1.23	1.04	
Cp/TQ	12.99	0.44	2.14	1.23	1.49	1.16	1.75	1.95	0.87	0.43	1.17	0.35	
Cp/All	100.00	1.01	5.02	3.15	3.50	3.48	3.46	4.23	2.94	3.46	10.02	7.68	52.05
Px/Cp	8.90	0.02	0.11	0.09	0.14	0.17	0.24	0.44	0.70	1.18	3.24	2.56	
Px/Gn	24.78	0.02	0.11	0.17	0.24	0.44	0.66	0.99	1.84	3.20	9.47	7.64	
Px/Sp	4.54	0.00	0.02	0.06	0.08	0.09	0.10	0.33	0.35	0.64	1.63	1.24	
Px/TQ	10.71	0.05	0.26	0.29	0.55	0.76	1.09	0.86	1.88	1.82	2.46	0.67	
Px/All	100.00	0.09	0.51	0.61	1.02	1.47	2.09	2.63	4.78	6.83	16.81	12.11	51.07
Gn/Cp	0.75	0.01	0.06	0.04	0.00	0.07	0.01	0.15	0.08	0.07	0.14	0.13	
Gn/Px	8.07	0.21	1.11	0.84	0.83	0.69	0.70	0.70	0.59	0.73	1.03	0.64	
Gn/Sp	5.78	0.09	0.51	0.51	0.58	0.77	0.54	0.47	0.52	0.64	0.76	0.41	
Gn/TQ	6.06	0.10	0.67	0.80	0.69	0.56	0.82	0.61	0.60	0.37	0.60	0.24	
Gn/All	100.00	0.40	2.34	2.19	2.10	2.09	2.06	1.93	1.79	1.81	2.54	1.42	79.33
Sp/Cp	8.19	0.01	0.05	0.04	0.06	0.13	0.18	0.21	0.31	0.53	3.41	3.26	
Sp/Px	3.30	0.06	0.36	0.31	0.30	0.43	0.20	0.28	0.35	0.44	0.41	0.16	
Sp/Gn	25.81	0.02	0.16	0.30	0.41	0.59	1.00	2.15	2.51	3.79	8.52	6.36	
Sp/TQ	24.40	0.11	0.83	1.11	1.04	1.58	1.87	2.40	1.80	4.01	7.96	1.68	
Sp/All	100.00	0.20	1.40	1.76	1.81	2.73	3.25	5.03	4.97	8.77	20.31	11.46	38.30

Sample: RC076 FINE AREA % DISTRIBUTION OF TOTAL MINERAL AS PARTICLES OF A GIVEN GRADE AND TYPE Table A1.48

		Particle Grade (% of First Mentioned Phase - eg. Cp in Cp/Px Binaries)											
Type	Total	0.0250	0.1000	0.2000	0.3000	0.4000	0.5000	0.6000	0.7000	0.8000	0.9000	0.9750	1.0000
Cp/Px	10.38	0.55	2.50	0.73	0.35	0.47	0.20	0.31	0.36	1.04	2.34	1.52	
Cp/Gn	0.82	0.01	0.05	0.03	0.00	0.00	0.00	0.00	0.00	0.00	0.35	0.38	
Cp/Sp	5.99	0.17	0.85	0.42	0.23	0.16	0.13	0.00	0.09	0.10	1.88	1.97	
Cp/TQ	73.50	1.75	9.57	7.50	7.03	4.53	3.39	3.05	2.73	5.31	15.94	12.70	
Cp/All	100.00	2.48	12.97	8.67	7.62	5.16	3.71	3.36	3.19	6.46	20.51	16.57	9.31
Px/Cp	15.01	0.01	0.08	0.08	0.05	0.05	0.06	0.21	0.25	0.89	6.83	6.49	
Px/Gn	0.37	0.00	0.01	0.01	0.02	0.02	0.02	0.02	0.08	0.09	0.07	0.02	
Px/Sp	0.40	0.00	0.02	0.01	0.00	0.00	0.00	0.00	0.00	0.00	0.18	0.19	
Px/TQ	41.78	0.24	1.27	0.99	1.17	1.11	1.52	2.39	3.57	6.20	14.65	8.67	
Px/All	100.00	0.26	1.38	1.08	1.24	1.19	1.60	2.63	3.90	7.18	21.73	15.37	42.44
Gn/Cp	0.44	0.00	0.02	0.00	0.00	0.00	0.00	0.00	0.00	0.05	0.21	0.17	
Gn/Px	0.64	0.00	0.01	0.03	0.05	0.02	0.03	0.03	0.08	0.05	0.16	0.17	
Gn/Sp	1.11	0.00	0.01	0.01	0.02	0.02	0.06	0.03	0.12	0.05	0.36	0.42	
Gn/TQ	21.01	0.39	2.18	1.90	1.97	1.89	1.64	2.14	1.69	2.07	3.11	2.02	
Gn/All	100.00	0.40	2.22	1.95	2.04	1.94	1.73	2.21	1.89	2.21	3.84	2.78	76.80
Sp/Cp	12.22	0.04	0.15	0.02	0.03	0.00	0.09	0.17	0.39	1.19	5.44	4.71	
Sp/Px	0.91	0.01	0.05	0.00	0.00	0.00	0.00	0.00	0.00	0.07	0.42	0.36	
Sp/Gn	0.81	0.02	0.07	0.02	0.08	0.04	0.09	0.06	0.07	0.07	0.17	0.14	
Sp/TQ	78.85	0.64	4.03	4.40	4.35	4.39	3.53	4.24	6.11	12.56	21.91	12.68	
Sp/All	100.00	0.70	4.29	4.44	4.46	4.42	3.72	4.46	6.57	13.90	27.93	17.89	7.20

Sample: RGHR TLS COARSE AREA % DISTRIBUTION OF TOTAL MINERAL AS PARTICLES OF A GIVEN GRADE AND TYPE Table A1 49

		Particle Grade (% of First Mentioned Phase - eg. Cp in Cp/Px Binaries)											
Type	Total	0.0250	0.1000	0.2000	0.3000	0.4000	0.5000	0.6000	0.7000	0.8000	0.9000	0.9750	1.0000
Cp/Px	1.50	0.09	0.37	0.13	0.25	0.23	0.08	0.07	0.05	0.06	0.10	0.07	
Cp/Gn	1.71	0.00	0.01	0.14	0.05	0.20	0.02	0.21	0.08	0 18	0.48	0.35	
Cp/Sp	55.41	0.04	0.52	0.83	0.41	1.04	1.95	3.11	1.98	5.19	21.74	18.61	
Cp/TQ	10.63	0.37	2.27	1.93	1.11	1.33	0.69	1.24	0.51	0.24	0.79	0.15	
Cp/All	100.00	0.50	3.16	3.03	1.82	2.79	2.73	4.63	2.62	5 68	23.12	19.18	30 74
Px/Cp	0.83	0.00	0.00	0.00	0.00	0.00	0.01	0.03	0.06	0.05	0.33	0.34	
Px/Gn	20.57	0.01	0.12	0.26	0.25	0.53	0.76	1.06	1.41	3.42	7.66	5.11	
Px/Sp	0.03	0.00	0.00	0.00	0.00	0.00	0.00	0.00	0.00	0.02	0.00	0 00	
Px/TQ	61.40	0.10	0.86	1.52	2.00	2.43	3.71	5.01	7.17	11.36	18.85	8.29	
Px/All	100.00	0.10	0.98	1.88	2.25	2.97	4.48	6.10	8.64	14.86	26.84	13.74	17.16
Gn/Cp	0.15	0.00	0.01	0.01	0.00	0 02	0.00	0.03	0.01	0.06	0.01	0.00	
Gn/Px	8.61	0.15	0.96	0.97	0.68	0.79	0.86	0.89	0.65	1.16	1.17	0.31	
Gn/Sp	14.83	0.20	1.33	1.54	1.38	1.47	1.42	1.09	1.34	1.92	2.18	0.96	
Gn/TQ	30.33	0.62	4.35	5.03	3.89	3.74	3.04	2.82	2.97	1.94	1.55	0.39	
Gn/All	100.00	0.97	6.64	7.54	5.96	6.02	5.33	4.83	4.98	5.09	4.91	1.06	46 08
Sp/Cp	2.23	0.05	0.25	0.14	0.09	0.22	0.21	0.16	0.10	0.35	0.49	0.17	
Sp/Px	0.03	0.00	0.00	0.01	0.00	0.00	0.00	0.00	0.01	0.01	0.00	0.00	
Sp/Gn	32.07	0.02	0.22	0.44	0.53	0.67	1.32	2.03	2.98	5.70	11.04	7.10	
Sp/TQ	46.07	0.39	2.32	2.29	2.33	2.30	3.20	4.22	4.87	6.40	12.02	5.73	
Sp/All	100.00	0.46	2.80	2.88	2.35	3.19	4.72	6.42	7.96	12.46	23.55	13 00	19 60

Sample RGHR TLS MEDIUM AREA % DISTRIBUTION OF TOTAL MINERAL AS PARTICLES OF A GIVEN GRADE AND TYPE Table A1.50

Particle Grade (% of First Mentioned Phase - eg. Cp in Cp/Px Binaries)

Type	Total	0.0250	0.1000	0.2000	0.3000	0.4000	0.5000	0.6000	0.7000	0.8000	0.9000	0.9750	1.0000
Cp/Px	12.09	0.46	2.41	1.32	0.54	1.69	0.30	0.36	1.69	0.48	1.08	1.76	
Cp/Gn	22.35	0.12	0.90	0.12	0.36	0.48	0.60	0.72	2.53	4.82	7.59	4.11	
Cp/Sp	14.17	0.94	4.76	2.29	0.90	0.72	0.60	2.53	0.84	0.00	0.00	0.59	
Cp/TQ	24.90	2.57	11.86	3.73	1.63	0.72	1.20	1.81	0.42	0.96	0.00	0.00	
Cp/All	100.00	4.09	19.93	7.46	3.43	3.61	2.71	5.42	5.48	6.26	8.67	6.46	26.49
Px/Cp	2.61	0.00	0.01	0.01	0.04	0.01	0.02	0.13	0.07	0.28	1.13	0.93	
Px/Gn	20.81	0.01	0.08	0.13	0.18	0.28	0.45	0.83	1.12	2.90	8.45	6.39	
Px/Sp	2.55	0.01	0.05	0.03	0.07	0.03	0.08	0.13	0.24	0.58	0.90	0.44	
Px/TQ	10.10	0.03	0.13	0.13	0.38	0.40	0.44	0.88	1.07	2.08	3.04	1.51	
Px/All	100.00	0.06	0.28	0.29	0.67	0.71	0.99	1.97	2.50	5.83	13.51	9.27	63.93
Gn/Cp	1.66	0.01	0.07	0.10	0.09	0.04	0.05	0.06	0.07	0.04	0.70	0.41	
Gn/Px	9.64	0.27	1.56	1.21	0.80	0.92	0.75	0.69	0.69	0.83	1.26	0.66	
Gn/Sp	5.42	0.07	0.47	0.50	0.33	0.44	0.36	0.87	0.40	0.71	0.89	0.38	
Gn/TQ	7.62	0.29	1.53	0.98	0.70	0.81	0.99	0.47	0.55	0.83	0.47	0.00	
Gn/All	100.00	0.64	3.64	2.79	1.92	2.21	2.16	2.09	1.71	2.41	3.32	1.45	75.66
Sp/Cp	10.76	0.00	0.00	0.00	0.04	0.19	0.07	0.12	0.24	1.04	4.87	4.18	
Sp/Px	3.62	0.02	0.22	0.32	0.23	0.19	0.17	0.08	0.34	0.27	1.05	0.74	
Sp/Gn	15.41	0.01	0.13	0.23	0.23	0.77	0.48	0.86	1.01	2.63	5.55	3.51	
Sp/TQ	37.51	0.12	0.74	0.77	0.78	0.99	2.09	2.10	2.69	4.39	12.83	10.02	
Sp/All	100.00	0.16	1.09	1.32	1.27	2.14	2.81	3.17	4.27	8.33	24.30	18.44	32.69

Sample: RGHR TLS FINE AREA % DISTRIBUTION OF TOTAL MINERAL AS PARTICLES OF A GIVEN GRADE AND TYPE Table A1 51

		Particle Grade (% of First Mentioned Phase - eg. Cp in Cp/Px Binaries)											
Type	Total	0.0250	0.1000	0.2000	0.3000	0.4000	0.5000	0.6000	0.7000	0.8000	0.9000	0.9750	1.0000
Cp/Px	13.17	0.73	3.51	1.49	0.96	0.85	1.59	0.64	0.74	1.70	0.96	0.00	
Cp/Gn	21.76	0.07	0.32	0.21	0.32	0.85	0.53	0.64	0.74	1.70	8.61	7.77	
Cp/Sp	13.67	0.97	4.57	1.70	0.96	0.85	0.00	0.64	0.00	0.00	1.91	2.07	
Cp/TQ	25.36	2.30	10.73	3.61	1.59	1.28	0.53	1.91	0.74	1.70	0.96	0.00	
Cp/All	100.00	4.07	19.13	7.01	3.83	3.83	2.66	3.83	2.23	5.10	12.44	9.84	26.04
Px/Cp	2.15	0.00	0.00	0.01	0.01	0.01	0.05	0.04	0.07	0.18	0.94	0.85	
Px/Gn	14.36	0.01	0.07	0.12	0.16	0.27	0.47	0.65	1.06	2.00	5.52	4.04	
Px/Sp	7.01	0.02	0.09	0.04	0.09	0.11	0.16	0.25	0.42	0.73	2.73	2.36	
Px/TQ	9.87	0.04	0.20	0.14	0.23	0.38	0.41	0.63	1.08	1.85	3.90	1.02	
Px/All	100.00	0.07	0.36	0.31	0.49	0.77	1.09	1.56	2.63	4.76	13.09	8.26	66.60
Gn/Cp	0.51	0.01	0.04	0.02	0.01	0.02	0.02	0.06	0.03	0.04	0.13	0.12	
Gn/Px	7.26	0.16	0.94	0.76	0.70	0.66	0.72	0.61	0.57	0.73	0.91	0.49	
Gn/Sp	4.80	0.10	0.59	0.56	0.45	0.41	0.39	0.41	0.34	0.54	0.70	0.33	
Gn/TQ	5.25	0.15	0.85	0.74	0.85	0.48	0.51	0.70	0.37	0.23	0.22	0.14	
Gn/All	100.00	0.42	2.41	2.09	2.01	1.56	1.64	1.77	1.32	1.55	1.96	1.08	82.19
Sp/Cp	6.51	0.00	0.02	0.00	0.00	0.03	0.00	0.09	0.16	0.49	2.98	2.74	
Sp/Px	7.98	0.15	0.74	0.45	0.44	0.40	0.38	0.42	0.54	0.37	2.01	2.10	
Sp/Gn	22.24	0.01	0.12	0.22	0.23	0.43	0.62	0.97	1.67	3.57	8.44	5.96	
Sp/TQ	20.37	0.14	0.74	0.63	0.74	0.98	1.11	1.38	2.21	3.20	6.16	3.07	
Sp/All	100.00	0.30	1.61	1.29	1.41	1.85	2.11	2.86	4.58	7.63	19.58	13.87	42.91

Sample RGHR CON COARSE AREA % DISTRIBUTION OF TOTAL MINERAL AS PARTICLES OF A GIVEN GRADE AND TYPE Table A1.52

Particle Grade (% of First Mentioned Phase - eg. Cp in Cp/Px Binaries)

Type	Total	0.0250	0.1000	0.2000	0.3000	0.4000	0.5000	0.6000	0.7000	0.8000	0.9000	0.9750	1.0000
Cp/Px	22.44	0.22	1.59	2.10	2.09	2.08	1.75	1.52	1.95	1.55	3.90	3.69	
Cp/Gn	2.09	0.01	0.06	0.04	0.07	0.07	0.14	0.21	0.27	0.21	0.51	0.49	
Cp/Sp	2.03	0.01	0.06	0.06	0.11	0.08	0.30	0.29	0.23	0.46	0.39	0.02	
Cp/TQ	25.60	0.30	1.85	2.25	2.97	2.24	3.30	2.72	2.55	3.78	3.10	0.53	
Cp/All	100.00	0.55	3.55	4.45	5.25	4.47	5.49	4.74	4.99	6.01	7.91	4.72	47.85
Px/Cp	23.90	0.05	0.24	0.21	0.46	0.55	0.95	1.70	2.66	4.58	7.79	4.71	
Px/Gn	11.87	0.02	0.17	0.24	0.28	0.38	0.54	0.68	1.01	1.62	3.94	2.99	
Px/Sp	0.89	0.00	0.02	0.03	0.02	0.02	0.04	0.04	0.10	0.25	0.30	0.08	
Px/TQ	28.56	0.08	0.50	0.81	1.45	1.13	2.42	2.31	3.92	5.17	7.15	3.62	
Px/All	100.00	0.16	0.93	1.30	2.20	2.08	3.95	4.73	7.69	11.61	19.17	11.41	34.78
Gn/Cp	0.69	0.00	0.02	0.02	0.04	0.05	0.05	0.04	0.06	0.06	0.18	0.17	
Gn/Px	4.43	0.05	0.28	0.26	0.27	0.29	0.34	0.36	0.41	0.62	0.98	0.59	
Gn/Sp	3.53	0.01	0.10	0.15	0.15	0.29	0.25	0.40	0.50	0.52	0.70	0.47	
Gn/TQ	7.84	0.12	0.71	0.66	0.69	0.66	0.87	0.86	0.81	0.95	1.00	0.49	
Gn/All	100.00	0.19	1.11	1.08	1.15	1.28	1.51	1.66	1.79	2.15	2.86	1.72	83.51
Sp/Cp	4.79	0.00	0.09	0.24	0.20	0.40	0.62	0.23	0.54	0.51	1.05	0.90	
Sp/Px	2.24	0.01	0.12	0.24	0.16	0.11	0.15	0.09	0.14	0.45	0.59	0.19	
Sp/Gn	21.74	0.07	0.46	0.78	1.28	1.58	1.47	2.57	2.08	3.48	5.17	2.80	
Sp/TQ	47.84	0.58	3.02	2.47	3.15	4.21	4.86	6.61	6.03	7.12	6.85	2.94	
Sp/All	100.00	0.66	3.69	3.72	4.80	6.29	7.10	9.50	8.79	11.56	13.66	6.83	23.40

Sample: RGHR CON MEDIUM AREA % DISTRIBUTION OF TOTAL MINERAL AS PARTICLES OF A GIVEN GRADE AND TYPE Table A1.53

		Particle Grade (% of First Mentioned Phase - eg. Cp in Cp/Px Binaries)											
Type	Total	0.0250	0.1000	0.2000	0.3000	0.4000	0.5000	0.6000	0.7000	0.8000	0.9000	0.9750	1.0000
Cp/Px	14.03	0.23	1.55	1.69	1.39	1.37	1.17	1.03	0.91	0.96	2.04	1.67	
Cp/Gn	2.46	0.01	0.05	0.08	0.14	0.08	0.07	0.08	0.10	0.36	0.90	0.60	
Cp/Sp	8.06	0.01	0.13	0.20	0.09	0.23	0.58	0.43	0.50	0.66	2.72	2.49	
Cp/TQ	21.07	0.18	1.26	1.88	2.47	1.87	1.80	2.25	2.28	1.54	3.52	2.01	
Cp/All	100.00	0.44	2.99	3.84	4.10	3.56	3.62	3.79	3.80	3.52	9.18	6.78	54.38
Px/Cp	14.31	0.02	0.09	0.09	0.15	0.26	0.44	0.78	1.22	2.55	5.27	3.45	
Px/Gn	9.46	0.02	0.12	0.15	0.23	0.25	0.32	0.51	0.95	1.75	3.18	1.98	
Px/Sp	4.41	0.01	0.04	0.05	0.05	0.10	0.12	0.16	0.39	0.46	1.60	1.45	
Px/TQ	14.56	0.04	0.26	0.35	0.46	0.69	1.03	1.45	2.17	3.07	3.50	1.56	
Px/All	100.00	0.08	0.50	0.64	0.89	1.30	1.91	2.91	4.73	7.82	13.54	8.43	57.26
Gn/Cp	0.53	0.00	0.03	0.02	0.01	0.02	0.02	0.03	0.09	0.08	0.12	0.09	
Gn/Px	3.90	0.04	0.26	0.32	0.30	0.25	0.24	0.28	0.39	0.45	0.79	0.57	
Gn/Sp	3.87	0.02	0.15	0.24	0.22	0.30	0.39	0.37	0.43	0.57	0.76	0.43	
Gn/TQ	2.40	0.06	0.33	0.27	0.23	0.23	0.28	0.28	0.15	0.35	0.23	0.00	
Gn/All	100.00	0.12	0.76	0.85	0.76	0.81	0.93	0.96	1.06	1.45	1.90	1.09	89.30
Sp/Cp	5.99	0.08	0.40	0.22	0.29	0.38	0.77	0.46	0.29	1.05	1.51	0.55	
Sp/Px	6.06	0.13	0.62	0.40	0.58	0.38	0.41	0.52	0.44	0.65	1.22	0.71	
Sp/Gn	23.26	0.05	0.40	0.67	0.87	1.16	1.86	2.15	2.47	4.49	6.19	2.96	
Sp/TQ	18.59	0.32	1.75	1.40	1.34	1.81	1.95	1.30	2.50	1.99	3.38	0.84	
Sp/All	100.00	0.58	3.16	2.69	3.08	3.73	4.98	4.43	5.70	8.18	12.30	5.05	46.10

Sample RGHR CON FINE AREA % DISTRIBUTION OF TOTAL MINERAL AS PARTICLES OF A GIVEN GRADE AND TYPE Table A1.54

Particle Grade (% of First Mentioned Phase - eg. Cp in Cp/Px Binaries)

Type	Total	0.0250	0.1000	0.2000	0.3000	0.4000	0.5000	0.6000	0.7000	0.8000	0.9000	0.9750	1.0000
Cp/Px	18.62	0.56	3.23	2.31	0.99	1.52	0.82	1.09	1.73	1.85	2.67	1.85	
Cp/Gn	2.59	0.03	0.12	0.03	0.05	0.07	0.08	0.00	0.12	0.66	1.04	0.40	
Cp/Sp	18.07	0.10	0.59	0.40	0.35	0.46	0.33	0.20	0.58	1.98	10.84	2.25	
Cp/TQ	54.45	0.63	3.76	3.69	3.66	2.84	3.30	3.66	3.69	7.13	16.77	5.31	
Cp/All	100.00	1.32	7.70	6.43	5.05	4.88	4.54	4.95	6.12	11.61	31.32	9.81	6.27
Px/Cp	35.67	0.02	0.16	0.24	0.39	0.38	0.43	1.20	1.21	4.85	15.29	11.49	
Px/Gn	4.55	0.03	0.14	0.10	0.10	0.14	0.39	0.52	0.55	0.83	1.25	0.51	
Px/Sp	2.42	0.01	0.06	0.02	0.00	0.03	0.00	0.16	0.06	0.35	1.01	0.72	
Px/TQ	29.23	0.27	1.41	1.11	1.27	1.63	1.99	3.12	3.82	5.62	7.72	1.27	
Px/All	100.00	0.33	1.77	1.47	1.77	2.18	2.82	4.99	5.64	11.65	25.27	13.98	28.12
Gn/Cp	1.72	0.01	0.07	0.10	0.03	0.00	0.05	0.06	0.07	0.08	0.63	0.63	
Gn/Px	5.11	0.01	0.16	0.24	0.27	0.40	0.45	0.24	0.28	0.48	1.43	1.16	
Gn/Sp	3.08	0.02	0.16	0.18	0.18	0.20	0.20	0.36	0.35	0.48	0.63	0.34	
Gn/TQ	10.89	0.21	1.29	1.31	1.25	1.47	1.44	1.67	0.76	0.95	0.54	0.00	
Gn/All	100.00	0.26	1.68	1.83	1.73	2.06	2.13	2.32	1.46	1.99	3.22	2.13	79.20
Sp/Cp	19.21	0.08	1.57	0.64	0.32	0.17	0.43	0.90	1.05	2.06	6.96	5.03	
Sp/Px	3.77	0.05	0.28	0.21	0.06	0.26	0.00	0.13	0.00	0.17	1.35	1.26	
Sp/Gn	9.97	0.02	0.15	0.26	0.32	0.52	0.43	0.64	0.90	1.55	3.09	2.09	
Sp/TQ	49.00	0.70	5.05	5.71	3.67	3.26	3.11	4.25	3.76	7.90	9.47	2.09	
Sp/All	100.00	0.84	7.05	6.83	4.38	4.21	3.97	5.93	5.71	11.68	20.88	10.47	18.04

Sample: CLNR TLS COARSE AREA % DISTRIBUTION OF TOTAL MINERAL AS PARTICLES OF A GIVEN GRADE AND TYPE Table A1.55

		Particle Grade (% of First Mentioned Phase - eg. Cp in Cp/Px Binaries)											
Type	Total	0.0250	0.1000	0.2000	0.3000	0.4000	0.5000	0.6000	0.7000	0.8000	0.9000	0.9750	1.0000
Cp/Px	22.37	0.68	3.38	2.12	2.41	2.12	2.51	1.19	1.50	1.90	2.80	1.76	
Cp/Gn	5.62	0.01	0.05	0.09	0.11	0.20	0.33	0.23	0.52	0.68	1.86	1.54	
Cp/Sp	4.77	0.02	0.23	0.37	0.18	0.58	0.18	0.47	0.25	0.62	1.19	0.70	
Cp/TQ	12.30	0.38	2.06	1.62	1.72	1.42	1.54	1.26	0.41	0.09	1.51	0.30	
Cp/All	100.00	1.09	5.72	4.20	4.40	4.31	4.55	3.15	2.67	3.30	7.36	4.31	54.93
Px/Cp	23.43	0.01	0.09	0.14	0.19	0.24	0.75	0.94	1.67	2.52	9.02	7.86	
Px/Gn	10.90	0.01	0.12	0.23	0.19	0.19	0.26	0.58	0.96	1.03	3.79	3.53	
Px/Sp	4.58	0.01	0.05	0.08	0.08	0.06	0.25	0.19	0.25	0.77	1.74	1.12	
Px/TQ	13.15	0.05	0.22	0.24	0.66	0.50	0.77	1.36	1.32	2.70	3.79	1.53	
Px/All	100.00	0.08	0.49	0.69	1.12	0.98	2.03	3.07	4.20	7.01	18.35	14.04	47.94
Gn/Cp	0.66	0.01	0.05	0.04	0.05	0.04	0.08	0.07	0.06	0.09	0.12	0.06	
Gn/Px	4.02	0.07	0.34	0.21	0.33	0.31	0.21	0.23	0.36	0.74	0.90	0.32	
Gn/Sp	5.10	0.01	0.14	0.31	0.29	0.31	0.23	0.29	0.51	0.49	1.32	1.19	
Gn/TQ	4.37	0.06	0.37	0.39	0.36	0.44	0.31	0.59	0.38	0.46	0.62	0.38	
Gn/All	100.00	0.15	0.90	0.94	1.03	1.10	0.83	1.19	1.32	1.78	2.96	1.95	85.84
Sp/Cp	6.82	0.02	0.14	0.16	0.11	0.33	0.18	0.90	0.43	1.53	2.20	0.81	
Sp/Px	7.40	0.10	0.68	0.68	0.38	0.46	0.88	0.29	0.66	1.03	1.47	0.74	
Sp/Gn	21.94	0.13	0.64	0.54	0.97	0.86	1.02	2.08	2.94	5.51	5.72	1.53	
Sp/TQ	21.61	0.19	1.24	1.30	1.09	2.44	1.67	2.84	2.54	2.71	4.36	1.23	
Sp/All	100.00	0.45	2.70	2.67	2.54	4.09	3.75	6.11	6.56	10.82	13.75	4.31	42.24

Sample CLNR TLS MEDIUM AREA % DISTRIBUTION OF TOTAL MINERAL AS PARTICLES OF A GIVEN GRADE AND TYPE Table A1.56

		Particle Grade (% of First Mentioned Phase - eg. Cp in Cp/Px Binaries)											
Type	Total	0.0250	0.1000	0.2000	0.3000	0.4000	0.5000	0.6000	0.7000	0.8000	0.9000	0.9750	1.0000
Cp/Px	19.04	0.24	1.86	2.51	2.09	1.63	1.90	2.03	1.55	1.61	2.16	1.46	
Cp/Gn	3.53	0.01	0.04	0.01	0.07	0.04	0.19	0.17	0.17	0.34	1.33	1.15	
Cp/Sp	6.90	0.00	0.17	0.20	0.38	0.32	0.42	0.87	0.74	0.39	1.62	1.79	
Cp/TQ	12.53	0.11	0.80	1.30	1.69	1.00	1.13	1.97	1.01	1.27	1.49	0.77	
Cp/All	100.00	0.36	2.86	4.02	4.24	3.00	3.65	5.03	3.48	3.61	6.59	5.17	58.00
Px/Cp	18.27	0.01	0.09	0.15	0.25	0.51	0.72	0.93	1.86	3.82	6.37	3.54	
Px/Gn	7.78	0.02	0.12	0.12	0.28	0.23	0.31	0.39	0.77	1.44	2.73	1.39	
Px/Sp	6.22	0.01	0.07	0.11	0.09	0.16	0.21	0.27	0.38	0.70	2.30	1.91	
Px/TQ	8.53	0.02	0.15	0.25	0.35	0.63	0.66	0.82	1.44	1.88	1.92	0.42	
Px/All	100.00	0.06	0.43	0.64	0.97	1.54	1.90	2.42	4.45	7.83	13.32	7.26	59.20
Gn/Cp	0.50	0.01	0.04	0.02	0.02	0.03	0.06	0.02	0.05	0.01	0.10	0.13	
Gn/Px	3.74	0.03	0.23	0.27	0.25	0.20	0.23	0.26	0.49	0.36	0.80	0.62	
Gn/Sp	3.03	0.02	0.13	0.21	0.23	0.33	0.28	0.38	0.31	0.57	0.50	0.06	
Gn/TQ	1.41	0.04	0.20	0.14	0.14	0.16	0.16	0.13	0.18	0.06	0.13	0.07	
Gn/All	100.00	0.09	0.61	0.65	0.64	0.73	0.73	0.79	1.03	0.99	1.53	0.88	91.33
Sp/Cp	6.54	0.06	0.22	0.12	0.38	0.70	0.51	0.59	1.08	0.99	1.81	0.08	
Sp/Px	8.88	0.16	0.82	0.56	0.53	0.58	0.66	0.77	0.66	1.44	1.92	0.79	
Sp/Gn	19.29	0.01	0.24	0.60	0.55	1.06	1.18	2.10	2.21	3.52	5.08	2.75	
Sp/TQ	14.04	0.29	1.36	0.87	1.38	1.42	1.00	1.23	1.59	1.54	2.27	1.08	
Sp/All	100.00	0.51	2.63	2.15	2.35	3.76	3.36	4.69	5.54	7.49	11.08	4.71	51.25

Sample: CLNR TLS FINE AREA % DISTRIBUTION OF TOTAL MINERAL AS PARTICLES OF A GIVEN GRADE AND TYPE Table A1.57

		Particle Grade (% of First Mentioned Phase - eg. Cp in Cp/Px Binaries)											
Type	Total	0.0250	0.1000	0.2000	0.3000	0.4000	0.5000	0.6000	0.7000	0.8000	0.9000	0.9750	1.0000
Cp/Px	25.09	0.15	0.81	0.79	0.99	1.50	1.54	1.85	2.00	3.70	7.14	4.62	
Cp/Gn	4.26	0.02	0.11	0.09	0.13	0.09	0.11	0.26	0.15	0.53	1.59	1.18	
Cp/Sp	3.93	0.04	0.44	0.35	0.46	0.09	0.33	0.53	0.31	0.35	0.59	0.43	
Cp/TQ	18.05	0.36	1.96	1.41	1.06	1.15	1.10	1.32	1.85	2.11	3.37	2.36	
Cp/All	100.00	0.56	3.33	2.64	2.64	2.82	3.08	3.96	4.32	6.70	12.69	8.59	48.67
Px/Cp	12.84	0.06	0.39	0.45	0.42	0.60	0.75	1.10	1.13	1.55	3.59	2.79	
Px/Gn	13.23	0.03	0.13	0.11	0.16	0.22	0.43	0.58	0.91	2.16	5.04	3.47	
Px/Sp	2.12	0.02	0.09	0.06	0.10	0.04	0.05	0.06	0.08	0.26	0.78	0.58	
Px/TQ	11.13	0.09	0.46	0.37	0.52	0.43	0.43	1.16	0.98	1.90	4.37	0.42	
Px/All	100.00	0.19	1.07	0.99	1.20	1.29	1.67	2.91	3.09	5.86	13.78	7.25	60.69
Gn/Cp	2.08	0.02	0.11	0.08	0.04	0.11	0.07	0.08	0.19	0.22	0.62	0.54	
Gn/Px	7.25	0.11	0.71	0.69	0.49	0.49	0.55	0.41	0.48	0.55	1.48	1.27	
Gn/Sp	1.71	0.03	0.19	0.19	0.21	0.27	0.21	0.16	0.10	0.22	0.12	0.00	
Gn/TQ	4.84	0.12	0.73	0.66	0.41	0.22	1.03	0.33	0.29	0.44	0.62	0.00	
Gn/All	100.00	0.28	1.74	1.62	1.15	1.10	1.85	0.99	1.06	1.43	2.84	1.81	84.12
Sp/Cp	15.58	0.02	0.11	0.15	0.23	0.61	0.57	0.23	1.85	2.42	6.81	2.58	
Sp/Px	8.09	0.05	0.30	0.23	0.11	0.15	0.19	0.23	0.79	0.91	2.72	2.40	
Sp/Gn	14.02	0.00	0.04	0.15	0.11	0.30	0.57	1.14	1.32	2.12	4.77	3.51	
Sp/TQ	35.82	0.20	1.29	1.44	1.36	1.21	1.89	2.72	3.71	5.45	13.96	2.58	
Sp/All	100.00	0.27	1.74	1.97	1.82	2.27	3.22	4.31	7.68	10.90	28.27	11.07	26.49

Sample· CLNR CON COARSE AREA % DISTRIBUTION OF TOTAL MINERAL AS PARTICLES OF A GIVEN GRADE AND TYPE Table A1.58

Particle Grade (% of First Mentioned Phase - eg Cp in Cp/Px Binaries)

Type	Total	0.0250	0.1000	0.2000	0.3000	0.4000	0.5000	0.6000	0.7000	0.8000	0.9000	0.9750	1.0000
Cp/Px	14.49	0.05	0.40	0.56	0.50	0.84	0.99	0.85	1.00	1.82	4.32	3.15	
Cp/Gn	1.39	0.00	0.02	0.01	0.03	0.04	0.07	0.05	0.22	0.24	0.41	0.30	
Cp/Sp	4.32	0.00	0.03	0.09	0.17	0.23	0.16	0.26	0.38	0.66	1.38	0.96	
Cp/TQ	15.03	0.04	0.25	0.43	0.73	0.78	1.07	1.11	1.69	2.04	3.94	2.95	
Cp/All	100.00	0.10	0.70	1.09	1.43	1.89	2.30	2.27	3.29	4.77	10.06	7.36	64.77
Px/Cp	37.92	0.23	1.37	1.31	1.22	1.63	2.85	3.60	3.35	6.42	10.29	5.66	
Px/Gn	2.27	0.00	0.01	0.06	0.07	0.09	0.13	0.09	0.19	0.38	0.76	0.50	
Px/Sp	2.41	0.00	0.03	0.05	0.07	0.08	0.07	0.10	0.18	0.62	0.89	0.33	
Px/TQ	27.32	0.24	1.50	1.70	1.94	2.19	2.68	2.94	3.06	4.78	4.79	1.50	
Px/All	100.00	0.48	2.91	3.11	3.30	3.99	5.72	6.72	6.78	12.19	16.73	7.99	30.08
Gn/Cp	9.14	0.09	0.54	0.72	1.10	0.37	0.80	0.69	0.71	0.71	2.03	1.40	
Gn/Px	4.44	0.05	0.35	0.39	0.33	0.24	0.52	0.53	0.69	0.99	0.35	0.00	
Gn/Sp	4.01	0.03	0.15	0.16	0.24	0.09	0.59	0.35	0.09	0.08	1.09	1.15	
Gn/TQ	15 99	0.51	2.60	1.80	1.96	3.26	2.14	1.18	1.30	0.86	0.38	0.00	
Gn/All	100.00	0.68	3.64	3.07	3.62	3.96	4.05	2.74	2.79	2.64	3.85	2.55	66.43
Sp/Cp	26.37	0.27	1.71	1.84	1.83	1.94	1.79	3.86	4.41	3.81	3.11	1.81	
Sp/Px	5.12	0.03	0.38	0.60	0.30	0.25	0.28	0.48	0.65	0.72	0.89	0.54	
Sp/Gn	4.52	0.03	0.11	0.02	0.04	0.22	0.56	0.13	0.52	0.62	1.28	0.99	
Sp/TQ	41.35	0.98	6.27	5.77	3.30	4.91	4.15	3.11	2.72	3.34	4.81	1.99	
Sp/All	100.00	1.32	8.48	8.23	5.46	7.31	6.78	7.58	8.30	8.48	10.09	5.33	22.64

Sample: CLNR CON MEDIUM AREA % DISTRIBUTION OF TOTAL MINERAL AS PARTICLES OF A GIVEN GRADE AND TYPE Table A1.51

		Particle Grade (% of First Mentioned Phase - eg. Cp in Cp/Px Binaries)											
Type	Total	0.0250	0.1000	0.2000	0.3000	0.4000	0.5000	0.6000	0.7000	0.8000	0.9000	0.9750	1.0000
Cp/Px	13.47	0.05	0.34	0.49	0.59	0.84	0.87	0.99	1.23	2.00	3.68	2.40	
Cp/Gn	1.42	0.00	0.01	0.02	0.02	0.02	0.05	0.05	0.11	0.15	0.52	0.47	
Cp/Sp	3.06	0.00	0.03	0.08	0.06	0.09	0.11	0.20	0.28	0.44	1.02	0.76	
Cp/TQ	3.62	0.01	0.09	0.16	0.18	0.29	0.21	0.31	0.52	0.55	0.97	0.33	
Cp/All	100.00	0.06	0.47	0.74	0.86	1.24	1.24	1.54	2.14	3.14	6.19	3.96	78.42
Px/Cp	45.01	0.22	1.46	1.79	1.88	2.35	3.11	4.49	4.91	6.99	11.00	6.82	
Px/Gn	2.83	0.01	0.03	0.02	0.03	0.10	0.06	0.12	0.29	0.64	1.01	0.51	
Px/Sp	2.90	0.00	0.02	0.03	0.04	0.08	0.16	0.33	0.29	0.46	0.89	0.61	
Px/TQ	8.91	0.05	0.36	0.56	0.69	0.60	0.69	1.15	1.53	2.27	1.01	0.00	
Px/All	100.00	0.28	1.87	2.39	2.64	3.14	4.02	6.10	7.02	10.36	13.90	7.93	40.35
Gn/Cp	22.80	0.55	2.67	1.67	2.20	1.47	2.34	1.40	2.57	3.47	3.31	1.14	
Gn/Px	17.43	0.17	1.44	2.07	1.60	1.07	0.83	2.00	0.94	1.07	3.31	2.93	
Gn/Sp	8.70	0.08	0.43	0.40	0.40	0.40	0.50	0.80	1.17	0.27	1.80	2.44	
Gn/TQ	18.35	0.63	3.54	2.81	2.30	1.47	1.17	0.80	1.87	1.60	1.50	0.65	
Gn/All	100.00	1.42	8.08	6.95	6.51	4.41	4.84	5.01	6.55	6.41	9.92	7.16	32.73
Sp/Cp	29.41	0.40	2.33	2.27	2.42	2.69	2.24	2.78	2.93	6.34	4.98	0.00	
Sp/Px	7.69	0.09	0.57	0.66	0.72	1.26	0.90	0.72	0.52	0.60	1.08	0.58	
Sp/Gn	5.31	0.03	0.09	0.03	0.22	0.24	0.22	0.27	0.42	0.72	1.75	1.31	
Sp/TQ	16.31	0.65	3.28	1.94	1.66	0.72	1.05	1.08	2.09	1.91	1.35	0.58	
Sp/All	100.00	1.16	6.27	4.91	5.03	4.91	4.41	4.85	5.97	9.57	9.16	2.48	41.29

Sample. CLNR CON FINE AREA % DISTRIBUTION OF TOTAL MINERAL AS PARTICLES OF A GIVEN GRADE AND TYPE Table A1.60

Particle Grade (% of First Mentioned Phase - eg. Cp in Cp/Px Binaries)

Type	Total	0.0250	0.1000	0.2000	0.3000	0.4000	0.5000	0.6000	0.7000	0.8000	0.9000	0.9750	1.0000
Cp/Px	9.97	0 03	0.21	0.28	0.34	0.34	0.50	0.56	0.57	1.12	3.35	2.66	
Cp/Gn	1.24	0.00	0.01	0.00	0.01	0.03	0.05	0.04	0.06	0.14	0.48	0.40	
Cp/Sp	3.50	0.01	0.07	0.05	0.08	0.10	0.18	0.19	0.14	0.38	1.28	1.02	
Cp/TQ	5.95	0.01	0.07	0.12	0.14	0.20	0.26	0.37	0.38	0.65	2.05	1.69	
Cp/All	100.00	0.06	0.37	0.45	0.57	0.68	0.99	1.16	1.14	2.29	7.17	5.77	79.35
Px/Cp	38.09	0.35	1.90	1.43	1.25	1.89	2.53	2.64	4.08	5.63	9.80	6.59	
Px/Gn	3.30	0.01	0.04	0.04	0.13	0.04	0.16	0.13	0.31	0.26	1.09	1.07	
Px/Sp	1.94	0.01	0.04	0.02	0.03	0.04	0.11	0.07	0.00	0.18	0.79	0.64	
Px/TQ	9.56	0.21	1.14	0.81	0.66	1.14	1.21	0.79	1.23	0.97	1.29	0.11	
Px/All	100.00	0.58	3.13	2.31	2.08	3.12	4.01	3.63	5.62	7.04	12.96	8.41	47.11
Gn/Cp	4.82	0.11	0.56	0.36	0.27	0.27	0.56	0.54	0.31	0.18	0.80	0.87	
Gn/Px	4.01	0.06	0.25	0.13	0.27	0.19	0.34	0.13	0.63	0.36	0.80	0.87	
Gn/Sp	1.74	0.03	0.13	0.04	0.13	0.09	0.11	0.13	0.16	0.18	0.40	0.33	
Gn/TQ	5.78	0.19	0.87	0.36	0.40	0.27	0.45	0.40	0.31	0.89	1.21	0.44	
Gn/All	100.00	0.39	1.81	0.89	1.07	0.80	1.45	1.21	1.41	1.61	3.22	2.50	83.64
Sp/Cp	39.40	0.45	2.45	1.64	1.00	2.23	3.16	2.68	3.12	3.27	11.04	8.34	
Sp/Px	4.23	0.06	0.30	0.15	0.00	0.15	0.37	0.22	0.26	0.30	1.34	1.09	
Sp/Gn	5.83	0.01	0.07	0.07	0.11	0.15	0.19	0.22	0.52	0.30	2.01	2.18	
Sp/TQ	18.19	0.33	1.97	1.64	1.12	0.89	1.86	1.56	2.60	3.87	2.34	0.00	
Sp/All	100.00	0.86	4.80	3.50	2.23	3.42	5.58	4.69	6.51	7.74	16.73	11.60	32.35

Sample: RC074 COARSE AREA DISTRIBUTIONS AS VARIOUS TYPES AND GRADE/RECOVERY DATA Table A1.61

Mineral Distributions

	Sample Grade	Low-Grade (00-15%)	Medium Grade (15-85%)	High Grade (85-100%)	Free (100%)	% of Binaries With Cp (All Grades)
Cp	2.54	2.62	25.21	12.03	60.14	
Px	38.08	0.80	31.68	37.40	30.12	1.94
Gn	27.13	8.13	32.03	4.18	55.65	3.22
Sp	32.14	2.07	31.81	36.21	29.91	1.44
Total	99.89					

MINERAL GRADE/RECOVERY RELATIONSHIPS

Cp Grade	61.3	66.7	76.9	83.7	86.9	89.7	92.8	94.4	96.8	98.6	99.8	100.0
Recovery	100.0	99.7	97.4	94.7	92.8	90.4	86.7	84.0	78.5	72.2	64.0	60.1
Px Grade	72.9	75.4	79.0	81.3	83.7	85.7	88.1	90.7	93.1	95.8	99.2	100.0
Recovery	100.0	99.9	99.2	98.3	96.6	94.6	91.1	85.8	79.1	67.5	43.8	30.1
Gn Grade	38.0	46.0	63.2	74.3	82.6	88.3	92.6	95.9	98.1	99.4	99.9	100.0
Recovery	100.0	98.8	91.9	85.9	80.4	75.9	71.6	67.3	63.5	59.8	56.9	55.7
Sp Grade	61.8	67.3	74.9	78.7	82.9	86.0	89.0	91.3	93.7	96.1	99.1	100.0
Recovery	100.0	99.7	97.9	96.2	93.3	90.3	86.3	81.9	75.5	66.1	45.4	29.9

Sample RC074 MEDIUM AREA DISTRIBUTIONS AS VARIOUS TYPES AND GRADE/RECOVERY DATA Table A1.62

Mineral Distributions

	Sample Grade	Low-Grade (00-15%)	Medium Grade (15-85%)	High Grade (85-100%)	Free (100%)	% of Binaries With Cp (All Grades)
Cp	6.31	7.16	25.42	14.77	52.65	
Px	40.06	0.73	22.39	33.65	43.23	6.65
Gn	31.46	5.48	22.11	5.62	66.79	9.50
Sp	22.18	2.17	31.55	49.28	17.00	14.56
Total	100.01					

MINERAL GRADE/RECOVERY RELATIONSHIPS

Cp Grade	42.6	51.4	70.6	81.8	86.8	90.5	92.8	95.0	96.4	98.3	99.8	100.0
Recovery	100.0	99.0	92.8	88.0	85.2	82.3	79.9	76.7	73.6	67.4	58.0	52.7
Px Grade	76.9	79.3	82.9	85.4	87.6	89.5	91.4	93.2	95.0	96.8	99.4	100.0
Recovery	100.0	99.9	99.3	98.4	97.0	95.3	93.0	89.6	84.9	76.9	57.6	43.2
Gn Grade	47.3	56.5	72.8	80.7	88.1	92.1	95.0	97.3	98.3	99.3	99.9	100.0
Recovery	100.0	99.1	94.5	91.1	86.9	83.8	80.9	77.7	75.8	72.4	68.4	66.8
Sp Grade	61.7	67.4	75.5	79.0	82.3	85.7	87.9	90.3	92.6	94.8	98.6	100.0
Recovery	100.0	99.6	97.8	96.3	93.9	90.5	87.6	82.7	76.4	66.3	38.8	17.0

Sample: RC074 FINE AREA DISTRIBUTIONS AS VARIOUS TYPES AND GRADE/RECOVERY DATA Table A1.63

Mineral Distributions

	Sample Grade	Low-Grade (00-15%)	Medium Grade (15-85%)	High Grade (85-100%)	Free (100%)	% of Binaries With Cp (All Grades)
Cp	9.63	17.73	32.94	24.89	24.43	
Px	46.79	1.28	16.97	32.87	48.88	45.36
Gn	29.56	3.49	17.96	5.98	72.57	5.05
Sp	15.71	3.62	40.85	44.88	10.65	58.55
Total	101.69					

MINERAL GRADE/RECOVERY RELATIONSHIPS

Cp Grade	24.5	33.3	57.3	71.9	80.3	85.5	89.6	93.1	94.9	96.5	99.2	100.0
Recovery	100.0	97.1	82.3	74.2	69.0	65.1	61.2	56.8	53.8	49.3	35.8	24.4
Px Grade	74.2	78.6	85.1	87.9	89.7	91.6	93.1	94.5	95.9	97.2	99.4	100.0
Recovery	100.0	99.8	98.7	97.8	96.7	95.2	93.3	91.0	87.3	81.7	64.0	48.9
Gn Grade	57.3	65.0	78.2	84.7	89.4	93.3	95.8	97.6	98.8	99.4	99.9	100.0
Recovery	100.0	99.5	96.5	94.0	91.3	88.4	85.8	83.3	80.8	78.5	75.2	72.6
Sp Grade	53.1	60.7	72.2	76.2	79.6	82.3	85.1	87.9	90.6	94.0	98.5	100.0
Recovery	100.0	99.4	96.4	94.4	91.9	89.0	84.6	78.6	70.4	55.5	27.3	10.6

Sample. RC076 COARSE AREA DISTRIBUTIONS AS VARIOUS TYPES AND GRADE/RECOVERY DATA Table A1.64

Mineral Distributions

	Sample Grade	Low-Grade (00-15%)	Medium Grade (15-85%)	High Grade (85-100%)	Free (100%)	% of Binaries With Cp (All Grades)
Cp	4.95	2.20	30.66	17.28	49.87	
Px	34.44	0.99	33.45	35.76	29.81	8.95
Gn	29.93	6.38	30.15	5.46	58.00	2.54
Sp	30.67	1.86	36.38	36.16	25.60	2.76
Total	100.00					

MINERAL GRADE/RECOVERY RELATIONSHIPS

Cp Grade	61.2	63.5	71.5	79.5	82.8	87.6	90.7	93.5	96.4	98.0	99.7	100.0
Recovery	100.0	99.8	97.8	94.1	91.9	87.4	83.6	79.0	72.5	67.1	56.2	49.9
Px Grade	70.2	72.9	77.1	79.9	83.0	85.3	87.9	90.4	93.2	95.8	99.2	100.0
Recovery	100.0	99.9	99.0	97.8	95.7	93.4	89.6	84.6	76.7	65.6	42.9	29.8
Gn Grade	42.9	50.1	65.6	76.2	83.4	89.0	93.0	96.0	98.0	99.3	99.9	100.0
Recovery	100.0	99.1	93.6	88.2	83.6	78.9	74.9	70.8	67.0	63.5	59.8	58.0
Sp Grade	61.9	66.3	72.9	77.0	81.0	85.0	87.7	90.2	92.8	95.7	99.1	100.0
Recovery	100.0	99.7	98.1	96.2	93.3	89.2	85.4	80.6	73.3	61.8	40.1	25.6

Sample: RC076 MEDIUM AREA DISTRIBUTIONS AS VARIOUS TYPES AND GRADE/RECOVERY DATA Table A1.65

Mineral Distributions

	Sample Grade	Low-Grade (00-15%)	Medium Grade (15-85%)	High Grade (85-100%)	Free (100%)	% of Binaries With Cp (All Grades)
Cp	7.44	6.03	24.22	17.70	52.05	
Px	37.63	0.60	19.42	28.92	51.07	23.28
Gn	35.79	2.73	13.98	3.95	79.33	5.16
Sp	19.16	1.60	28.33	31.77	38.30	21.96
Total	100.02					

MINERAL GRADE/RECOVERY RELATIONSHIPS

Cp Grade	45.4	55.0	72.5	79.7	85.4	89.6	92.8	95.7	97.1	98.2	99.7	100.0
Recovery	100.0	99.0	94.0	90.8	87.3	83.8	80.4	76.1	73.2	69.7	59.7	52.0
Px Grade	80.0	82.4	85.6	87.3	89.1	90.8	92.5	93.9	95.7	97.3	99.5	100.0
Recovery	100.0	99.9	99.4	98.8	97.8	96.3	94.2	91.6	86.8	80.0	63.2	51.1
Gn Grade	63.2	70.0	81.8	88.0	92.1	94.9	96.9	98.3	99.1	99.6	100.0	100.0
Recovery	100.0	99.6	97.3	95.1	93.0	90.9	88.8	86.9	85.1	83.3	80.8	79.3
Sp Grade	66.9	70.7	77.3	81.6	84.4	87.2	89.7	92.4	94.3	96.5	99.4	100.0
Recovery	100.0	99.8	98.4	96.6	94.8	92.1	88.8	83.8	78.8	70.1	49.8	38.3

Sample RC076 FINE AREA DISTRIBUTIONS AS VARIOUS TYPES AND GRADE/RECOVERY DATA Table A1.66

Mineral Distributions

	Sample Grade	Low-Grade (00-15%)	Medium Grade (15-85%)	High Grade (85-100%)	Free (100%)	% of Binaries With Cp (All Grades)
Cp	13.14	15.45	38.17	37.08	9.31	
Px	43.30	1.64	18.82	37.10	42.44	95.08
Gn	29.71	2.61	13.97	6.62	76.80	20.27
Sp	18.41	5.00	41.97	45.83	7.20	87.62
Total	104.56					

MINERAL GRADE/RECOVERY RELATIONSHIPS

Cp Grade	26.0	34.1	54.1	67.1	77.9	84.4	88.2	90.8	92.4	94.5	98.4	100.0
Recovery	100.0	97.5	84.6	75.9	68.3	63.1	59.4	56.0	52.8	46.4	25.9	9.3
Px Grade	70.8	76.3	84.1	87.2	89.4	90.8	92.1	93.5	95.0	96.6	99.3	100.0
Recovery	100.0	99.7	98.4	97.3	96.0	94.8	93.2	90.6	86.7	79.5	57.8	42.4
Gn Grade	64.1	71.1	82.6	88.2	92.1	94.8	96.4	97.9	98.8	99.4	99.9	100.0
Recovery	100.0	99.6	97.4	95.4	93.4	91.5	89.7	87.5	85.6	83.4	79.6	76.8
Sp Grade	46.0	52.5	64.9	72.9	78.8	83.2	85.9	88.2	90.5	93.7	98.2	100.0
Recovery	100.0	99.3	95.0	90.6	86.1	81.7	78.0	73.5	66.9	53.0	25.1	7.2

Sample: RGHR TLS COARSE AREA DISTRIBUTIONS AS VARIOUS TYPES AND GRADE/RECOVERY DATA Table A1.67

Mineral Distributions

	Sample Grade	Low-Grade (00-15%)	Medium Grade (15-85%)	High Grade (85-100%)	Free (100%)	% of Binaries with Cp (All Grades)
Cp	3.42	3.67	23.30	42.30	30.74	
Px	33.92	1.08	41.18	40.58	17.16	3.89
Gn	30.03	7.61	39.73	6.58	46.08	0.64
Sp	32.46	3.26	40.39	36.55	19.60	6.50
Total	99.83					

MINERAL GRADE/RECOVERY RELATIONSHIPS

Cp Grade	55.6	62.2	75.1	82.5	85.4	88.6	90.8	93.6	94.6	96.0	99 0	100 0
Recovery	100.0	99.5	96.3	93.3	91.5	88.7	86.0	81.3	78.7	73.0	49.9	30 7
Px Grade	67.0	68.8	73.0	77.0	80.0	82.6	85.5	88.3	91.2	94.5	98.9	100.0
Recovery	100.0	99.9	98.9	97.0	94.8	91.8	87.3	81.2	72.6	57.7	30.9	17 2
Gn Grade	38.0	44.1	58.5	70.5	78.5	85.3	90.4	94.0	96.9	98 9	99 9	100 0
Recovery	100.0	99.0	92.4	84.9	78.9	72.9	67.6	62.7	57.7	52.7	47.7	46.1
Sp Grade	54.1	59.8	69.9	75.7	79.6	82.6	85.8	89.0	91.9	95.0	99.0	100.0
Recovery	100.0	99.5	96.7	93.9	90.9	87.7	83.0	76.6	68.6	56.1	32 6	19.6

Sample RGHR TLS MEDIUM AREA DISTRIBUTIONS AS VARIOUS TYPES AND GRADE/RECOVERY DATA Table A1.68

Mineral Distributions

	Sample Grade	Low-Grade (00-15%)	Medium Grade (15-85%)	High Grade (85-100%)	Free (100%)	% of Binaries With Cp (All Grades)
Cp	2.47	24.01	34.37	15.13	26.49	
Px	47.45	0.33	12.95	22.78	63.93	10.05
Gn	28.53	4.28	15.29	4.77	75.66	9.92
Sp	21.65	1.25	23.31	42.75	32.69	36.11
Total	100.10					

MINERAL GRADE/RECOVERY RELATIONSHIPS

Cp Grade	20.3	29.1	58.2	73.4	79.5	84.4	87.2	91.4	94.7	97.4	99.5	100.0
Recovery	100.0	95.9	76.0	68.5	65.1	61.5	58.8	53.4	47.9	41.6	32.9	26.5
Px Grade	87.0	88.6	90.6	91.5	92.8	93.7	94.6	95.7	96.7	98.0	99.7	100.0
Recovery	100.0	99.9	99.7	99.4	98.7	98.0	97.0	95.0	92.5	86.7	73.2	63.9
Gn Grade	55.0	63.6	79.8	87.7	91.4	94.4	96.5	98.0	98.8	99.5	100.0	100.0
Recovery	100.0	99.4	95.7	92.9	91.0	88.8	86.7	84.6	82.8	80.4	77.1	75.7
Sp Grade	71.7	75.0	80.8	84.3	86.3	88.7	90.8	92.6	94.1	96.0	99.1	100.0
Recovery	100.0	99.8	98.7	97.4	96.2	94.0	91.2	88.0	83.8	75.4	51.1	32.7

Sample: RGHR TLS FINE AREA DISTRIBUTIONS AS VARIOUS TYPES AND GRADE/RECOVERY DATA Table A1.69

Mineral Distributions

	Sample Grade	Low-Grade (00-15%)	Medium Grade (15-85%)	High Grade (85-100%)	Free (100%)	% of Binaries With Cp (All Grades)
Cp	1.42	23.20	28.48	22.28	26.04	
Px	47.73	0.43	11.61	21.36	66.60	9.16
Gn	31.26	2.83	11.94	3.04	82.19	4.05
Sp	19.63	1.92	21.72	33.45	42.91	17.72
Total	100.04					

MINERAL GRADE/RECOVERY RELATIONSHIPS

Cp Grade	20.7	30.0	59.7	74.6	81.7	87.3	90.3	93.5	94.8	96.7	99.3	100.0
Recovery	100.0	95.9	76.8	69.8	66.0	62.1	59.5	55.7	53.4	48.3	35.9	26.0
Px Grade	86.4	88.6	91.2	92.2	93.1	94.1	95.1	96.0	97.0	98.1	99.7	100.0
Recovery	100.0	99.9	99.6	99.3	98.8	98.0	96.9	95.3	92.7	88.0	74.9	66.6
Gn Grade	63.5	70.8	83.4	89.6	93.6	95.8	97.4	98.7	99.3	99.7	100.0	100.0
Recovery	100.0	99.6	97.2	95.1	93.1	91.5	89.9	88.1	86.8	85.2	83.3	82.2
Sp Grade	67.6	73.4	81.9	85.5	87.9	90.0	91.7	93.3	95.0	96.8	99.4	100.0
Recovery	100.0	99.7	98.1	96.8	95.4	93.5	91.4	88.6	84.0	76.4	56.8	42.9

Sample: RGHR CON COARSE AREA DISTRIBUTIONS AS VARIOUS TYPES AND GRADE/RECOVERY DATA Table A1.70

Mineral Distributions

	Sample Grade	Low-Grade (00-15%)	Medium Grade (15-85%)	High Grade (85-100%)	Free (100%)	% of Binaries With Cp (All Grades)
Cp	16.06	4.10	35.41	12.64	47.85	
Px	29.45	1.09	33.56	30.58	34.78	65.19
Gn	46.60	1.30	10.61	4.59	83.51	7.94
Sp	7.82	4.35	51.76	20.49	23.40	16.65
Total	99.93					

MINERAL GRADE/RECOVERY RELATIONSHIPS

Cp Grade	49.1	54.8	65.7	73.9	81.2	86.0	90.7	93.9	96.4	98.4	99.8	100.0
Recovery	100.0	99.4	95.9	91.4	86.2	81.7	76.2	71.5	66.5	60.5	52.6	47.9
Px Grade	69.5	72.7	77.2	80.3	83.5	85.6	88.4	90.8	93.5	96.4	99.4	100.0
Recovery	100.0	99.8	98.9	97.6	95.4	93.3	89.4	84.7	77 0	65.4	46.2	34.8
Gn Grade	76.6	81.2	88.2	91.7	94.0	95.7	97.1	98.2	99.0	99.6	99.9	100.0
Recovery	100.0	99.8	98.7	97.6	96.5	95.2	93.7	92.0	90.2	88.1	85.2	83.5
Sp Grade	46.3	52.3	62.5	68.4	73 6	78.8	83.4	88.5	92.4	96.3	99.4	100.0
Recovery	100.0	99.3	95.6	91.9	87.1	80.8	73.7	64.2	55.4	43.9	30.2	23.4

Mineral Distributions

	Sample Grade	Low-Grade (00-15%)	Medium Grade (15-85%)	High Grade (85-100%)	Free (100%)	% of Binaries With Cp (All Grades)
Cp	12.52	3.43	26.23	15.96	54.38	
Px	33.22	0.58	20.19	21.97	57.26	50.77
Gn	44.86	0.38	6.83	2.99	89.30	6.39
Sp	9.50	3.75	32.79	17.36	46.10	16.97
Total	100.11					

MINERAL GRADE/RECOVERY RELATIONSHIPS

Cp Grade	54.3	59.8	70.7	78.9	85.4	89.6	92.9	95.5	97.3	98.3	99.7	100.0
Recovery	100.0	99.6	96.6	92.7	88.6	85.1	81.5	77.7	73.9	70.3	61.2	54.4
Px Grade	80.8	82.9	86.0	87.9	89.5	91.0	92.5	94.2	95.9	97.9	99.7	100.0
Recovery	100.0	99.9	99.4	98.8	97.9	96.6	94.7	91.8	87.0	79.2	65.7	57.3
Gn Grade	83.0	86.3	91.6	94.6	96.2	97.4	98.3	98.9	99.4	99.7	100.0	100.0
Recovery	100.0	99.9	99.1	98.3	97.5	96.7	95.8	94.8	93.7	92.3	90.4	89.3
Sp Grade	53.0	60.1	72.0	77.8	82.3	86.2	90.1	92.8	95.3	97.7	99.7	100.0
Recovery	100.0	99.4	96.3	93.6	90.5	86.8	81.8	77.3	71.6	63.5	51.2	46.1

Sample RGHR CON FINE AREA DISTRIBUTIONS AS VARIOUS TYPES AND GRADE/RECOVERY DATA Table A1.72

Mineral Distributions

	Sample Grade	Low-Grade (00-15%)	Medium Grade (15-85%)	High Grade (85-100%)	Free (100%)	% of Binaries With Cp (All Grades)
Cp	19.22	9.02	43.58	41.13	6.27	
Px	36.59	2.10	30.52	39.26	28.12	83.64
Gn	31.95	1.93	13.52	5.34	79.20	17.33
Sp	14.76	7.89	42.72	31.35	18.04	58.29
Total	102.52					

MINERAL GRADE/RECOVERY RELATIONSHIPS

Cp Grade	35.4	42.9	59.5	70.0	76.5	81.4	84.8	87.6	89.9	92.7	98.5	100.0
Recovery	100.0	98.7	91.0	84.5	79.5	74.6	70.1	65.1	59.0	47.4	16.1	6.3
Px Grade	63.8	69.4	77.8	81.4	84.1	86.3	88.3	90.9	92.9	95.5	99.2	100.0
Recovery	100.0	99.7	97.9	96.4	94.7	92.5	89.7	84.7	79.0	67.4	42.1	28.1
Gn Grade	69.1	74.2	83.3	88.6	91.9	94.7	96.7	98.3	99.0	99.5	99.9	100.0
Recovery	100.0	99.7	98.1	96.2	94.5	92.4	90.3	88.0	86.5	84.5	81.3	79.2
Sp Grade	39.1	44.6	60.7	72.5	78.5	82.8	85.9	89.4	91.7	95.0	99.1	100.0
Recovery	100.0	99.2	92.1	85.3	80.9	76.7	72.7	66.8	61.1	49.4	28.5	18.0

Sample: CLNR TLS COARSE AREA DISTRIBUTIONS AS VARIOUS TYPES AND GRADE/RECOVERY DATA Table A1.73

Mineral Distributions

	Sample Grade	Low-Grade (00-15%)	Medium Grade (15-85%)	High Grade (85-100%)	Free (100%)	% of Binaries With Cp (All Grades)
Cp	10.50	6.81	26.59	11.66	54.93	
Px	35.36	0.57	19.11	32.39	47.94	60.22
Gn	44.13	1.05	8.19	4.91	85.84	6.77
Sp	10.02	3.15	36.55	18.06	42.24	18.86
Total	100.02					

MINERAL GRADE/RECOVERY RELATIONSHIPS

Cp	Grade	42.2	51.1	68.4	77.2	84.1	89.4	93.8	96.2	97.6	98.6	99.8	100.0
	Recovery	100.0	98.9	93.2	89.0	84.6	80.3	75.7	72.6	69.9	66.6	59.2	54.9
Px	Grade	80.4	82.5	85.5	87.5	89.5	90.6	92.2	93.9	95.5	97.1	99.4	100.0
	Recovery	100.0	99.9	99.4	98.7	97.6	96.6	94.6	91.5	87.3	80.3	62.0	47.9
Gn	Grade	80.1	84.0	90.1	93.3	95.4	97.0	97.8	98.5	99.1	99.6	99.9	100.0
	Recovery	100.0	99.8	98.9	98.0	97.0	95.9	95.0	93.8	92.5	90.8	87.8	85.8
Sp	Grade	55.7	61.6	72.0	77.7	81.3	85.4	88.2	91.6	94.2	97.4	99.8	100.0
	Recovery	100.0	99.6	96.9	94.2	91.6	87.5	83.8	77.7	71.1	50.3	46.5	42.2

Sample: CLNR TLS MEDIUM AREA DISTRIBUTIONS AS VARIOUS TYPES AND GRADE/RECOVERY DATA Table A1.74

Mineral Distributions

	Sample Grade	Low-Grade (00-15%)	Medium Grade (15-85%)	High Grade (85-100%)	Free (100%)	% of Binaries With Cp (All Grades)
Cp	12.65	3.22	27.02	11.76	58.00	
Px	33.23	0.49	19.74	20.58	59.20	56.61
Gn	43.74	0.70	5.55	2.41	91.33	6.84
Sp	10.42	3.14	29.83	15.79	51.25	18.85
Total	100.04					

MINERAL GRADE/RECOVERY RELATIONSHIPS

Cp Grade	55.4	60.0	70.4	79.0	85.7	89.3	92.5	95.9	97.6	98.8	99.8	100.0
Recovery	100.0	99.6	96.8	92.8	88.5	85.5	81.9	76.8	73.4	69.8	63.2	58.0
Px Grade	81.7	83.3	86.0	87.9	89.6	91.4	93.0	94.3	96.0	98.0	99.7	100.0
Recovery	100.0	99.9	99.5	98.9	97.9	96.4	94.5	92.0	87.6	79.8	66.5	59.2
Gn Grade	85.9	88.6	93.1	95.4	96.8	97.9	98.6	99.1	99.5	99.8	100.0	100.0
Recovery	100.0	99.9	99.3	98.6	98.0	97.3	96.6	95.8	94.7	93.7	92.2	91.3
Sp Grade	56.7	63.7	74.6	79.5	83.8	87.9	90.7	93.5	95.9	98.0	99.8	100.0
Recovery	100.0	99.5	96.9	94.7	91.9	88.1	84.8	80.1	74.5	67.0	56.0	51.2

Mineral Distributions

	Sample Grade	Low-Grade (00-15%)	Medium Grade (15-85%)	High Grade (85-100%)	Free (100%)	% of Binaries With Cp (All Grades)
Cp	19.19	3.89	26.16	21.27	48.67	
Px	39.21	1.26	17.02	21.03	60.69	45.55
Gn	30.78	2.03	9.20	4.65	84.12	18.84
Sp	11.17	2.01	32.16	39.34	26.49	41.34
Total	100.35					

MINERAL GRADE/RECOVERY RELATIONSHIPS

Cp Grade	54.4	61.7	75.1	81.5	85.7	89.0	91.6	94.0	95.9	97.7	99.6	100.0
Recovery	100.0	99.4	96.1	93.5	90.8	88.0	84.9	81.0	76.6	69.9	57.3	48.7
Px Grade	74.7	79.1	85.4	88.4	90.6	92.1	93.6	95.3	96.5	97.9	99.7	100.0
Recovery	100.0	99.8	98.7	97.7	96.6	95.3	93.6	90.7	87.6	81.7	67.9	60.7
Gn Grade	70.8	76.8	87.1	92.3	94.7	96.2	98.1	98.7	99.2	99.6	99.9	100.0
Recovery	100.0	99.7	98.0	96.4	95.2	94.1	92.2	91.3	90.2	88.8	85.9	84.1
Sp Grade	63.6	68.1	75.9	80.6	83.3	85.5	87.8	89.9	92.6	95.1	99.2	100.0
Recovery	100.0	99.7	98.0	96.0	94.2	91.9	88.7	84.4	76.7	65.8	37.6	26.5

Sample: CLNR CON COARSE AREA DISTRIBUTIONS AS VARIOUS TYPES AND GRADE/RECOVERY DATA Table A1.76

Mineral Distributions

	Sample Grade	Low-Grade (00-15%)	Medium Grade (15-85%)	High Grade (85-100%)	Free (100%)	% of Binaries With Cp (All Grades)
Cp	65.91	0.79	17.03	17.41	64.77	
Px	23.03	3.39	41.81	24.72	30.08	89.02
Gn	5.60	4.31	22.87	6.39	66.43	51.94
Sp	5.92	9.79	52.14	15.42	22.64	73.25
Total	100.46					

MINERAL GRADE/RECOVERY RELATIONSHIPS

Cp Grade	78.0	80.3	84.5	87.6	90.2	92.5	94.5	95.9	97.2	98.4	99.7	100.0
Recovery	100.0	99.9	99.2	98.1	96.7	94.8	92.5	90.2	86.9	82.2	72.1	64.8
Px Grade	52.9	58.5	68.5	74.6	78.8	82.6	86.6	90.2	92.9	96.4	99.5	100.0
Recovery	100.0	99.5	96.6	93.5	90.2	86.2	80.5	73.8	67.0	54.8	38.1	30.1
Gn Grade	51.5	59.5	73.3	80.4	86.3	91.2	95.1	97.1	98.5	99.3	99.9	100.0
Recovery	100.0	99.3	95.7	92.6	89.0	85.0	81.0	78.2	75.5	72.8	69.0	66.4
Sp Grade	33.0	39.4	54.5	65.9	72.0	78.7	83.9	88.8	93.2	96.8	99.5	100.0
Recovery	100.0	98.7	90.2	82.0	76.5	69.2	62.4	54.8	46.5	38.1	28.0	22.6

Sample: CLNR CON MEDIUM AREA DISTRIBUTIONS AS VARIOUS TYPES AND GRADE/RECOVERY DATA Table A1.77

Mineral Distributions

	Sample Grade	Low-Grade (00-15%)	Medium Grade (15-85%)	High Grade (85-100%)	Free (100%)	% of Binaries With Cp (All Grades)
Cp	74.13	0.53	10.90	10.15	78.42	
Px	20.76	2.15	35.67	21.83	40.35	88.71
Gn	1.62	9.51	40.68	17.08	32.73	46.60
Sp	3.61	7.43	39.64	11.64	41.29	69.35
Total	100.11					

MINERAL GRADE/RECOVERY RELATIONSHIPS

Cp Grade	84.6	86.4	89.6	92.0	93.7	95.3	96.4	97.4	98.3	99.1	99.9	100.0
Recovery	100.0	99.9	99.5	98.7	97.9	96.6	95.4	93.9	91.7	88.6	82.4	78.4
Px Grade	61.2	65.4	73.2	78.4	82.2	85.3	88.2	91.5	94.4	97.3	99.6	100.0
Recovery	100.0	99.7	97.9	95.5	92.8	89.7	85.7	79.6	72.5	62.2	48.3	40.3
Gn Grade	34.3	42.0	58.8	70.1	79.0	84.0	88.2	91.7	95.1	97.5	99.5	100.0
Recovery	100.0	98.6	90.5	83.5	77.0	72.6	67.8	62.8	56.2	49.8	39.9	32.7
Sp Grade	39.3	47.6	63.9	72.8	79.7	85.0	88.8	91.9	94.7	98.0	99.9	100.0
Recovery	100.0	98.8	92.6	87.7	82.6	77.7	73.3	68.5	62.5	52.9	43.8	41.3

Sample: CLNR CON FINE AREA DISTRIBUTIONS AS VARIOUS TYPES AND GRADE/RECOVERY DATA Table A1.78

Mineral Distributions

	Sample Grade	Low-Grade (00-15%)	Medium Grade (15-85%)	High Grade (85-100%)	Free (100%)	% of Binaries With Cp (All Grades)
Cp	74.14	0.42	7.29	12.94	79.35	
Px	14.51	3.71	27.80	21.38	47.11	87.90
Gn	7.14	2.19	8.44	5.72	83.64	45.58
Sp	4.29	5.65	33.66	28.34	32.35	79.65
Total	100.09					

MINERAL GRADE/RECOVERY RELATIONSHIPS

Cp Grade	88.2	89.9	92.6	94.2	95.4	96.3	97.2	97.9	98.4	99.0	99.8	100.0
Recovery	100.0	99.9	99.6	99.1	98.6	97.9	96.9	95.7	94.6	92.3	85.1	79.4
Px Grade	55.0	62.7	75.6	81.2	84.4	87.9	91.1	93.3	95.7	97.6	99.6	100.0
Recovery	100.0	99.4	95.3	94.0	91.9	88.8	84.8	81.1	75.5	68.5	55.5	47.1
Gn Grade	70.3	78.5	89.9	92.9	95.1	96.3	97.7	98.5	99.1	99.5	99.9	100.0
Recovery	100.0	99.6	97.8	96.9	95.8	95.0	93.6	92.4	91.0	89.4	86.1	83.6
Sp Grade	46.2	54.4	70.3	77.8	81.1	84.5	88.8	91.6	94.4	96.6	99.3	100.0
Recovery	100.0	99.1	94.3	90.9	88.6	85.2	79.6	74.9	68.4	60.7	44.0	32.4